Springer Theses
Recognizing Outstanding Ph.D. Research

Jamie Hicks

Preparation, Characterisation and Reactivity of Low Oxidation State d-Block Metal Complexes Stabilised by Extremely Bulky Amide Ligands

Springer

Springer Theses

Recognizing Outstanding Ph.D. Research

Aims and Scope

The series "Springer Theses" brings together a selection of the very best Ph.D. theses from around the world and across the physical sciences. Nominated and endorsed by two recognized specialists, each published volume has been selected for its scientific excellence and the high impact of its contents for the pertinent field of research. For greater accessibility to non-specialists, the published versions include an extended introduction, as well as a foreword by the student's supervisor explaining the special relevance of the work for the field. As a whole, the series will provide a valuable resource both for newcomers to the research fields described, and for other scientists seeking detailed background information on special questions. Finally, it provides an accredited documentation of the valuable contributions made by today's younger generation of scientists.

Theses are accepted into the series by invited nomination only and must fulfill all of the following criteria

- They must be written in good English.
- The topic should fall within the confines of Chemistry, Physics, Earth Sciences, Engineering and related interdisciplinary fields such as Materials, Nanoscience, Chemical Engineering, Complex Systems and Biophysics.
- The work reported in the thesis must represent a significant scientific advance.
- If the thesis includes previously published material, permission to reproduce this must be gained from the respective copyright holder.
- They must have been examined and passed during the 12 months prior to nomination.
- Each thesis should include a foreword by the supervisor outlining the significance of its content.
- The theses should have a clearly defined structure including an introduction accessible to scientists not expert in that particular field.

More information about this series at http://www.springer.com/series/8790

Jamie Hicks

Preparation, Characterisation and Reactivity of Low Oxidation State d-Block Metal Complexes Stabilised by Extremely Bulky Amide Ligands

Doctoral Thesis accepted by
Monash University, Clayton, VIC, Australia

Springer

Author
Dr. Jamie Hicks
School of Chemistry
Monash University
Clayton, VIC
Australia

Supervisor
Prof. Cameron Jones
School of Chemistry
Monash University
Clayton, VIC
Australia

ISSN 2190-5053 ISSN 2190-5061 (electronic)
Springer Theses
ISBN 978-981-10-2904-2 ISBN 978-981-10-2905-9 (eBook)
DOI 10.1007/978-981-10-2905-9

Library of Congress Control Number: 2016954625

Printed on acid-free paper

This Springer imprint is published by Springer Nature
The registered company is Springer Nature Singapore Pte Ltd.
The registered company address is: 152 Beach Road, #22-06/08 Gateway East, Singapore 189721, Singapore

Dedicated to the memory of my grandparents
Clarence and Nellie Hicks
who sadly passed away during the progress
of this work

Supervisor's Foreword

It gives me great pleasure to introduce the thesis of my former Ph.D. student, Dr. Jamie Hicks, which has been selected for publication in this prestigious Springer Thesis series. Jamie's thesis presents an outstanding piece of research, which describes the synthesis, characterisation and reactivity of a series of unprecedented metal-metal bonded complexes stabilised by extremely bulky amide ligands.

Compounds bearing homonuclear metal-metal bonds have been intensively studies for over 50 years, not only due to their fundamental appeal, but also because of their wide range of applications, including sensing, small molecule activation, catalysis and enzyme mimicry. In comparison, compounds that contain mixed metal-metal bonds, especially in low-coordinate states, are relatively unexplored, likely due to their difficult synthesis and unstable nature.

Jamie commenced his Ph.D. studies in 2012, when he started investigating the synthesis and reactivity of complexes containing homonuclear metal-metal bonds. However, during this time, Jamie developed a novel and elegant route towards compounds bearing mixed metal-metal bonds, utilizing "inorganic Grignard reagents". This led to the synthesis and isolation of a number of unprecedented compounds, featuring the first examples of manganese–magnesium, zinc–magnesium and zinc–cadmium bonds in molecular compounds. The reactivity of these new compounds towards a variety of gases and small organic molecules was extensively studied, leading to a number of remarkable results.

Jamie's thesis is exceptional on every level, developed at the frontier of our current knowledge and understanding of inorganic and organometallic chemistry. It is both beautifully written and well presented, making it an enjoyable and effortless read. I am confident that Jamie will continue to produce work of an outstanding standard in his future career, and I wish him all the very best.

Clayton, Australia
June 2016

Prof. Cameron Jones

Abstract

Chapter 1 gives a general introduction into d-block elements, including some of the fundamental concepts, such as the 18 electron rule and metal-metal bonding. It also includes an overview of low oxidation state metal complexes, in addition to some of the ligands that have been used to stabilize such complexes. Finally, dimeric magnesium(I) complexes are introduced showing their use as effective reducing agents in organic and inorganic synthesis.

Chapter 2 focuses on the preparation of extremely bulky amido d-block metal(II) halide complexes, including those of chromium, manganese, iron, cobalt, zinc, cadmium and mercury. The synthesis, structure and magnetic properties of these complexes were explored and compared to related terphenyl d-block metal(II) halide complexes. These amido d-block metal(II) halide complexes could potentially serve as precursors for low-coordinate, low-oxidation state d-block chemistry.

Low-coordinate, low-oxidation state manganese complexes are discussed in Chap. 3. These include the characterisation of the first two-coordinate manganese(I) dimer $[\{(Ar^*(SiMe_3)NMn\}_2]$ (Ar^* = 2,6-$\{Ph_2CH\}_2$-4-Me-C_6H_2) synthesised by the reduction of $[Ar^*(SiMe_3)NMn(THF)(\mu\text{-}Br)\}_2]$ with the magnesium(I) reducing agent $[\{(^{Mes}Nacnac)Mg\}_2]$ ($^{Mes}Nacnac$ = $[(MesNCMe)_2CH]^-$, Mes = mesityl). The reduction of the bulkier precursor complex $[Ar^\dagger(Si^iPr_3)NMn(THF)(\mu\text{-}Br)\}_2]$ ($Ar^\dagger$ = 2,6-$\{Ph_2CH\}_2$-4-^{i}Pr-C_6H_2) with the same magnesium(I) reducing agent yielded the unprecedented Mn(0)Mg(II) heterobimetallic complex $[Ar^\dagger(Si^iPr_3)NMnMg(^{Mes}Nacnac)]$ possessing an unsupported Mn–Mg bond. The complex was utilized as an "inorganic Grignard reagent", in the preparation of the asymmetric manganese(I) dimer $[Ar^\dagger(Si^iPr_3)NMnMn(SiMe_3)Ar^*]$ and the related mixed valence, bis(amido)-heterobimetallic complex $[CrMn\{Ar^\dagger(Si^iPr_3)N\}\{Ar^*(SiMe_3)N\}]$. It is also shown to act as a two-electron reducing agent in reactions with unsaturated substrates.

Chapter 4 concentrates on low oxidation state group 12 complexes with metal-metal bonds. This includes the synthesis and characterisation of a homologous series of two-coordinate amido group 12 metal(I) dimers $[\{(Ar^\dagger(SiMe_3)NM\}_2]$ (M = Zn, Cd, Hg). The reduction of the extremely bulky amido zinc(II) bromide complex $[Ar^*(Si^iPr_3)NZnBr]$ with $[\{(^{Mes}Nacnac)Mg\}_2]$ gave the novel Zn(0)Mg(II)

heterobimetallic complex [Ar*(Si^iPr_3)NZnMg(^{Mes}Nacnac)], which bears the first example of a Zn–Mg bond in a molecular complex. The complex was utilized as a transfer reagent in the preparation of the unprecedented trimetallic zinc complex [{Ar*(Si^iPr_3)NZn}$_2$Zn], which bears a string of two-coordinate zinc atoms. The related group 12 trimetallic complexes [{Ar*(Si^iPr_3)NZn}$_2$M] (M = Cd, Hg) were also isolated.

Chapter 5 investigates the synthesis, structure and reactivity of low-coordinate, low-oxidation state cobalt complexes. A series of low coordinate, high-spin cobalt(I) complexes bearing the extremely bulky amide ligand Ar*($SiPh_3$)N^- are described. These include the benzene capped cobalt(I) complex [Ar*($SiPh_3$)NCo(η^6-benzene)], which readily looses its benzene ligand upon dissolution in THF or fluorobenzene, to give the dimeric cobalt(I) complex [{Ar*($SiPh_3$)NCo}$_2$]. The first neutral two-coordinate cobalt(I) complex [Ar*($SiPh_3$)NCo(IPriMe)] (IPriMe = :C{N(^{i}Pr)C(Me)}$_2$) was also isolated by exchange of the benzene ligand with the N-heterocyclic carbene IPriMe.

Finally, Chap. 6 discusses transition metal tetrelyne complexes, which are heavier group 14 analogues of transition metal carbyne complexes. The synthesis and structure of the two singly bonded Mo–Ge complexes [$Cp(CO)_3$Mo–GeN(Ph)Ar*] (Cp = η^5-C_5H_5) and [$Cp(CO)_3$Mo–GeN($SiMe_3$)Ar*] is discussed. The latter readily eliminates a molecule of CO when heated or irradiated with UV light to give the unprecedented amino-germylyne complex [$Cp(CO)_3$Mo≡GeN($SiMe_3$)Ar*]. The spectroscopic and structural data for this complex, in combination with the results of computational studies, show that this compound is best viewed as having a bent Mo–Ge "triple" bond, with little multiple bond character to its Ge–N interaction.

Parts of this thesis have been published in the following journal articles:

J. Hicks, E. Underhill, C. E. Kefalidis, L. Maron, C. Jones, A Mixed-Valence Tri-Zinc Complex, LZnZnZnL (L = Bulky Amide), Bearing a Linear Chain of Two-Coordinate Zinc Centres, *Angew. Chem., Int. Ed.*, **2015**, *54*, 10000. Highlighted in *Nature Chemistry*, *Chemistry in Australia* and as a *Hot Paper* in *Angew. Chem. Int. Ed.*

J. Hicks, C. Jones, Low-Coordinate Cobalt(I) Complexes Stabilized by an Extremely Bulky Amide Ligand, *Organometallics*, **2015**, *34*, 2118.

J. Hicks, C. E. Hoyer, B. Moubaraki, G. L. Manni, E. Carter, D. M. Murphy, K. Murray, L. Gagliardi, C. Jones, A Two-Coordinate Manganese(0) Complex with an Unsupported Mn–Mg Bond: Allowing Access to Low Coordinate Homo- and Heterobimetallic Compounds, *J. Am. Chem. Soc.*, **2014**, *136*, 5283. Highlighted in *J. Am. Chem. Soc. Spotlights, Chem. & Eng. News* and *Chemistry in Australia*.

J. Hicks, C. Jones, Extremely Bulky Amido First Row Transition Metal(II) Halide Complexes: Potential Precursors to Low Coordinate Metal–Metal Bonded Systems, *Inorg. Chem.*, **2013**, *52*, 3900.

J. Hicks, T. J. Hadlington, C. Schenk, J. Li, C. Jones, Utilizing Steric Bulk to Stabilize Molybdenum Aminogermylyne and Aminogermylene Complexes, *Organometallics*, **2012**, *32*, 323.

Acknowledgements

First and foremost I would like to thank my supervisor Prof. Cameron Jones for offering me a Ph.D. candidate position in his group. It has been a fantastic experience and a privilege. His guidance and enthusiasm have made this undertaking possible; his support and sometimes slightly weird sense of humour will not be forgotten. I will also never mispronounciate the words angstrom, nuclear or synchrotron again.

To the many members of the Jones Group who have come and gone over the last three years; Dr. Andreas Stasch, Dr. Simon Bonyhady, Dr. Lea Fohlmeister, Dr. Jiaye Li, Dr. Tobias Böttcher, Dr. Lalrempuia Ralte (Puia), Dr. Edwin Wong, Dr. Mengtao Ma, Dr. María Pastor, Dr. Brant Maitland, Anastas Sidiropoulos (Tash), Brooke Osborne and Sarah Keller, thank you all. You have all contributed to the work in this thesis in some way. A special thank you goes to Emma Underhill (Cardiff University), who worked alongside me for 6 months as part of her 3rd year undergraduate product. Her hard work and "angelic" singing voice will not be forgotten.

To the current Jones Group members; Dr. Deepak Dange, Terrance Hadlington (T-Bone), John Kelly, Mike Dawkins, Aaron Boutland, Caspar de Bruin-Dickason, Jacques Atkinson-Bodourian and Ewart Middleton, thank you. Your friendship and banter over the last three years have made this whole experience so much fun. A special thank you goes to Dr. Indrek Pernik, who spent the time to proof read this thesis cover to cover. You are also a great pool partner. A massive thank you goes to my lab partner and beautiful girlfriend Amelia Davey. Her constant support and kindness throughout the last three years has made it an amazing experience.

Thank you to various staff around the university that have made this research possible. A special thanks goes to Dr. Craig Forsyth, Dr. Andreas Stasch and Dr. David Turner, for teaching me the basics of X-ray crystallography, for taking the time to answer numerous crystallography questions, and also for the many late nights "socialising". Thank you to Peter Nichols who has taught me more about NMR spectroscopy than I ever thought possible.

A number of collaborators have contributed to the work reported in this thesis. Thank you to Prof. Keith Murray and Dr. Boujemaa Moubaraki (Monash University), who helped collect and interpret a number of solid-state variable temperature magnetic susceptibility measurements reported in this thesis. Thank you also to Prof. Laura Gagliardi and Giovanni Manni (University of Minnesota), who performed computational studies on a number of compounds reported in Chap. 3. Thank you to Prof. Laurent Maron and Christos Kefalidis (Université de Toulouse) who performed calculations on the group 12 complexes reported in this work (Chap. 4). Thank you to Dr. Christian Schenk (Universität Heidelberg) who performed computational studies on a number of complexes reported in Chap. 6.

Finally, thank you to my parents, grandparents and family back in England, for their support and encouragement over the years; even though I'm pretty sure they would prefer me working or studying a little closer to home.

Declaration

The work presented in this thesis was carried out between January 2012 and May 2015 under the supervision of Prof. Cameron Jones. This thesis contains no material which has been accepted for the award of any other degree or diploma at any university or equivalent institution and that, to the best of my knowledge and belief, this thesis contains no material previously published or written by another person, except where due reference is made in the text of the thesis.

May 2015

Contents

1 General Introduction 1
1.1 Transition Metals 1
1.2 Low Oxidation State Transition Metal Complexes 2
1.2.1 Bulky Ligands Used into Stabilise Low Oxidation State Complexes 2
1.2.2 Preparation of Low Oxidation State Transition Metal Complexes 3
1.3 Metal–Metal Bonding in Transition Metal Complexes 4
1.3.1 History 4
1.3.2 Quintuple Bonds 5
1.4 Magnesium(I) Complexes 7
1.4.1 Reactivity of β-Diketiminate Stabilised Magnesium(I) Complexes 8
1.4.2 Using β-Diketiminate Stabilised Magnesium(I) Complexes as Reducing Agents in Inorganic Synthesis . . . 9
References 12

2 Extremely Bulky Amido d-Block Metal(II) Halide Complexes 15
2.1 Introduction 15
2.1.1 Previously Reported Bulky Amido Transition Metal(II) Halide Complexes 16
2.1.2 Previously Reported Bulky Amido Group 12 Metal(II) Halide Complexes 18
2.1.3 Terphenyl Stabilised D-Block Metal Halide Complexes . . . 20
2.1.4 Extremely Bulky Monodentate Amido Ligands 25
2.2 Research Outline 27
2.3 Results and Discussion 28
2.3.1 Preparation of Bulky Potassium Amide Salts 28
2.3.2 Bulky Amido First Row Transition Metal(II) Halide Complexes 29
2.3.3 Bulky Amido Group 12 Metal(II) Halide Complexes 36

2.4 Conclusion . . . 43
2.5 Experimental . . . 43
References . . . 53

3 Preparation of Low Oxidation State Manganese Complexes Stabilised by Bulky Amide Ligands . . . 55
3.1 Introduction . . . 55
3.1.1 Low Oxidation State Manganese Complexes . . . 55
3.2 Research Outline . . . 62
3.3 Results and Discussion . . . 62
3.3.1 Preparation and Characterisation of a Two-Coordinate Manganese(I) Dimer with an Unsupported Metal–Metal Bond . . . 62
3.3.2 Preparation and Characterisation of a Two-Coordinate Manganese(0) Heterobimetallic Complex with an Unsupported Mn–Mg Bond . . . 66
3.3.3 Reactivity of a Two-Coordinate Manganese(0) Heterobimetallic Complex . . . 70
3.4 Conclusion . . . 81
3.5 Experimental . . . 81
References . . . 84

4 Preparation of Low Oxidation State Group 12 Metal Complexes Stabilised by Bulky Amide Ligands . . . 87
4.1 Introduction . . . 87
4.1.1 The First Molecular Compounds Possessing Group 12 Metal–Metal Bonds . . . 87
4.1.2 Isolation of the First Zinc(I) Dimer . . . 89
4.1.3 Other Metal–Metal Bonded Zinc(I) Compounds . . . 91
4.2 Research Outline . . . 102
4.3 Results and Discussion . . . 103
4.3.1 Preparation and Characterisation of a Homologous Series of Group 12 Metal(I) Dimers . . . 103
4.3.2 Preparation and Characterisation of a Two-Coordinate Zinc(0) Heterobimetallic Complex with an Unsupported Zn–Mg Bond . . . 108
4.3.3 Attempts to Synthesise Two-Coordinate Cadmium(0) or Mercury(0) Heterobimetallic Complexes with Unsupported M–Mg Bonds . . . 111
4.3.4 Reactivity of a Two-Coordinate Zinc(0) Heterobimetallic Complex with an Unsupported Zn–Mg Bond . . . 114
4.4 Conclusion . . . 122
4.5 Experimental . . . 123
References . . . 129

5 Preparation of Low Oxidation State Cobalt Complexes Stabilised by a Bulky Amide Ligand 131
5.1 Introduction 131
5.1.1 Low Oxidation State Cobalt Complexes Stabilised by Bulky Bidentate Monoanionic Ligands 131
5.1.2 Low Oxidation State Cobalt Complexes Stabilised by Bulky Monodentate Monoanionic Ligands. 140
5.1.3 Other Relevant Low Coordinate, Low Oxidation State Cobalt Complexes 144
5.2 Research Outline 148
5.3 Results and Discussion 148
5.3.1 Preparation and Characterisation of Two Low Coordinate Amido Cobalt(I) Complexes 148
5.3.2 Reactivity of the Two Amido Cobalt(I) Complexes 152
5.4 Conclusion 155
5.5 Experimental. 156
References. 158

6 Preparation of Molybdenum Aminogermylene and Aminogermylyne Complexes 161
6.1 Introduction 161
6.1.1 Previously Reported Transition Metal Tetrelyne Complexes 161
6.2 Research Outline 171
6.3 Results and Discussion 172
6.3.1 Preparation of Two Molybdenum Aminogermylene Complexes 172
6.3.2 Preparation of a Molybdenum Aminogermylyne Complex 176
6.4 Conclusion 180
6.5 Experimental. 180
References. 182

7 Appendix 185
7.1 General Procedures. 185
7.1.1 X-Ray Crystallography 185
7.1.2 Magnetic Susceptibility Measurements 185
7.1.3 EPR Spectroscopy Studies 192
7.1.4 Computational Studies 192
7.2 Miscellaneous Data. 193
7.3 Summary of Crystallographic Data. 195
References. 196

Abbreviations

Ad	1-adamantyl
Ar	A general aryl substituent
Ar*	2,6-$\{Ph_2CH\}_2$-4-Me-C_6H_2
$Ar^{\dagger}$	2,6-$\{Ph_2CH\}_2$-4-^{i}Pr-C_6H_2
Ar^{Dipp}	2,6-$Dipp_2$-C_6H_3
Ar^{F}	3,5-$(F_3C)_2C_6H_3$
Ar^{Mes}	2,6-Mes_2-C_6H_3
Ar^{Tripp}	2,6-$Tripp_2$-C_6H_3
bipy	2,2′-bipyridine
br.	Broad
^{t}Bu	Tertiary butyl
^{n}Bu	Primary butyl
ca.	*circa*
CAAC	Cyclic alkyl amino carbene
cm^{-1}	Unit of wavenumber
Cp	Cyclopentadienyl, C_5H_5
Cp*	Pentamethyl cyclopentadienyl, C_5Me_5
crypt-222	Cryptand [2.2.2]
Cy	Cyclohexyl
IMes	:C$\{N(Mes)CH\}_2$
IPr	:C$\{N(Dipp)CH\}_2$
IPriMe	:C$\{N(^{i}Pr)C(Me)\}_2$
^{i}Pr	Isopropyl
IR	Infrared
J_{xy}	Coupling constant between nuclei X and Y in Hz
K	Kelvin
kJ	Kilojoule
λ	Wavelength
L	A general ligand
LUMO	Lowest occupied molecular orbital

μ_B	Bohr magneton (J T^{-1})
μ_{eff}	Effective magnetic moment in Bohr magnetons
μ_{so}	Spin only magnetic moment
μ	Bridging
m	*meta*-substituent
m	Multiplet (NMR) or medium (IR)
M	A general metal or molar (mol dm^{-3})
M^+	A molecular ion
Py	Pyridine
q	Quartet
R, R′, R″	General organic substituent
s	Singlet (NMR) or strong (IR)
S	Spin state
sept	Septet
t	Triplet
^{tBu}Nacnac	$[(DippNC^tBu)_2CH]^-$
Tf	Triflate
δ	Chemical shift in NMR spectroscopy (ppm)
d	Doublet
DMAP	4-dimethylaminopyridine
dec.	Decomposition
DFT	Density functional theory
Dipp	2,6-diisopropylphenyl
^{Dipp}DAB	$\{(DippNC(CH_3)\}_2$
^{Dipp}Nacnac	$[(DippNCMe)_2CH]^-$
DME	1,2-dimethoxyethane
DMF	Dimethylformamide
dmpe	$(Me_2PCH_2)_2$
dppe	$(Ph_2PCH_2)_2$
EPR	Electron paramagnetic resonance
Et	Ethyl
Et_2-CAAC	$:C(CEt_2)(CH_2)(CMe_2)NDipp$
Giso	$[(DippN)_2CN^iPr_2]^-$
HOMO	Highest occupied molecular orbital
Hz	Hertz, s^{-1}
IR	Infrared spectroscopy
Me	Methyl
Me_2-CAAC	$:C(CH_2)(CMe_2)_2N$-Dipp
Mes	Mesityl (2,4,6-trimethylphenyl)
^{Mes}Nacnac	$[(MesNCMe)_2CH]^-$
mol	Mole
Mp	Melting point
MS/CI	Chemical ionisation mass spectrometry
MS/EI	Electron ionisation mass spectrometry
m/*z*	Mass/charge ratio

ν	Wavenumber
N_2P_2	$^{t}BuN^{(-)}SiMe_2N$-$(CH_2CH_2P^{i}Pr_2)_2$
NHC	N-heterocyclic carbene
o	*ortho*-substituent
p	*para*-substituent
Ph	Phenyl
Pipiso	$(DippN)_2C(cis\text{-}2,6\text{-}Me_2NC_5H_8)^-$
Piso	$(DippN)_2CH)^-$
Priso	$(DippN)_2C(N^{i}Pr_2)^-$
ppm	Parts per million
THF	Tetrahydrofuran
TMC	Tetramethyl carbene, $:C\{N(Me)C(Me)\}_2$
TMS	Trimethylsilyl or tetramethylsilane
Tripp	2,4,6-triisopropylphenyl
UV	Ultraviolet
WBI	Wiberg bond index
X	A general halide
Xyl	2,6-dimethylphenyl
^{Xyl}Nacnac	$[(XylNCMe)_2CH]^-$

Summary of Compounds

Chapter 2

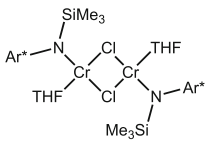

2-41

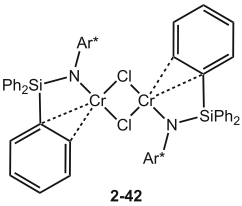

2-42

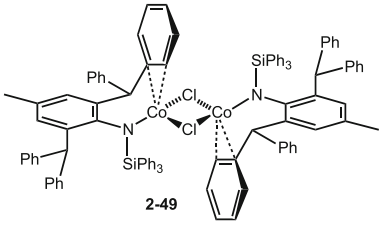

2-49

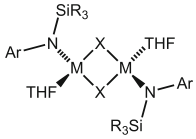

M = Mn, X = Br, Ar = Ar*, R = Me, **2-43**
M = Mn, X = Br, Ar = Ar*, R = Ph, **2-44**
M = Mn, X = Br, Ar = Ar†, R = ^{i}Pr, **2-45**
M = Fe, X = Br, Ar = Ar*, R = Me, **2-46**
M = Fe, X = Br, Ar = Ar*, R = Ph, **2-47**
M = Co, X = Cl, Ar = Ar*, R = Ph, **2-48**

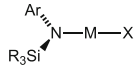

Ar = Ar*, R = Ph, M = Zn, X = Br, **2-53**
Ar = Ar*, R = ^{i}Pr, M = Zn, X = Br, **2-54**
Ar = Ar†, R = ^{i}Pr, M = Zn, X = Br, **2-55**
Ar = Ar*, R = Ph, M = Cd, X = I, **2-57**
Ar = Ar*, R = Me, M = Hg, X = I, **2-58**
Ar = Ar†, R = Me, M = Hg, X = I, **2-59**
Ar = Ar*, R = Ph, M = Hg, X = I, **2-60**
Ar = Ar*, R = ^{i}Pr, M = Hg, X = I, **2-61**
Ar = Ar†, R = ^{i}Pr, M = Hg, X = I, **2-62**

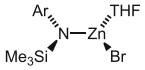

Ar = Ar*, **2-51**
Ar = Ar†, **2-52**

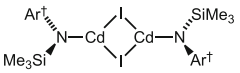

2-56

Chapter 3

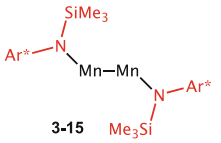

3-15

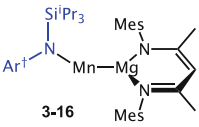

3-16

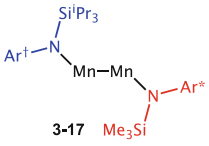

3-17

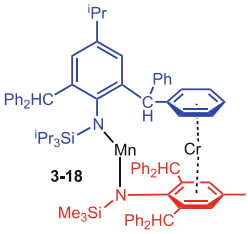

3-18

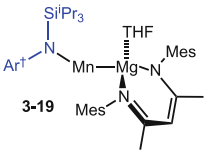

3-19

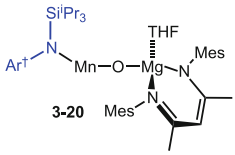

3-20

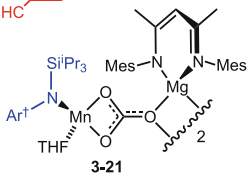

3-21

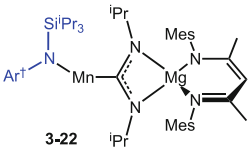

3-22

Chapter 4

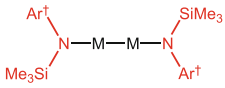

M = Zn, **4-18**
M = Cd, **4-19**
M = Hg, **4-20**

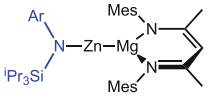

Ar = Ar†, **4-26a**
Ar = Ar*, **4-26b**

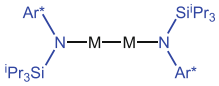

M = Hg, **4-27**
M = Zn, **4-28**

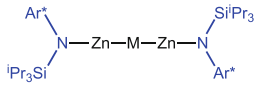

M = Zn, **4-29**
M = Cd, **4-30**
M = Hg, **4-31**

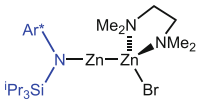

4-32

Chapter 5

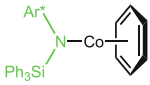

5-43

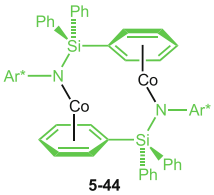

5-44

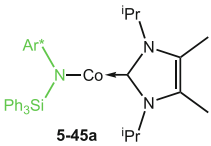

5-45a

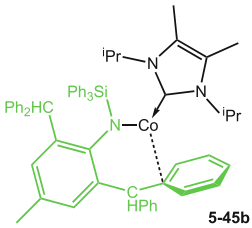

5-45b

Chapter 6

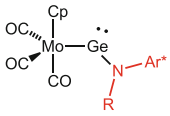

R = Ph, **6-40**

R = $SiMe_3$, **6-41**

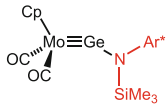

6-42

Chapter 1
General Introduction

1.1 Transition Metals

The term "transition", in regards to the elements, was first used by English chemist Charles Bury in 1921, who referred to a transition series of elements during the change of an inner layer of electrons, taking the number of elements in a row from 8 to 18 [1]. This series is now known as the d-block. To date, the definition of a transition metal, or transition element can vary between authors and publications, however most chemists now agree with the IUPAC definition, as "an element whose atom has a partially filled d sub-shell, or which can give rise to cations with an incomplete d sub-shell" [2]. This definition includes all elements in groups 3 through to 11 in the periodic table. The elements of group 12 (zinc, cadmium and mercury) have been disputed over for many years, as to whether they should be classed as transition metals or not; as they contain the maximum number of 10 d electrons in both their elemental state, as well as in their most of their compounds. This debate was reignited in 2007, when the first experimental evidence for HgF_4, a d^8 square planar mercury(IV) complex was reported [3]. However, in this thesis, the term "transition metal" or "transition element" will only be referring to elements in groups 3-11 of the periodic table, while the elements of group 12 are classed as "post-transition metals".

In 1921, Irving Langmuir proposed a rule for predicting the stability of a transition metal complex, known as the 18 Electron Rule [4]. The rule is based on the valence shells of transition metals, which consist of nine valence orbitals (1s, 5d and 3p) that can each accommodate two electrons. Once all of these orbitals have been filled, i.e. have 18 electrons, the transition metal complex is said to have achieved the same electronic configuration as the noble gas in its period, and as a consequence is likely stable. However, 18 electron complexes can be notoriously unreactive, for example ferrocene and molybdenum hexacarbonyl are two examples of 18 electron complexes. The useful and interesting transition metal complexes will usually violate this rule, and hence their reactivity, for example Grubb's

J. Hicks, *Preparation, Characterisation and Reactivity of Low Oxidation State d-Block Metal Complexes Stabilised by Extremely Bulky Amide Ligands*, Springer Theses,
DOI 10.1007/978-981-10-2905-9_1

Catalyst and *cis*-platin do not have 18 valence electrons. In low coordinate, low oxidation state transition metal chemistry, complexes with significantly less than 18 electrons are targeted, and hence are often extremely reactive.

1.2 Low Oxidation State Transition Metal Complexes

Oxidation state is a fundamental concept in chemistry, and is particularly important in transition metal chemistry, as d-block elements often have a wide range of stable oxidation states. According to IUPAC, the oxidation state of an element is defined as "a measure of the degree of oxidation of an atom in a substance" [2]. The highest oxidation state of an element can be determined by the number of valence electrons, this can be achieved for many of the early transition metals, for example Sc^{3+}, Ti^{4+}, however this is not the case for many of the later transition metals.

Transition metal complexes in oxidation states below +2, with the exception of group 11, are almost always stabilised by π-acid ligands, such as CO, NO or PR_3. Complexes with transition metals in oxidation states below +2, without coordinated π-acid ligands are quite rare, and this type of complex is the primary focus for this work.

These low oxidation state metal centres are usually highly reactive, often difficult to handle and readily oxidise in the presence of an oxidising agent such as O_2. However, in recent years considerable progress has been made in this field. The use of bulky ligands has proven successful in kinetically stabilising a number of unprecedented low oxidation state transition metal complexes. Several of these have shown novel bonding modes [5], previously unseen reactivity [6], interesting magnetic properties [7] and even catalytic abilities [8].

1.2.1 Bulky Ligands Used into Stabilise Low Oxidation State Complexes

A number of different classes of sterically demanding ligands have been used to stabilise low oxidation state transition metal complexes, ranging from multidentate pincer ligands to neutral N-heterocyclic carbenes (NHC's). Arguably, the most widely used of these are the *β*-diketiminate, amidinate, guanidinate and terphenyl ligand classes, which are all monoanionic ligands (Fig. 1.1).

Amidinates, guanidinates and *β*-diketiminates are all types of chelating N-donor ligands, and possess a number of desirable properties for low oxidation state transition metal chemistry. Firstly, they have sufficient bulk to sterically protect a highly reactive, low oxidation state metal centre. They are also relatively easy to synthesise and modify, to fine-tune the sterics and electronics of the ligand as desired. Finally, they mostly coordinate as bidentate ligands (with a few exceptions reported), and therefore provide extra stabilising properties from the chelate effect.

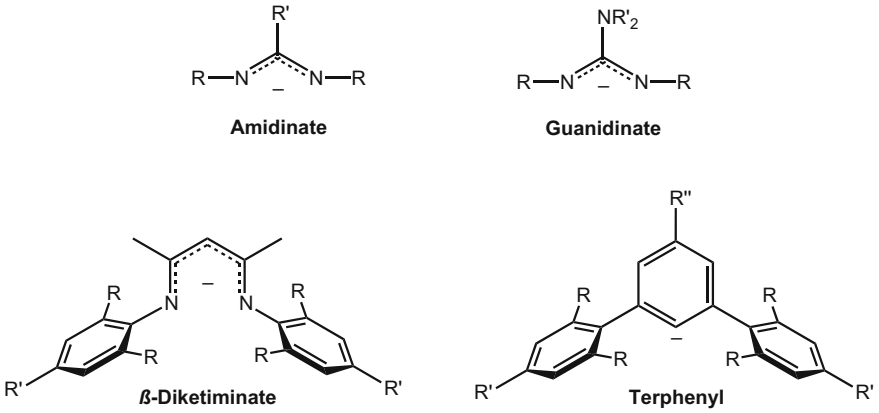

Fig. 1.1 General structure of the amidinate, guanidinate, β-diketiminate and terphenyl ligand classes. R, R′ and R″ = alkyl or aryl group

Terphenyl ligands on the other hand, are monodentate aryl donor ligands. This class of ligand is highly interesting for this type of chemistry, as they can stabilise metals with low coordination numbers as well as low oxidation states. As a result, terphenyl stabilised metal complexes are often more difficult to synthesise, but can show increased reactivity.

1.2.2 Preparation of Low Oxidation State Transition Metal Complexes

Low oxidation state transition metal complexes have been prepared via a number of different routes, the most common being from the reduction of a ligand metal halide precursor complex "L_nMX_m" (L = a ligand, M = a transition metal, X = a halide) with a reducing agent such as an alkali metal, potassium graphite (KC_8), sodium mercury amalgam (Na/Hg), activated magnesium or sodium naphthalide. Following this route, a variety of different compound types have been isolated, ranging from metal–metal bonded dimers, aryl capped/bridged complexes, dinitrogen coordination/activation compounds, as well as three or even two coordinate monomeric species (when using monodentate ligands). An example of each of these binding modes containing a first row transition metal stabilised by a sterically hindering *β*-diketiminate ligand is shown in Fig. 1.2 [9].

All of the complexes in Fig. 1.2 were prepared by reduction of their corresponding *β*-diketiminate stabilised metal(II) halide precursors, with either KC_8, magnesium metal or a sodium/potassium alloy. The different compound types arise due to different reaction conditions; for example, solvent, atmosphere, steric and electronic properties of the ligand, as well as the transition metal used all play a part in the final structure.

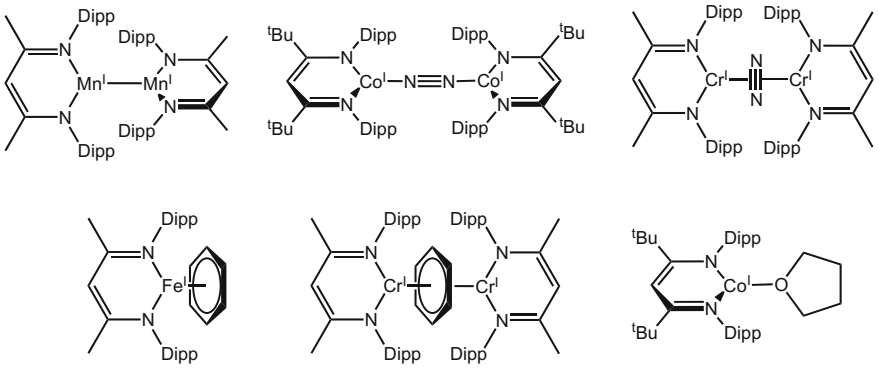

Fig. 1.2 Examples of low oxidation state first row transition metal complexes stabilised by β-diketiminates ligands

Low coordinate, low oxidation state transition metal chemistry gives an elegant route into highly reactive complexes. The main focus of this work will be on synthesising low oxidation state transition metal complexes with metal–metal bonds, however some emphasis will be on isolating low oxidation state monometallic transition metal species with extremely low coordination numbers.

1.3 Metal–Metal Bonding in Transition Metal Complexes

1.3.1 History

Today, the existence of metal–metal bonds in stable, isolable compounds is well known, and routinely covered in textbooks [10]. However, for more than half of the 20th century, metal-to-metal bonds were unknown to chemists, and even the idea of a bond order higher than three was absent from chemical theory. The coordination chemistry involving transition metals was based almost entirely on Alfred Werner's ideas of "one-centre coordination chemistry", where metal complexes are described as a single metal ion surrounded by a set of ligands. Complexes involving more than one metal centre were simply described as an arrangement of individual metal ions, each with their own metal-ligand bonds, and no metal–metal bonds or interactions.

In the early 1960s, this idea was about to change; with the development of analytical techniques such as X-ray crystallography, which were becoming more accessible. In 1963, the groups of Cotton (MIT, USA) and Penfold (University of Canterbury, NZ) almost simultaneously, independently published the results of X-ray crystallographic studies on the previously reported "$CsReCl_4$" complex [11, 12]. Both groups correctly assigned the molecular formula as $Cs_3Re_3Cl_{12}$, and found the structure contains a triangular $[Re_3Cl_{12}]^{3-}$ anion, with a mean Re–Re distance of 2.47 Å. Cotton went on and discussed the electronic confirmation of the

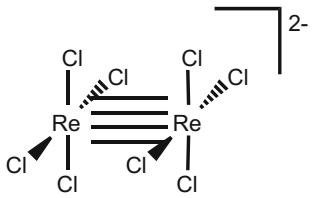

Fig. 1.3 Representation of the structure of the $[Re_2Cl_8]^{2-}$ ion

anion further, and concluded that "…the d_{xy}, d_{xz} and d_{yz} orbitals of each rhenium atom combine to give bonding and antibonding 3-center MO's. There are just six bonding orbitals, which are filled by the twelve electrons…", thus proposing double bonds between the metal atoms [12]. In the following year, the group published a second paper with the analysis leading to this conclusion [13].

The discovery of Re=Re double bonds was a landmark in chemistry, however it was rather overshadowed by events to come. Later that year, a group from the USSR reported the synthesis and structure of another rhenium chloride complex, containing a new Re_2Cl_8 anion, which due to crystal twinning had assigned with a 4− charge [14]. Cotton and co-workers were working on similar chemistry at the time and felt that the Soviet group had incorrectly assigned the charge of the complex. This turned out to be the case, and in the last few months of 1964, Cotton reported the new rhenium chloride salt $K_2[Re_2Cl_8]\cdot 2H_2O$ that contained the same Re_2Cl_8 anion, where he correctly concluded that the anion contains a 2− charge [15] (Fig. 1.3).

The structure of the $[Re_2Cl_8]^{2-}$ anion presented Cotton with a tantalising theoretical challenge, as there were two major structural artefacts that could not be explained by conventional chemistry. The first was the unprecedented short bond distance between the metal centres (Re1–Re2 = 2.24 Å), which was even shorter than in rhenium metal. The second was that the four chlorine atoms on each Re centre were in an unexpected eclipsed confirmation, rather than the apparently lower energy staggered confirmation. Soon after, Cotton proposed a radical explanation that explained both the extremely short metal–metal bond and the eclipse confirmation; a metal–metal quadruple bond [16]. He went on to explain that the four-fold bond was made up of a single σ bond, two π bonds, and a new type of bond, a δ bond, formed by the side on overlap of the two d_{xy} orbitals.

Today, there are over a thousand metal–metal quadruple bonded complexes that have been structurally characterised, comprising of a number of metals, including vanadium, niobium, chromium, molybdenum, tungsten, rhenium and ruthenium [10].

1.3.2 Quintuple Bonds

Shortly after the discovery of the quadruple bond, chemists started to ask if we have now reached the highest bond order, or are higher bond orders possible? During the next half a century, groups started to investigate transition metal diatomics (of the

form M_2), by trapping the M_2 units in atom-argon matrix cocondensation experiments [17]. Experimental and theoretical studies on a number of these molecules suggested that fivefold, and in the case of Cr_2 and Mo_2, sixfold bonding is possible. Unfortunately, these diatomics cannot be isolated and structurally characterised. To accomplish the goal of identifying complexes with metal–metal bond orders greater than four, chemists turned their attention to quintuple bonded complexes. A number of theoretical papers were published on the problem, for example in 1979, Hoffmann and co-workers suggested that M_2L_6 with D_{3h} symmetry could possibly contain a metal–metal quintuple bond [18]. Furthermore, in 2001, Weinhold and Landis introduced natural bond orbital theory (NBO) [19], and in 2005, extended this work to transition metals by drawing Lewis-like structures and bonding concepts. Based on their theory, they suggested that the most probable geometry of a complex containing a metal–metal quintuple bond is one with *trans*-bent geometry and C_{2h} symmetry [20].

All of this was good evidence that bond orders higher than four are possible, however no one had yet synthesised an isolable complex with a bond of order greater than four. The major synthetic problem was that if ligands were used to stabilise multiple bonded centres, their binding reduces the number of valence orbitals available to form metal–metal bonds, therefore the number of ligands must be minimised. However, minimising the number of ligands can leave the reactive dimetallic core open to intermolecular reactions, which can yield polymers or clusters with lower bond orders.

In 2005, Power's group came up with a solution. By using sterically demanding monodentate terphenyl ligands, the low coordinate chromium(I) dimer $[(Ar^{Dipp}Cr)_2]$ **1-01** (Ar^{Dipp} = 2,6-$Dipp_2$-C_6H_3, Dipp = 2,6-diisopropylphenyl) was isolated, and it contains a chromium-chromium quintuple bond (Fig. 1.4) [5]. Use of bulky terphenyl ligands reduces the coordination number of the chromium centres, which

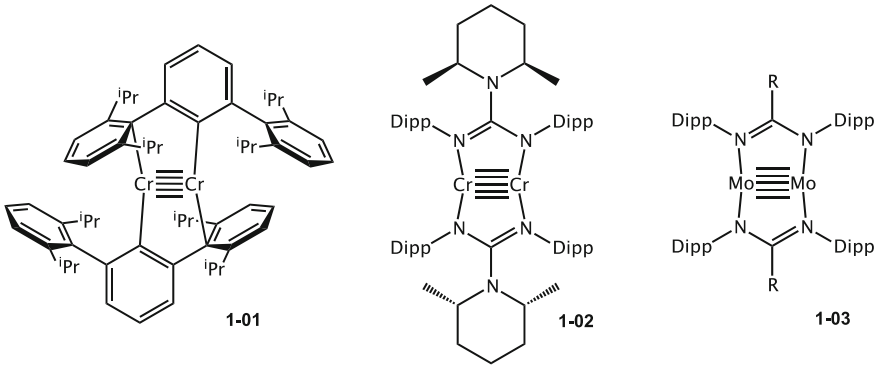

Fig. 1.4 Representations of the structures of the first isolated chromium(I) dimer **1-01** with fivefold bonding, the chromium dimer with shortest metal–metal bond **1-02** and the first complex with a molybdenum–molybdenum quintuple bond **1-03**. R = H or Ph

maximises the number of valence orbitals available to form metal–metal bonds, whilst providing sufficient steric protection to prevent intermolecular reactions.

Since then, the groups of Kempe and Tsai have stabilised a number of other chromium(I) dimers containing quintuple bonds, using bridging amidinate and guanidinate ligands; [21] the latest of which $[Cr_2(\mu\text{-N,N}'\text{-Pipiso})_2]$ **1-02** (Pipiso = $(DippN)_2C(cis\text{-}2,6\text{-}Me_2NC_5H_8)^-$) by Kempe, contains the shortest reported metal–metal bond of any coordination complex (Fig. 1.4) [22]. In 2009, Tsai also reported the first non-chromium quintuple bonded complex, a molybdenum-molybdenum quintuple bond in $[Mo_2(\mu\text{-N,N}'\text{-Piso})_2]$ **1-03** (Piso = $(DippN)_2CH^-$) [23].

1.4 Magnesium(I) Complexes

The chemistry of the group 2 metals, including magnesium is dominated by the +2 oxidation state. Less than a decade ago, in every thermally stable reported compound involving magnesium, the metal was found in the +2 oxidation state. Due to the recent developments in low oxidation state zinc chemistry, with Carmona isolating the first zinc(I) dimer [24], groups started to question whether a magnesium(I) complex was also isolable, as zinc and magnesium have similar electronic properties.

The breakthrough came in 2007, by Jones and Stasch, with the isolation of the first two thermally stable magnesium(I) dimers $[\{(^{Dipp}Nacnac)Mg\}_2]$ **1-04** ($^{Dipp}Nacnac$ = $[(DippNCMe)_2CH]^-$) and $[\{(Priso)Mg\}_2]$ **1-05** (Priso = $(DippN)_2C(N^iPr_2)^-$) [25]. The dimers **1-04** and **1-05** were synthesised by the reduction of their magnesium iodide etherate precursors $[(^{Dipp}Nacnac)MgI(OEt_2)]$ **1-06** and $[\{(Priso)Mg(\mu\text{-I})\}_2OEt_2]$ **1-07** respectively, with an excess of potassium metal (Scheme 1.1).

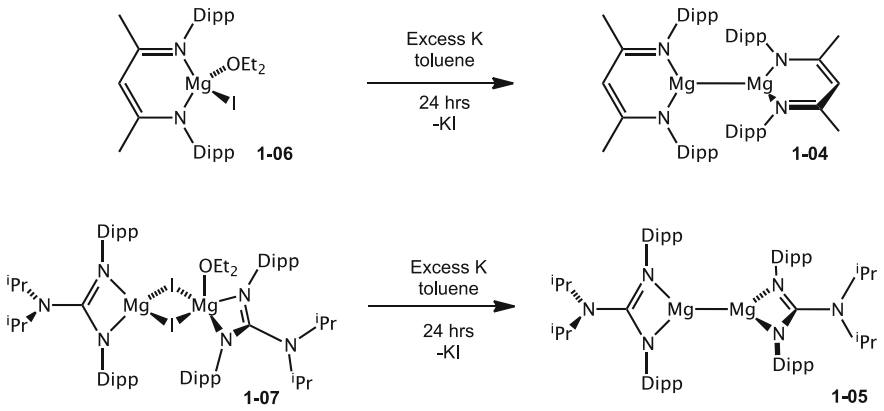

Scheme 1.1 Preparation of the magnesium(I) dimers $[\{(^{Dipp}Nacnac)Mg\}_2]$ **1-04** and $[\{(Priso)Mg\}_2]$ **1-05**

The two dimers contain a Mg_2^{2+} core, which in **1-04** is stabilised by two sterically demanding β-diketiminate ligands and in **1-05**, two sterically demanding guanidinate ligands.

Since the isolation of **1-04** and **1-05**, the Jones and Stasch groups have continued research on low oxidation state magnesium chemistry, investigating the reactivity of magnesium(I) dimers [26], whilst isolating a number of new magnesium(I) complexes, including the less bulky β-diketiminate stabilised magnesium(I) dimer, [{(^{Mes}Nacnac)Mg}$_2$] **1-08** (^{Mes}Nacnac = [(MesNCMe)$_2$CH]$^-$; Mes = mesityl) [27]. This complex shows increased in reactivity (as will be discussed) compared with **1-04**, due to the decrease in bulk of its stabilising ligands.

1.4.1 Reactivity of β-Diketiminate Stabilised Magnesium(I) Complexes

β-Diketiminate stabilised magnesium(I) dimers have proved to be versatile reducing agents in both organic and inorganic synthesis [26]. The $\{Mg_2\}^{2+}$ core acts as two-centre, two-electron reductant towards a number of small molecules and organic substrates, some of which are highlighted in Scheme 1.2.

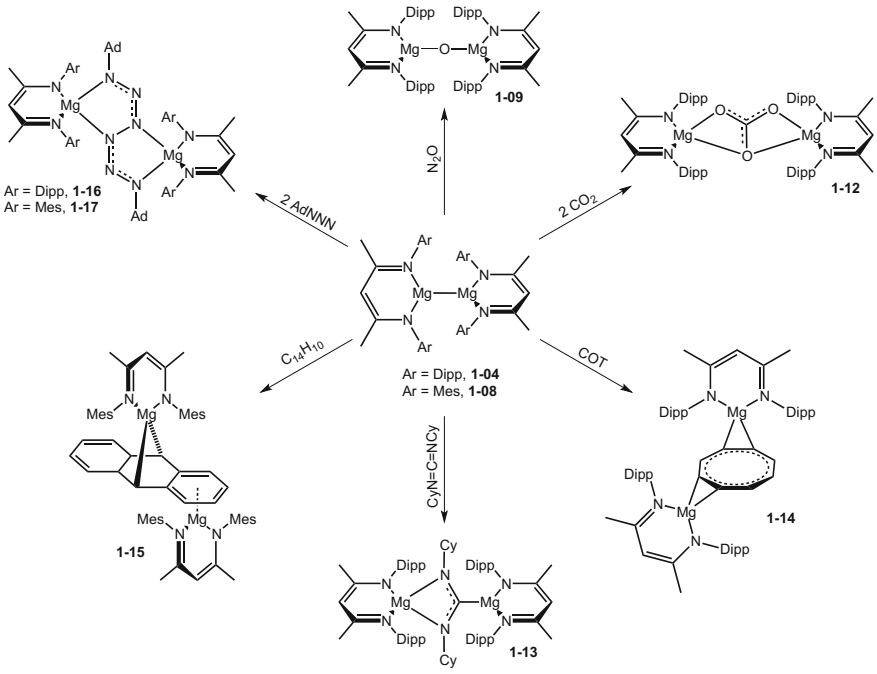

Scheme 1.2 Reactions of the magnesium(I) dimers **1-04** and **1-08** with a selection of small molecules and organic substrates

When **1-04** is exposed to one of the simplest oxidizing agents N_2O, it is oxidized to give the bridging magnesium(II) oxide [{(^{Dipp}Nacnac)Mg}$_2$(μ-O)] **1-09** [28]. This oxo-bridged complex is unprecedented in magnesium chemistry, and is highly reactive. Further chemistry has been performed on **1-09**, including reactions with CS_2 and dicyclohexyl carbodiimide to give [{(^{Dipp}Nacnac)Mg}(μ-CS_2O){Mg(^{Dipp}Nacnac)(OEt_2)}] **1-10** and [{(^{Dipp}Nacnac)Mg}$_2${μ-(NCy)$_2$O}] **1-11** respectively. It is of note that the synthesis of **1-09** was attempted using O_2 in place of N_2O, however no evidence for the formation of **1-09** was seen. Complex **1-04** also reacts with two equivalents of carbon dioxide to give good yields of the magnesium carbonate complex [(^{Dipp}Nacnac)Mg}$_2$(μ-CO_3)] **1-12** [28]. The reaction was shown to proceed through the initial reduction of CO_2 to the bridging magnesium oxide **1-09** and CO, as determined by ^{13}C labelling studies. Complex **1-09** then reacts with a further equivalent of CO_2 to afford **1-12**.

In reactions of magnesium(I) dimers with unsaturated organic substrates such as a carbodiimides, reductive insertion into the metal–metal bond is common. For example, the reaction of **1-04** with dicyclohexyl carbodiimide gives the insertion product [{(^{Dipp}Nacnac)Mg}$_2${μ-C(NCy)$_2$}] **1-13** [27]. Interestingly, **1-04** can also reduce cyclooctatetraene (COT), albeit under fairly forcing conditions (refluxing toluene) to give [{(^{Dipp}Nacnac)(THF)Mg}$_2$(μ-COT)] **1-14** after the addition of THF to aid crystallisation [29]. This is the first crystallographically characterised example of a magnesium complex of dianionic cyclooctatetraenide, although other examples have been characterised by other spectroscopic techniques [30].

The difference in reactivity between the highly sterically hindered **1-04** and the lesser sterically hindered **1-08** is highlighted in their reactivity towards anthracene. Complex **1-04** shows no reactivity towards anthracene in solution at ambient temperature, while heating to 100 °C gives an intractable mixture of products. In contrast, **1-08** reacts with one equivalent of anthracene quickly at room temperature, to cleanly yield [{(^{Mes}Nacnac)Mg}$_2$(μ-$C_{14}H_{10}$)] **1-15** [31].

Finally, magnesium(I) dimers have also shown to reductively couple unsaturated substrates, such as azides, forming new N–N bonds [27]. The reaction of **1-04** or **1-08** with two equivalents of adamantyl azide gives the azide coupled products [{(^{Dipp}Nacnac)Mg}$_2$(μ-Ad_2N_6)] **1-16** and [{(^{Mes}Nacnac)Mg}$_2$(μ-Ad_2N_6)] **1-17** respectively, containing a bridging hexazene moiety.

1.4.2 Using β-Diketiminate Stabilised Magnesium(I) Complexes as Reducing Agents in Inorganic Synthesis

Since the discovery of magnesium(I) dimers, arguably the most useful reactivity has been found as novel reducing agents for inorganic synthesis. The chemistry of low oxidation state transition metal and main group complexes has always been heavily reliant on the reducing agents available. The typical reducing agents used in this type of chemistry are; the s-block metals in their elemental form, such as lithium, sodium, potassium or magnesium; potassium graphite (KC_8) or alkali metal

naphthalenide solutions [32]. Although these traditional reducing agents have been effective in the past, their use in reducing metal precursor complexes to lower oxidation state species, is often problematic. Using magnesium(I) complexes as reducing agents for this type of chemistry has some key advantages over the traditional reductants. One of these is that they have high solubility in hydrocarbon solvents such as toluene or diethyl ether, which allows more controlled and selective reaction conditions, than with insoluble alkali metals for instance. Furthermore, where accurately measuring a stoichiometric amount of an alkali metal is difficult, magnesium(I) complexes are "easy to handle" crystalline solids that can be used in stoichiometric amounts. This can prevent "over-reduction" of a metal precursor complex to elemental metal, which is often seen when using an excess of an alkali metal. Finally, the alkali metals, KC_8 etc. are known for their potential fire risk on use, whereas magnesium(I) complexes are air and moisture sensitive, but not pyrophoric, making them a much safer alternative.

To date, there are numerous reports of magnesium(I) dimers being used as reducing agents for inorganic synthesis, many of which were employed because traditional reducing agents had failed [33]. One example of this was their use in low oxidation state main group chemistry, with the isolation of the first germanium(0) dimer [{(IPr)Ge}$_2$] (IPr = :C{N(Dipp)CH}$_2$) **1-18**, stabilised by bulky NHC's [34]. The complex was originally targeted from the reduction of the germanium(II) chloride precursor complex [(IPr)$GeCl_2$] **1-19** with a stoichiometric amount of KC_8, or a sodium mirror. In both cases, there was no evidence for the formation of **1-18**, and the only isolable product was free IPr (Scheme 1.3). However, when the reduction of **1-19** was carried out using either **1-04** or **1-08** as the reducing agent, the reaction solution instantly turned dark red on addition, producing a white precipitate of the magnesium(II) chloride by-product, [{(^{Dipp}Nacnac)Mg(μ-Cl)}$_2$] **1-20-Cl** when using **1-04**, or [{(^{Mes}Nacnac)Mg(μ-Cl)}$_2$] **1-21-Cl** when using **1-08**. After workup, **1-18** could be isolated as dark red crystals in low yields (20 % using **1-08**, <5 % when using **1-04**) (Scheme 1.3).

The use of magnesium(I) complexes as reducing agents in low oxidation state d-block chemistry is limited, however there is some precedence. In 2012, the Jones group published the synthesis of the iron(I) metal–metal bonded dimer [Fe^{I}_2(μ-N,N′-Pipiso)$_2$] **1-22**, stabilised by two bridging guanidinate ligands, and the related manganese(I) complex [{(Piso)Mn^{I}}$_2$] **1-23** (Piso = [(DippN)$_2$C^{t}Bu]) [35]. Both complexes were synthesised by reduction of their corresponding guanidinato and amindinato metal(II) bromide precursor complexes [{(Pipiso)Fe^{II}(μ-Br)}$_2$] **1-24** and [{(Piso)Mn^{II}(μ-Br)}$_3$(THF)$_2$] **1-25** with stoichiometric amounts of **1-08**. Compounds **1-22** and **1-23** were structurally characterised by X-ray crystallography, and both were found to posses metal–metal bonds. In **1-22**, the iron-iron bond was found to be extremely short, just 2.198 Å, which is the shortest Fe–Fe interaction to date [36] (Scheme 1.4).

As shown in the synthesis of **1-18**, **1-22** and **1-23**, the magnesium(I) compounds can act as reducing agents by the extraction of halogens from the precursor complex. However, in the case of aluminium hydrides, it has been shown that magnesium(I) complexes can also act as reducing agents via hydrogenation of their

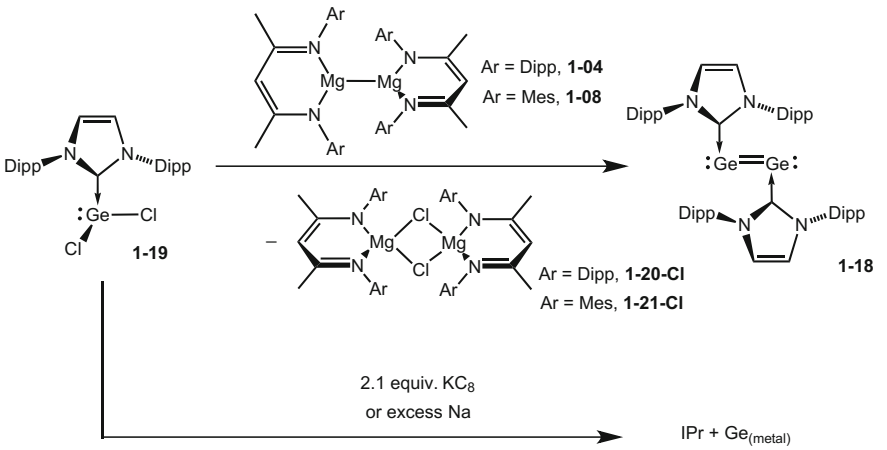

Scheme 1.3 Preparation of **1-18** using the magnesium(I) dimers **1-04** and **1-08** as reducing agents

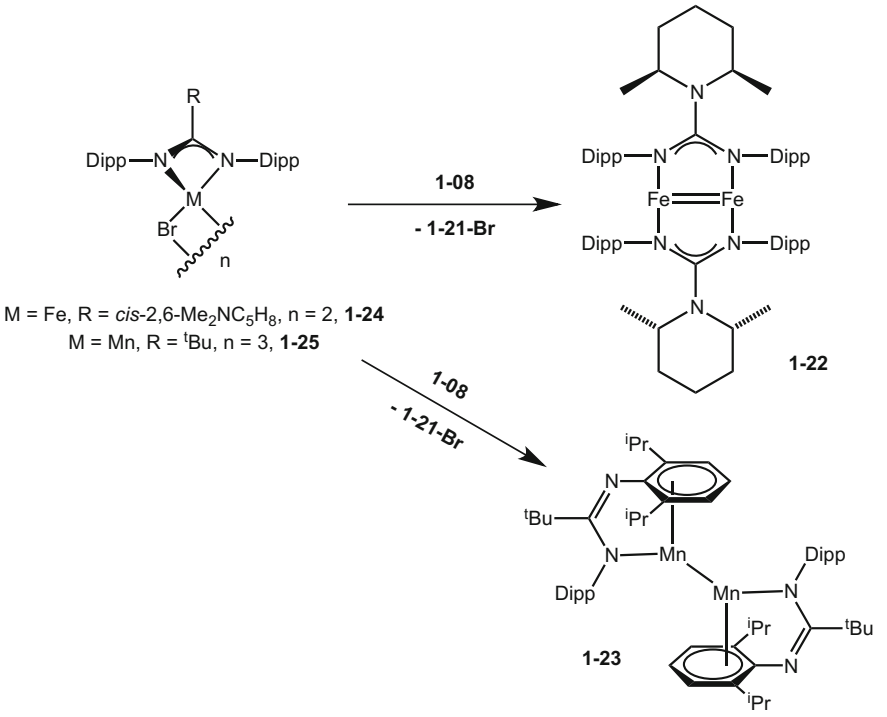

Scheme 1.4 Preparation of **1-22** and **1-23**

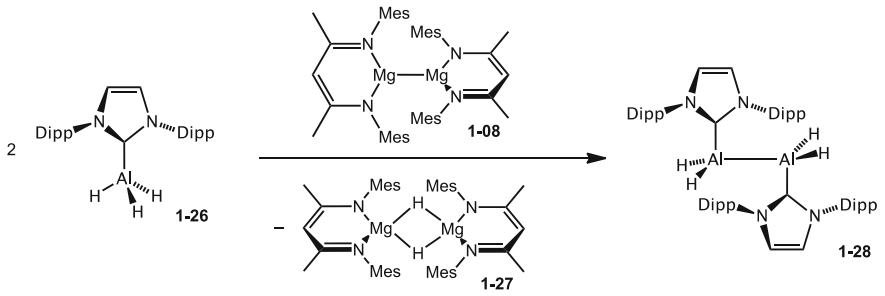

Scheme 1.5 Synthesis of the NHC stabilised aluminium(II) hydride **1-28** via hydrogenation of the magnesium(I) dimer **1-08**

magnesium centres [37]. When the NHC stabilised aluminium(III) hydride complex [(IPr)AlH_3] **1-26** is treated with half an equivalent of **1-08**, a redox reaction occurs with the transfer of a hydrogen from the aluminium centre to the magnesium, resulting in the formation of the magnesium(II) hydride complex [{(^{Mes}Nacnac)Mg(μ-H)}$_2$] **1-27** and the NHC stabilised aluminium(II) hydride complex [{(IPr)AlH_2}$_2$] **1-28** (Scheme 1.5).

Complex **1-28** is a NHC stabilised adduct of the elusive parent dialane(4) (Al_2H_4), which has only been observed in solid H_2 matrices at temperatures of *c.a.* 5 K [38].

Similar reactivity of the magnesium(I) dimers was found when **1-08** was reacted with other aluminium hydride compounds, for example amindinate and guanidinate stabilised aluminium dihydrides [37].

References

1. C.R. Bury, J. Am. Chem. Soc. **43**, 1602 (1921)
2. A.D. McNaught, A. Wilkinson, *Compendium of Chemical Terminology*, 2nd edn. (Blackwell, Science, UK, 1997)
3. X. Wang, L. Andrews, S. Riedel, M. Kaupp, Angew. Chem. Int. Ed. **46**, 8371 (2007)
4. (a) I. Langmuir, Science **54**, 1386 (1921); (b) W.B. Jenson, J. Chem. Educ. **82**, 28 (2005)
5. T. Nguyen, A.D. Sutton, M. Brynda, J.C. Fettinger, G.J. Long, P.P. Power, Science **310**, 844 (2005)
6. M.M. Rodriguez, E. Bill, W.W. Brennessel, P.L. Holland, Science **334**, 780 (2011)
7. J.M. Zadrozny, D.J. Xiao, M. Atanasov, G.J. Long, F. Grandjean, F. Neese, J.R. Long, Nat. Chem. **5**, 577 (2013)
8. K. Weber, E.-M. Schnöckelborg, R. Wolf, Chem. Cat. Chem. **3**, 1572 (2011)
9. (a) J. Chai, H. Zhu, A.C. Stückl, H.W. Roesky, J. Magull, A. Bencini, A. Caneschi, D. Gatteschi, J. Am. Chem. Soc. **127**, 9201 (2005); (b) K. Ding, A. W. Pierpont, W.W. Brennessel, G. Lukat-Rodgers, K.R. Rodgers, T.R. Cundari, E. Bill, P.L. Holland, J. Am. Chem. Soc. **131**, 9471 (2009); (c) W.H. Monillas, G.P.A. Yap, L.A. MacAdams, K.H. Theopold, J. Am. Chem. Soc. **129**, 8090 (2007); (d) J.M. Smith, A.R. Sadique, T.R. Cundari, K.R. Rodgers, G. Lukat-Rodgers, R.J. Lachicotte, C.J. Flaschenriem, J. Vela,

P.L. Holland, J. Am. Chem. Soc. **128**, 756 (2006); (e) W.H. Monillas, G.P.A. Yap, K.H. Theopold, Angew. Chem. Int. Ed. **46**, 6692 (2007); (f) T.R. Dugan, X. Sun, E.V. Rybak-Akimova, O. Olatunji-Ojo, T.R. Cundari, P.L. Holland, J. Am. Chem. Soc. **133**, 12418 (2011)
10. F.A. Cotton, C.A. Murillo, R.A. Walton, *Multiple Bonds Between Metal Atoms*, 3rd edn. (Springer Science and Business Media, New York, 2005) and references therein
11. W.T. Robinson, J.E Fergusson, B.R. Penfold, Proc. Chem. Soc. 101 (1963)
12. J.A. Bertrand, F.A. Cotton, W.A. Dollase, J. Am. Chem. Soc. **85**, 1349 (1963)
13. F.A. Cotton, T.E. Haas, Inorg. Chem. **3**, 10 (1964)
14. V.G. Kuznetzov, P.A. Koz'min, J. Struct. Chem. **4**, 49 (1963)
15. F.A. Cotton, C.B. Harris, Inorg. Chem. **4**, 330 (1965)
16. (a) F.A. Cotton, N.F. Curtis, C.B. Harris, B.F.G. Harris, S.J. Lippard, J.T.Mague, E.R. Robinson, J.S. Wood, Science **145**, 1305 (1964); (b) F.A. Cotton, Inorg. Chem. **4**, 334 (1965)
17. (a) M.D. Morse, Chem. Rev. **86**, 1049 (1986); (b) M.H. Chisholm, A.M. Macintosh, Chem. Rev. **105**, 2949 (2005) and references therein
18. A. Dedieu, T.A. Albright, R. Hoffmann, J. Am. Chem. Soc. **101**, 3141 (1979)
19. F. Weinhold, C.R. Landis, Chem. Educ. Res. Pract. **2**, 9 (2001)
20. F. Weinhold, C.R. Landis, *Valency and Bonding: A Natural Bond Orbital Donor-Acceptor Perspective* (Cambridge University Press, Cambridge, 2005)
21. N.V.S. Harisomayajula, A.K. Nair, Y.-C. Tsai, Chem. Commun. **50**, 3391 (2014) and references therein
22. A. Noor, T. Bauer, T.K. Todorova, B. Weber, L. Gagliardi, R. Kempe, Chem. Eur. J. **30**, 9825 (2013)
23. Y.-C. Tsai, H.-Z. Chen, C.-C. Chang, J.-S.K. Yu, G.-H. Lee, Y. Wang, T.-S. Kuo, J. Am. Chem. Soc. **131**, 12534 (2009)
24. I. Resa, E. Carmona, E. Gutierrez-Puebla, A. Monge, Science **305**, 1136 (2004)
25. S.P. Green, C. Jones, A. Stasch, Science **318**, 1754 (2007)
26. A. Stasch, C. Jones, Dalton Trans. **40**, 5659 (2011)
27. S.J. Bonyhady, C. Jones, S. Nembenna, A. Stasch, A. Edwards, G.J. McIntyre, Chem. Eur. J. **16**, 938 (2010)
28. R. Lalrempuia, A. Stasch, C. Jones, Chem. Sci. **4**, 4383 (2013)
29. S.J. Bonyhady, S.P. Green, C. Jones, S. Nembenna, A. Stasch, Angew. Chem. Int. Ed. **48**, 2973 (2009)
30. T. Alonso, S. Harvey, P.C. Junk, C.L. Raston, B. Skelton, A.H. White, Organometallics **6**, 2110 (1987)
31. C. Jones, L. McDyre, D.M. Murphy, A. Stasch, Chem. Commun. **46**, 1511 (2010)
32. N.G. Connelly, W.E. Geiger, Chem. Rev. **96**, 877 (1996) and references therein
33. C. Jones, A. Stasch, Top. Organomet. Chem. **45**, 73 (2013) and references therein
34. A. Sidiropoulos, C. Jones, A. Stasch, S. Klein, G. Frenking, Angew. Chem. Int. Ed. **48**, 9701 (2009)
35. L. Fohlmeister, S. Liu, C. Schulten, B. Moubaraki, A. Stasch, J.D. Cashion, K.S. Murray, L. Gagliardi, C. Jones, Angew. Chem. Int. Ed. **51**, 8294 (2012)
36. As determined by a survey of the Cambridge Crystallographic Database, Feb (2015)
37. S.J. Bonyhady, D. Collis, G. Frenking, N. Holzmann, C. Jones, A. Stasch, Nat. Chem. **2**, 865 (2010)
38. X. Weng, L. Andrews, S. Tam, M.E. DeRose, M.E. Fajardo, J. Am. Chem. Soc. **125**, 9218 (2003)

Chapter 2
Extremely Bulky Amido d-Block Metal(II) Halide Complexes

2.1 Introduction

It is perhaps surprising that bulky monodentate amide ligands (–NR_2, R = an alkyl or aryl group), which have been utilized for decades to stabilize low coordinate d-block metal complexes [1], e.g. two-coordinate [$M(NR_2)_2$] complexes [2], have not been successfully employed in the preparation of related metal(I) dimers. This may result from the fact that reports of the amido d-block metal(II) halide precursor complexes are sparse, despite the many hundreds of structurally characterized amido d-block metal complexes that populate the literature [1].

Though monodentate amido d-block metal(II) halide complexes are limited in number, they are not unknown. However, this complex type usually requires either sterically demanding ligands, or strongly coordinating π-acid ligands such as phosphines or carbon monoxide to be isolated. Examples of amido d-block metal(II) halides with coordinating π-acid ligands include [{(dtma)Cu(PPh_3)(μ-Cl)}$_2$] [3] (dtma = di-*p*-tolylmethylamido) and [Ni(PMe_3)$_2$(pyr)Cl] [4] (pyr = pyrrolyl). However, in low-coordinate, low oxidation state chemistry, precursor complexes that do not possess strongly coordinating π-acid ligands are desired, as these ligands will likely be present in the final product, increasing the coordination number of the metal centre, thereby lowering its reactivity.

Attempting to prepare a monodentate amido metal(II) halide complex without the use of sterically demanding or π-acid ligands will almost always lead to the formation of the homoleptic species [$M(NR_2)_2$] and the metal(II) halide, via redistribution. However, utilizing steric bulk on its own, without π-acid ligands, has led to a handful of monodentate amido d-block metal(II) halide complexes.

J. Hicks, *Preparation, Characterisation and Reactivity of Low Oxidation State d-Block Metal Complexes Stabilised by Extremely Bulky Amide Ligands*, Springer Theses,
DOI 10.1007/978-981-10-2905-9_2

2.1.1 Previously Reported Bulky Amido Transition Metal(II) Halide Complexes

In 1996, the group of Cummins reported the synthesis and isolation of the low valent amido iron(II) chloride complex [FeCl{N(R)(Ar#)}(tmeda)] [5] **2-01** (R = C$(CD_3)_2CH_3$, Ar# = 2,5-FMeC_6H_3). The complex is stabilized by a bulky amide ligand, along with a molecule of chelating tetramethylethylenediamine (tmeda) coordinating to the iron centre. Complex **2-01** was prepared by a salt metathesis reaction between iron(II) bromide and the lithium amide salt [Ar#(R)NLi], in the presence of tmeda (Scheme 2.1).

The four-coordinate iron(II) complex was found to be monomeric, with the iron(II) centre having a distorted tetrahedral geometry. The four coordination sites of the metal are occupied by the bulky amide ligand, the chloride, and a chelating molecule of tmeda. Complex **2-01** has an effective magnetic moment in solution of 5.29 μ_B at room temperature, determined by the Evans method, which is slightly above the spin only value for a d^6 high spin Fe^{2+} centre (4.90 μ_B). As far as we are aware, no attempts to reduce **2-01**, in order to synthesise a low oxidation state amido iron complex have been reported.

Following this, in 2007, Lee and co-workers reported the synthesis and structure of the similar tmeda stabilised amido iron(II) chloride complex [FeCl{N($SiMe_3$)(Xyl)}(tmeda)] **2-02** (Xyl = 2,6-xylyl) and the isostructual cobalt(II) complex [CoCl{N($SiMe_3$)(Xyl)}(tmeda)] **2-03** [6]. Similar to the synthesis of **2-01**, compounds **2-02** and **2-03** were prepared by reactions of the lithium amide salt [Xyl($SiMe_3$)NLi(tmeda)] and the corresponding metal(II) chloride (Scheme 2.2). However, in the synthesis of **2-02** and **2-03**, no tmeda was added to the reaction

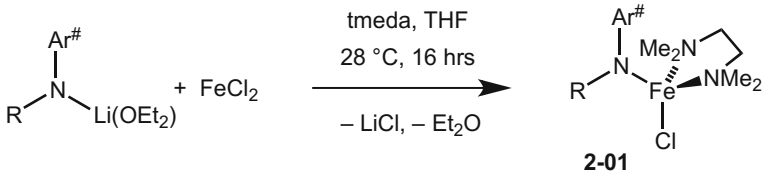

Scheme 2.1 Preparation of **2-01**

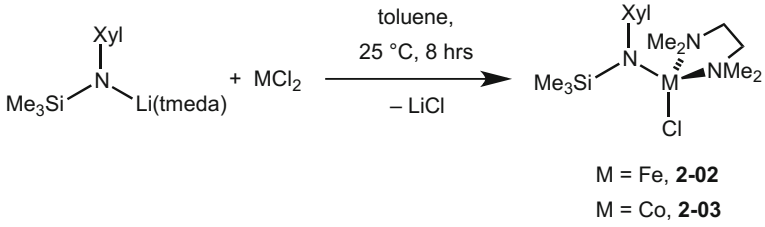

Scheme 2.2 Preparation of **2-02** and **2-03**

mixture as it was in the synthesis of **2-01**, but was introduced through coordination to the lithium amide reactant.

The structures of **2-02** and **2-03** were determined by X-ray crystallography, and were found to be essentially isostructual to the previously reported amido iron(II) chloride **2-01**. Magnetic measurements were also performed on of **2-02** and **2-03**, yielding effective magnetic moments of 4.79 μ_B and 3.77 μ_B respectively, which in both cases are only slightly less than the spin only value for the high spin M^{2+} centre (4.90 μ_B for high spin Fe^{2+} and 3.87 μ_B for high spin Co^{2+} with Td geometry). Complexes **2-02** and **2-03** were further reacted with methyl lithium, resulting in moderate yields of the corresponding methylated complexes [Fe(Me){N(SiMe$_3$)(Xyl)}(tmeda)] **2-04** and [Co(Me){N(SiMe$_3$)(Xyl)}(tmeda)] **2-05** [6]. However, once again, no attempts were made to reduce the complexes, in order to isolate a low oxidation state amido iron or cobalt complex.

In 2011, Duchateau and co-workers reported the bulky amido chromium(II) chloride complex [{Cr(NC$_4$H$_2^t$Bu$_2$-2,5)(THF)(μ-Cl)}$_2$] **2-06** [7]. Complex **2-06** was synthesized in a rather unusual way, firstly via the alkylation of the chromium(III) dichloride complex [{η^5-(^{t}Bu)$_2$C$_4$H$_2$N}CrCl$_2$(THF)] **2-07** with triethyl aluminium, to give the alkylated product [{η^5-(^{t}Bu)$_2$C$_4$H$_2$N}CrEt(μ-Cl)]$_2$ **2-08**, which was followed by the reduction of the complex with a further equivalent of AlEt$_3$ (Scheme 2.3). THF was added to aid crystallisation, and **2-06** was isolated in moderate yields.

X-ray crystallography was once again used to determine the structure of **2-06**, which was found to be dimeric in the solid state, with approximately symmetrically bridging chlorides. The metal centres were found to be four-coordinate, and in a distorted square planar geometry. The coordination sites of the chromium centres are occupied by the two bridging chlorides, the bulky amide ligand, and a THF molecule. The square planar geometry of the metal centres in **2-06** differs from that for the three previously reported amido metal(II) chloride complexes **2-01**–**2-03**, as in all those cases, the metal possessed a distorted tetrahedral environment. However, the coordination geometry of the metal in **2-06** was not unexpected, as numerous four-coordinate square planar chromium(II) complexes have been characterised [8].

Complex **2-06** exhibits an effective magnetic moment in the solid state of 4.95 μ_B at 298 K, which is almost 2.0 μ_B less than the spin only value for two non-interacting

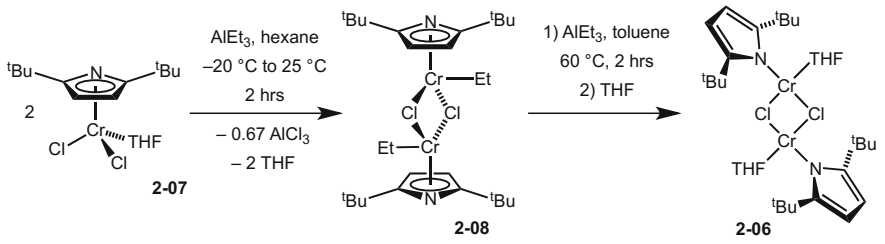

Scheme 2.3 Preparation of **2-06** and **2-08**

Cr^{2+} high spin centres (6.93 μ_B), showing relatively strong antiferromagnetic coupling within the Cr_2Cl_2 core. However, the value of 4.95 μ_B is indicative of two high spin Cr^{2+} centres, as low spin d^4 square planar complexes are expected to be diamagnetic.

Complex **2-06** was tested for catalytic activity in the polymerisation of ethylene, but was found to be inactive. No attempts to reduce **2-06** to a low oxidation state amido chromium complex have been reported.

2.1.2 *Previously Reported Bulky Amido Group 12 Metal(II) Halide Complexes*

To the best of our knowledge, apart from in publications arising from this work, there are no terminal amido zinc(II) halide or amido cadmium(II) halide complexes that have been structurally authenticated. There are however a number of low coordinate zinc metal halide complexes stabilised by bulky N,N′ bidentate ligands, e.g. [(^{Mes}Nacnac)ZnI(THF)] [9] (^{Mes}Nacnac = $[(MesNCMe)_2CH]^-$) and [(Giso)ZnI] (Giso = $[(DippN)_2CNCy_2]^-$) [10]. There are also multiple zinc and cadmium halide complexes stabilised by amide substituents on tridentate or higher dentate ligands [11]. However, as this chapter is focused primarily on bulky monodentate ligands, these complexes will not be further discussed.

A good number of amido mercury(II) halide complexes are known, the simplest of which is the mercuric amidochloride, $[Hg(NH_2)Cl]$ [12]. However, single crystal X-ray crystallographic analysis of the compound reveals that its solid state structure is actually a salt, consisting of a zig-zag 1-dimensional polymer $(HgNH_2)_n$ with chloride counterions, and not a sigma bonded complex [13].

Rather surprisingly, the first crystallographically characterised terminal amido mercury(II) halide complex, employed a N-aminoporphyrin compound as a ligand [14]. Porphyrin rings usually act as rigid, dianionic, tetradentate ligands to most metals, forming some extremely stable complexes [15]. However, when the N-aminooctaethyl-porphyrin **2-09** (NAOEP-H_2) [16] is reacted with mercury(II) chloride, two metal centres bond to one aminoporphyrin unit, to give the bis-chloromercury(II)-N-aminoporphyrin complex $[NAOEP(HgCl)_2]$ **2-10** (Scheme 2.4). The first mercury centre sits above the plane of the ring, bonded to one of the porphyrin pyrrole nitrogen atoms, and loosely coordinated by the two neighbouring pyrrole units. The second metal sits below the ring, and is bonded to the nitrogen atom of the amino group, resulting in a two-coordinate amido mercury(II) chloride moiety.

In 2010, Niemeyer and co-workers reported on a series of mercury(II) halide complexes stabilised by bulky diaryl-substituted triazenide ligands [17]. Triazenide ligands are related to amidinate and guanidinate ligand classes, in that they are N-donor bidentate ligands, which chelate to a metal centre forming a four membered ring. However, triazenide ligands contain a N_3 motif as their backbone, in

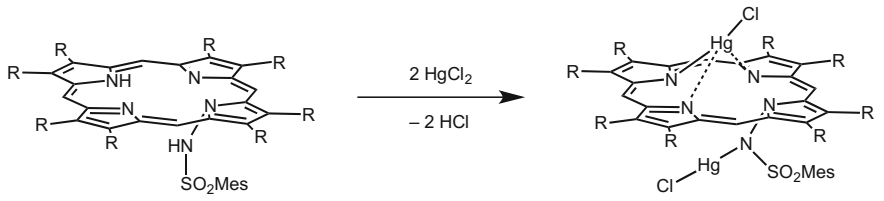

Scheme 2.4 Synthesis of bis-chloromercury(II)-N-aminoporphyrin complex [NAOEP($HgCl_2$)$_2$] **2-10**

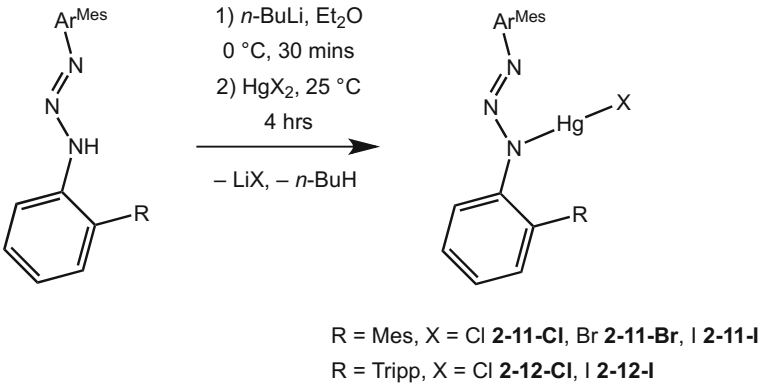

Scheme 2.5 Synthesis of **2-11-X** and **2-12-X**. X = Cl, Br or I

comparison to the amidinates and guanidinates NCN backbone. This subtle change in the ligand's backbone can lead to large electronic differences in a complex.

The complexes were synthesised by a simple deprotonation of the bulky triazenide $Ar^{Mes}(Ar)N_3H$ (Ar^{Mes} = 2,6-Mes_2-C_6H_3, Ar = Mph or Tph, Mph = 2-$MesC_6H_4$, Tph = 2-$Tripp_2C_6H_4$) with *n*-butyl lithium, followed by a salt metathesis reaction with the corresponding mercury(II) halide, to give the complexes [Ar^{Mes}(Mph)N_3HgX] (X = Cl **2-11-Cl**, Br **2-11-Br** or I **2-11-I**) and Ar^{Mes}(Tph)N_3HgX (X = Cl **2-12-Cl** or I **2-12-I**) in moderate to good yields (Scheme 2.5).

All of the triazenide mercury halide complexes (apart from **2-11-I**) were characterised by X-ray crystallography, which revealed that the triazenide is coordinating to the mercury in an η^1-bonding mode, rather than the more common N,N′-chelating arrangement. This unusual bonding mode makes the mercury two-coordinate, albeit with a weak aryl interaction from one of the flanking phenyl groups.

Further reactivity of the triazenide mercury halide complexes towards a number of alkaline earth metals and lanthanide metals was investigated. When **2-12-I** was reacted with magnesium metal in THF, a redox-transmetallation reaction occurred,

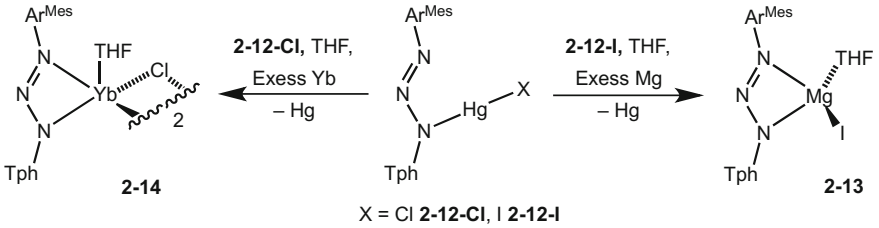

Scheme 2.6 Synthesis of **2-13** and **2-14**

leading to the formation and isolation of $[Ar^{Mes}(Tph)N_3MgI(THF)]$ **2-13** in good yields (Scheme 2.6). A similar reaction between **2-12-Cl** and ytterbium chips in THF, led to the isolation of the corresponding triazenide ytterbium(II) chloride complex $[\{Ar^{Mes}(Tph)N_3Yb(THF)(\mu\text{-}Cl)\}_2]$ **2-14**, also in high yields.

Apart from the reaction of **2-12-I** with magnesium, which may have initially been an attempt to reduce the triazenide mercury(II) halide to a low oxidation state mercury complex, no other attempts to reduce of the triazenide mercury halide complexes have been reported.

2.1.3 Terphenyl Stabilised D-Block Metal Halide Complexes

The only monodentate ligands that have been successfully applied to the preparation of two-coordinate transition metal(I) dimers, apart from the work presented in this thesis, are the bulky terphenyls, which were introduced in Sect. 1.2.1. This is partly because the precursors to these complexes, terphenyl transition metal(II) halide complexes, e.g. $[\{Ar^{Dipp}Cr(\mu\text{-}Cl)\}_2]$ **2-15** (Ar^{Dipp} = 2,6-$Dipp_2$-C_6H_3), the precursor complex to the Cr–Cr quintuple bonded complex $[(Ar^{Dipp}Cr)_2]$ **1-01**, are readily available and are stable to redistribution reactions [18].

2.1.3.1 Terphenyl Transition Metal(II) Halide Complexes

Power and co-workers have published a range of terphenyl stabilised transition metal(II) halide complexes, including the metals chromium, manganese, iron, and cobalt (Fig. 2.1) [19]. The majority of these complexes were synthesised via salt metathesis reactions between the terphenyl lithium salt and the corresponding metal(II) halide, however a small number have been synthesised by different routes, such as oxidative addition of halogens to metal(I) dimers, and decomposition of terphenyl metal(II) halides during their attempted reductions. X-ray crystallographic studies of the reported terphenyl transition metal(II) halide complexes revealed them all to exist as dimers, with bridging halides in the solid state, in essentially one of four common structural motifs (Fig. 2.1).

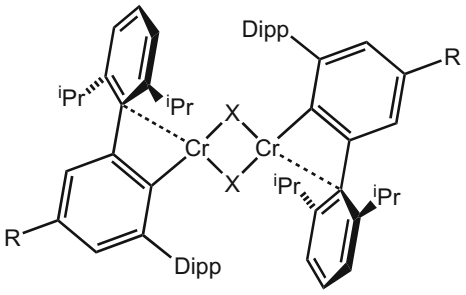

X = Cl, R = H, **2-15**
X = Cl, R = OMe, **2-16**
X = Cl, R = $SiMe_3$, **2-17**
X = I, R = H, **2-18**

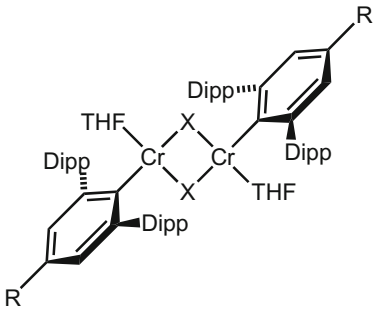

X = Cl, R = F, **2-19**
X = F, R = CF_3, **2-20**

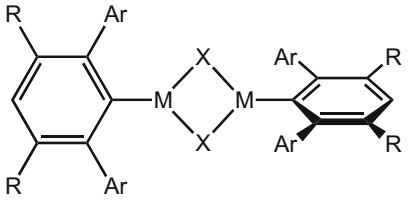

M = Mn, X = I, Ar = Tripp, R = ^{i}Pr, **2-22**
M = Fe, X = Br, Ar = Tripp, R = ^{i}Pr, **2-23**
M = Co, X = I, Ar = Tripp, R = H, **2-25**
M = Co, X = I, Ar = Dipp, R = H, **2-26**

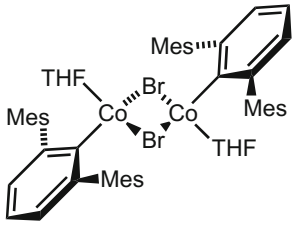

2-27

Fig. 2.1 Diagrammatic representations of the structurally characterised terphenyl transition metal(II) halide complexes **2-15**–**2-20**, **2-22**, **2-23** and **2-25**–**2-27**

To date, six terphenyl chromium(II) halide complexes have been crystallographically characterised. These are [{4-R-Ar^{Dipp}Cr(μ-Cl)}$_2$] (R = H **2-15**, OMe **2-16**, $SiMe_3$ **2-17**), [{Ar^{Dipp}Cr(μ-I)}$_2$] **2-18**, [{4-F-Ar^{Dipp}Cr(THF)(μ-Cl)}$_2$] **2-19** and [{4-CF_3-Ar^{Dipp}Cr(THF)(μ-F)}$_2$] **2-20** [19–21]. Complexes **2-15**–**2-17** are essentially isostructual, differing only by the substituent in the para position of the central ring. The chromium centres in these three complexes exist in distorted square planar geometries, similar to that observed for the amido chromium(II) chloride **2-06**. However, **2-06** contains a molecule of THF coordinating to the Cr centre, whereas in complexes **2-15**–**2-17**, the four coordination sites occupied by one terphenyl ligand, two bridging chlorides and a relatively strong interaction with the *ipso*-carbon of one of the terphenyl's flanking rings, instead of a coordinating solvent molecule. Complex **2-18** is similar to **2-15**–**2-17**, but has a slightly different structure in the solid state, in that the bridging halides are iodides rather than

chlorides. Due to the large ionic radius of iodine, the chromium halide bonds in **2-18** are considerably longer than in any of the chromium chloride complexes. As a result, one of the iodides has a weak interaction with one of the ligand's flanking aryl rings.

Depending on the steric and/or electronic properties of the metal centre, the coordination of a solvent molecule in the above complexes can be favoured over a ligand interaction. For instance, in **2-19** and **2-20**, a molecule of THF is coordinated to the metal centre, yielding a square planar geometry, similar to **2-06**. This structural change has come about as a result of a fluorine atom in the para position of the terphenyl ligand central ring in **2-19**, or the bridging fluorides in **2-20**. In both cases, the highly electronegative fluorine atoms withdraw electron density from the metal centre, which favours the coordination of a donor molecule, such as THF, rather than an aryl interaction.

Complexes **2-15**–**2-17** and **2-19** were synthesised via salt metathesis reactions between the appropriate terphenyl lithium salt, such as [$Ar^{Dipp}Li$] for **2-15**, and chromium(II) chloride THF adduct [$CrCl_2(THF)_2$] in diethyl ether at 0 °C [20, 21]. Complex **2-21** was not synthesised by salt metathesis, but via oxidative addition of iodine to the quintuple bonded chromium(I) dimer **1-01**.[19] The synthesis of **2-20** was rather unusual, as it was the decomposition product in the attempted reduction of another terphenyl chromium(II) chloride complex [{(4-CF_3-$Ar^{Dipp}Cr(\mu$-Cl)$\}_2$] **2-21** with KC_8 (Scheme 2.7) (N.B. No structural analysis of **2-21** has been reported) [20]. Unlike the terphenyl chromium(II) chloride complexes **2-15**–**2-17**, **2-19** and **2-21**, which are all blue compounds, **2-20** is a pale purple colour.

In contrast to the range of terphenyl chromium(II) halide complexes reported, there is only one terphenyl manganese(II) halide and one terphenyl iron(II) halide complex reported, which are the isostructual complexes [{3,5-$^iPr_2$-Ar^{Tripp}M (μ-X)$\}_2$] (M = Mn, X = I, **2-22**; M = Fe, X = Br, **2-23**; Ar^{Tripp} = 2,6-$Tripp_2$-C_6H_3) [22]. Similar to the complexes **2-15**–**2-17**, **2-19** and **2-21**, complexes **2-22** and **2-23** were synthesised via salt metathesis reactions between the terphenyl lithium salt [3,5-$^iPr_2$-Ar^{Tripp}Li] and either MnI_2 (for **2-22**) or $FeBr_2$ (for **2-23**), in diethyl ether. The metal centres in both complexes were found to possess distorted trigonal geometries; the coordination sites being occupied by the terphenyl ligand

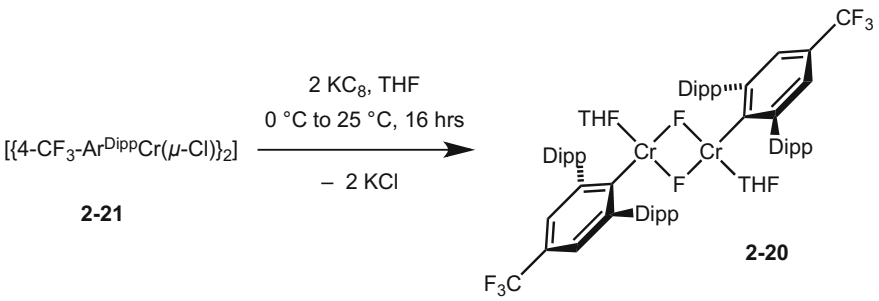

Scheme 2.7 Synthesis of **2-20**

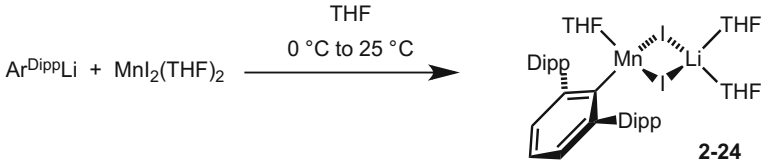

Scheme 2.8 Preparation of **2-24**

and the two bridging halides, with no strong interactions with the flanking aryl rings. The low coordination number of the metal centres in these compounds is a direct effect of the significant bulk of the [3,5-^{i}Pr$_2$-Ar^{Tripp}] ligands. The related iron(II) chloride complex [{3,5-^{i}Pr$_2$-Ar^{Tripp}Fe(μ-Cl)}$_2$] was also targeted by salt metathesis, i.e. the reaction between [3,5-^{i}Pr$_2$-Ar^{Tripp}Li] and $FeCl_2$. However, due to small amounts of the impurity LiI in the terphenyl lithium salt, the complex [{3,5-^{i}Pr$_2$-Ar^{Tripp}Fe(μ-Cl)}$_2$] could never be isolated in a pure form, as halogen exchange occurred between LiI and the product. Consequently the crystallised product always contained a percentage of the iron(II) iodide complex [{3,5-^{i}Pr$_2$-Ar^{Tripp}Fe(μ-I)}$_2$] [19].

One reason for the lack of terphenyl manganese(II), and iron(II) halide complexes, is that reactions of the smaller terphenyl lithium salts, with manganese(II) or iron(II) halides, often favours the formation of '-ate' complexes, over the elimination of the lithium halide salt. For example, the reaction between [Ar^{Dipp}Li] and manganese(II) iodide in THF, leads to high yields of the manganese iodide lithiate complex [Ar^{Dipp}Mn(THF)(μ-I)$_2$Li(THF)$_2$] **2-24** (Scheme 2.8) [16]. The extreme bulk of the 3,5-^{i}Pr$_2$-Ar^{Tripp} ligands in **2-22** and **2-23** proved to be sufficient to drive the elimination of LiI, and therefore makes their isolation possible [22].

Finally, three terphenyl cobalt(II) halide complexes have been structurally characterised. These are [{Ar^{Dipp}Co(μ-I)}$_2$] **2-25**, [{Ar^{Tripp}Co(μ-I)}$_2$] **2-26**, and [{Ar^{Mes}Co(THF)(μ-Br)}$_2$] **2-27** [23], with a fourth reported [{3,5-^{i}Pr$_2$-Ar^{Tripp}Co(μ-Cl)}$_2$] **2-28**, but not structurally characterised [24]. Initially, the terphenyl cobalt (II) chloride complexes were targeted by reactions of the terphenyl lithium salts, [Ar^{Dipp}Li] and [Ar^{Tripp}Li], with $CoCl_2$. However, as was found with iron, small amounts of the corresponding terphenyl cobalt(II) iodide complexes were found in the product, formed by halogen exchange with a LiI impurity. However, when the reactions were repeated, adding an excess of LiI to the reaction mixture, the chloride was fully exchanged with iodide, and **2-25** and **2-26** could be isolated cleanly and in good yields (Scheme 2.9) [19].

Complexes **2-25** and **2-26** are essentially isostructual with the previously discussed terphenyl manganese(II) iodide **2-22** and terphenyl iron(II) bromide **2-23**, in that they have three-coordinate metal centres with distorted trigonal geometries.

Along with the two terphenyl cobalt(II) iodide complexes, one terphenyl cobalt (II) bromide complex has also been reported and structurally characterised, viz. [{(Ar^{Mes}Co(μ-Br)}$_2$] **2-27** [23]. The complex was not synthesised from the terphenyl lithium salt, but via a terphenyl Grignard reagent. The terphenyl iodide

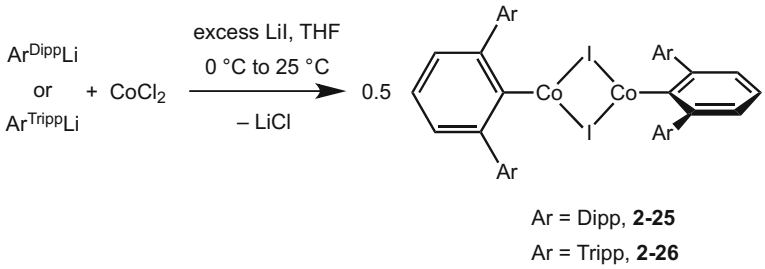

Scheme 2.9 Preparation of **2-25** and **2-26**

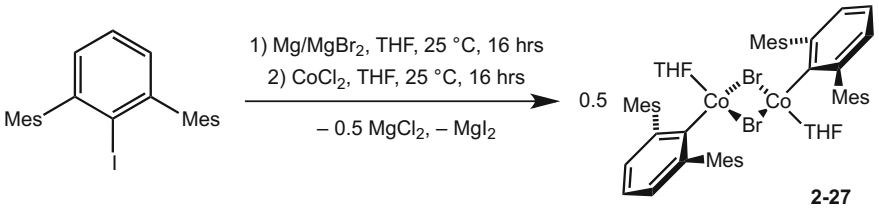

Scheme 2.10 Preparation of **2-27**

$Ar^{Mes}I$ was reacted with activated magnesium (a mixture of magnesium metal and $MgBr_2$) and the mixture subsequently treated with $CoCl_2$ in THF (Scheme 2.10). Once again halogen exchange occurs, this time involving $MgBr_2$, and the bromide bridged complex **2-27** is isolated instead of the chloride.

The smaller Ar^{Mes} ligands on **2-27**, compared with Ar^{Dipp} and Ar^{Tripp} on **2-25** and **2-26** respectively, favour the coordination of a molecule of THF to the metal centre, thus increasing the coordination from three in **2-25** and **2-26**, to four in **2-27**. Complex **2-27** bears some resemblance to the chromium(II) halide complexes **2-19** and **2-20**, in that it possesses four coordinate metal centres, with the coordination sites occupied by a terphenyl ligand, two bridging halides and a molecule of THF. However, as the chromium centres in **2-22** and **2-23** were found to be in a distorted square planar geometry, the cobalt centres in **2-27** were found to possess distorted tetrahedral geometries.

2.1.3.2 Terphenyl Group 12 Metal(II) Halide Complexes

In addition to terphenyl transition metal(II) halide complexes, Power, Robinson and co-workers have also isolated and structurally characterised a handful of terphenyl group 12 metal(II) halide complexes, including those of zinc, cadmium and mercury. These are $[\{Ar^{Dipp}Zn(\mu\text{-}I)\}_2]$ **2-29**, $[\{Ar^{Tripp}Zn(\mu\text{-}I)\}_2]$ **2-30**, $[\{Ar^{Dipp}Cd(\mu\text{-}I)\}_2]$ **2-31** and $[Ar^{Dipp}HgI]$ **2-32** (Fig. 2.2) [25, 26].

All four compounds **2-29**–**2-32** were initially synthesised via salt metathesis reactions between terphenyl lithium salts and the appropriate group 12 metal(II)

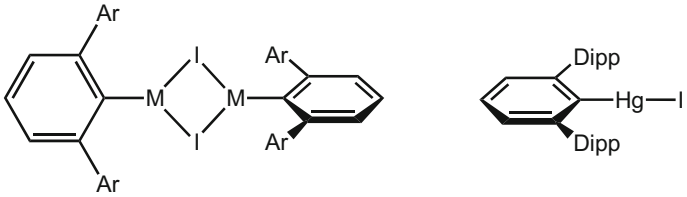

M = Zn, Ar = Dipp, **2-29**

M = Zn, Ar = Tripp, **2-30**

M = Cd, Ar = Dipp, **2-31**

2-32

Fig. 2.2 Diagrammatic representations of the structurally characterised terphenyl group 12 metal(II) halide complexes **2-29**–**2-32**

iodide, which gave moderate yields of all four complexes. However, it was later found that **2-32** could be synthesised in considerably higher yields (92 % compared with 60 %) when the terphenyl Grignard reagent was used in place of the lithium salt [25].

Complexes **2-29**–**2-31** are essentially isostructual, existing as dimers in the solid state with bridging iodine atoms. The metal centres are three coordinate, in distorted trigonal geometries, with the coordination sites occupied by the two bridging iodine atoms and the terphenyl ligand. The metal centres in all three compounds do not exhibit any close interactions with flanking aryl groups.

The terphenyl mercury(II) iodide complex **2-32** is the only d-block terphenyl metal(II) halide complex reported to date, and is monomeric, two-coordinate in the solid state. However, this was not unexpected, as there are numerous monomeric two-coordinate mercury(II) halide complexes that have been structurally characterised [8]. The majority of these complexes bear much less sterically hindering ligands than terphenyls, e.g. the two-coordinate complex, phenyl mercury(II) iodide, the structure of which was first reported by Pachomov in 1963 [27].

2.1.4 Extremely Bulky Monodentate Amido Ligands

Over the past four years, the Jones group has developed a range of extremely bulky monodentate amide ligands, with the general structure of the secondary amine (or protonated ligand) shown in Fig. 2.3 [28–31].

A large proportion of the bulk, and consequent kinetic protection supplied by these ligands comes from the common pentaaryl substituent [2,6-{$Ph_2C(H)$}$_2$-4-R′-C_6H_2] bound to the nitrogen atom. The other nitrogen substituent is an R group. This R group is typically either a trisubstituted silyl group or aryl ring, however ligands with alkyl and disubstituted phosphorus substituents have also been synthesised [32]. The overall steric bulk of the ligand can easily be tuned, by changing the size of this

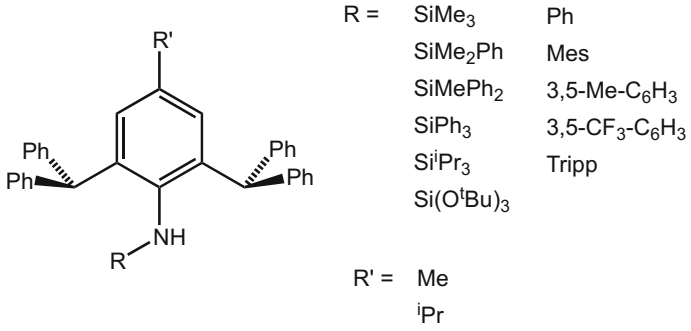

Fig. 2.3 A range of extremely bulky secondary amines

R group, from something relatively small, e.g. a phenyl ring, to an extremely bulky group, such as tri(tertbutoxy)silyl. The R′ group in the *para* position of the central ring is generally either methyl or isopropyl. Changing this R′ group from methyl to isopropyl, has little effect on the overall bulk of the ligand, and consequently little effect on the stability of a metal complex bearing it. However, it does influence the solubility and crystallising properties of the ligand itself, as well as derived coordination complexes.

The extremely bulky secondary amines are easily synthesised, in two steps for the bis(aryl) amines, and three steps for the silyl containing ligands (Scheme 2.11). The first step is common to both ligand types, i.e. the synthesis of the bulky aniline, either Ar*NH_2 **2-33** (Ar* = 2,6-$(Ph_2CH)_2$-4-Me-C_6H_2) or Ar$^{\dagger}NH_2$ **2-34** (Ar† = 2,6-$(Ph_2CH)_2$-4-^{i}Pr-C_6H_2). These are prepared via a solvent free Friedel-Crafts alkylation reaction between diphenylmethanol and a *para*-substituted aniline, to give good yields of the corresponding bulky aniline.

The silyl amine pro-ligands are synthesised by deprotonation of the bulky aniline **2-33** or **2-34** with *n*-butyl lithium in THF, followed by the addition of the corresponding silyl chloride, to give the bulky secondary amines in moderate to good yields. The diaryl pro-ligands on the other hand, are synthesised by palladium-catalysed cross-coupling reactions between the bulky aniline, **2-33** or **2-34**, and the corresponding aryl bromide.

These extremely bulky amide ligands have been used to stabilise a number of p-block element(I) dimers, such as the first amido digermyne [{Ar*$(SiMe_3)$NGe$\}_2$] **2-35** [33], the first amido distannyne [{Ar†$(Si^{i}Pr_3)$NSn$\}_2$] **2-36** [34] and a range of dipnictenes [{Ar*$(SiPh_3)$NE$\}_2$] (E = As **2-37**, Sb **2-38** and Bi **2-39**) [35]. All of these unprecedented p-block compounds were synthesised by reductions of the amido metal halide (or dihalide) precursor complexes with the magnesium(I) reducing agent [{(^{Mes}Nacnac)Mg$\}_2$] **1-08** (Scheme 2.12). The only other monodentate ligand class used to successfully stabilise this range of low oxidation state p-block compounds are the terphenyls.

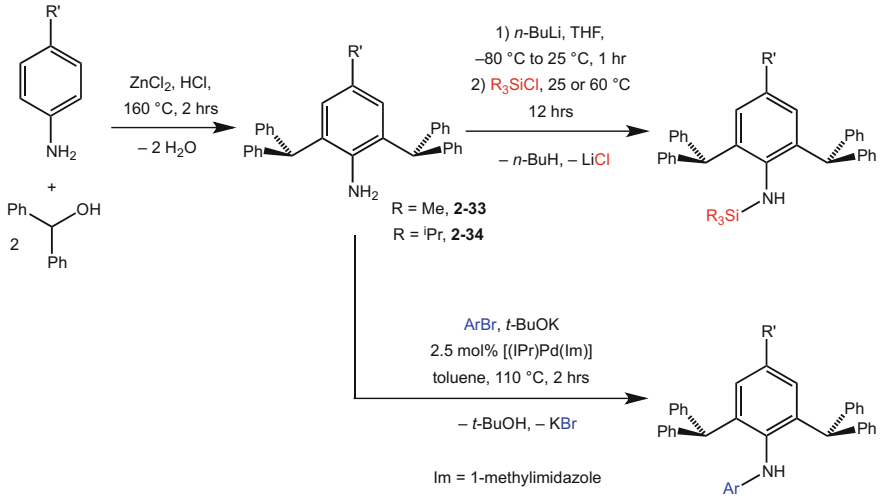

Scheme 2.11 Preparation of a series of bulky secondary amines

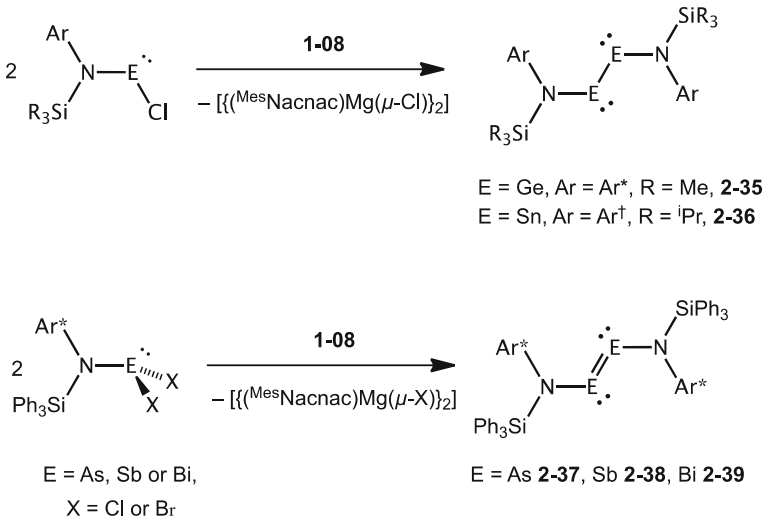

Scheme 2.12 Preparation of **2-35**–**2-39**

2.2 Research Outline

With the recent success that the extremely bulky amide ligands, developed in the Jones group, have had in low oxidation state p-block chemistry, it seemed reasonable that they could also be used to stabilise low coordinate, low oxidation state d-block metal complexes. With this in mind, a range of first row transition metal(II)

halide and group 12 metal(II) halide complexes, stabilised by the bulky amido ligands were targeted. The bulk and the electronic properties of the ligand were proposed to be modified, to investigate how these change the structure of the amido metal(II) halide complex. These complexes would hopefully serve as precursors to novel amide stabilised low oxidation state d-block metal complexes in later studies.

2.3 Results and Discussion

Bulky amido metal(II) halide complexes were initially targeted via salt metathesis reactions between metal(II) halides and bulky lithium amide salts, generated in situ by deprotonation of the bulky secondary amine pro-ligands with *n*-butyl lithium in THF. However, these reactions, e.g. involving [Ar*($SiMe_3$)NLi(THF)] and [Ar*($SiPh_3$)NLi], typically led to complex mixtures of unidentifiable products. That said, one reaction between [Ar*($SiMe_3$)NLi(THF)] and $MnBr_2$ in THF, followed by crystallisation from a diethyl ether solution, afforded a very low yield (<5 %) of the "-ate" complex, [Ar*($SiMe_3$)NMn(THF)(μ-Br)$_2$Li(OEt_2)$_2$] **2-40**. The complex is reminiscent of **2-24**, the terphenyl manganese(II) bromide lithiate complex, isolated from the reaction of [Ar^{Dipp}Li] and MnI_2. In an attempt to prevent the formation of these "-ate" complexes, potassium amide salts were chosen as an alternative to lithium amide salts, in the preparation of the amido d-block metal(II) halide complexes, as discussed below.

2.3.1 Preparation of Bulky Potassium Amide Salts

The potassium amide salt [Ar*($SiMe_3$)NK(η^6-toluene)] was reported prior to this work, prepared by the deprotonation of the bulky secondary amine Ar*($SiMe_3$)NH with 1.1 equivalents of [K(N($SiMe_3$)$_2$] (KN″) in THF [36]. After purification by crystallisation from toluene, a modest yield (71 %) of the complex was isolated. However, scaling this reaction up from the reported 2 to 10 g (or above) proved problematic. This was partly due to the reaction not going fully to completion, because it is essentially an equilibrium between the potassium salt of bulky amine and the potassium salt of N″. Therefore the product was repeatedly contaminated with small amounts of the starting Ar*($SiMe_3$)NH (≈10 %), even after crystallisation. The equilibrium point of the reaction can be shifted to favour the formation of [Ar*($SiMe_3$)NK(η^6-toluene)], by adding a large excess of KN″, however then the product was found to be contaminated with KN″. The deprotonation was also attempted with KH, however this does not react with bulky amine Ar*($SiMe_3$)NH, even in THF at reflux over the course of several days.

A new and improved synthesis for [Ar*($SiMe_3$)NK] was developed, replacing the use of stoichiometric amounts of KN″ with a cleaner and more atom efficient route. By using a slight excess of KH (1.1–1.3 equiv.) with a catalytic amount of

Scheme 2.13 Improved synthesis of [Ar*(SiMe$_3$)NK(THF)]

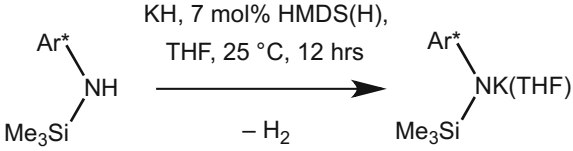

(Me$_3$Si)$_2$NH (5–10 mol%) in THF, KN″ is generated in situ, by deprotonation of (Me$_3$Si)$_2$NH with KH. This then deprotonates the bulky secondary amine Ar*(SiMe$_3$)NH, to give [Ar*(SiMe$_3$)NK(THF)], whilst regenerating the catalyst. With the release of H_2, the reaction is driven to competition over the course 12 h, with no Ar*(SiMe$_3$)NH observed in the product by ^{1}H NMR spectroscopy. Furthermore, workup and purification of the potassium amide is achieved by simply filtering away the remaining KH, removing the solvent *in vacuo*, and finally washing the residue with warm hexane to remove excess KN″. This gives [Ar*(SiMe$_3$)NK(THF)] in significantly higher yields (95 %) (Scheme 2.13).

The coordinated THF in [Ar*(SiMe$_3$)NK(THF)] is relatively labile, and can be exchanged for other weakly coordinating or aromatic solvent molecules, such as diethyl ether or toluene, by simply dissolving (or suspending in the case of Et$_2$O) the potassium amide in the appropriate solvent.

The improved synthetic route to [Ar*(SiMe$_3$)NK(THF)] was found to be effective for the synthesis of many other bulky potassium amides, such as [Ar*(SiPh$_3$)NK] and [Ar†(SiMe$_3$)NK(THF)]. However, for the deprotonation of extremely sterically hindered secondary amines, such as Ar†(Si^{i}Pr$_3$)NH or Ar*(Si^{i}Pr$_3$)NH, the reaction mixtures required heating to 60 °C for 12 h to proceed. This new route is how all of the potassium amides presented in this work were prepared.

2.3.2 *Bulky Amido First Row Transition Metal(II) Halide Complexes*

A range of bulky amido transition metal(II) halide complexes were synthesised by the addition of THF solutions of the potassium amides [Ar*(SiMe$_3$)NK(η^6-toluene)], [Ar*(SiPh$_3$)NK] or [Ar†(Si^{i}Pr$_3$)NK] to a solution (or suspensions) of one equivalent of either CrCl$_2$, MnBr$_2$, FeBr$_2$, or CoCl$_2$, in THF and −80 °C. The reaction mixtures were slowly warmed to room temperature, where they were stirred for between 5 min and 12 h. Work-up, followed by recrystallization of the crude reaction mixture gave moderate to good yields (43–81 %) of the amido metal halide complexes **2-41**–**2-49** (Scheme 2.14).

Reactions of the three potassium amides with NiBr$_2$ and CuCl$_2$ were also attempted. However, in every case these led to intractable mixtures of products, with no amido metal halide complex isolated. Furthermore, reactions of the three potassium amides with CoBr$_2$ were also targeted, however in every case these led to the recovery of the potassium amide and the reproducible generation of the new

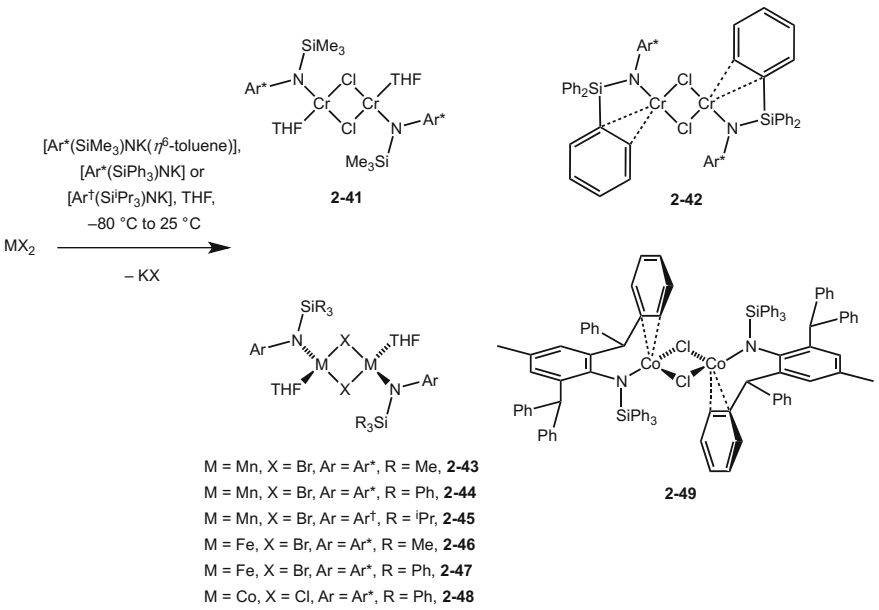

Scheme 2.14 Preparation of **2-41**–**2-49**

cobalt bromide contact ion-pair complex, $[(THF)_4Co(\mu\text{-}Br)_2CoBr_2]$ **2-50**. It seems that dissolution of $CoBr_2$ in THF yields **2-50**, which has a low reactivity towards the potassium amide starting materials. In addition, no identifiable product could be isolated from the reaction of [[Ar*($SiMe_3$)NK(η^6-toluene)] with $CoCl_2$. However, depending on the solvent of crystallization, two amido cobalt(II) chloride complexes **2-48** and **2-49** bearing the same Ar*($SiPh_3$)N^- ligand could be isolated (see structural discussions below for further details).

Unfortunately, in the repeated reactions between the most bulky of the three potassium amides [Ar†(Si^iPr_3)NK], and the metal(II) halides $CrCl_2$, $FeBr_2$ or $CoCl_2$, no amido metal halide complex was isolated. The only isolated product from all three reactions was the protonated bulky secondary amine Ar†(Si^iPr_3)NH. The only reaction to yield an amido transition metal(II) halide bearing the bulky Ar†(Si^iPr_3)N^- ligand was between [Ar†(Si^iPr_3)NK] and $MnBr_2$, which gave good yields of the amido manganese(II) bromide **2-45**.

All of the complexes **2-41**–**2-49** were characterised by X-ray crystallography (Figs. 2.4, 2.5 and 2.6), which revealed them to possess varying coordination geometries, depending on the ligand and metal involved. However, they were all found to be dimeric in the solid state, with bridging halides.

The two amido chromium(II) chloride complexes **2-41** and **2-42** differ to the other amido metal(II) halides, in that they both posses distorted square planar metal geometries, whereas complexes **2-43**–**2-49** all contain metals in distorted tetrahedral environments. The metal coordination sites in **2-41** and **2-42**, are occupied by the

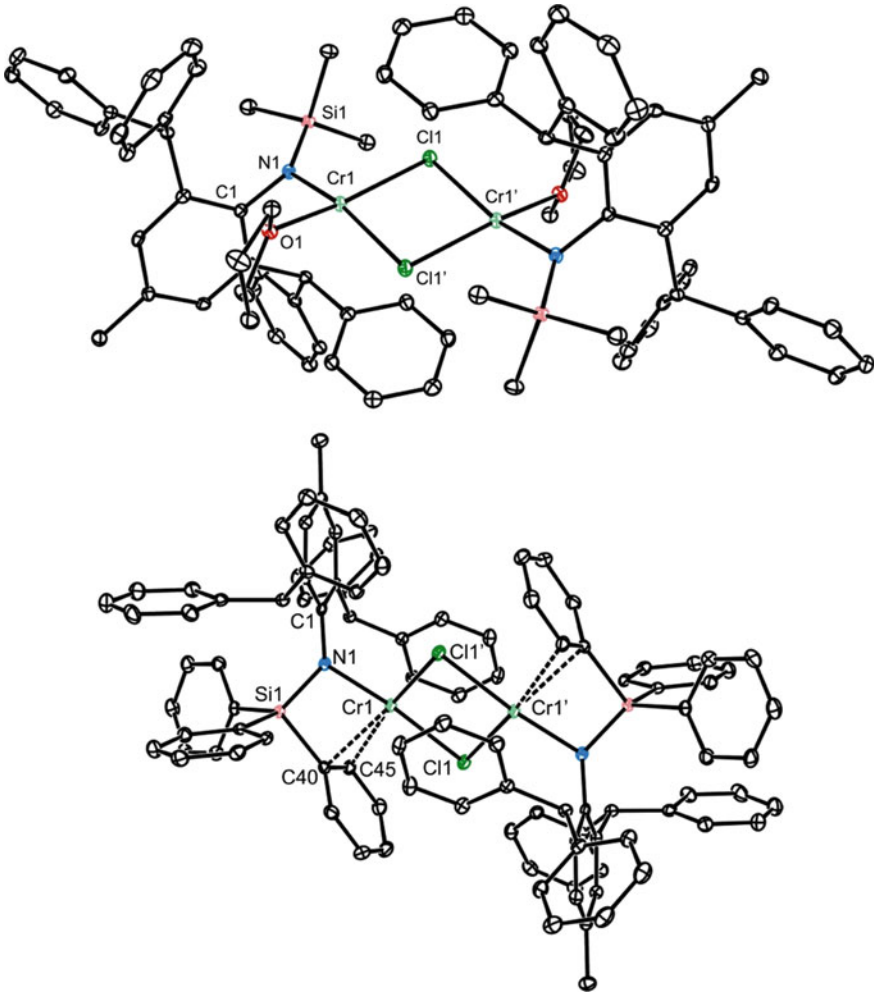

Fig. 2.4 Thermal ellipsoid plots (25 % probability surface) of the molecular structures of **2-41** (*top*) and **2-42** (*bottom*). Hydrogen atoms have been omitted for clarity. Selected interatomic distances (Å) and angles (°) for complexes **2-41** and **2-42** can be found in Table 2.1

amide, two approximately symmetrically bridging chlorides and either a molecule of THF in **2-41**, or an η^2-phenyl interaction to one of the phenyl rings of the triphenyl silyl group in **2-42**. The difference in the chromium coordination sites suggests that there is competition between THF and ligand arene interactions in these complexes, as both complexes were synthesized in THF. The resulting structures can be explained by the bulk of the ligand; the smaller Ar*$(SiMe_3)N^-$ ligand in **2-41** favours the coordination of a molecule of THF, whereas the more sterically demanding Ar*$(SiPh_3)N^-$ ligand in **2-42** favours an η^2-phenyl interaction. The $SiPh_3$ groups on the Ar*$(SiPh_3)N^-$ ligands of **2-42** provide the possibility of an

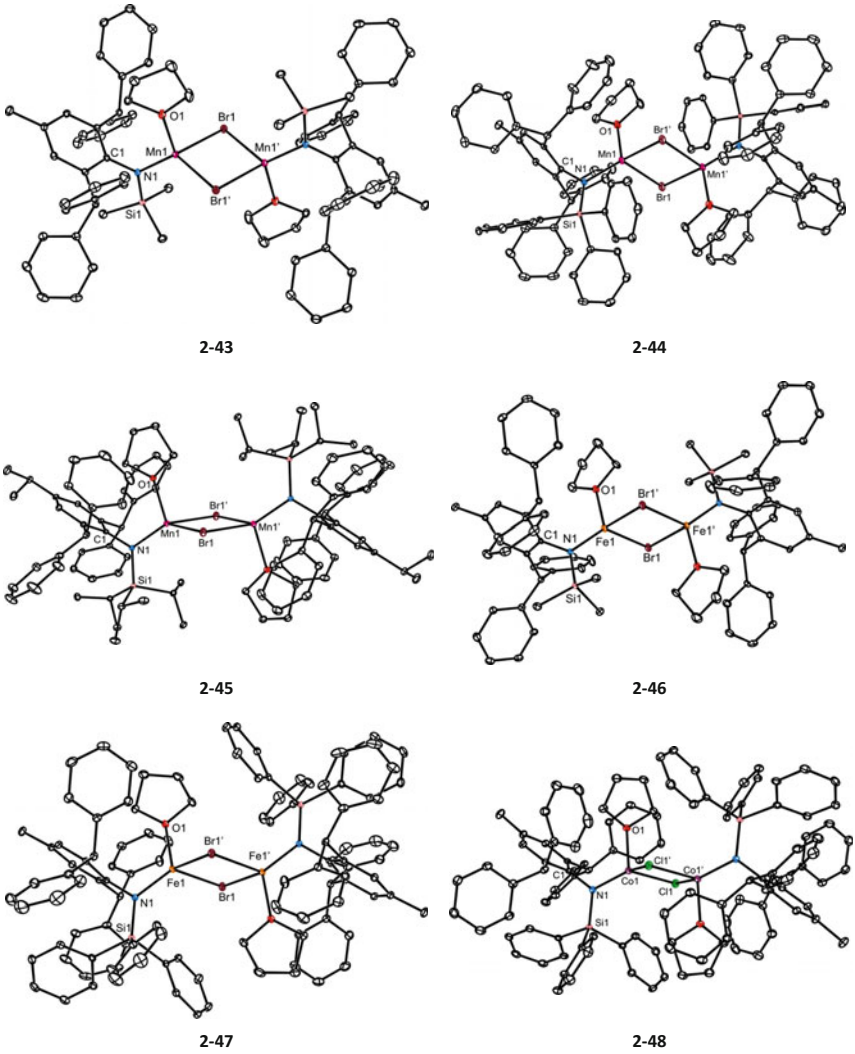

Fig. 2.5 Thermal ellipsoid plots (25 % probability surface) of the molecular structures of **2-43**–**2-48**. Hydrogen atoms have been omitted for clarity Selected interatomic distances (Å) and angles (°) for complexes **2-43**–**2-48** can be found in Table 2.1

η^2-phenyl interaction, which is not available in **2-41**. However, as chromium(II) is generally considered a hard acid, the coordination to THF would be favoured over the softer η^2-phenyl interaction, therefore the steric bulk of the ligand is the main driving force for this change in coordination.

Complex **2-41** closely resembles the previously reported amido chromium(II) complex **2-06**, as well as the two terphenyl chromium(II) halide complexes **2-19** and **2-20**. That is, all four complexes are dimeric, square planar chromium(II) halide

Table 2.1 Selected interatomic distances (Å) and angles (°) for **2-41**–**2-49**

	2-41 (Cr)	**2-42 (Cr)**	**2-43 (Mn)**	**2-44 (Mn)**	**2-45 (Mn)**	**2-46 (Fe)**	**2-47 (Fe)**	**2-48 (Co)**	**2-49 (Co)**
M–N	2.016(2)	2.014(2)	1.9849(13)	2.024(2)	1.924(2)	1.9363(15)	2.0137(17)	1.936(2)	1.909(3)
M–X	2.3654(8)	2.3945(9)	2.5790(3)	2.6196 (5)	2.5514(6)	2.5552(3)	2.6329(4)	2.3500(9)	2.3508(10)
M–X′	2.4248(8)	2.3567(8)	2.5968 (3)	2.5912 (5)	2.5671(5)	2.5455(3)	2.6410(4)	2.3487(8)	2.3209(9)
M–O or M–$CC_{mid\ point}$	2.0766(19)	2.423(2)	2.1034(12)	2.127(2)	2.041(2)	2.0507(13)	2.1335(14)	2.027(2)	2.365(2)
M···M′	3.523(1)	3.503(1)	3.574(1)	3.724(1)	3.620(1)	3.685(1)	3.918(11)	3.342(1)	3.310(1)
X–M–X′	85.32(3)	84.99(3)	92.65(1)	88.76(2)	89.98(2)	87.48(1)	84.031(12)	89.34(3)	89.77(3)
M–X–M′	94.68(3)	95.01(3)	87.35(1)	91.24(2)	90.02(2)	92.52(1)	95.969(12)	90.66(3)	90.23(3)
N–M–O or N–M–$CC_{mid\ point}$	97.41(8)	81.48(7)	113.28(5)	114.96(8)	118.17(9)	118.71(6)	109.07(6)	108.60(10)	97.14(8)

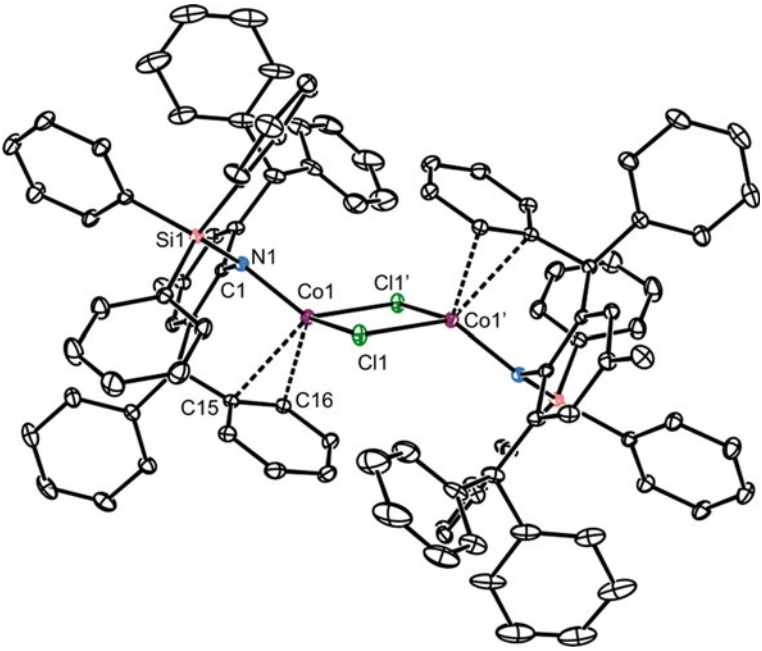

Fig. 2.6 Thermal ellipsoid plot (25 % probability surface) of the molecular structure of **2-49**. Hydrogen atoms have been omitted for clarity. Selected interatomic distances (Å) and angles (°) for complex **2-49** can be found in Table 2.1

complexes in the solid state, with bridging halides and a molecule of THF occupying coordination sites. Complex **2-42** is more closely associated with the terphenyl chromium(II) chloride complexes **2-15**–**2-18**, which are also dimeric, square planar complexes, but do not possess a coordinating solvent. Instead, the fourth coordination site is occupied by a strong interaction with the *ipso*-carbon of one of the terphenyl flanking aryl groups.

The Cr-N distances in **2-41** and **2-42** are in the normal range for chromium(II) amides [8], but are slightly less than the sum of the covalent radii for Cr and N (2.10 Å) [37]. Although the Cr···η^2–C–$C_{mid\ point}$ distances in **2-42** (2.423(2) Å) are longer than normal Cr–C covalent bonds, e.g. 2.020(7) Å in [Cr(η^6-benzene)$_2$] [38] and 2.041(3) Å in **2-15** [21], they clearly signify relatively strong Cr···phenyl interactions.

The three amido manganese(II) bromide complexes **2-43**, **2-44** and **2-45**; the two amido iron(II) bromide complexes **2-46** and **2-47**, along with the amido cobalt(II) chloride complex **2-48**, are essentially isostructual in the solid state. All of the metals in complexes **2-43**–**2-48** possess distorted tetrahedral coordination geometries, with their sites occupied in a similar fashion to **2-41**, i.e. with the terminal amide, two bridging halides and a molecule of THF coordinated to the metal. Rather surprisingly, the amido manganese bromide **2-45**, which bears the most sterically demanding ligand [$Ar^{\dagger}(Si^{i}Pr_3)N^{-}$, still possesses this geometry, even

though the extra bulk would be thought to favour a η^2-phenyl interaction, and not a coordinating THF molecule.

There are no other reported terminal amido manganese(II) halide complexes to compare complexes **2-43**–**2-45** with, however the manganese complexes reported here contrast to the previously reported monomeric amido iron(II) chloride complexes **2-01** and **2-02**, and the amido cobalt(II) chloride **2-03**. Complexes **2-01**–**2-03** all contain a bidentate coordinating tmeda molecule, which occupies two of the four coordination sites; this disfavours dimerisation, therefore **2-01**–**2-03** are all monomeric in the solid state. There are no equivalent structural types for terphenyl manganese or iron halide complexes either, as the only reported terphenyl manganese(II) halide **2-22** and terphenyl iron(II) halide **2-23** possess one of the most sterically demanding terphenyl ligands 3,5-$^{i}Pr_2$-Ar^{Tripp}. These extremely bulky terphenyl ligands force the metal to occupy a three-coordinate trigonal geometry, with no space for the coordination of a solvent molecule. Comparisons can, however, be made between the cobalt complex **2-49**, and the terphenyl cobalt bromide complex **2-27**, both of which are dimeric, have similar distorted tetrahedral cobalt geometries, with a coordinating molecule of THF.

Within the series of essentially isostructual complexes **2-43**–**2-48**, there is a general decrease in the M–N and/or M–O distances with increasing relative atomic mass of the metal. This is consistent with the decreasing high spin covalent radii reported for the metal sequence Mn (1.61 Å) > Fe (1.52 Å) > Co (1.50 Å) [37]. Although the N-centers in all of the complexes **2-43**–**2-48** have planar geometries, none of their M-N distances are especially short, and therefore they do not indicate significant degrees of N → M π-bonding. In addition, their metal-metal separations are not indicative of any substantial metal-metal bonding.

As previously mentioned in the discussion of the amido chromium halide complexes **2-41** and **2-42**, there is a competition in these complexes for the metal's coordination to THF, or the formation of a ligand arene interaction. In the amido cobalt(II) chloride complexes **2-48** and **2-49**, this is apparently a relatively finely balanced competition, as both the THF coordinated complex **2-48** and the THF free, arene interacting complex **2-49** can be isolated with the same Ar*($SiPh_3$)N^- ligand. Complex **2-48** is obtained when the vacuum dried crude reaction product is recrystallized from a toluene/hexane solution. However, if that solution is kept at room temperature for several days before crystallization occurs, only **2-49** is obtained. Moreover, solid samples of **2-48** appear to slowly lose their coordinated THF at ambient temperature, while dissolution of **2-49** in THF leads to the immediate and quantitative regeneration of compound **2-48**.

The solid state structure of **2-49** resembles those of **2-43**–**2-48**, in that it has a distorted tetrahedral cobalt geometry, though the fourth coordination site of the metal is instead taken up by an η^2-phenyl interaction rather than a coordinating molecule of THF. At first glance, this appears similar to the situation in **2-42**. However, in **2-42** the interaction derives from a phenyl group of the $SiPh_3$ fragment, whereas in **2-49**, it comes from a phenyl substituent of the Ar* ligand. This difference presumably results from the contrasting metal geometries in the two complexes.

All of the amido transition metal(II) halide compounds reported (except **2-48**) are very thermally stable solids, and are indefinitely stable in solution at ambient temperature. Little information can be gained from their NMR spectroscopic data, due to the paramagnetic nature of the compounds. This gives rise to broad signals in the ^{1}H NMR spectra, which are typically observed over wide chemical shift ranges, e.g. −53 to 123 ppm for **2-49**.

Solution state effective magnetic moments of the amido transition metal(II) complexes were determined using the Evans method [39]. Unfortunately, the very low solubility of the chromium chloride complex **2-42** in non-coordinating deuterated solvents prevented an accurate magnetic moment determination. The magnetic moment obtained for the amido chromium chloride **2-41** (μ_{eff} = 5.81 μ_B per dimer) is less than the spin-only value for two non-interacting high-spin Cr^{2+} centers (μ_{so} = 6.93 μ_B). However, it lies in the range previously reported for related square-planar halide bridged chromium(II) dimers, e.g. the terphenyl chromium fluoride complex **2-20** (μ_{eff} = 6.94 μ_B per dimer) [20] and the previously reported amido chromium(II) chloride complex **2-06** (μ_{eff} = 4.95 μ_B per dimer) [7]. This suggests the compound is high-spin and exhibits a degree of antiferromagnetic coupling over the Cr_2Cl_2 core. Similarly, the magnetic moments obtained for all the tetrahedral dimers, **2-43**–**2-49**, indicate that they are high-spin complexes, the metal centers of which are antiferromagnetically coupled to varying extents. Specifically, the effective magnetic moments for the manganese complexes, **2-43** (5.90 μ_B per dimer), **2-44** (6.85 μ_B per dimer), and **2-45** (6.90 μ_B per dimer) are markedly less than the spin-only value (μ_{so} = 8.36 μ_B). It is difficult to draw comparisons here as we are not aware of any other structurally authenticated tetrahedral, halide bridged manganese(II) dimers that have been the subjects of magnetochemical studies. The only exceptions are several dimeric, tetrahedral manganese dihalide adducts, e.g. [{Mn(NEt$_3$)I(μ-I)}$_2$] (μ_{eff} = 6.8 μ_B), for which significant antiferromagnetic coupling between the Mn centers was proposed [40]. The magnetic moments obtained for the iron(II) and cobalt(II) dimers, **2-46** (5.38 μ_B per dimer), **2-47** (6.61 μ_B per dimer), **2-48** (4.86 μ_B per dimer) and **2-49** (5.20 μ_B per dimer), are also somewhat less than the spin-only values (Fe: 6.93 μ_B, Co: 5.40 μ_B,). The observed magnetic moments are, however, comparable to those for related four-coordinate complexes, e.g. the β-diketiminato iron fluoride complex [{(^{Dipp}Nacnac)Fe(μ-F)}$_2$] (6.2 μ_B per dimer) [41] and the terphenyl cobalt bromide complex **2-27** (4.7 μ_B per dimer) [23].

2.3.3 Bulky Amido Group 12 Metal(II) Halide Complexes

Bulky amido group 12 halide complexes were prepared here, using similar methods to those for the synthesis of the amido transition metal(II) halide complexes, i.e. via reactions of the bulky potassium amides with metal(II) halides. However, for the group 12 complexes, two additional bulky potassium amides were employed, these are [Ar†(SiMe$_3$)NK(OEt$_2$)] and [Ar*(Si^{i}Pr$_3$)NK].

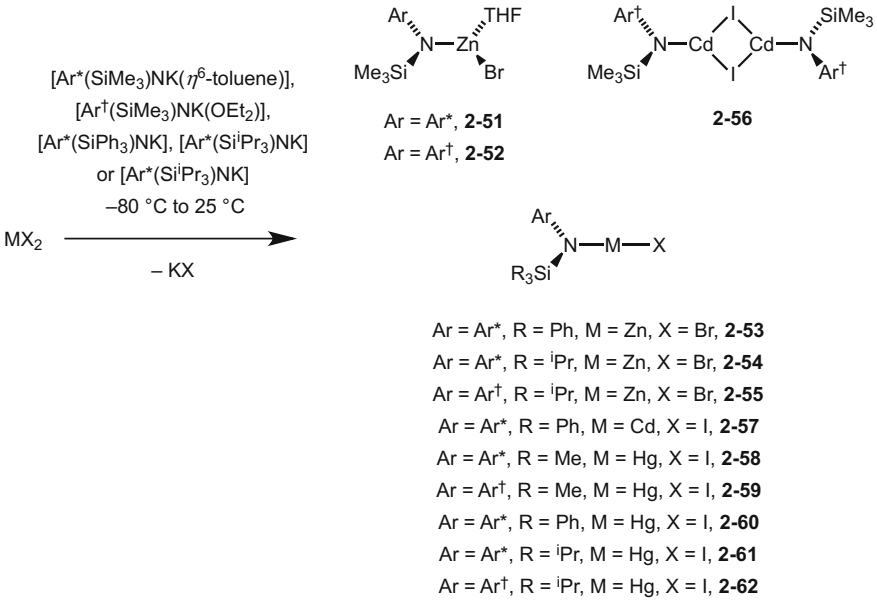

Scheme 2.15 Preparation of **2-51**–**2-62**

The bulky amido group 12 metal(II) halide complexes were synthesised by the addition of either THF, toluene or diethyl ether solutions of the potassium amides [Ar*($SiMe_3$)NK(η^6-toluene)], [Ar*($SiPh_3$)NK], [Ar†(Si^iPr_3)NK], [Ar†($SiMe_3$)NK(OEt_2)] and [Ar*(Si^iPr_3)NK] to suspensions of one equivalent of either $ZnBr_2$, CdI_2 or HgI_2 in the same solvent and −80 °C. The reactions were slowly warmed to room temperature, where they were stirred for between 30 min and 4 h. Work-up, followed by recrystallization of the crude reaction mixture gave moderate to excellent yields (53–90 %) of the amido metal halide complexes **2-51**–**2-62** (Scheme 2.15).

Amido zinc and mercury halide complexes bearing all five ligands have been isolated and characterised. However, reactions between the potassium amides [Ar*($SiMe_3$)NK(η^6-toluene)], [Ar*(Si^iPr_3)NK] or [Ar†(Si^iPr_3)NK], and one equivalent of CdI_2, in THF, toluene or diethyl ether repeatedly lead to the formation of cadmium metal and the corresponding protonated amine.

All of the complexes **2-51**–**2-62** were crystallographically characterised (Figs. 2.7, 2.8 and 2.9), which once again revealed them to possess varying coordination geometries, depending on the ligand and metal involved. These complexes differ to the equivalent transition metal complexes, in that, with the exception of **2-56**, they are all monomeric in the solid state.

The two amido zinc bromide complex **2-51** and **2-52** are essentially isostructual, and differ from the other amido group 12 metal halide complexes in that they are the only two to possess a coordinating solvent molecule, likely due to the fact that they possess the two least sterically demanding amido ligands. The coordination of THF

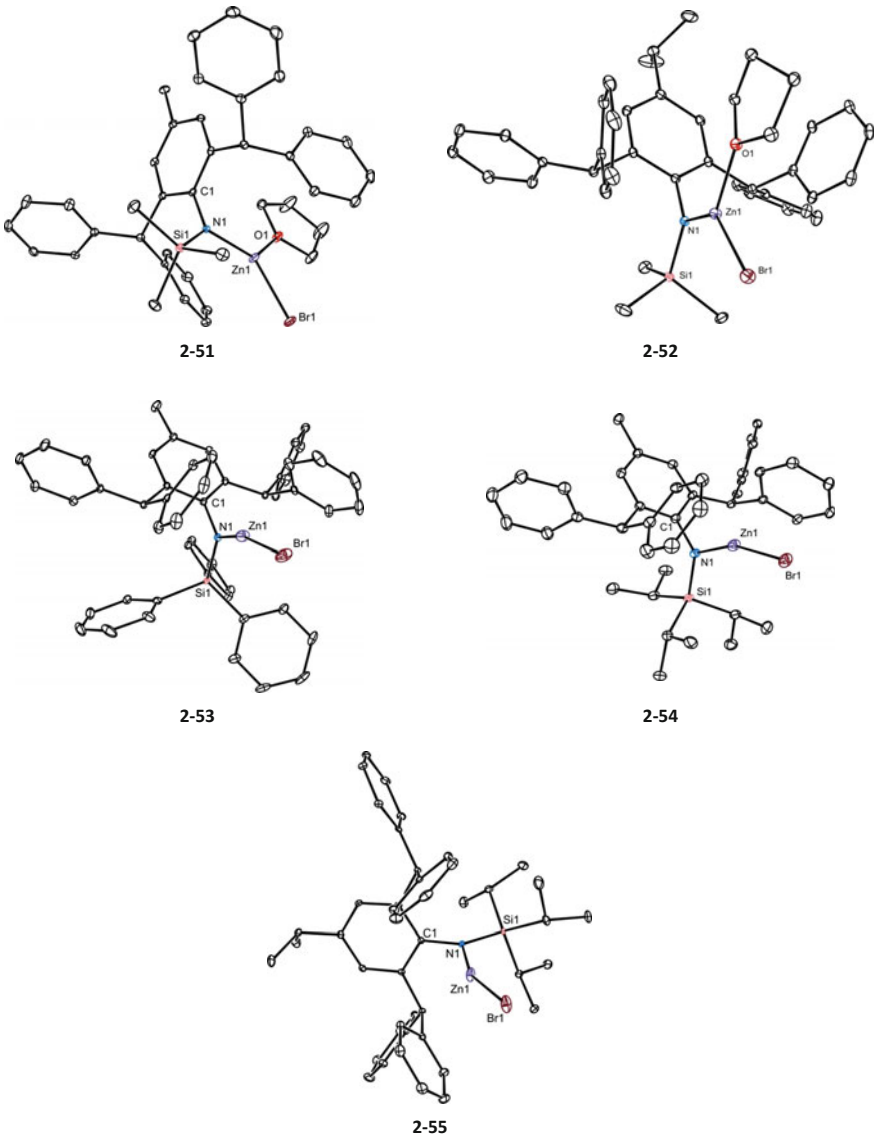

Fig. 2.7 Thermal ellipsoid plots (25 % probability surface) of the molecular structures of **2-51**–**2-55**. Hydrogen atoms have been omitted for clarity. Selected interatomic distances (Å) and angles (°) for complexes **2-51**–**2-55** can be found in Table 2.2

to the zinc centre in **2-51** and **2-52**, results in a three-coordinate zinc centre, in a distorted trigonal geometry. Although in both structures two phenyl rings from the pentaaryl substituent lie above and below the zinc coordination plane, the closest Zn···C_{phenyl} distance (3.048 Å in **2-51**, and 3.109 Å in **2-52**) in both cases is too

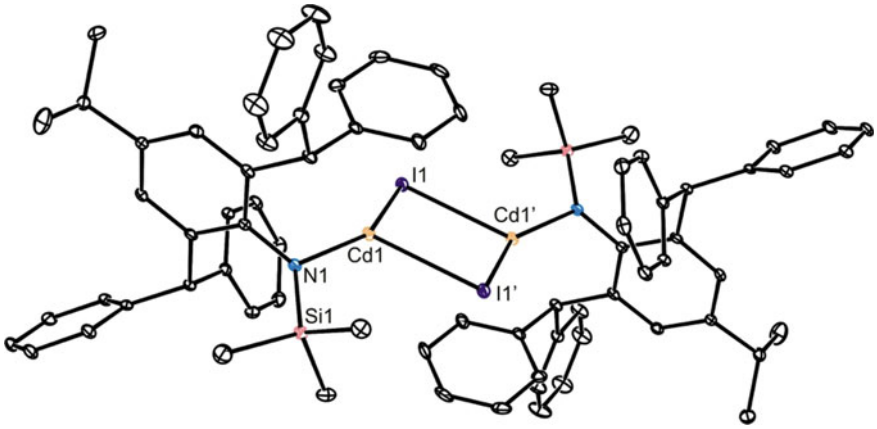

Fig. 2.8 Thermal ellipsoid plot (25 % probability surface) of the molecular structure of **2-56**. Hydrogen atoms have been omitted for clarity. Selected interatomic distances (Å) and angles (°) for complex **2-56** can be found in Table 2.2

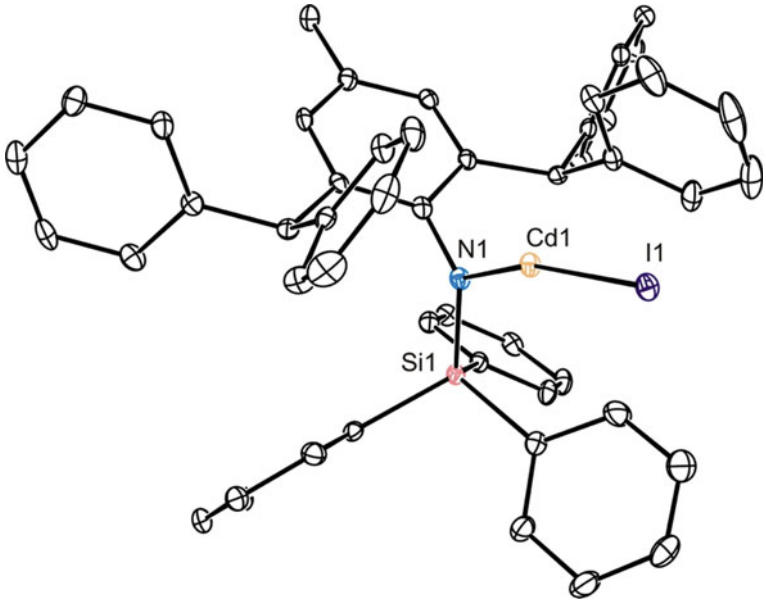

Fig. 2.9 Thermal ellipsoid plot (25 % probability surface) of the molecular structure of **2-57**. Hydrogen atoms have been omitted for clarity. Selected interatomic distances (Å) and angles (°) for complex **2-57** can be found in Table 2.2

long to imply any significant interaction. It is worth noting that the synthesis of amido zinc bromide complexes bearing $[Ar^*(SiMe_3)N]^-$ and $[Ar^\dagger(SiMe_3)N]^-$ without a coordinating molecule of THF was attempted, by carrying out reactions of the potassium amides $[Ar^*(SiMe_3)NK(\eta^6\text{-toluene})]$ and $[Ar^\dagger(SiMe_3)NK(OEt_2)]$ with $ZnBr_2$ in toluene, benzene and diethyl ether. However, in every case decomposition occurred, yielding the protonated amine and zinc metal. Therefore it is thought that the steric protection provided by the $Ar^*(SiMe_3)N^-$ and $Ar^\dagger(SiMe_3)N^-$ ligands is not sufficient to stabilise two-coordinate zinc halide complexes.

In contrast to **2-51** and **2-52**, there is no solvent coordinated to the three amido zinc bromide complexes **2-53**, **2-54** and **2-55**, likely due to the increase in ligand bulk. As a result, complexes **2-53**–**2-55** possess two-coordinate zinc centres. All three structures have slightly bent N-Zn-Br angles (160.41° in **2-53**, 159.37° in **2-54** and 158.63° in **2-55**) which may be due to an interaction between the Zn center and one of the flanking phenyl rings, but as the closest $Zn\cdots C_{phenyl}$ distance is long in all cases (2.824 Å in **2-53,** 2.854 Å in **2-54** and 2.812 Å in **2-55**), these interactions must be considered weak at best. Compounds **2-53**–**2-55** represent the first structurally characterised examples of amido zinc halide complexes, and differ from the corresponding terphenyl zinc halide complexes **2-29** and **2-30**, which have three-coordinate zinc centres and are dimeric in the solid state [25, 26].

Two amido cadmium iodide complexes, **2-56** and **2-57**, were also isolated and structurally characterised (Figs. 2.9 and 2.10). Compound **2-56** differs from all of the other amido group 12 metal halide complexes reported here, in that it is the only one to exist as a dimer in the solid state, even though the complex bears the same ligand, and was prepared in the same solvent as the monomeric zinc bromide complex **2-52**. The two cadmium centres are three-coordinate, and have distorted trigonal geometries. Flanking phenyl rings from the $Ar^\dagger$ substituent lie above and below the cadmium coordination plane, but as the closest $Cd\cdots C_{phenyl}$ distance is 2.952 Å, these distances are considered too long to imply any significant interaction. Complex **2-56** is similar to the corresponding terphenyl cadmium iodide complex **2-31**, which also possesses three-coordinate metal centres, and also exists as a dimer with bridging iodides in the solid state.

In contrast to **2-56**, the amido cadmium iodide complex **2-57** is monomeric in the solid state, due to an increase in ligand bulk, and is also solvent free, resulting in a two-coordinate cadmium centre. The structure of **2-57** is essentially isostructual with the related zinc complex **2-53**, with a slightly bent N–Cd–I fragment (164.8°), which is possibly due to an interaction between the Cd centre and one of the flanking phenyl rings of the $Ar^\dagger$ substituent. However, as the closest $Cd\cdots C_{phenyl}$ distance is quite long (2.903 Å), this interaction must once again be considered weak. Compounds **2-56** and **2-57** represent the first examples of amido cadmium halide complexes.

Finally, five amido mercury iodide complexes, **2-58**–**2-62**, have been synthesised and crystallographically characterised (Fig. 2.10). All complexes were found to be essentially isostructual, monomeric and solvent free in the solid state, resulting in two-coordinate mercury centres. As with the two-coordinate zinc and cadmium

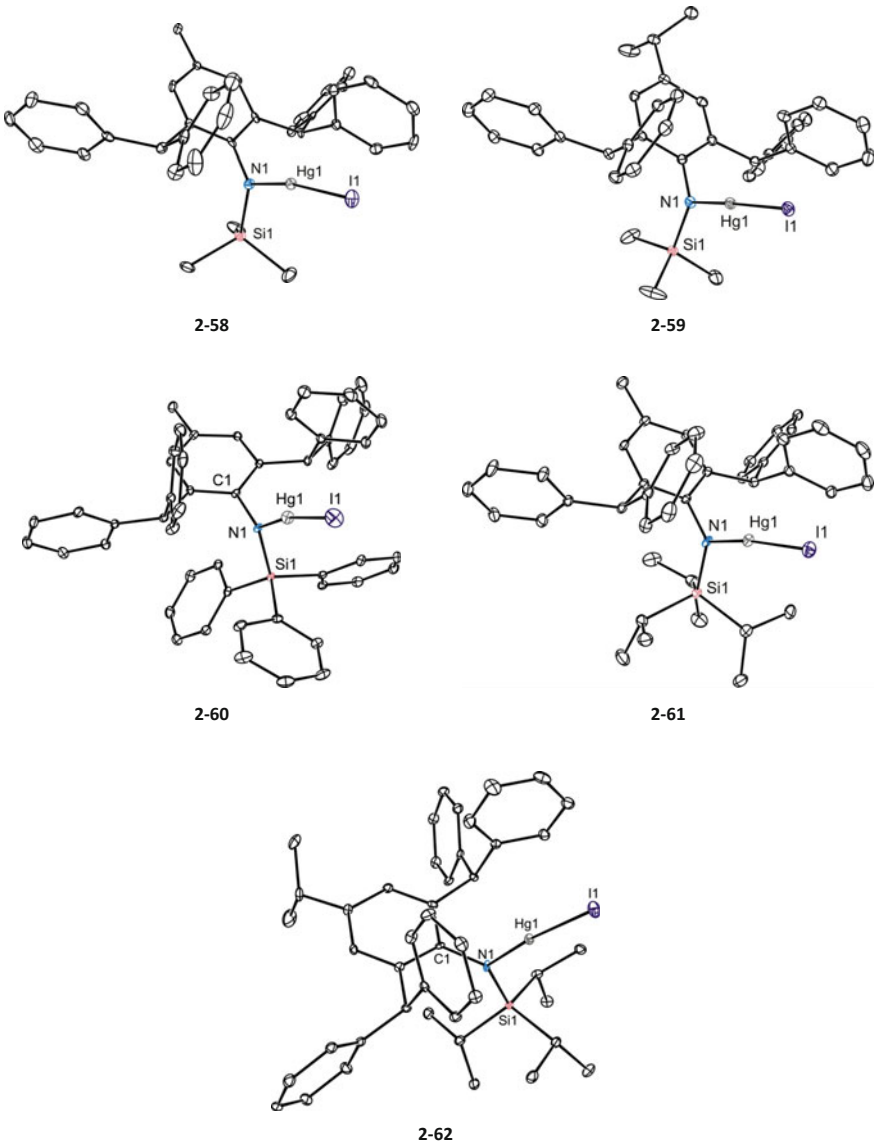

Fig. 2.10 Thermal ellipsoid plots (25 % probability surface) of the molecular structures of **2-58**–**2-62**. Hydrogen atoms have been omitted for clarity. Selected interatomic distances (Å) and angles (°) for complexes **2-58–2-62** can be found in Table 2.2

structures, **2-53**–**2-55** and **2-57**, the N-Hg-I angles in the complexes are slightly bent (171.0° (avg) in **2-58**, 174.3° (avg.) in **2-59**, 170.3° in **2-60**, 173.4° in **2-61**, 174.4° in **2-62**) but to a lesser extent than in the related zinc and cadmium complexes. In addition, there are no strong Hg···C interactions with the phenyl groups

Table 2.2 Selected interatomic distances (Å) and angles (°) for **2-51–2-62**

	2-51 (Zn)	**2-52 (Zn)**	**2-53 (Zn)**	**2-54 (Zn)**	**2-55 (Zn)**	**2-56 (Cd)**	**2-57 (Cd)**	**2-58 (Hg)**	**2-59 (Hg)**	**2-60 (Hg)**	**2-61 (Hg)**	**2-62 (Hg)**
M–N	1.8765(16)	1.8781(19)	1.833(3)	1.867(4) 1.855(4)	1.841(2)	2.099(4)	2.100(4)	2.040(7) 2.040(6)	2.035(5) 2.047(5)	2.049(5)	2.012(4)	2.013(4)
M–X	2.2993(3)	2.2969(7)	2.2180(6)	2.2722(12) 2.2677(10)	2.2218(4)	2.7292(9)	2.6104(7)	2.5629(6) 2.5596(5)	2.5690(8) 2.5638(7)	2.5713(8)	2.5647(9)	2.5570(8)
N–M–X	131.30(5)	130.44(6)	160.41	159.38(11) 160.15(11)	158.62(6)	145.96(10)	164.84(11)	171.16(18) 17081(17)	177.62(15) 170.90(15)	170.31(13)	173.44(11)	174.40(13)
M–O	1.9936(16)	1.9869(18)	–	–	–	–	–	–	–	–	–	–
N–M–O	119.76(7)	121.73(8)	–	–	–	–	–	–	–	–	–	–
M···M′	–	–	–	–	–	3.822	–	–	–	–	–	–
M–X′	–	–	–	–	–	2.8889(10)	–	–	–	–	–	–
M–X–M′	–	–	–	–	–	85.68(4)	–	–	–	–	–	–
X–M–X′	–	–	–	–	–	94.32(4)	–	–	–	–	–	–

of the ligand (closest Hg···C_{phenyl} = 3.240 Å **2-58**, 3.265 Å **2-59**, 3.166 Å **2-60**, 3.203 Å **2-61** and 3.376 Å **2-62**). The complexes mirror the previously reported amido mercury halide complexes, **2-10**–**2-12**, as well as the corresponding terphenyl mercury iodide compound **2-32**, with no large structural diversity over the series.

2.4 Conclusion

In summary, five extremely bulky amide ligands have been utilized in the preparation of rare examples of monodentate amido first row transition metal(II) halide and group 12 metal halide complexes in moderate to high yields on multigram scales. All prepared complexes have been spectroscopically characterized and their X-ray crystal structures determined. The Cr, Mn, Fe and Co complexes are all high-spin, antiferromagnetically coupled halide bridged dimers, which possess square-planar (Cr) or tetrahedral (Mn, Fe and Co) metal coordination geometries.

The amido group 12 metal halides are almost exclusively monomeric, with the exception of the iodide bridge cadmium complex **2-56**. The amido zinc and cadmium halide complexes were found to display either planar three-coordinate, or distorted linear metal geometries, depending on the steric bulk of the ligand. All of the amido mercury iodide complexes, independent of the ligand size, were found to possess two coordinate metal centres.

2.5 Experimental

General methods. All manipulations were carried out using standard Schlenk and glove box techniques under an atmosphere of high purity dinitrogen. THF, hexane, cyclohexane and toluene were distilled over molten potassium, while diethyl ether and pentane were distilled over sodium/potassium alloy (1:1). ^{1}H, $^{13}C\{^{1}H\}$, $^{29}Si\{^{1}H\}$ $^{113}Cd\{^{1}H\}$ and $^{199}Hg\{^{1}H\}$ NMR spectra were recorded on either Bruker DPX300, Bruker AvanceIII 400 or Varian Inova 500 spectrometers and were referenced to the resonances of the solvent used, external $SiMe_4$, $Cd(ClO_4)_2$ or Me_2Hg. Mass spectra were recorded on an Agilent Techonlogies 5975D inert MSD with a solid-state probe or obtained from the EPSRC National Mass Spectrometric Service at Swansea University. IR spectra were recorded using a Perkin-Elmer RX1 FT-IR spectrometer as Nujol mulls between NaCl plates or recorded as solid samples using an Agilent Cary 630 attenuated total reflectance (ATR) spectrometer. Microanalyses were carried out by the Science Centre, London Metropolitan University. A reproducible microanalysis for **2-44** could not be obtained because of its highly air sensitive nature, and because total removal of the hexane and THF of crystallization proved difficult by vacuum drying the compound at elevated temperature. A reproducible microanalysis for **2-48** could also not be obtained as it

slowly loses its THF of coordination in the solid state, yielding **2-49**. Melting points were determined in sealed glass capillaries under dinitrogen and are uncorrected. Solution state effective magnetic moments were determined by the Evans method [39]. The potassium amides [Ar*($SiMe_3$)NK(η^6-toluene)], [Ar*($SiPh_3$)NK], and [Ar†(Si^iPr_3)NK] were prepared as discussed in Sect. 2.3.1. All other reagents were used as received.

Preparation of [Ar*(Si^iPr_3)NH]. To a suspension of Ar*NH_2 (10.0 g, 22.7 mmol) in THF (100 mL) was added ^{n}BuLi (14.9 mL of a 1.6 M solution in hexanes) at −80 °C over 10 min. The reaction mixture was warmed to room temperature and stirred for a further 2 h, producing a white precipitate. Subsequently, neat triisopropylsilyl chloride (4.82 g, 25.0 mmol) was added, and the reaction mixture was warmed to 60 °C and stirred for 12 h, whereupon volatiles were removed *in vacuo*. The residue was extracted with toluene (100 mL), the extract filtered and volatiles removed *in vacuo* to give an off white solid, which was washed with hexane (3 × 25 mL) to give [Ar*(Si^iPr_3)NH] as an off white powder (9.80 g, 73 %). Mp: 224–226 °C; ^{1}H NMR (499 MHz, C_6D_6, 298 K): δ = 1.05 (d, $^3J_{HH}$ = 7.5 Hz, 18H, CH(CH_3)$_2$), 1.31 (sept, $^3J_{HH}$ = 7.5 Hz, 3H, C*H*(CH_3)$_2$), 1.83 (s, 3H, ArCH_3), 6.28 (s, 2H, Ph_2CH), 6.89 (s, 2H, *o*-Ar*H*), 7.01–7.21 (m, 20H, Ar*H*); ^{13}C{^{1}H} NMR (75 MHz, C_6D_6): δ = 14.9 (Si{*C*H(CH_3)$_2$}$_3$), 19.1 (Si{CH(*C*H_3)$_2$}$_3$), 21.2 (Ar*C*H_3), 52.5 (*C*HPh_2), 126.6, 128.6, 130.1, 130.3, 132.5, 141.0, 141.1, 144.9 (Ar-*C*); ^{29}Si{^{1}H} NMR (80 MHz, C_6D_6): δ = 3.3(s); IR υ/cm^{-1} (Nujol): 1598(m), 1493(m), 1443(s), 1354(m), 1255(m), 1128(m), 1076(m), 1030 (m), 914(m), 879(s), 762(m), 721(s), 698(s), 661(s); MS/EI *m/z* (%): 595.5 (M^+, 41), 552.4 (M^+–^{i}Pr, 100), 167.1 (Ph_2CH^+, 84); acc. mass MS/ESI calc. for $C_{42}H_{50}NSi$ (Ar*N(H)Si^iPr_3 +H^+): 596.3713, found: 596.3701.

Preparation of [Ar†($SiMe_3$)NK(OEt_2)]. To a suspension of KH (0.557 g, 13.9 mmol) in THF (40 mL) was added a solution of Ar†($SiMe_3$)NH (5.00 g, 9.26 mmol) in THF (40 mL) at room temperature. To the reaction mixture was added 7 mol% of hexamethyldisilazane (0.10 ml, 0.62 mmol), and the mixture warmed to 60 °C, where the evolution of hydrogen gas was observed. The reaction was stirred for a further 12 h at 60 °C, whereupon it was cooled to room temperature, filtered and volatiles removed *in vacuo*. The brown red residue was washed with hot hexane (2 × 30 mL) and diethyl ether (2 × 30 mL) to give [Ar†($SiMe_3$)NK(OEt_2)] as an off white powder (5.10 g, 84 %). Mp: 241–244 °C; ^{1}H NMR (499 MHz, C_6D_6, 298 K): δ = 0.41 (s, 9H, Si(CH_3)$_3$), 1.12 (d, $^3J_{HH}$ = 6.9 Hz, 6H, CH(CH_3)$_2$), 2.67 (sept, $^3J_{HH}$ = 6.9 Hz, 1H, C*H*(CH_3)$_2$), 6.51–7.39 (m, 24H, Ph_2CH and Ar*H*); ^{13}C{^{1}H} NMR (101 MHz, C_6D_6): δ = 5.5 (Si(*C*H_3)$_3$), 25.0 (ArCH(*C*H_3)$_2$), 33.9 (Ar*C*H(CH_3)$_2$), 53.6 (*C*HPh_2), 124.6, 125.8, 125.9, 126.6, 127.5, 128.6, 130.1, 130.3, 130.6, 131.2, 139.2, 144.9, 146.6, 151.3, 155.4 (Ar-*C*); ^{29}Si{^{1}H} NMR (80 MHz, C_6D_6): δ = −32.8(s); IR υ/cm^{-1} (Nujol): 1596(m), 1491(m), 1428(s), 1328(s), 1230(m), 1103(m), 1070(m), 1028(m), 979(s), 955(s), 860(m), 827(s), 811(s), 761(s), 704(s); MS/EI *m/z* (%): 577.5 (Ar†N(K)$SiMe_3^+$, 9), 539.5 (Ar†N(H)$SiMe_3^+$, 100), 466.4 (Ar†NH^+, 22), 167.2 (Ph_2CH^+, 41), 73.2 (Me_3Si^+, 53); anal. calc. for $C_{42}H_{50}KNOSi$: C 77.37 %, H 7.73 %, N 2.15 %, found: C 77.28 %, H 7.78 %, N 2.24 %.

Preparation of [Ar*(Si^{i}Pr$_3$)NK(OEt$_2$)]. To a suspension of KH (0.505 g, 12.6 mmol) in THF (40 mL) was added a solution of Ar*(Si^{i}Pr$_3$)NH (5.00 g, 8.40 mmol) in THF (40 mL) and hexamethyldisilazane (0.10 mL, 0.62 mmol, 7 mol%) at ambient temperature. The reaction mixture was warmed to 60 °C, whereupon the evolution of hydrogen gas was observed. The mixture was stirred for a further 12 h. It then was allowed to cool to ambient temperature before it was filtered, and volatiles removed from the filtrate *in vacuo*. The red brown residue was washed with hot hexane (2 × 30 mL) and ice cold diethyl ether (2 × 20 mL) to give [Ar*(Si^{i}Pr$_3$)NK(OEt$_2$)] as an off white powder (5.30 g, 89 %). Mp: >260 °C; N.B. diethyl ether resonances appear at the same chemical shifts as for uncoordinated Et$_2$O in C_6D_6; ^{1}H NMR (499 MHz, C_6D_6, 298 K): δ = 1.34 (d, $^3J_{HH}$ = 7.4 Hz, 18H, CH(CH_3)$_2$), 1.52 (sept, $^3J_{HH}$ = 7.4 Hz, 3H, CH(CH$_3$)$_2$), 2.10 (s, 3H, ArCH_3), 6.60–7.41 (m, 24H, Ph$_2$CH and ArH); ^{13}C{^{1}H} NMR (101 MHz, C_6D_6): δ = 17.7 (*C*H(CH$_3$)$_2$), 21.1 (CH(*C*H$_3$)$_2$), 21.4 (Ar*C*H$_3$), 52.7 (Ph$_2$*C*H), 119.8, 125.4, 125.9, 127.5, 128.5, 129.0, 130.5, 130.9, 139.2, 147.0, 150.9, 156.9 (Ar-*C*); ^{29}Si{^{1}H} NMR (80 MHz, C_6D_6): δ = −23.4 (s); IR υ/cm^{-1} (Nujol): 1599 (m), 1492(m), 1421(s), 1308(s), 1075(m), 1030(m), 997(m), 946(m), 910(m), 880 (m), 764(m), 700(s), 674(m); MS/EI *m/z* (%): 633.5 (Ar*N(K)Si^{i}Pr$_3^+$, 5), 595.5 (Ar*N(H)Si^{i}Pr$_3^+$, 33), 552.4 (Ar*N(H)Si^{i}Pr$_2^+$, 64), 167.1 (Ph$_2$CH$^+$, 100); anal. calc. for $C_{46}H_{58}KNOSi$: C 78.02 %, H 8.26 %, N 1.98 %, found: C 77.91 %, H 8.26 %, N 2.01 %.

Preparation of [{Ar*(SiMe$_3$)NCr(THF)(μ-Cl)}$_2$], 2-41. To a solution of $CrCl_2$ (0.096 g, 0.779 mmol) in THF (30 mL) was added a solution of [Ar*(SiMe$_3$)NK (η^6-toluene)] (0.500 g, 0.779 mmol) in THF (10 mL) at −80 °C over 5 min. The reaction mixture was warmed to room temperature and stirred for a further 2 h, whereupon volatiles were removed *in vacuo*. The residue was extracted with warm toluene (40 mL), the extract filtered and volatiles removed from the filtrate *in vacuo* to give **2-41** as a turquoise solid (0.38 g, 73 %). N.B. X-ray quality crystals of **2-41** were obtained by recrystallizing this solid from warm THF. Mp: 305–308 °C (248–250° C decomp.); ^{1}H NMR (499 MHz, C_6D_6, 298 K): δ = −11.71, −4.42(br.), 6.72, 10.15(br.), 10.94(br.), 16.61(br.), 36.09(br.); IR υ/cm^{-1} (Nujol): 1597(m), 1491(s), 1346(m), 1254(s), 1207(m), 1067(s), 1030(m), 1015(m), 917(s), 857(s), 829(s), 748(m), 716(m), 702(s), 603(m), 559(m); MS/EI *m/z* (%): 511.3 (Ar*N(H)SiMe$_3^+$, 87), 439.2 (Ar*NH$_2^+$, 79), 167.0 (Ph$_2$CH$^+$, 33), 73.0 (Me$_3$Si$^+$, 20); μ_{eff} (Evans, C_6D_6, 298 K): 5.81 μ_B; anal. calc. for $C_{80}H_{88}Cl_2Cr_2N_2O_2Si_2$: C 71.67 %, H 6.62 %, N 2.09 %, found: C 71.82 %, H 6.51 %, N 2.13 %.

Preparation of [{Ar*(SiPh$_3$)NCr(μ-Cl)}$_2$], 2-42. To a solution of $CrCl_2$ (0.092 g, 0.747 mmol) in THF (30 mL) was added a solution of [Ar*(SiPh$_3$)NK] (0.500 g, 0.679 mmol) in THF (10 mL) at −80 °C over 5 min. The reaction mixture was warmed to room temperature and stirred for a further 2 h, whereupon volatiles were removed *in vacuo*. The residue was extracted with toluene (40 mL), the extract filtered and volatiles removed from the filtrate *in vacuo* to give **2-42** as a green solid (0.41 g, 81 %). N.B. X-ray quality crystals of **2-42** were obtained by recrystallizing this solid from toluene. Mp: 156–159 °C; ^{1}H NMR (499 MHz, d_8-toluene, 298 K): δ = −12.88, 0.89, 1.23, 1.83, 3.02(br.), 6.00, 6.75, 7.51, 10.05

(br.), 14.97(br.); IR υ/cm^{-1} (Nujol): 1597(m), 1491(s), 1283(m), 1263(s), 1138(m), 1103(s), 1087(m), 1076(m), 1029(m), 944(m), 790(m), 720(s), 700(s), 604(m), 560 (m), 539(m), 507(m); MS/EI *m/z* (%): 697.4 ($Ar^*N(H)SiPh_3^+$, 81), 439.2 ($Ar^*NH_2^+$, 83), 259.1 (Ph_3Si^+, 100) 167.0 (Ph_2CH^+, 17); anal. calc. for $C_{102}H_{84}Cl_2Cr_2N_2Si_2$: C 78.09 %, H 5.40 %, N 1.79 %, found: C 77.99 %, H 5.49 %, N 1.83 %.

Preparation of [{Ar*(SiMe$_3$)NMn(THF)(μ-Br)}$_2$], 2-43. To a suspension of $MnBr_2$ (0.184 g, 0.857 mmol) in THF (30 mL) was added a solution of [Ar*($SiMe_3$)NK(η^6-toluene)] (0.500 g, 0.779 mmol) in THF (10 mL) at −80 °C over 5 min. The reaction mixture was warmed to room temperature and stirred for a further 2 h, whereupon volatiles were removed *in vacuo*. The residue was extracted with warm toluene (40 mL), the extract filtered and slowly cooled to 5 °C overnight to give **2-43** as pink crystals (0.42 g, 75 %). Mp: 222–224 °C; ^{1}H NMR (499 MHz, C_6D_6, 298 K): δ = 0.92(br.), 1.36(br.), 7.54(br.), 34.45(br.), 41.06(br.); IR ν/cm^{-1} (Nujol): 1598(m), 1493(m), 1260(s), 1241(s), 1208(m), 1130(m), 1076 (m), 1030(m), 1013(m), 916(s), 906(s), 856(s), 832(s), 727(s), 700(s), 674(m), 622 (m), 606(m), 554(m), 531(m); MS/EI *m/z* (%): 511.2 ($Ar^*N(H)SiMe_3^+$, 100), 438.2 (Ar^*NH^+, 23), 167.0 (Ph_2CH^+, 25); μ_{eff} (Evan's, C_6D_6, 298 K): 5.90 μ_B; anal. calc. for $C_{80}H_{88}Br_2Mn_2N_2O_2Si_2$: C 66.94 %, H 6.18 %, N 1.95 %, found: C 66.84 %, H 6.26 %, N 1.98 %.

Preparation of [{Ar*(SiPh$_3$)NMn(THF)(μ-Br)}$_2$], 2-44. To a suspension of $MnBr_2$ (0.143 g, 0.747 mmol) in THF (30 mL) was added a solution of [Ar*($SiPh_3$)NK] (0.500 g, 0.679 mmol) in THF (10 mL) at −80 °C over 5 min. The reaction mixture was warmed to room temperature and stirred for a further 2 h, whereupon volatiles were removed *in vacuo*. The residue was extracted with toluene (40 mL), the extract filtered and volatiles removed from the filtrate *in vacuo* to give **2-44** as a pale pink solid (0.38 g, 62 %). N.B. X-ray quality crystals were obtained from crystallizing this solid from a mixture of toluene and hexane. Mp: 296–299 °C (decomp. on melting); ^{1}H NMR (499 MHz, C_6D_6, 298 K): δ = −34.71(br) 0.87, 0.93, 1.37, 33.04(br), 40.81(br); IR υ/cm^{-1} (Nujol): 1597(m), 1492(s), 1425(s), 1260(m), 1229(m), 1207(m), 1128(m), 1101(s), 1029(m), 903(s), 798(m), 736(m), 729(s), 702(s), 605(m), 577(m), 556(m), 540(m), 504(m); MS/EI *m/z* (%): 697.3 ($Ar^*N(H)SiPh_3^+$, 54), 439.2 ($Ar^*NH_2^+$, 18), 259.0 (Ph_3Si^+, 100), 167.0 (Ph_2CH^+, 11); μ_{eff} (Evans, C_6D_6, 298 K): 6.85 μ_B.

Preparation of [{Ar†(Si^{i}Pr$_3$)NMn(THF)(μ-Br)}$_2$], 2-45. To a suspension of $MnBr_2$ (0.160 g, 0.747 mmol) in THF (30 mL) was added a solution of [$Ar^\dagger(Si^iPr_3)$NK(OEt_2)] (0.500 g, 0.679 mmol) in THF (10 mL) at −80 °C over 5 min. The reaction mixture was warmed to room temperature and stirred for a further 12 h, whereupon volatiles were removed *in vacuo*. The residue was extracted with warm benzene (40 mL), the extract filtered and slowly cooled to 6 °C overnight to give **2-45** as pink crystals (0.365 g, 65 %). Mp: 191–194 °C; ^{1}H NMR (499 MHz, C_6D_6, 298 K): δ = 2.47 (br.), 15.51 (br.); IR ν/cm^{-1} (Nujol): 1595(m), 1491(s), 1227(s), 1205(m), 1166(m), 1120(m), 1070(m), 1032(m), 1013(m), 891(s), 863(m), 850(m), 798(m), 764(m), 726(s), 702(s), 679(s), 658(m), 604(m), 594(m); MS/EI *m/z* (%): 715.2 ($Ar^\dagger(Si^iPr_2)NMnBr^+$, 1), 623.4 ($Ar^\dagger N(H)Si^iPr_3^+$, 46), 580.4 ($Ar^\dagger N(H)Si^iPr_2^+$, 100), 467.3 ($Ar^\dagger NH_2^+$, 80), 167.0 ($Ph_2CH^+$, 48); μ_{eff} (Evan's, C_6D_6,

298 K): 6.9 μ_B; anal. calc. for $C_{96}H_{120}Br_2Mn_2N_2O_2Si_2$: C 69.47 %, H 7.29 %, N 1.69 %, found: C 69.53 %, H 7.33 %, N 1.73 %.

Preparation of [{Ar*(SiMe$_3$)NFe(THF)(μ-Br)}$_2$], 2-46. To a suspension of $FeBr_2$ (0.185 g, 0.857 mmol) in THF (30 mL) was added a solution of [Ar*(SiMe$_3$)NK(η^6-toluene)] (0.500 g, 0.779 mmol) in THF (10 mL) at −80 °C over 5 min. The reaction mixture was warmed to room temperature and stirred for a further 2 h, whereupon volatiles were removed from the filtrate *in vacuo*. The residue was extracted with toluene (40 mL), the extract filtered and volatiles removed from the filtrate *in vacuo* to give **2-46** as a yellow solid (0.32 g, 57 %). N.B. X-ray quality crystals of **2-46** were obtained by crystallizing this solid from a mixture of THF and hexane. Mp: 210-212 °C (88-92 °C decomp.); ^{1}H NMR (400 MHz, C_6D_6, 298 K): δ = −21.01(br.), −4.07, 3.99, 13.36, 15.19, 21.35, 28.35(br.), 71.19(br.); IR υ/cm^{-1} (Nujol): 1598(m), 1493(s), 1260(s), 1242(s), 1208(m), 1129(m), 1077(m), 1030(m), 1015(m), 917(m), 902(s), 860(s), 836(s), 766(m), 749(m), 730(s), 703(s), 605(m), 555(m), 535(m); MS/CI *m/z* (%): 647.0 ({M/2 –THF}$^+$, 100), 435.1 (Ar*NH$_2^+$, 17); μ_{eff} (Evans, C_6D_6, 298 K): 5.38 μ_B; anal. calc. for $C_{80}H_{88}Br_2Fe_2N_2O_2Si_2$: C 66.85 %, H 6.17 %, N 1.95 %, found: C 66.92 %, H 6.25 %, N 2.06 %.

Preparation of [{Ar*(SiPh$_3$)NFe(THF)(μ-Br)}$_2$], 2-47. To a suspension of $FeBr_2$ (0.161 g, 0.747 mmol) in THF (30 mL) was added a solution of [Ar*(SiPh$_3$)NK] (0.500 g, 0.679 mmol) in THF (10 mL) at −80 °C over 5 min. The reaction mixture was warmed to room temperature and stirred for a further 2 h, whereupon volatiles were removed *in vacuo*. The residue was extracted with toluene (40 mL), the extract filtered and volatiles removed from the filtrate *in vacuo* to give **2-47** as a yellow solid (0.43 g, 70 %). N.B. X-ray quality crystals of **2-47** were obtained from crystallizing this solid from a mixture of toluene and hexane. Mp: 276–279 °C; ^{1}H NMR (400 MHz, C_6D_6, 298 K): δ = −41.70(br.), 3.50(br.), 5.57(br.), 12.64(br.), 64.17(br.), 73.59(br.); IR υ/cm^{-1} (Nujol): 1596(m), 1492(m), 1237(m), 1209(m), 1130(m), 1105(s), 1030(m), 918(m), 903(s), 884(m), 852(m), 791(m), 743(m), 725 (s), 696(s), 604(m), 579(m), 558(m), 548(m), 506(m); MS/EI *m/z* (%): 833.3 (Ar*(SiPh$_3$)NFeBr$^+$, <1), 697.3 (Ar*N(H)SiPh$_3^+$, 82), 439.2 (Ar*NH$_2^+$, 20), 259.0 (Ph$_3$Si$^+$, 100), 167.0 (Ph$_2$CH$^+$, 10); μ_{eff} (Evans, C_6D_6, 298 K): 6.61 μ_B; anal. calc. for $C_{110}H_{100}Br_2Fe_2N_2O_2Si_2$: C 73.01 %, H 5.57 %, N 1.55 %, found: C 72.96 %, H 5.41 %, N 1.57 %.

Preparation of [{Ar*(SiPh$_3$)NCo(THF)(μ-Cl)}$_2$], 2-48. Compound **2-49** (0.100 g, 0.063 mmol) was dissolved in THF (5 mL) and stirred for 5 min at room temperature to give a blue/green solution. Volatiles were removed *in vacuo* to yield **2-48** as a green solid (0.107 g, 99 %). N.B. X-ray quality crystals of **2-48** were obtained by recrystallizing this solid from a mixture of toluene and hexane. Mp: 239–243 °C (118–121 °C turns orange/brown); ^{1}H NMR (499 MHz, C_6D_6/d_8-THF, 298 K): δ = −22.13, −14.11, −0.99, 5.10, 10.22, 11.88, 18.07, 49.56, 54.56; IR υ/cm^{-1} (Nujol): 1597(m), 1492(m), 1260(s), 1100(s), 1076(s), 1018(s), 896(m), 880(m), 799(s), 738(m), 697(s), 604(m), 542(m), 504(m); μ_{eff} (Evans, C_6D_6/d_8-THF, 298 K): 5.20 μ_B.

Preparation of [{Ar*(SiPh$_3$)NCo(μ-Cl)}$_2$], 2-49. To a suspension of $CoCl_2$ (0.088 g, 0.679 mmol) in THF (30 mL) was added a solution of [Ar*(SiPh$_3$)NK] (0.500 g, 0.679 mmol) in THF (10 mL) at −80 °C over 5 min. The reaction mixture was warmed to room temperature and stirred for a further 2 h, whereupon volatiles were removed *in vacuo*. The residue was extracted with toluene (40 mL), the extract filtered and volatiles removed *in vacuo* and washed with hexane (20 mL) to give **2-49** as an orange solid (0.23 g, 43 %). N.B. X-ray quality crystals of **2-49** were obtained from crystallizing this solid from a mixture of toluene and hexane. Mp: 241–244 °C; ^{1}H NMR (499 MHz, C_6D_6/d_8-THF, 298 K): δ = −52.82, −49.44, −40.48, 1.37, 7.01, 7.58, 12.11, 14.29, 16.29, 25.62, 59.17, 75.70, 123.04(br); IR υ/cm^{-1} (Nujol): 1598(m), 1425(s), 1257(m), 1216(m), 1130(m), 1100(s), 1029(m), 895(s), 797(m), 722(s), 708(s), 697(s), 624(m), 574(m), 557(m), 540(m), 502(m); MS/EI *m/z* (%): 790.3 (Ar*(SiPh$_3$)NCoCl$^+$, 1), 755.3 (Ar*(SiPh$_3$)NCo$^+$, 5), 697.4 (Ar*N(H)SiPh$_3^+$, 76), 438.2 (Ar*NH$^+$, 10), 259.1 (Ph$_3$Si$^+$, 100), 167.0 (Ph$_2$CH$^+$, 13); μ_{eff} (Evans, C_6D_6, 298 K): 4.86 μ_B; anal. calc. for $C_{102}H_{84}Cl_2Co_2N_2Si_2$: C 77.40 %, H 5.35 %, N 1.77 %, found: C 77.31 %, H 5.37 %, N 1.80 %.

Preparation of [Ar*(SiMe$_3$)NZnBr(THF)], 2-51. To a suspension of $ZnBr_2$ (0.192 g, 0.857 mmol) in THF (30 mL) was added a solution of [Ar*(SiMe$_3$)NK (η^6-toluene)] (0.500 g, 0.779 mmol) in THF (10 mL) at −80 °C over 5 min. The reaction mixture was warmed to room temperature and stirred for a further 2 h, whereupon volatiles were removed *in vacuo*. The residue was extracted with toluene (40 mL), the extract filtered and volatiles removed from the filtrate *in vacuo* to give **2-51** as an off white solid (0.43 g, 76 %). N.B. X-ray quality crystals of **2-51** were obtained by recrystallizing this solid from a mixture of THF and hexane. Mp: 176–180 °C; ^{1}H NMR (400 MHz, C_6D_6, 298 K): δ = 0.52 (s, 9H, Si(C*H*$_3$)$_3$), 0.83 (m, 4H, C*H*$_2$), 1.98 (s, 3H, ArC*H*$_3$), 2.66 (m, 4H, C*H*$_2$O), 6.54 (s, 2H, Ph$_2$C*H*), 6.91 (t, *J* = 7.6 Hz, 2H, Ar*H*), 7.02–7.18 (m, 12H, Ar*H*), 7.35 (d, *J* = 8.0 Hz, 4H, Ar*H*), 7.50 (d, *J* = 6.8 Hz, 4H, Ar*H*); ^{13}C{^{1}H} NMR (101 MHz, C_6D_6): δ = 4.0 (Si(*C*H$_3$)$_3$), 21.3 (Ar*C*H$_3$), 24.6 (*C*H$_2$), 52.0 (Ph$_2$*C*H), 70.1 (*C*H$_2$O), 126.4, 126.8, 128.5, 129.4, 129.7, 129.8, 130.2, 130.4, 141.7, 144.7, 145.4, 150.2 (Ar-*C*); ^{29}Si{^{1}H} NMR (80 MHz, C_6D_6): δ = 1.0 (s); IR υ/cm^{-1} (Nujol): 1597(m), 1492(s), 1262(s), 1244(s), 1207(m), 1125(m), 1075(m), 1032(m), 1014(m), 931(s), 860(s), 849(s), 829(s), 767(m), 733(s), 709(s), 697(s), 604(m), 554(m); MS/CI *m/z* (%): 656.1 (M$^+$ –THF, 2), 512.3 (Ar*N(H)SiMe$_3$ +H$^+$, 100), 440.2 (Ar*NH$_2$ +H$^+$, 35), 167.0 (Ph$_2$CH$^+$, 19); anal. calc. for $C_{40}H_{44}BrNOSiZn$: C 65.98 %, H 6.09 %, N 1.92 %, found: C 66.07 %, H 6.13 %, N 2.06 %.

Preparation of [Ar†(SiMe$_3$)NZnBr(THF)], 2-52. To a suspension of $ZnBr_2$ (0.190 g, 0.844 mmol) in THF (30 mL) was added a solution of [Ar†(SiMe$_3$)NK (OEt$_2$)] (0.500 g, 0.767 mmol) in THF (10 mL) at −80 °C over 5 min. The reaction mixture was warmed to room temperature and stirred for a further 2 h, whereupon volatiles were removed *in vacuo*. The residue was extracted with toluene (40 mL), the extract filtered and concentrated *in vacuo* (to *ca.* 10 ml). Hexane (50 mL) was added, and stirred for a further 10 min producing a white precipitate, which was filtered and dried to give **2-52** as a white powder (0.370 g, 64 %). X-ray quality crystals of **2-52** were obtained by recrystallizing this solid from hot toluene. Mp:

176–178 °C; ^{1}H NMR (499 MHz, C_6D_6, 298 K): δ = 0.50 (s, 9H, Si(CH_3)$_3$), 0.80 (br., 4H, CH_2), 0.98 (d, $^{3}J_{HH}$ = 6.9 Hz, 6H, CH(CH_3)$_2$), 2.51 (br., 4H, CH_2O), 2.54 (sept., $^{3}J_{HH}$ = 6.9 Hz, 1H, CH(CH$_3$)$_2$), 6.55 (s, 2H, Ph$_2$CH), 6.92–7.54 (m, 22H, ArH); ^{13}C{^{1}H} NMR (75 MHz, C_6D_6): δ = 4.0 (Si(CH_3)$_3$), 24.4 (CH(CH_3)$_2$), 24.6 (CH_2), 33.8 (CH(CH$_3$)$_2$), 52.1 (Ph$_2$CH), 70.3 (CH_2O), 126.4, 126.7, 126.8, 128.4, 129.7, 129.9, 130.2, 141.5, 141.6, 145.0, 145.5, 150.6 (Ar-C); ^{29}Si{^{1}H} NMR (80 MHz, C_6D_6): δ = 1.2 (s); IR υ/cm^{-1} (Nujol): 1599(m), 1493(m), 1446(s), 1247 (s), 1223(m), 1031(m), 1016(m), 923(s), 849(s), 831(s), 767(m), 731(s), 699(s); MS/CI *m/z* (%): 683.3 (M$^+$ –THF, <1), 539.5 (Ar†N(H)SiMe$_3^+$, 69), 467.4 (Ar†NH$_2^+$, 100), 167.0 (Ph$_2$CH$^+$, 31), 73.1 (THF +H$^+$, 11); anal. calc. for $C_{42}H_{48}BrNOSiZn$: C 66.71 %, H 6.40 %, N 1.85 %, found: C 66.61 %, H 6.48 %, N 1.91 %.

Preparation of [Ar*(SiPh$_3$)NZnBr], 2-53. To a suspension of $ZnBr_2$ (0.168 g, 0.747 mmol) in THF (30 mL) was added a solution of [Ar*(SiPh$_3$)NK] (0.500 g, 0.679 mmol) in THF (10 mL) at −80 °C over 5 min. The reaction mixture was warmed to room temperature and stirred for a further 2 h, whereupon volatiles were removed *in vacuo*. The residue was extracted with toluene (40 mL), the extract filtered and volatiles removed from the filtrate *in vacuo* to give **2-53** as an off white solid (0.45 g, 79 %). N.B. X-ray quality crystals of **2-53** were obtained by recrystallizing this solid from a mixture of toluene and hexane. Mp: 248–250 °C; ^{1}H NMR (400 MHz, C_6D_6, 298 K): δ = 1.89 (s, 3H, ArCH_3), 6.14 (s, 2H, Ph$_2$CH), 6.45 (d, $^{3}J_{HH}$ = 7.0 Hz, 4H, ArH), 6.73 (s, 2H, ArH), 6.81 (d, J = 7.0 Hz, 2H, ArH), 6.94–7.27 (m, 23H, ArH), 7.66 (d, $^{3}J_{HH}$ = 8.0 Hz, 6H, ArH); ^{13}C{^{1}H} NMR (101 MHz, C_6D_6): δ = 21.3 (ArCH$_3$), 53.0 (Ph$_2$$C$H), 126.5, 128.4, 128.5, 128.6, 129.1, 129.8, 130.2, 130.4, 130.5, 131.3, 132.5, 136.8, 142.3, 144.6, 144.7 (Ar-C); ^{29}Si{^{1}H} NMR (80 MHz, C_6D_6): δ = −18.9 (s); IR υ/cm^{-1} (Nujol): 1597(m), 1586 (m), 1489(m), 1237(s), 1216(s), 1136(m), 1105(s), 1076(m), 1031(m), 924(s), 909 (s), 879(m), 849(s), 763(m), 756(m), 737(s), 700(s), 602(s), 575(m), 555(s), 506(s); MS/EI *m/z* (%): 841.2 (M$^+$, 7), 697.4 (Ar*N(H)SiPh$_3^+$, 100), 439.2 (Ar*NH$_2^+$, 81), 259.1 (Ph$_3$Si$^+$, 71), 167.0 (Ph$_2$CH$^+$, 16); anal. calc. for $C_{51}H_{42}BrNSiZn$: C 72.73 %, H 5.03 %, N 1.66 %, found: C 72.84 %, H 5.13 %, N 1.56 %.

Preparation of [Ar*(Si^{i}Pr$_3$)NZnBr], 2-54. To a suspension of $ZnBr_2$ (0.350 g, 1.55 mmol) in diethyl ether (25 mL) was added a fine suspension of [Ar*(Si^{i}Pr$_3$)NK(OEt$_2$)] (1.00 g, 1.41 mmol) in diethyl ether (25 mL) at −80 °C over 5 min. The reaction mixture was warmed to room temperature and stirred for a further 12 h, whereupon volatiles were removed *in vacuo*. The residue was extracted with pentane (40 mL), the extract filtered, concentrated (to *ca.* 10 mL) and slowly cooled to −30 °C overnight to give **2-54** as colourless crystals (0.690 g, 66 %). Mp: 107–110 °C; ^{1}H NMR (499 MHz, C_6D_6, 298 K): δ = 1.25 (d, $^{3}J_{HH}$ = 7.5 Hz, 18H, Si{CH(CH_3)$_2$}$_3$), 1.53 (sept, $^{3}J_{HH}$ = 7.5 Hz, 3H, Si{CH(CH$_3$)$_2$}$_3$), 1.87 (s, 3H, ArCH_3), 6.43 (s, 2H, Ph$_2$CH), 6.81–7.22 (m, 22H, ArH); ^{13}C{^{1}H} NMR (75 MHz, C_6D_6): δ = 15.6 (Si{CH(CH$_3$)$_2$}$_3$), 19.1 (Si{CH(CH_3)$_2$}$_3$), 21.2 (ArCH$_3$), 52.8 (CHPh$_2$), 126.8, 128.4, 128.9, 129.4, 129.5, 130.5, 131.5, 131.8, 142.5, 144.5, 144.7 (Ar-C); ^{29}Si{^{1}H} NMR (80 MHz, C_6D_6): δ = 2.5 (s); IR υ/cm^{-1} (Nujol): 1598(m), 1493(m), 1439(s), 1233(s), 1212(m), 1133(m), 1075(m), 914(m), 899(s), 879(s), 842(s), 762(m), 746(s), 699(s), 657(s); MS/EI *m/z* (%):

595.5 (Ar*N(H)Si^{i}Pr$_3^+$, 36), 552.5 (Ar*N(H)Si^{i}Pr$_2^+$, 100), 439.3 (Ar*NH$_2^+$, 39), 167.1 (Ph$_2$CH$^+$, 88); anal. calc. for $C_{42}H_{48}BrNSiZn$: C 68.15 %, H 6.54 %, N 1.89 %, found: C 68.08 %, H 6.63 %, N 1.87 %.

Preparation of [Ar†(Si^{i}Pr$_3$)NZnBr], 2-55. To a suspension of $ZnBr_2$ (0.336 g, 1.49 mmol) in diethyl ether (20 mL) was added a fine suspension of [Ar†(Si^{i}Pr$_3$)NK(OEt$_2$)] (1.00 g, 1.36 mmol) in diethyl ether (20 mL) at −80 °C over 5 min. The reaction mixture was warmed to room temperature and stirred for a further 12 h, whereupon volatiles were removed *in vacuo*. The residue was extracted with pentane (40 mL), the extract filtered, concentrated (to *ca.* 10 mL) and slowly cooled to −30 °C overnight to give **2-55** as pale orange crystals (0.81 g, 78 %). Mp: 178–181 °C; ^{1}H NMR (499 MHz, C_6D_6, 298 K): δ = 0.93 (d, $^3J_{HH}$ = 7.0 Hz, 6H, ArCH(C*H*$_3$)$_2$), 1.24 (d, $^3J_{HH}$ = 7.5 Hz, 18H, Si{CH(C*H*$_3$)$_2$}$_3$), 1.53 (sept, $^3J_{HH}$ = 7.5 Hz, 3H, Si{C*H*(CH$_3$)$_2$}$_3$), (sept, $^3J_{HH}$ = 7.0 Hz, 1H, ArC*H*(CH$_3$)$_2$), 6.44 (s, 2H, Ph$_2$C*H*), 6.85–7.23 (m, 22H, Ar*H*); ^{13}C{^{1}H} NMR (75 MHz, C_6D_6): δ = 15.6 (Si{*C*H(CH$_3$)$_2$}$_3$), 19.8 (Si{CH(*C*H$_3$)$_2$}$_3$), 24.2 (ArCH(*C*H$_3$)$_2$), 33.8 (Ar*C*H(CH$_3$)$_2$), 53.0 (*C*HPh$_2$), 126.6, 126.7, 126.8, 128.4, 128.6, 128.9, 129.4, 130.1, 130.3, 131.5, 142.4, 142.9, 144.6, 144.8, 145.0, 146.6 (Ar-*C*); ^{29}Si{^{1}H} NMR (80 MHz, C_6D_6): δ = 2.53 (s); IR υ/cm^{-1} (Nujol): 1599(m), 1492(m), 1437 (s), 1382(m), 1259(m), 1234(m), 1158(m), 1125(m), 1074(m), 1031(m), 897(s), 883(s), 867(s), 839(s), 750(s), 699(s), MS/EI *m/z* (%): 767.2 (M$^+$, 2), 724.2 (M$^+$ –^{i}Pr, 10), 623.5 (Ar†N(H)Si^{i}Pr$_3^+$, 39), 580.4 (Ar†N(H)Si^{i}Pr$_2^+$, 100), 467.3 (Ar†NH$_2^+$, 14), 167.0 (Ph$_2$CH$^+$, 35); anal. calc. for $C_{44}H_{52}BrNSiZn$: C 68.79 %, H 6.82 %, N 1.82 %, found: C 68.66 %, H 6.90 %, N 1.78 %.

Preparation of [{Ar†(SiMe$_3$)NCd(μ-I)}$_2$], 2-56. To a solution of CdI_2 (0.62 g, 1.69 mmol) in THF (30 mL) was added a solution of [Ar†(SiMe$_3$)NK(OEt$_2$)] (1.00 g, 1.53 mmol) in THF (10 mL) at −80 °C over 5 min. The reaction mixture was slowly warmed to room temperature and stirred for a further 30 min, whereupon volatiles were removed *in vacuo*. The residue was extracted with toluene (40 mL), the extract filtered and concentrated (to *ca.* 10 mL). Hexane (50 mL) was added to the stirring solution producing a white precipitate, which was filtered and dried *in vacuo* to give **2-56** as a white powder (0.79 g, 66 %). N.B. X-ray quality crystals of **2-56** were grown by crystallizing this powder from hot cyclohexane. Mp: 205–208 °C (180–190 °C decomp.); ^{1}H NMR (499 MHz, C_6D_6, 298 K): δ = 0.37 (s, 18H, Si(C*H*$_3$)$_3$), 0.94 (d, $^3J_{HH}$ = 6.9 Hz, 12H, ArCH(C*H*$_3$)$_2$), 2.49 (sept, $^3J_{HH}$ = 6.9 Hz, 2H, ArC*H*(CH$_3$)$_2$), 6.34 (s, 4H, Ph$_2$C*H*), 6.89−7.21 (m, 44H, Ar*H*); ^{13}C{^{1}H} NMR (101 MHz, C_6D_6): δ = 4.0 (Si(*C*H$_3$)$_3$), 24.2 (ArCH(*C*H$_3$)$_2$), 33.8 (Ar*C*H(CH$_3$)$_2$), 53.2 (*C*HPh$_2$), 126.6, 126.7, 127.0, 128.7, 128.8, 129.3, 130.1, 130.3, 131.2, 141.7, 141.8, 144.5, 144.9 (Ar-*C*); ^{29}Si{^{1}H} NMR (80 MHz, C_6D_6): δ = −1.3(s); ^{113}Cd{^{1}H} NMR (89 MHz, C_6D_6): δ = 110.2(s); IR υ/cm^{-1} (Nujol): 1597(m), 1493(m), 1437(s), 1256(s), 1238(s), 1162(m), 1126(m), 1075(m), 1031 (m), 927(s), 894(m), 831(s), 751(s), 720(m), 697(s), 676(s); MS/EI *m/z* (%): 539.5 (Ar†N(H)SiMe$_3^+$, 75), 467.4 (Ar†NH$_2^+$, 100), 452.4 (Ar†NH$_2^+$ –CH$_3$, 74), 167.0 (Ph$_2$CH$^+$, 37); anal. calc. for $C_{76}H_{80}Cd_2I_2N_2Si_2$: C 58.65 %, H 5.18 %, N 1.80 %, found: C 58.72 %, H 5.27 %, N 1.74 %.

Preparation of [Ar*(SiPh$_3$)NCdI], 2-57. To a suspension of CdI_2 (0.274 g, 0.747 mmol) in THF (30 mL) was added a solution of [Ar*(SiPh$_3$)NK] (0.500 g, 0.679 mmol) in THF (10 mL) at −80 °C over 5 min. The reaction mixture was warmed to room atmospheric temerature and stirred for a further 2 h, whereupon volatiles were removed *in vacuo*. The residue was extracted with benzene (40 mL), the extract filtered and volatiles removed from the filtrate *in vacuo* to give **2-57** as a pale yellow solid (0.420 g, 72 %). N.B. X-ray quality crystals of **2-57** were obtained by recrystallizing this solid from diethyl ether. Mp: 255–258 °C (decomp. 203–205 °C); ^{1}H NMR (400 MHz, C_6D_6, 298 K): δ = 1.92 (s, 3H, ArCH_3), 6.20 (s, 2H, Ph_2CH), 6.44−7.69 (m, 37H, ArH); ^{13}C{^{1}H} NMR (75 MHz, C_6D_6): δ = 21.4 (ArCH$_3$), 52.9 (Ph_2CH), 128.4, 128.5, 128.7, 129.7, 130.2, 130.4, 130.6, 131.2, 131.9, 136.7, 142.2, 144.4, 144.7, 146.3 (Ar-C); ^{29}Si{^{1}H} NMR (80 MHz, C_6D_6): δ = −20.1 (s); ^{113}Cd{^{1}H} NMR (C_6D_6, 89 MHz): δ = 104.8; IR υ/cm^{-1} (Nujol): 1597(m), 1490(m), 1447(m), 1426(s), 1257(m), 1232(m), 1103(s), 1030(m), 926(s), 910(m), 835(m), 799(m), 765(m), 745(s), 733(s), 697(s); MS/CI *m/z* (%): 937.4 (M$^+$, 2), 697.6 (Ar*N(H)SiPh$_3^+$, 10), 438.3 (Ar*NH$^+$, 3), 259.1 (SiPh$_3^+$, 100), 167.1 (Ph_2CH^+, 17); anal. calc. for $C_{51}H_{42}CdINSi$: C 65.42 %, H 4.52 %, N 1.50 %, found: C 65.36 %, H 4.57 %, N 1.53 %.

Preparation of [Ar*(SiMe$_3$)NHgI], 2-58. To a suspension of HgI_2 (0.389 g, 0.857 mmol) in THF (30 mL) was added a solution of [Ar*(SiMe$_3$)NK(η^6-toluene)] (0.500 g, 0.779 mmol) in THF (10 mL) at −80 °C over 5 min. The reaction mixture was warmed to room temperature and stirred for a further 2 h, whereupon volatiles were removed *in vacuo*. The residue was extracted with toluene (20 mL), the extract filtered and volatiles removed from the filtrate *in vacuo* to give **2-58** as an orange solid (0.308 g, 79 %). N.B. X-ray quality crystals of **2-58** were obtained by recrystallizing this solid from hot toluene. Mp: 181–182 °C; ^{1}H NMR (400 MHz, C_6D_6, 298 K): δ = 0.32 (s, 9H, Si(CH_3)$_3$), 1.87 (s, 3H, ArCH_3), 6.31 (s, 2H, Ph_2CH), 6.82–7.18 (m, 22H, ArH); ^{13}C{^{1}H} NMR (75 MHz, C_6D_6): δ = 3.4 (Si(CH$_3$)$_3$), 21.2 (ArCH$_3$), 52.8 (Ph_2CH), 126.7, 128.7, 128.9, 129.5, 129.8, 130.0, 130.2, 130.3, 133.4, 143.0, 143.3, 143.4, 145.1 (Ar-C); ^{29}Si{^{1}H} NMR (80 MHz, C_6D_6): δ = 2.9 (s); ^{199}Hg{^{1}H} NMR (C_6D_6, 107.4 MHz): δ = −2001.6 (br.); IR υ/cm^{-1} (Nujol): 1598(m), 1492(s), 1442(s), 1247(s), 1215(m), 1075(m), 1030(m), 932(s), 846(s), 829(s), 754(s), 697(s); MS/EI *m/z* (%): 511.4 (Ar*N(H)SiMe$_3^+$, 100), 438.3 (Ar*NH$^+$, 47), 167.0 (Ph_2CH^+, 53), 73.1 (Me_3Si^+, 42); anal. calc. for $C_{36}H_{36}HgINSi$: C 51.58 %, H 4.33 %, N 1.67 %, found: C 51.62 %, H 4.32 %, N 1.76 %

Preparation of [Ar†(SiMe$_3$)NHgI], 2-59. To a solution of HgI_2 (0.77 g, 1.69 mmol) in THF (30 mL) was added a solution of [Ar†(SiMe$_3$)NK(OEt$_2$)] (1.00 g, 1.53 mmol) in THF (10 mL) at −80 °C over 5 min. The reaction mixture was slowly warmed to room temperature and stirred for a further 2 h, whereupon volatiles were removed *in vacuo*. The residue was extracted with toluene (40 mL), the extract filtered and concentrated (to *ca.* 10 mL). Hexane (50 mL) was added to the stirring solution producing a white precipitate, which was filtered and dried *in vacuo* to give **2-59** as a white powder (0.71 g, 53 %). N.B. X-ray quality crystals of **2-59** were obtained by recrystallizing this powder from a concentrated solution of

hot benzene. Mp: 202–204 °C; ^{1}H NMR (300 MHz, C_6D_6, 298 K): δ = 0.31 (s, 9H, Si(CH_3)$_3$), 0.90 (d, $^{3}J_{HH}$ = 6.9 Hz, 6H, ArCH(CH_3)$_2$), 2.45 (sept, $^{3}J_{HH}$ = 6.9 Hz, 1H, ArC*H*(CH$_3$)$_2$), 6.33 (s, 2H, Ph$_2$C*H*), 6.90–7.22 (m, 22H, Ar*H*); ^{13}C{^{1}H} NMR (75 MHz, C_6D_6): δ = 3.5 (Si(CH_3)$_3$), 24.2 (ArCH(CH_3)$_2$), 33.8 (ArCH(CH$_3$)$_2$), 53.0 (Ph$_2$CH), 126.6, 126.7, 128.9, 127.1, 127.3, 128.6, 128.7, 128.8, 128.9, 129.4, 130.0, 130.2, 130.3, 140.8, 141.7, 143.1, 143.2, 143.4, 143.7, 144.3, 144.9, 145.2 (Ar-*C*); ^{29}Si{^{1}H} NMR (80 MHz, C_6D_6): δ = 3.2 (s); ^{199}Hg{^{1}H} NMR (72 MHz, C_6D_6): δ = −2002.9; IR υ/cm^{-1} (Nujol): 1599(m), 1492(s), 1438(s), 1246(s), 1161(m), 1126(m), 1075(m), 1030(m), 927(s), 857(m), 830(s), 756(s), 734(m), 697(s); MS/EI *m/z* (%): 852.5 (M$^+$ –Me, <1), 539.5 (Ar†N(H)SiMe$_3^+$, 100), 167.2 (Ph$_2$CH$^+$, 48), 73.2 (SiMe$_3^+$, 72); anal. calc. for $C_{38}H_{40}HgINSi$: C 52.68 %, H 4.65 %, N 1.62 %, found: C 52.71 %, H 4.71 %, N 1.64 %.

Preparation of [Ar*(SiPh$_3$)NHgI], 2-60. To a suspension of HgI_2 (0.340 g, 0.747 mmol) in toluene (30 mL) was added a solution of [Ar*(SiPh$_3$)NK] (0.500 g, 0.679 mmol) in toluene (10 mL) at −80 °C over 5 min. The reaction mixture was warmed to room temperature and stirred for a further 4 h, whereupon volatiles were removed *in vacuo*. The residue was extracted with benzene (40 mL), the extract filtered and volatiles removed from the filtrate *in vacuo* to give **2-60** as an orange solid (0.440 g, 63 %). N.B. X-ray quality crystals of **2-60** were obtained by recrystallizing this solid from hexane and benzene layer. Mp: 210–213 °C; ^{1}H NMR (400 MHz, C_6D_6, 298 K): δ = 1.89 (s, 3H, ArCH_3), 6.40 (s, 2H, Ph$_2$C*H*), 6.44–7.71 (m, 37H, Ar*H*); ^{13}C{^{1}H} NMR (75 MHz, C_6D_6): δ = 21.3 (ArCH_3), 52.3 (Ph$_2$*C*H), 126.4, 128.6, 128.9, 129.3, 130.2, 130.4, 130.5, 136.8, 143.6, 143.8, 144.3, 145.1 (Ar-*C*); ^{29}Si{^{1}H} NMR (80 MHz, C_6D_6): δ = −16.6 (s); ^{199}Hg{^{1}H} NMR (C_6D_6, 107.4 MHz): δ = −2092.7 (br.); IR υ/cm^{-1} (Nujol): 1597(m), 1491 (s), 1438(s) 1426(s), 1259(m), 1238(m), 1212(m), 1107(s) 1030(m), 928(s), 912(s) 881(m), 837(m) 737(s), 697(s) 676(s); MS/EI *m/z* (%): 697.5 (Ar*N(H)SiPh$_3^+$, 20), 439.2 (Ar*NH$_2^+$, 10), 259.1 (SiPh$_3^+$, 100), 167.0 (Ph$_2$CH$^+$, 45); anal. calc. for $C_{51}H_{42}HgINSi$: C 59.79 %, H 4.13 %, N 1.37 %, found: C 59.89 %, H 4.17 %, N 1.33 %.

Preparation of [Ar*(Si^{i}Pr$_3$)NHgI], 2-61. To a suspension of HgI_2 (0.706 g, 1.55 mmol) in toluene (30 mL) was added a solution of [Ar*(Si^{i}Pr$_3$)NK(OEt$_2$)] (1.00 g, 1.41 mmol) in toluene (10 mL) at −80 °C over 5 min. The reaction mixture was warmed to room temperature and stirred for a further 2 h, whereupon volatiles were removed *in vacuo*. The residue was extracted with hexane (40 mL), the extract filtered and volatiles removed from the filtrate *in vacuo* to give **2-61** as a pale orange solid (0.75 g, 58 %). N.B. X-ray quality crystals of **2-61** were obtained by recrystallizing this solid from pentane. Mp: 235–238 °C; ^{1}H NMR (400 MHz, C_6D_6, 298 K): δ = 1.24 (d, $^{3}J_{HH}$ = 7.5 Hz, 18H, CH(CH_3)$_2$), 1.54 (sept, $^{3}J_{HH}$ = 7.5 Hz, 3H, C*H*(CH$_3$)$_2$), 1.88 (s, 3H, ArCH_3), 6.58 (s, 2H, Ph$_2$C*H*), 6.88–7.28 (m, 22H, Ar*H*); ^{13}C{^{1}H} NMR (75 MHz, C_6D_6): δ = 15.2 (*C*H(CH$_3$)$_2$), 19.6 (CH(*C*H$_3$)$_2$), 21.2 (Ar*C*H$_3$), 51.9 (Ph$_2$*C*H), 126.7, 128.6, 128.9, 129.1, 129.5, 130.2, 130.4, 143.6, 143.7, 145.3 146.2 (Ar-*C*); ^{29}Si{^{1}H} NMR (80 MHz, C_6D_6): δ = 5.6 (s); ^{199}Hg{^{1}H} NMR (C_6D_6, 107.4 MHz): δ = −1943.8; IR υ/cm^{-1} (Nujol): 1597(m), 1490(m), 1435(s), 1231(m), 1126(m), 1074(m), 1029(m), 883(s),

830(m), 809(m), 733(s), 698(s); MS/EI *m/z* (%): 880.5 (M^+ $-^iPr$, 2) 595.5 ($Ar^*NSi^iPr_3^+$, 42), 552.5 ($Ar^*N(H)Si^iPr_2^+$, 79), 167.0 (Ph_2CH^+, 100); anal. calc. for $C_{42}H_{48}HgINSi$: C 54.69 %, H 5.25 %, N 1.52 %, found: C 54.80 %, H 5.30 %, N 1.58 %.

Preparation of [$Ar^\dagger(Si^iPr_3)NHgI$], 2-62. To a suspension of HgI_2 (0.679 g, 1.49 mmol) in toluene (30 mL) was added a solution of [$Ar^\dagger(Si^iPr_3)NK(OEt_2)$] (1.00 g, 1.36 mmol) in toluene (10 mL) at −80 °C over 5 min. The reaction mixture was warmed to room temperature and stirred for a further 2 h, whereupon volatiles were removed *in vacuo*. The residue was extracted with hexane (40 mL), the extract filtered and volatiles removed from the filtrate *in vacuo* to give **2-62** as a pale orange solid (1.29 g, 90 %). N.B. X-ray quality crystals of **2-62** were obtained by recrystallizing this solid from hot hexane. Mp: 188–192 °C; ^{1}H NMR (400 MHz, C_6D_6, 298 K): δ = 0.92 (d, $^3J_{HH}$ = 6.9 Hz, 6H, ArCH(CH_3)$_2$), 1.22 (d, $^3J_{HH}$ = 7.5 Hz, 18H, Si{CH(CH_3)$_2$}$_3$), 1.54 (sept, $^3J_{HH}$ = 7.5 Hz, 3H, Si{CH(CH_3)$_2$}$_3$), 2.49 (sept, $^3J_{HH}$ = 6.9 Hz, 1H, ArCH(CH_3)$_2$), 6.59 (s, 2H, Ph_2CH), 6.93–7.29 (m, 22H, ArH); ^{13}C{^{1}H} NMR (75 MHz, C_6D_6): δ = 15.2 (Si{CH(CH_3)$_2$}$_3$), 19.6 (Si{CH(CH_3)$_2$}$_3$), 24.2 (ArCH(CH_3)$_2$), 33.8 (ArCH(CH_3)$_2$), 52.0 (Ph_2CH), 126.7, 127.0, 128.6, 128.8, 129.1, 129.5, 130.1, 130.3, 143.6, 143.7, 145.4 (Ar-C); ^{29}Si{^{1}H} NMR (80 MHz, C_6D_6): δ = 5.6 (s); ^{199}Hg{^{1}H} NMR (C_6D_6, 107.4 MHz): δ = −2017.1; IR υ/cm^{-1} (Nujol): 1598(m), 1491(s), 1448(s) 1426(s), 1379(m), 1233 (s), 1098(m), 1075(m), 1031(m), 910(s), 835(m), 757(m), 736(s), 697(s); MS/EI *m/z* (%): 951.4 (M^+, < 1) 908.5 (M^+ $-^iPr$, 3) 622.5 ($Ar^\dagger NSi^iPr_3^+$, 86), 580.5 ($Ar^\dagger N(H)Si^iPr_2^+$, 24), 167.0 ($Ph_2CH^+$, 100); anal. calc. for $C_{44}H_{52}HgINSi$: C 55.60 %, H 5.51 %, N 1.47 %, found: C 55.80 %, H 5.40 %, N 1.52 %.

References

1. M.F. Lappert, P.P. Power, A.V. Protchenko, A.L. Seeber, *Metal Amide Chemistry* (Wiley-VCH, Weinheim, 2009)
2. Selected recent examples: (a) A.M. Bryan, W.A. Merrill, W.M. Reiff, J.C. Fettinger, P. P. Power, Inorg. Chem. **51**, 3366 (2012); (b) J.N. Boynton, W.A. Merrill, W.M. Reiff, J.C. Fettinger, P.P. Power, Inorg. Chem. **51**, 3212 (2012); (c) A.E. Ashley, A.R. Cowley, J.C. Green, D.R. Johnston, D.J. Watkin, D.L. Kays, Eur. J. Inorg. Chem. 2547 (2009); (d) J.M. Zadrozny, D.J. Xiao, M. Atanasov, G.J. Long, F. Grandjean, F. Neese, J.R. Long, Nat. Chem. **5**, 577 (2013)
3. S.C. Nyburg, A.W. Parkins, M. Sidi-Boumedine, Polyhedron **12**, 1119 (1993)
4. M. Mathis, W. Harsha, T.W. Hanks, R.D. Bailey, G.L. Schimek, W.T. Pennington, Chem. Mater. **10**, 3568 (1998)
5. S.L. Stokes, W.M. Davis, A.L. Odom, C.C. Cummins, Organometallics **15**, 4521 (1996)
6. H.Y. Au-Yeung, C.H. Lam, C.-K. Lam, W.-Y. Wong, H.K. Lee, Inorg. Chem. **46**, 7695 (2007)
7. S. Licciulli, K. Albahily, V. Fomitcheva, I. Korobkov, S. Gambarotta, R. Duchateau, Angew. Chem. Int. Ed. **50**, 2346 (2011)
8. As determined from a survey of the Cambridge Crystallographic Database, March, 2015
9. S. Schulz, T. Eisenmann, U. Westphal, S. Schmidt, U. Florke, Z. Anorg, Allg. Chem. **635**, 216 (2009)

10. C. Jones, L. Furness, S. Nembenna, R.P. Rose, S. Aldridge, A. Stasch, Dalton Trans. **39**, 8788 (2010)
11. Selected recent examples: (a) G.-F. Chang, C.-H. Wang, H.-C. Lu, L.-S. Kan, I. Chao, W.H. Chen, A. Kumar, L. Lo, M.A.C. dela Rosa, C.-H. Hung, Chem. Eur. J. **17**, 11332 (2011); (b) W.-P. Chang, W.-C. Lin, J.-H, Chen, S.-S. Wang, J.-Y. Tung, Dalton Trans. **41**, 13454 (2012); (c) L.F. Sanchez-Barba, C. Alonso-Moreno, A. Garces, M. Fajardo, J. Fernandez-Baeza, A. Otero, A. Lara-Sanchez, A.M. Rodriguez, I. Lopez-Solera, Dalton Trans. 8054 (2009); (d) B. Liu, X. Li, X. Xu, M. Stepien, P. J. Chmielewski, J. Org. Chem. **78**, 1354 (2013); (e) M.J. Chmielewski, M. Pawlicki, N. Sprutta, L. Szterenberg, L. Latos-Grazynski, Inorg. Chem. **45**, 8664 (2006)
12. S.D. Arora, W.N. Lipscomb, M.C. Sneed, J. Am. Chem. Soc. **73**, 1015 (1951)
13. W.N. Libscomb, Acta Cryst. **4**, 266 (1951)
14. S.J. Simpson, H.W. Turner, R.A. Anderson, J. Am. Chem. Soc. **101**, 7729 (1979)
15. P.J. Brothers, J.P. Collman, Acc. Chem. Res. **19**, 209 (1986)
16. H.J. Callot, Tetrahedron **35**, 1455 (1979)
17. S.-O. Hauber, J.W. Seo, M. Niemeyer, Z. Anorg, Allg. Chem. **636**, 750 (2010)
18. T. Nguyen, A.D. Sutton, M. Brynda, J.C. Fettinger, G.J. Long, P.P. Power, Science **310**, 844 (2005)
19. C. Ni, P.P. Power, Struct. Bond. **136**, 59 (2010) and references therein
20. R. Wolf, C. Ni, T. Nguyen, M. Brynda, G.J. Long, A.D. Sutton, R.C. Fischer, M. Hellman, L. Pu, P.P. Power, Inorg. Chem. **46**, 11277 (2007)
21. A.D. Sutton, T. Ngyuen, J.C. Fettinger, M.M. Olmstead, G.J. Long, P.P. Power, Inorg. Chem. **46**, 4809 (2007)
22. C. Ni, B.D. Ellis, J.C. Fettinger, G.J. Long, P.P. Power, Chem. Commun. **8**, 1014 (2008)
23. J.J. Ellison, P.P. Power, J. Organomet. Chem. **526**, 263 (1996)
24. H. Lei, B.D. Ellis, C. Ni, F. Grandjean, G.J. Long, P.P. Power, Inorg. Chem. **47**, 10205 (2008)
25. Z. Zhu, M. Brynda, R.J. Wright, R.C. Fischer, W.A. Merrill, E. Rivard, R. Wolf, J.C. Fettinger, M.M. Olmstead, P.P. Power, J. Am. Chem. Soc. **129**, 10847 (2007)
26. Y. Wan, B. Quillian, C.S. Wannere, P. Wei, P.V.R. Schleyer, G.H. Robinson, Organometallics **26**, 3054 (2007)
27. V.I. Pakhomov, Zh. Strukt. Khim. (Russ.) **4**, 594 (1963)
28. J. Li, A. Stasch, C. Schenk, C. Jones, Dalton Trans. **40**, 10448 (2011)
29. E.W.Y. Wong, D. Dange, L. Fohlmeister, T.J. Hadlington, C. Jones, Aust. J. Chem. **66**, 1144 (2013)
30. T.J. Hadlington, J. Li, C. Jones, Can. J. Chem. **92**, 427 (2014)
31. J. Hicks, T.J. Hadlington, C. Jones, Organometallics **32**, 323 (2013)
32. T. Böttcher, J. Kelly, C. Jones, unpublished work
33. J. Li, C. Schenk, C. Goedecke, G. Frenking, C. Jones, J. Am. Chem Soc. **133**, 18622 (2011)
34. T.J. Hadlington, C. Jones, Chem. Commun. **50**, 2321 (2014)
35. A.M. Davey, D. Dange, C. Jones, unpublished work
36. D. Dange, J. Li, C. Schenk, H. Schnockel, C. Jones, Inorg. Chem. **51**, 13050 (2012)
37. B. Cordero, V. Gómez, A.E. Platero-Prats, M. Revés, J. Echeverría, E. Cremades, F. Barragán, S. Alvarez, Dalton Trans. 2832 (2008)
38. (a) F.A. Cotton, W.A. Dollase, J.S. Wood, J. Am. Chem. Soc. **85**, 1543 (1963); (b) J.A. Ibers, J. Chem. Phys. **40**, 3129 (1964)
39. (a) D.F. Evans, J. Chem. Soc. 2003 (1959); (b) E.M. Schubert, J. Chem. Ed. **69**, 62 (1992); (c) T. Ayers, R. Turk, C. Lane, J. Goins, D. Jameson, S. J. Slattery, Inorg. Chim. Acta **357**, 202 (2004)
40. H.P. Lane, S.M. Godfrey, R.G. Pritchard, C.A. McAuliffe, J. Chem. Soc. Dalton Trans. 701 (1995)
41. J. Vela, J.M. Smith, Y. Yu, N.A. Ketterer, C.J. Flaschenriem, R.J. Lachicotte, P.L. Holland, J. Am. Chem. Soc. **127**, 7857 (2005)

Chapter 3
Preparation of Low Oxidation State Manganese Complexes Stabilised by Bulky Amide Ligands

3.1 Introduction

As discussed in Chap. 1, metal–metal bonded compounds have been intensively studied for many decades, not only due to their fundamental appeal, but also because of their many applications, such as small molecule activations, catalysis, enzyme mimicry etc. [1]. With respect to transition metals, the vast majority of efforts in this field have lain with the second and third row elements [2]. Recently, the kinetic stabilisation of carbonyl free, first row metal–metal bonded dimers has become a hot topic, as they are often open shell and consequently highly reactive. Therefore it is not surprizing that they are also finding applications in a variety of areas, such as catalysis and small molecule activation [1].

3.1.1 Low Oxidation State Manganese Complexes

Manganese has one of the widest ranges of stable oxidation states of any element, ranging in isolable complexes at least from −1 to +7. Compounds with manganese in oxidation state of +1 or lower have been found to be highly effective in photochemical processes, and therefore are a popular class of compound to study [3]. That said, it is no surprise that numerous manganese(I) complexes populate the literature [4], some of which are commercially available, such as methylcyclopentadienyl manganese tricarbonyl (MMT) [(MeCp)$Mn(CO)_3$] (MeCp = methylcyclopentadienyl), which is used globally as a petrol additive [5]. However, the vast majority of these low oxidation state manganese compounds are stabilised by carbonyl ligands, e.g. MMT. Carbonyl free manganese(I) complexes are rare, particularly examples that possess Mn–Mn bonds. This class of compound is the primary focus of this chapter.

J. Hicks, *Preparation, Characterisation and Reactivity of Low Oxidation State d-Block Metal Complexes Stabilised by Extremely Bulky Amide Ligands*, Springer Theses,
DOI 10.1007/978-981-10-2905-9_3

3.1.1.1 Metal–Metal Bonded Manganese(I) Dimers

The first carbonyl-free manganese(I) dimer that contained an unsupported Mn–Mn bond was the β-diketiminate stabilised complex $[\{(^{Dipp}Nacnac)Mn\}_2]$ **3-01**, reported by Roesky and co-workers in 2005 [6]. The complex was synthesised by reduction of the manganese(II) iodide precursor complex $[\{(^{Dipp}Nacnac)Mn(\mu\text{-}I)\}_2]$ **3-02** with a sodium potassium alloy, in toluene over 4 days (Scheme 3.1). After workup and crystallisation, a small amount of the highly air sensitive red crystalline solid **3-01** was isolated (15 % yield).

The red crystals were analysed by X-ray crystallography, which showed the complex to be a manganese(I) metal–metal bonded dimer with a central Mn_2^{2+} core. The two Mn centres are three-coordinate, possessing distorted trigonal geometries, with no strong interactions from the flanking aryl groups of the ligand. The Mn–Mn bond length in **3-01** was found to be 2.721(1) Å, which is considerably shorter than the unsupported Mn–Mn bond in the Mn(0) compound $[Mn_2(CO)_{10}]$ [7] (2.90 Å), but comparable to bridged manganese(I) dimers such as $[Mn_2(CO)_7(\mu\text{-}S_2)]$ (2.67 Å) [8].

Variable-temperature magnetic susceptibility measurements were performed on a polycrystalline sample of **3-01**. The measurement was conducted using a SQUID magnetometer in the temperature range 2–300 K and in an applied field of 1 Torr, which gave an effective magnetic moment for the dimer of 3.93 μ_B at 298 K [6]. This value indicates that the two metal centres are high-spin, although it is significantly less than the expected spin only value for two non-interacting high-spin Mn(I) centres (9.8 μ_B for $4s^13d^5$ or 6.9 μ_B for $3d^6$). Backed up with computational calculations on a model of the complex, the authors concluded that strong antiferromagnetic coupling is occurring between the two metal centres. This result was later supported by variable-temperature W-band EPR studies [9].

The reactivity of **3-01** towards the oxidizing agents O_2 and $KMnO_4$ was also investigated. When a toluene solution of **3-01** was treated with one equivalent of $KMnO_4$ or an excess of dry O_2, the dioxo-bridged manganese(III) complex $[\{(^{Dipp}Nacnac)Mn(\mu\text{-}O)\}_2]$ **3-03** was formed in good yields (Scheme 3.2) [6].

In 2011, Tsai and co-workers reported the results of theory driven experiments, which included isolation of three low oxidation state metal–metal bonded manganese complexes, supported by dianionic, diamido ligands [10]. The paper was a follow up to their previous reported work, where they reported the synthesis of the

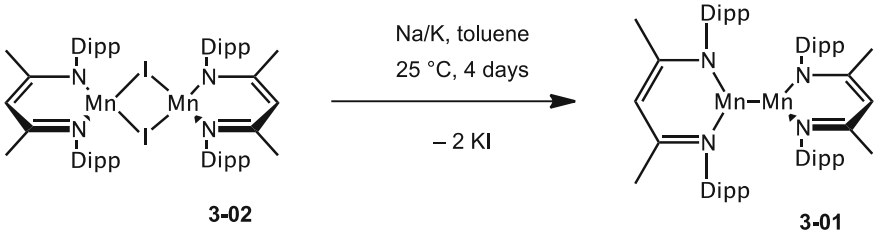

Scheme 3.1 Preparation of **3-01**

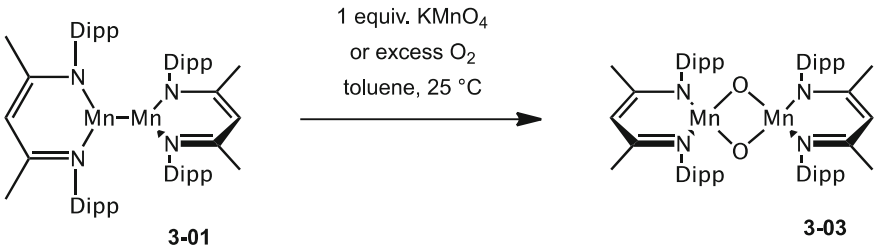

Scheme 3.2 Preparation of **3-03**

related dianionic metal–metal bonded zinc(I) complex $K_2[\{Me_2Si(DippN)_2Zn\}_2]$ (see Sect. 4.1.3 for further discussion) [11].

The three low oxidation state manganese complexes were prepared from the dinuclear manganese(II) precursor $[\{\kappa^2\text{-}Me_2Si(DippN)_2Mn\}_2]$ **3-04**, which was itself prepared from the reaction between $[Me_2Si(DippNLi)_2]$ and manganese(II) chloride in THF. Stepwise reductions of compound **3-04** were performed, using one and two equivalents of KC_8, which led to the isolation of the monoanionic complex $[\{\mu\text{-}\kappa^2\text{-}Me_2Si(DippN)_2Mn\}_2]^-$ **3-05** and dianionic complex $[\kappa^2\text{-}Me_2Si(DippN)_2Mn\}_2]^{2-}$ **3-06** respectively (Scheme 3.3). As expected, complex **3-05** can be reacted with a further equivalent of KC_8 to yield **3-06**, showing that it is in fact an intermediate in formation of **3-06**. As mentioned, complexes **3-05** and **3-06** are anionic and dianaionic complexes respectively, which are isolated as potassium salts, with either 18-crown-6 or cryptand [2.2.2] (crypt-222) coordinated to the cation (N.B. the donors were added to the reaction prior to reduction). A variation of **3-06** can also be isolated if no 18-crown-6 or crypt-222 is added, where the potassium cations sit in-between the two adjacent flanking phenyl rings of each ligand, in a sandwich like motif **3-06a** (Scheme 3.3).

All four compounds were crystallographically characterised, and it was found that both **3-05** and **3-06** are examples of low coordinate manganese dimers, containing metal–metal bonds, albeit in different coordination modes [11]. Complex **3-05** is a rare example of a dinuclear mixed valence manganese(I/II) complex, where the two diamido ligands bridge the two metal centres. Although the complex is mixed-valent, the two metal centres are essentially indistinguishable, as **3-05** has C_i symmetry.

Complex **3-06** is a three-coordinate manganese(I) dimer, with a unsupported Mn–Mn bond. The ligands in **3-06** are terminal and chelating, forming four-membered rings with the manganese centres. The one electron reduction of **3-05** to yield **3-06**, has resulted in a dramatic change of the ligand's coordination mode, from bridging in **3-05** to terminal chelating in **3-06**.

Interestingly, the Mn–Mn bond length in **3-05** [2.6848(8) Å] was found to be considerably shorter than that in **3-06** [2.7871(8) Å], even though the formal bond order of the metal–metal bond is 0.5 less (0.5 in **3-05** compared with 1.0 in **3-06**) [11]. This difference was calculated to be due to the difference in coordination modes of the ligands, where the bridging motif in **3-05** forces the metal atoms closer together.

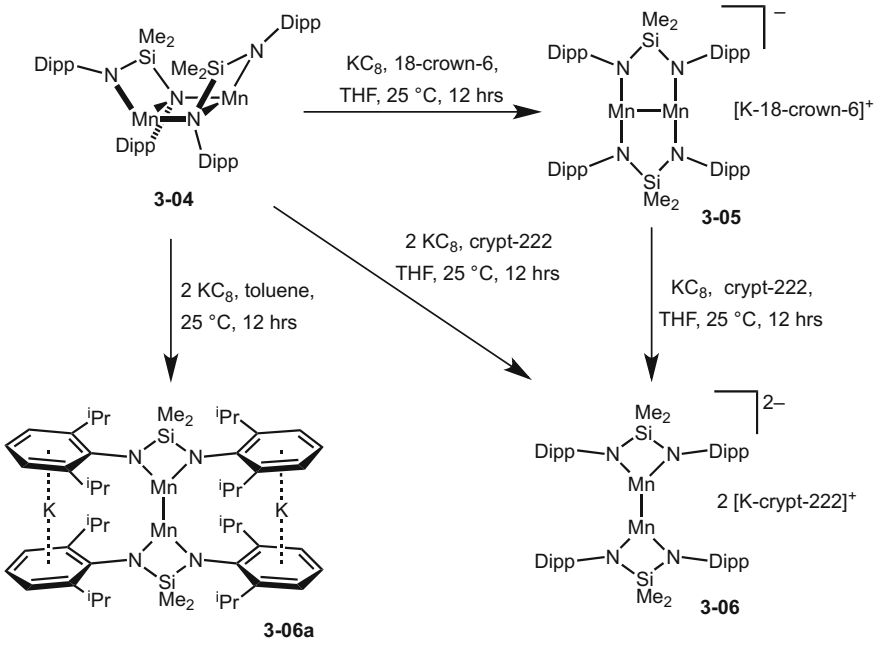

Scheme 3.3 Preparation of **3-05**, **3-06** and **3-06a**. Crypt-222 = Cryptand [2.2.2]

Variable-temperature magnetic susceptibility measurements were performed on polycrystalline samples of **3-05** and **3-06a**, using a SQUID magnetometer in the temperature range 2–300 K. The measurements found the two complexes to have room temperature effective magnetic moments of 6.10 μ_B and 4.84 μ_B respectively, both indicative of high spin manganese centres [11]. However, both magnetic moment values are significantly lower than the spin only values for two non-interacting Mn(I) or Mn(II) centres, indicating a high degree of antiferromagnetic coupling between the two metal centres. Further reactivity studies of the metal–metal bonded dimers are yet to be reported.

The most recently reported carbonyl free metal–metal manganese(I) dimer, which is stabilised by bulky amidinate ligands, was reported by the Jones group in 2012 [12]. The dimer was synthesised by the reduction of the trinuclear manganese(II) bromide complex $[\{(Piso)Mn(\mu\text{-}Br)\}_3(THF)_2]$ (Piso = $(DippN)_2CH$) **3-07** with 1.5 equivalents of the magnesium(I) reducing agent $[\{(^{Mes}Nacnac)Mg\}_2]$ **1-08** (Scheme 3.4). After workup and subsequent crystallisation, a moderate yield of the manganese(I) dimer $[\{(Piso)Mn\}_2]$ **3-08** was isolated as dark red-green crystals.

The dark red-green crystals of complex **3-08** were analysed by X-ray crystallography. The Mn–Mn bond length in the complex of 2.7170(9) Å [12], was found to be significantly shorter than in the dianionic manganese(I) compound **3-06** [2.7871(8) Å] [10], but almost identical to that in **3-01** [2.721(1) Å] [6]. Interestingly, the two amidinate ligands that are stabilising the Mn_2^{2+} core, adopt an

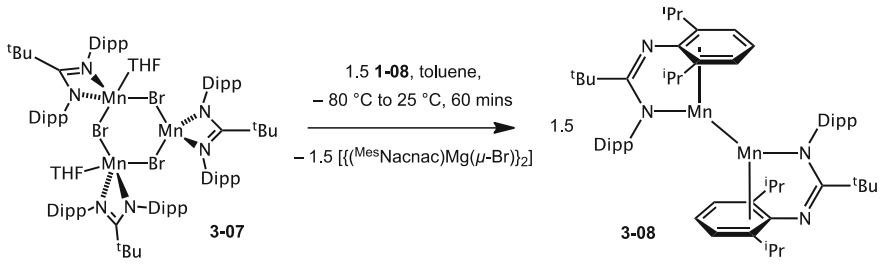

Scheme 3.4 Preparation of **3-08**

unusual geometry. Amidinate ligands are usually considered as monoanionic N,N′-chelating ligands, forming four-membered rings with a coordinated metal, as is the case in the precursor complex **3-07**. However, in **3-08**, the ligands are coordinating to the metal through one nitrogen atom, and an η^3-arene interaction of the opposing flanking aryl group. The complex is the first example of this unusual N,η^3-arene-chelating bonding mode with a first-row transition metal element. However it has been observed for much larger metals, such as indium [13], thallium [14], ytterbium [15] and samarium [16].

Variable-temperature magnetic susceptibility measurements were performed on a polycrystalline sample of **3-08**. The measurement was conducted using a SQUID magnetometer in the temperature range 2–300 K and in an applied field of 1 Torr, which revealed the dimer to have an effective magnetic moment of 4.39 μ_B at 298 K [12]. This is once again characteristic of a high spin manganese(I) dimer, and significantly lower than the expected value for two non-interacting high-spin manganese(I) centres, thus indicating strong antiferromagnetic coupling between the two metal centres. The effective magnetic moment value of 4.39 μ_B lies in the range of the other two manganese(I) dimers that have been magnetically studied (3.93 μ_B for **3-01** and 4.84 μ_B for **3-06a**) [6, 10].

The reactivity of **3-08** towards the gases O_2, N_2O and CO was investigated (Scheme 3.5) [17]. When a toluene solution of **3-08** was exposed to one atmosphere of O_2 or N_2O, an immediate colour change from dark red to brown was observed. After workup and subsequent crystallisation, the bridging manganese(III) oxide [{(Piso)Mn(μ-O)}$_2$] **3-09** was isolated in moderate yields. The structure of **3-09** resembles that of the β-diketiminate stabilised manganese(III) oxide **3-03**, however

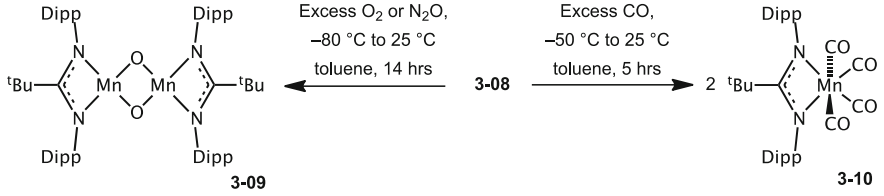

Scheme 3.5 Preparation of **3-09** and **3-10**

in that complex, the four-coordinate metal centres possessed distorted tetrahedral geometries, whereas in **3-09** they possess square planar geometries. The difference in metal geometry is likely due to the different steric demands of the two ligands.

A toluene solution of **3-08** was also exposed to an excess of carbon monoxide gas, which resulted in a colour change from dark red to orange-brown. After workup and crystallisation, the monomeric tetracarbonyl manganese(I) complex [(Piso)Mn(CO)$_4$] **3-10** was isolated [17]. The addition of CO resulted in breaking the metal–metal bond, and the coordination of four molecules of CO per metal centre, yielding the octahedral manganese(I) complex **3-10**.

3.1.1.2 Carbonyl-free Manganese(I) Complexes Without Metal–Metal Bonds

As discussed in Chap. 1, low oxidation state complexes can be isolated as different compound types, and not just those possessing metal–metal bonds. Depending on a combination of the ligand's steric and electronic properties, as well as the metal, reducing agent, atmosphere and solvent used, different types of complex can be isolated.

In 2008, Power and co-workers reported the reduction of the extremely bulky terphenyl manganese(II) iodide complex [{3,5-^{i}Pr-Ar^{Tripp}Mn(μ-I)}$_2$] **2-22** (Ar^{Tripp} = 2,6-Tripp$_2$-C$_6$H$_3$), the only reported terphenyl manganese(II) halide complex (previously discussed in Chap. 2) [18]. The reduction of **2-22** was carried out using a stoichiometric amount of KC_8 in THF. After workup and crystallisation from toluene, a modest yield (29 %) of the dimeric manganese(I) complex [(3,5-^{i}Pr-Ar^{Tripp}Mn)$_2$(μ-η^6:η^6-C$_7$H$_8$)] **3-11** was isolated as red-brown crystals (Scheme 3.6).

Complex **3-11** was crystallographically characterised, and was found to be an inverted sandwich complex, with a molecule of toluene inserted between the two metal centres [18]. The two metal centres coordinate to either side of the toluene in an η^6 fashion, in addition to coordination to the terphenyl ligand. The molecular structure of **3-11** also shows that the central toluene molecule maintains its planar geometry. Moreover, the C–C bond lengths are comparable to those in free toluene, indicating that toluene is simply coordinating and not activated. This inverted sandwich structure, with an aromatic molecule inserted between two metal centres is unique to manganese, but has been seen in other first row transition metal

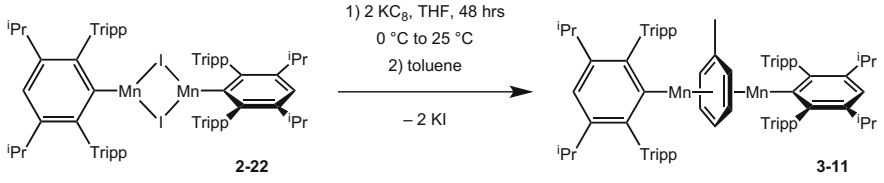

Scheme 3.6 Preparation of **3-11**

complexes, for example, scandium [19], titanium [20], vanadium [21], chromium [22] and nickel [23]. The inverted sandwich structure was proposed to have formed because of the extreme bulk of the ligands, disfavouring the formation of a metal–metal bond. In addition, the Mn···Mn separation in **3-11** was found to be 3.561 Å [18], which is well outside the sum of the covalent radii of two high spin manganese centres (3.22 Å) [24], and therefore too long for any significant interaction.

Variable-temperature magnetic susceptibility measurements were performed on a polycrystalline sample of **3-11**. The measurement was conducted using a SQUID magnetometer in the temperature range 2–320 K and in an applied field of 0.01 Torr, which revealed the complex to have an effective magnetic moment of 5.17 μ_B per manganese(I) centre at room temperature [18]. This value is slightly above the expected μ_{eff} of a non-interacting high-spin manganese(I) centre (4.90 μ_B), and significantly above the μ_{eff} value of the metal–metal bonded manganese dimer **3-01** (3.93 μ_B), clearly supporting the lack of a metal–metal bond.

In the following year, Chomitz and Arnold published the reduction of the monomeric manganese(II) chloride complex [(N_2P_2)MnCl] **3-12** (N_2P_2 = $^tBuN^{(-)}SiMe_2N$-$(CH_2CH_2P^iPr_2)_2$) stabilised by a multidentate amido diphosphine ligand [25]. The tetrahedral precursor complex **3-12** was reduced using a THF solution of sodium naphthalide, under a nitrogen atmosphere. After workup and subsequent crystallisation, dark red crystalline blocks of [{(N_2P_2)Mn}$_2$(μ-N_2)] **3-13** were isolated (Scheme 3.7) [26]. These dark red crystals of **3-13** were subsequently analysed by X-ray crystallography.

Complex **3-13** was found to be a manganese(I) dimer, but instead of a metal–metal bond, a molecule of dinitrogen inserted between two metal centres in an end-on fashion. The two metal centres possess tetrahedral geometries, with three coordination sites occupied by the ligand and the fourth by the bridging dinitrogen. The coordination of the dinitrogen molecule between the metal centres yields a similar structure to that of **3-11**, where a toluene molecule bridges the two metal centres. Complex **3-13** is only the second reported compound to contain a N_2 bridge between two manganese centres, the first being the carbonyl stabilised complex [{$(MeCp)Mn(CO)_2$}$_2$(μ-N_2)] **3-14** reported in 1979 by Ziegler and co-workers [27].

The N–N bond length in **3-13** shows a modest elongation compared with free N_2 (1.208 Å in **3-13** compared with 1.098 Å in free N_2), indicating a small degree of

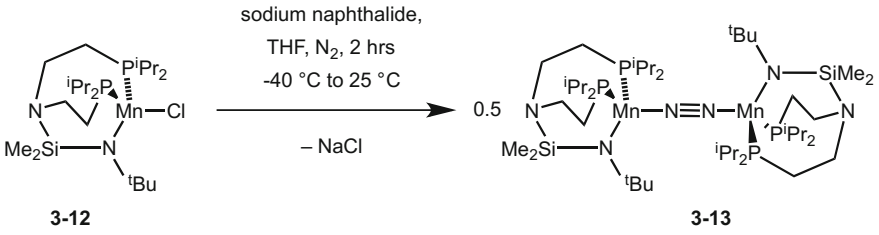

Scheme 3.7 Preparation of **3-13**

activation, due to π back-bonding into the π* orbitals of the N_2 ligand [26]. This elongation is significantly enhanced compared to **3-14** (1.118 Å) [27], as the lower coordination number, in addition to the lack of π-accepting ligands such as CO, increases the electron density available for back-bonding into the N_2 π* orbitals. Further reactivity of **3-13** has yet to be reported.

3.2 Research Outline

As discussed in Chap. 2, the three bulky amido manganese(II) bromide complexes [{Ar*($SiMe_3$)NMn(μ-Br)(THF)}$_2$] **2-43**, [{Ar*($SiPh_3$)NMn(μ-Br)(THF)}$_2$] **2-44** and [{Ar†($Si^{i}Pr_3$)NMn(μ-Br)(THF)}$_2$] **2-45** have been prepared as potential precursors for low coordinate, low oxidation state manganese complexes. As only a handful of low oxidation state metal–metal bonded manganese dimers have been isolated, none of which are stabilised by a monodentate ligand, the goal of this chapter was to attempt to reduce these complexes to hopefully isolate the first two-coordinate manganese(I) dimer. The reductions of the three amido manganese (II) bromide complex were to be carried out using a variety of experimental conditions and reducing agents, including the magnesium(I) dimer **1-08**.

If successful in the isolation of low oxidation state manganese complexes, their reactivity towards a number of small gaseous molecules, as well as some organic unsaturated substrates was to be explored.

3.3 Results and Discussion

3.3.1 Preparation and Characterisation of a Two-Coordinate Manganese(I) Dimer with an Unsupported Metal–Metal Bond

At the outset of this study, the reduction of the amido manganese(II) bromide complex [{Ar*($SiMe_3$)NMn(μ-Br)(THF)}$_2$] **2-43**, bearing the least sterically demanding amide ligand Ar*($SiMe_3$)N^{-}, was attempted using excess magnesium metal in THF. However, after stirring for one week at room temperature, almost complete recovery of the starting material **2-43** resulted. The reduction of **2-43** was also attempted over sodium and potassium mirrors in cyclohexane, toluene and diethyl ether independently, which in all cases led to the isolation of decomposition products, such as elemental manganese and the secondary amine Ar*($SiMe_3$)NH. However, when the reduction was attempted using a stoichiometric amount of KC_8 in cyclohexane, the reaction mixture slowly turned deep red over the course of several days. After workup and crystallization, a low yield of the amido manganese(I)

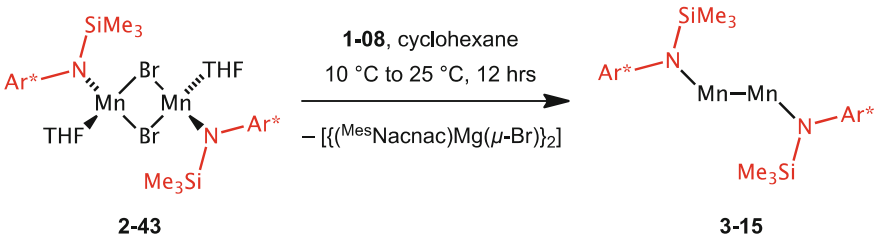

Scheme 3.8 Improved synthesis of **3-15**

dimer [{Ar*($SiMe_3$)NMn}$_2$] **3-15** was isolated as extremely air and moisture sensitive dark red crystalline blocks. It was later found that the yield of **3-15** can be significantly enhanced (70 % compared with 10 %) by using the magnesium(I) reducing agent [{(^{Mes}Nacnac)Mg}$_2$] **1-08** rather than KC_8 (Scheme 3.8).

Compound **3-15** was analysed by X-ray crystallography, and its molecular structure depicted in Fig. 3.1. The complex is a two-coordinate, amido stabilised manganese(I) dimer, with an unsupported Mn–Mn bond. The complex has a mildly trans-bent structure, with N–Mn–Mn angles of 148.39(5)°, and a Mn–Mn bond length of 2.7224(6) Å, which is in good agreement with the singly bonded β-diketiminate stabilized manganese(I) dimer **3-01** [2.721(1) Å] [6] and the amidinate stabilised dimer **3-08** [2.7170(9) Å] [12]. The Mn centres do not exhibit any close interactions with the flanking phenyl rings [closest Mn···C_{phenyl} = 3.043(3) Å].

Compound **3-15** is paramagnetic in solution, and exhibits a room temperature solution-state magnetic moment of 3.4 μ_B, determined by the Evans Method [28]. This value is indicative of two high-spin manganese centres that are

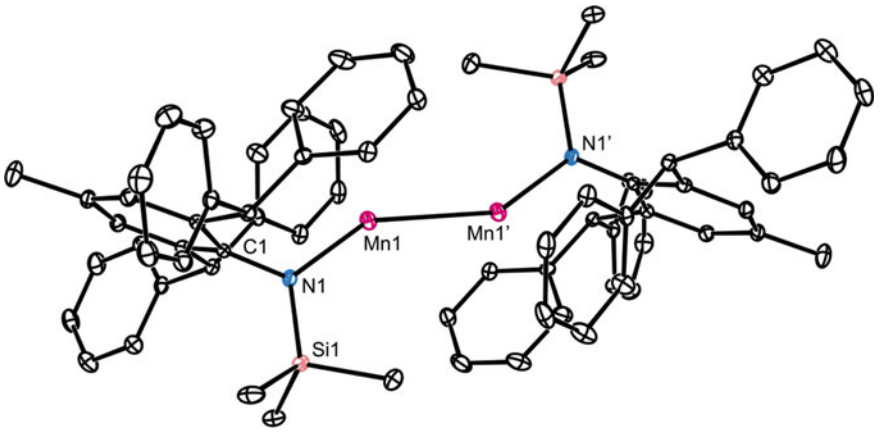

Fig. 3.1 Thermal ellipsoid plot (25 % probability surface) of the molecular structure of **3-15**. Hydrogen atoms have been omitted for clarity. Selected bond lengths (Å) and angles (°): Mn(1)-Mn(1′) 2.7224(6), N(1)-Mn(1) 1.9904(15), N(1)-Si(1) 1.7254(16), N(1)-Mn(1)-Mn(1′) 148.39(5)

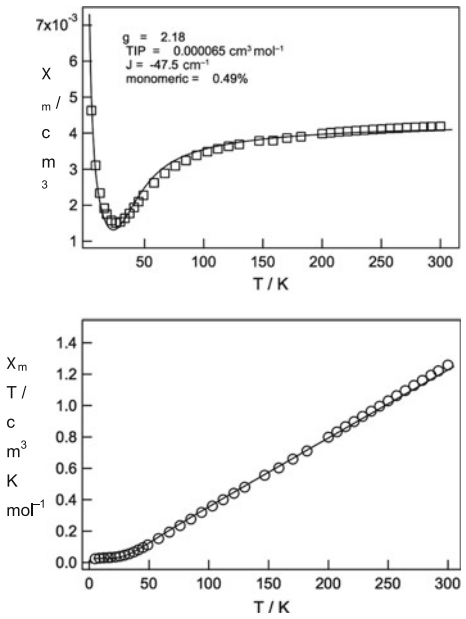

Fig. 3.2 Plots of χ_M (per Mn) versus T (*top*) and $\chi_M T$ (per Mn) versus T (*bottom*) for **3-15**. *Solid lines* are the best fits to an S = 5/2 dimer model using the parameters given with 0.49 % paramagnetic impurity

anti-ferromagnetically coupled together, as the expected magnetic moment for two non-interacting high-spin manganese(I) centres is much higher (9.8 μ_B for $4s^1 3d^5$ or 6.9 μ_B for $3d^6$). To further investigate the magnetic properties of **3-15**, variable-temperature magnetic susceptibility measurements were performed on a polycrystalline sample of **3-15**. The measurement was conducted using a SQUID magnetometer in the temperature range 2–300 K and in an applied field of 1 Torr, the results of which are highlighted in Fig. 3.2.

Compound **3-15** exhibits an $\chi_M T$ value (χ_M = molar magnetic susceptibility) of 1.28 $cm^3\ mol^{-1}$ K per manganese centre at 300 K, corresponding to a μ_{eff} value of 3.20 μ_B per manganese centre at this temperature (the Curie temperature however is significantly higher than 300 K). The $\chi_M T$ value decreases almost linearly from 300 K down to approximately 50 K, reaching 0.1 $cm^3\ mol^{-1}$ K, before plateauing at close to 0 $cm^3\ mol^{-1}$ K below that. The corresponding χ_M versus T plot is typical of an antiferromagnetic coupled system, the data for which were fitted to an $S = 5/2$ (per manganese centre) dimer model ($-2J\mathbf{S}_1 \cdot \mathbf{S}_2$) using $g = 2.18$, $J = -47.5\ cm^{-1}$. The two plots in Fig. 3.2 strongly resemble those for the higher coordinate manganese(I) dimers **3-01** and **3-08**, which were both shown to have Mn–Mn single bonds, with strong antiferromagnetic coupling between the two metal centres.

To further investigate the metal–metal bonding in **3-15**, calculations (in collaboration with Prof. L. Gagliardi, University of Minnesota) using the theory methods CASSCF (complete active space self-consistent field) and CASPT2 (complete active space perturbation theory), were carried out on a full model of the dimer, in order to

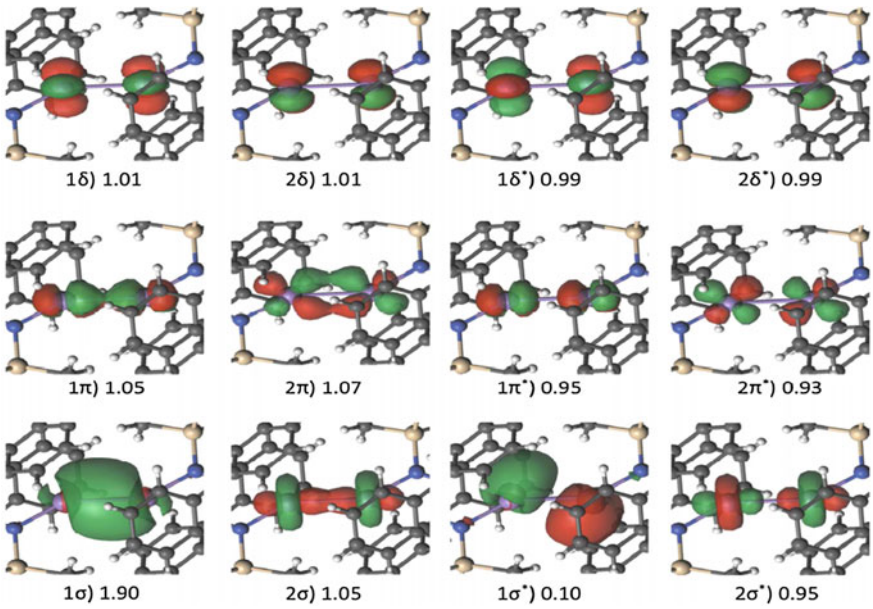

Fig. 3.3 Active orbitals and corresponding occupation numbers for the singlet ground state of **3-15**. The manganese atoms are *purple*. Iso-surface value 0.03 a.u.

determine its ground-state electronic structure. For the low-energy states, the wave function was highly multiconfigurational, with no configuration exceeding a weight of 10 %. At CASSCF and CASPT2 levels of theory, the singlet spin state was calculated to be the ground state, but the triplet and quintet states lie only approximately 1 and 2 kcal/mol above respectively. In the ground state, **3-15** was calculated to have a single Mn–Mn bond, with a calculated effective bond order (EBO) of 0.90. The molecular orbitals and corresponding occupation numbers for the singlet ground state are shown in Fig. 3.3. A singlet ground state is in good agreement with the magnetic measurements above.

The results of the computational studies performed on **3-15** are comparable to those for the higher coordinate manganese(I) dimer **3-08**. That is, the low-energy states are highly multiconfigurational, with a dominant singlet ground state. The two complexes were also calculated to possess a manganese-manganese single bond, with each high-spin metal centre encompassing five singly occupied 3d orbitals that are essentially non-bonding.

Combining the results of X-ray crystallography, magnetic studies and computational calculations, it can be concluded that **3-15** is a high-spin, two coordinate amido manganese(I) dimer with a unsupported metal–metal bond. The complex represents the first example of a two-coordinate manganese(I) dimer, and is the first open shell, two-coordinate d-block metal(I) dimer.

3.3.2 Preparation and Characterisation of a Two-Coordinate Manganese(0) Heterobimetallic Complex with an Unsupported Mn–Mg Bond

With the successful reduction of the amido manganese bromide **2-43**, the reductions of the two bulkier amido manganese bromide complexes [{Ar*($SiPh_3$)NMn(μ-Br)(THF)}$_2$] **2-44** and [{Ar†(Si^iPr_3)NMn(μ-Br)(THF)}$_2$] **2-45** were also attempted. Using the same magnesium(I) reducing agent **1-08**, the initial expectation was that similar, bulkier versions of the manganese(I) dimer **3-15** would be formed. With that in mind, **2-44** and **2-45** were each reacted with one equivalent of the magnesium(I) reducing agent **1-08**. However, in both cases, the reaction mixture turned an intense royal blue colour on addition of the reducing agent, in contrast to the deep red colour of the manganese(I) dimer **3-15**. Approximately half of the amido manganese bromide starting materials were recovered from both reactions. Due to the extremely high solubility of the blue product in the reaction between **2-44** and **1-08**, no X-ray quality crystals of it were isolated. However, blue X-ray quality crystals were isolated from the reaction between **2-45** and **1-08**, by extraction of the reaction mixture into pentane, with subsequent cooling of the extract to −30 °C overnight. These crystals were crystallographically characterized, revealing the structure [Ar†(Si^iPr_3)NMnMg(^{Mes}Nacnac)] **3-16** (Fig. 3.4). Repeating the reaction, using two equivalents of the magnesium(I) reducing agent **1-08**, resulted in full consumption of the starting material **2-45**, and gave a good yield (71 %) of **3-16** (Scheme 3.9).

As expected, the blue product was not a manganese(I) dimer, but the manganese-magnesium heterobimetallic complex **3-16**. The complex is monomeric, with an unsupported Mn–Mg bond [2.8244(13) Å], and a two-coordinate non-linear manganese centre (N–Mn–Mg = 160.9°) in the solid state. It is worth noting that there are no strong interactions between the manganese and the flanking phenyl rings of the Ar† substituent [closest Mn···C_{phenyl} is between Mn1 and C17, Mn1–C17 = 3.033(3) Å].

Compound **3-16** is of considerable fundamental interest for a number of reasons. Firstly, while a handful of d-block metal-magnesium bonded complexes have been reported [29], none include manganese, therefore the complex possesses the first crystallographically characterised example of a Mn–Mg bond. Furthermore, all of the reported d-block metal-magnesium complexes are higher coordinate, closed shell systems, where **3-16** is open shell (as discussed below). In addition, formal oxidation states can be assigned to the metal centres in the complex, as Mn(0) and Mg(II), due to the difference in electronegativity of the two elements (1.31 for Mg and 1.55 for Mn on the Pauling scale) [30]. Consequently, compound **3-16** is the first example of a two-coordinate manganese(0) complex.

Compound **3-16** is paramagnetic, and exhibits a solution state magnetic moment of 5.3 μ_B at 298 K, as determined by the Evans method. This is slightly lower than the spin only value for a non interacting high-spin Mn(0) centre ($4s^23d^5$ = 5.9 μ_B),

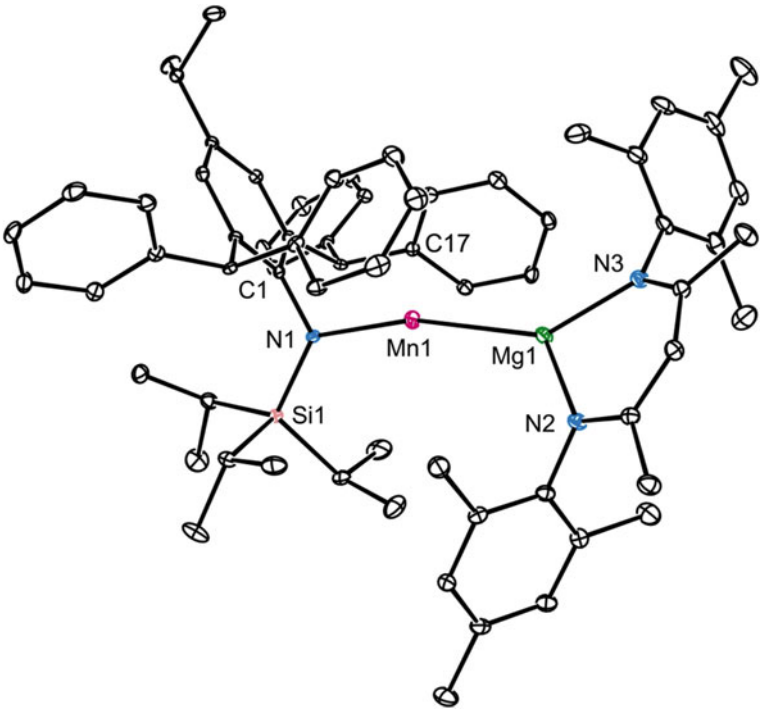

Fig. 3.4 Thermal ellipsoid plot (25 % probability surface) of the molecular structure of **3-16**. Hydrogen atoms have been omitted for clarity. Selected bond lengths (Å) and angles (°): Mn(1)-Mg(1) 2.8244(13), Mn(1)-N(1) 2.024(3), Mg(1)-N(2) 2.044(3), Mg(1)-N(3) 2.057(3), N(1)-Mn(1)-Mg(1) 160.85(9), N(2)-Mg(1)-N(3) 91.47(13)

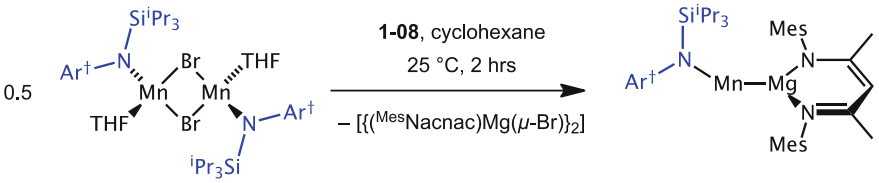

Scheme 3.9 Preparation of **3-16**

but clearly indicates the presence of a high-spin manganese centre. Variable-temperature magnetic susceptibility measurements were performed on a polycrystalline sample of **3-16**, in the temperature range 2–320 K and in an applied field of 0.01 Torr; the results of which are highlighted in Fig. 3.5. The $\chi_M T$ value for the complex at 300 K, is 4.14 cm^3 mol^{-1} K, corresponding to an effective magnetic moment of 5.76 μ_B. The $\chi_M T$ value decreases gradually, in a Curie-Weiss fashion, to $\sim$3.9 cm^3 mol^{-1} K at 6 K, then more rapidly due to zero-field splitting,

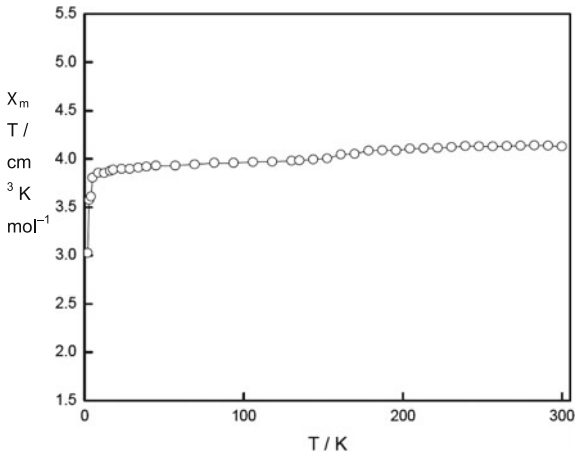

Fig. 3.5 Plot of $\chi_M T$ versus T for **3-16**. The *solid line* is a guide to the eye

reaching 3.0 cm^3 mol^{-1} K at 2 K. The data are suggestive of an isolated $S = 5/2$ ground state, supporting the proposal of a high-spin $4s^2$ $3d^5$ manganese centre.

To further investigate the spin state of complex **3-16**, low-temperature (10 K), low and high field EPR spectroscopic studies (X band—9 GHz, Q band—35 GHz) were performed on frozen toluene solutions of **3-16**. The results, along with the associated simulations of the complex, are shown in Fig. 3.6. The complexity of

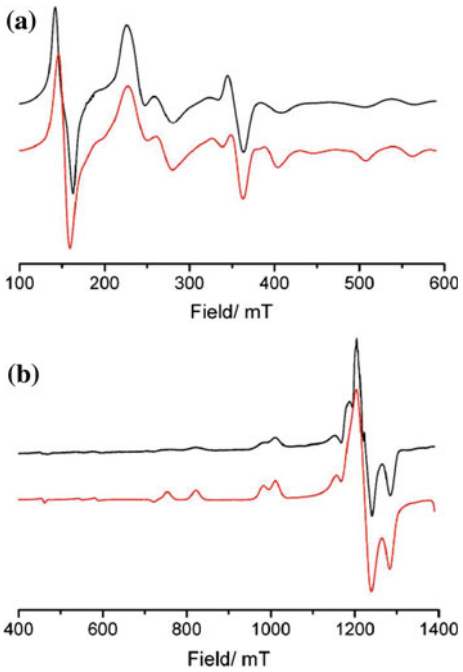

Fig. 3.6 Experimental (*black line*) and simulated (*red line*) EPR spectra for complex **3-16**, recorded at 10 K. a = X-band and b = Q band frequency

both spectra arises from zero field splitting, which dominates the spectra at 10 K. The EPR simulations are based on the spin Hamiltonian parameters of g = 2.004, S = 5/2, D = 0.1 cm^{-1} (2850 MHz) and E = 0.04 cm^{-1} (1250 Mz) and, as can be seen in Fig. 3.6, are a close fit to the experimental data for both X and Q band (D = axial zero field splitting parameter, E = rhombic zero field splitting parameter). However, the ^{55}Mn hyperfine could not be detected, and the g anisotropy remained unresolved, at these two frequencies, owing to the zero field splitting contributions from D and E. That said, the best fits for the band data are certainly based on an isolated S = 5/2 spin state, which is consistent with the magnetic measurements.

In order to further investigate the metal–metal bonding in **3-16**, calculations using the theory methods CASSCF and CASPT2, were carried out on a model of the complex, where the isopropyl groups are replaced with methyl groups (viz. **3-16^{Me}**). Consistent with the magnetic studies and EPR results, both levels of theory predict a sextet ground state for **3-16^{Me}**, with the dominant configuration of $1\sigma^2(3d^{a}_{Mn})^1(3d^{b}_{Mn})^1(3d^{c}_{Mn})^1(3d^{d}_{Mn})^1(3d^{e}_{Mn})^1$, with a weight of 98 % (Fig. 3.7). This configuration arises from a single σ bond between the two metal centres, and five singly occupied non-bonding 3*d* orbitals. The Mn–Mg single bond was calculated to have an EBO of 0.97, which largely originates from the 4s and 3s orbitals on the Mn and Mg respectively.

As previously mentioned, the two metal centres have different electronegativities (1.31 for Mg and 1.55 for Mn on the Pauling scale) [30], resulting in a formal Mn(0)Mg(II) complex. However, this difference in electronegativities is not great, and therefore the Mn–Mg bond should not be heavily polarised, and therefore should possess significant covalent character. Indeed this is the case, and an only

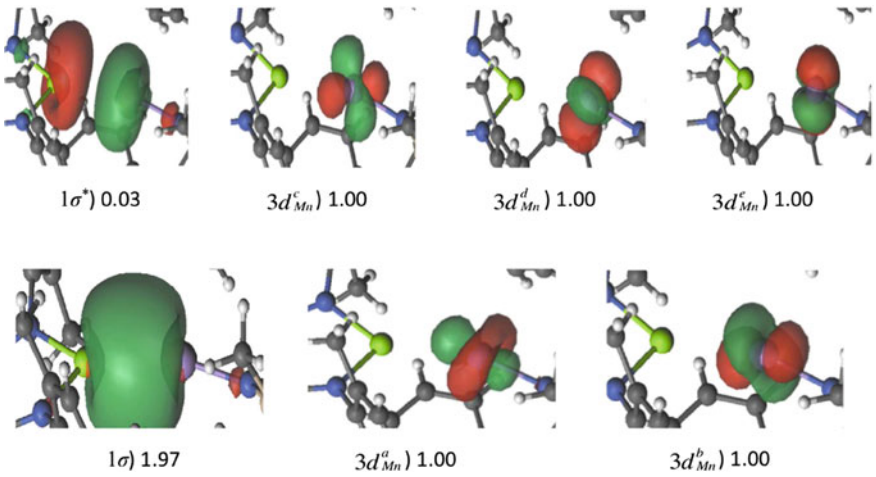

Fig. 3.7 Active orbitals and corresponding occupation numbers for the sextet ground state of compound **3-16^{Me}**. The *green* atom (*left*) is Mg, and the *purple* atom (*right*) is Mn. Iso-surface value 0.03 a.u

slightly polarised covalent bond is calculated between the two metal centres (Fig. 3.7). To add further support, the LoProp atom charges were calculated for the two metal centres in **3-16^{Me}** (Mn +0.69 and Mg +0.83), which are similar and positive for both metals.

Combining the results of X-ray crystallography, magnetic measurements, EPR spectroscopy and computational calculations, it can be concluded that **3-16** is a singly bonded manganese-magnesium heterobimetallic complex with a two-coordinate manganese centre. The Mn centre is formally in the zero oxidation state and is high-spin. The spin state of the complex is 5/2, supported by magnetic measurements, low and high field EPR spectroscopy as well as computation calculations.

3.3.3 Reactivity of a Two-Coordinate Manganese(0) Heterobimetallic Complex

3.3.3.1 Reactivity of an Mn–Mg Bonded Complex Towards Inorganic Complexes

The isolation of the manganese-magnesium heterobimetallic complex **3-16** was at first rather surprizing, as we were initially targeting the manganese(I) dimer [{(Ar†(Si^{i}Pr$_3$)NMn}$_2$]. It is therefore likely that the mechanism of this reaction involves the generation of the transient manganese(I) fragment "Ar†(Si^{i}Pr$_3$)NMn", but with the increase in ligand bulk (compared with the reduction of **2-43**) the dimerization of this fragment has become less favourable. A similar mechanism can be proposed for the isolation of the inverted sandwich manganese(I) complex **3-11**, which bears extremely bulky 3,5-^{i}Pr$_2$-Ar^{Tripp} ligands. However, in the case of **3-11**, a molecule of toluene inserts between the metal centres, increasing the distance between the two 3,5-^{i}Pr$_2$-Ar^{Tripp}Mn fragments, whereas in the **3-16**, the transient fragment is further reduced by the magnesium(I) reducing agent **1-08**, yielding **3-16**.

It was therefore proposed that the formation of the initially targeted manganese(I) complex [{(Ar†(Si^{i}Pr$_3$)NMn}$_2$] could still be possible, and **3-16** is simply an intermediate in the reduction process. To test this hypothesis, a further equivalent of the amido manganese bromide **2-45** was added to a solution of **3-16**, and the mixture stirred at room temperature for a week, which resulted in almost complete recovery of the starting materials. The reaction was repeated, heating the reaction mixture to 60 °C. However, after a couple of hours at this temperature, complete decomposition of **3-16** was observed by ^{1}H NMR spectroscopy. It was therefore concluded that the formation of [{(Ar†(Si^{i}Pr$_3$)NMn}$_2$] is simply unfavourable, due to large steric demands of the two Ar*(Si^{i}Pr$_3$)N^{-} ligands.

It was later proposed, that even though the formation of [{(Ar†(Si^{i}Pr$_3$)NMn}$_2$] is unfavourable, **3-16** could possibly be utilized as a reagent in the synthesis of a less bulky asymmetrical manganese(I) dimer. If **3-16** acts as a reducing agent towards a

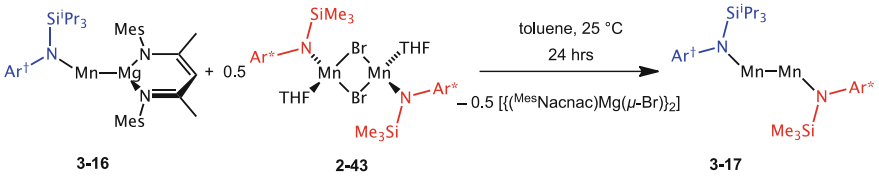

3-16 2-43 3-17

Scheme 3.10 Preparation of **3-17**

less sterically demanding amido manganese bromide complex, the isolation of an unprecedented asymmetrical manganese(I) dimer could be possible. With this in mind, **3-16** was reacted with half an equivalent of **2-43**, the less bulky amido manganese(II) bromide complex, in toluene at room temperature (Scheme 3.10). Over 24 h, the intense blue colour of **3-16** slowly disappeared and the mixture turned dark red. After workup and subsequent crystallisation, deep red crystals of the proposed asymmetrical amido manganese(I) dimer [Ar†(Si^{i}Pr$_3$)NMnMnN(SiMe$_3$)Ar*] **3-17** were isolated. These crystals were analysed by X-ray crystallography and the structure of the complex determined (Fig. 3.8).

Compound **3-17** is a two-coordinate, asymmetrical amido manganese(I) bimetallic complex with an unsupported metal–metal bond. The complex is unprecedented, as it is the only carbonyl free asymmetrical transition metal(I) dimer

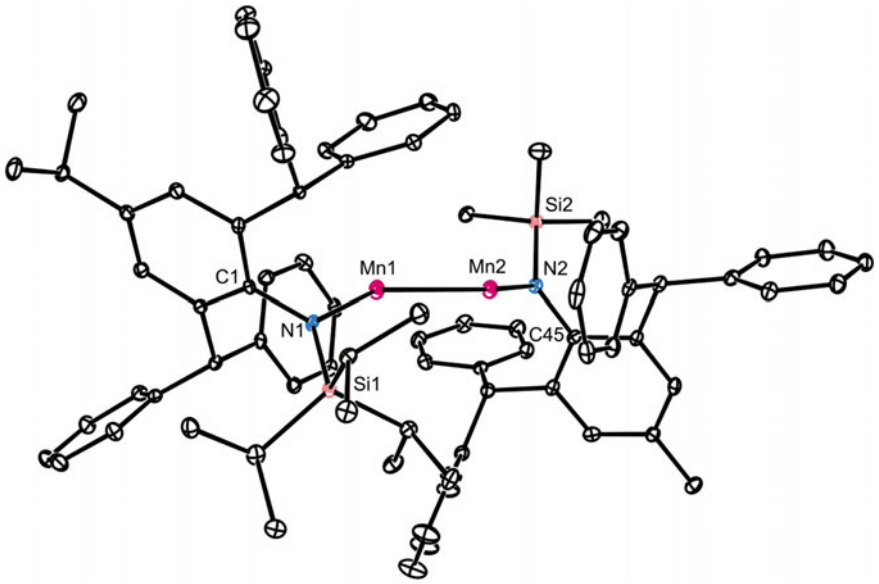

Fig. 3.8 Thermal ellipsoid plot (25 % probability surface) of the molecular structure of **3-17**. Hydrogen atoms have been omitted for clarity. Selected bond lengths (Å) and angles (°): Mn(1)-N(1) 2.027(3), Mn(1)-Mn(2) 2.7431(7), Mn(2)-N(2), 2.010(3), N(1)-Mn(1)-Mn(2) 154.08(7), N(2)-Mn(2)-Mn(1) 152.01(9)

reported to date. The complex resembles that of the previously discussed amido manganese(I) dimer **3-15**, but with a few minor differences. Complex **3-17** has a slightly longer Mn–Mn bond than **3-15** [2.7431(7) Å compared with 2.7224(6) Å], and a twisted central N–Mn–Mn–N unit [torsion angle = 138.34(13)°] compared with the planar N–Mn–Mn–N unit in **3-15**. These differences are likely due to the larger steric demands of the Ar*(Si^{i}Pr$_3$)N$^-$ ligand in **3-17**, causing extra strain on the complex to accommodate it. The two metal centres are non-linear and two-coordinate, with no strong interactions to the ligand's flanking phenyl rings [closest Mn···C$_{Phenyl}$ = 3.043(3) Å].

Compound **3-17** is paramagnetic in solution, and has an effective magnetic moment (μ_{eff} = 3.4 μ_B) in solution at room temperature, identical to that of the symmetrical complex **3-15**, as determined by the Evans method [28]. This is once again indicative of two high-spin manganese(I) centres that are strongly antiferromagnetically coupled. It was therefore concluded that **3-17** is similar structurally, and electronically to the previously discussed **3-15**.

The reaction between the Mn–Mg bonded complex **3-16**, and the amido manganese(II) bromide system **2-43**, to yield the asymmetrical manganese(I) dimer **3-17** is rather interesting, as **3-16** is acting as an "inorganic Grignard reagent", in the transfer of the "Ar†(Si^{i}Pr$_3$)NMn" group onto a second metal centre, thus creating a new metal–metal bond. We wanted to further explore the reactivity of complex **3-16** as an "inorganic Grignard reagent", to potentially synthesise a number of low coordinate heterobimetallic complexes with unsupported metal–metal bonds. Accordingly, complex **3-16** was reacted in turn, with the amido chromium chloride **2-41**, the amido iron bromide **2-46** and the amido zinc bromide **2-51**, in the hope that heterobimetallic complexes, essentially isostructual to the asymmetrical manganese(I) dimer **3-17** would be isolated (Scheme 3.11).

Unfortunately, even after multiple attempts, including changing the reaction conditions, none of these reactions led to the isolation of a heterobimetallic complex with an unsupported metal–metal bond. The reactions between **3-16** and both **2-46** and **2-51**, led to intractable mixtures of products on multiple occasions, with signs of decomposition seen by the precipitation of elemental metal in every case. However, crystals of a heterobimetallic complex were isolated from the reaction between **3-16** and the amido chromium chloride complex **2-41**, when the reaction

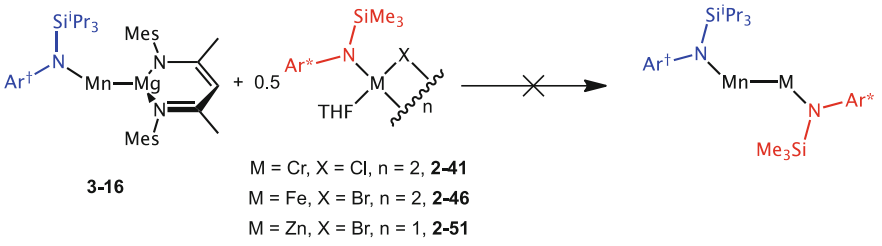

Scheme 3.11 Unsuccessful reactions of **3-16** carried out in order to isolate heterobimetallic complexes with unsupported metal–metal bonds

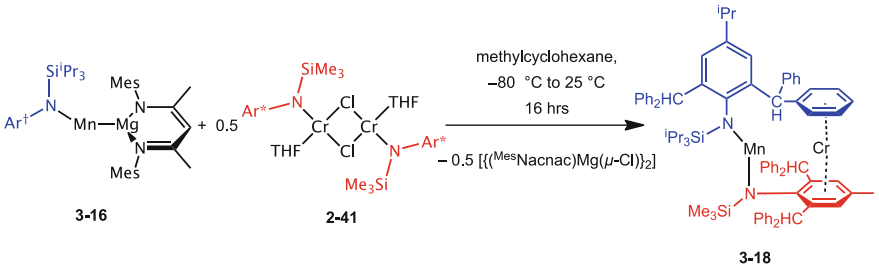

Scheme 3.12 Preparation of **3-18**

was performed in methylcyclohexane (Scheme 3.12). These dark yellow/gold crystals were analysed by X-ray crystallography, and the structure of the new heterobimetallic complex **3-18** was determined (Fig. 3.9).

Complex **3-18** is a chromium-manganese heterobimetallic complex, bearing one $Ar^{\dagger}(Si^{i}Pr_3)N^{-}$ and one $Ar^{*}(SiMe_3)N^{-}$ ligand, i.e. one from each reactant. The product shows that once again, **3-16** has been successfully utilized as an "inorganic Grignard reagent" in the transfer of the "$Ar^{\dagger}(Si^{i}Pr_3)NMn$" fragment onto another

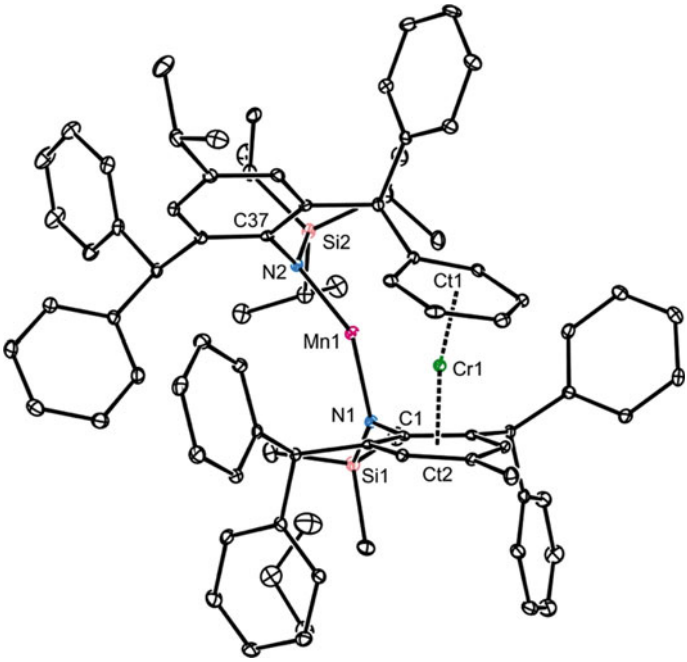

Fig. 3.9 Thermal ellipsoid plot (25 % probability surface) of the molecular structure of **3-18**. Hydrogen atoms have been omitted for clarity. Selected bond lengths (Å) and angles (°): Cr(1)···Mn(1) 3.0443(6), Mn(1)-N(1) 1.952(2), Mn(1)-N(2) 1.998(2), N(1)-Mn(1)-N(2) 140.00(9), Ct(1)-Cr(1)-Ct(2) 164.42(6)

metal fragment, but this time yielding a complex in a different arrangement. It is likely that the reaction mechanism proceeds via the initially targeted Cr–Mn bonded intermediate, which subsequently undergoes an internal redox process to give **3-18**, however no evidence for this has been obtained.

Complex **3-18** is mixed valance, with a two-coordinate Mn(II) bis-amido fragment [N–Mn–N = 140.00(9)°]. The Cr(0) centre is η^6 coordinated to the central ring of the Ar*($SiMe_3$)N^- ligand, and a flanking phenyl ring of the Ar*(Si^iPr_3)N^- ligand, in a sandwich type motif. The separation between the two metal centres is 3.0443(6) Å, which is only slightly greater than the sum of the covalent radii of Cr and high-spin Mn (3.00 Å) [24]. This implies that there could be an interaction, or even a weak bond between the two metal centres. To further investigate the possibility that the two metal centres are interacting, magnetic studies were performed on the complex.

The solution-state effective magnetic moment of complex **3-18**, determined by the Evans method, was found to be 5.5 μ_B, which is only slightly less than the spin only value for a non-interacting high-spin manganese(II) centre (5.9 μ_B). The chromium(0) centre is expected to have negligible input to the overall paramagnetism of the complex, as coordination of two η^6 rings result in a saturated diamagnetic 18 electron centre, as previously seen in complexes such as bis-(η^6-benzene)chromium [31]. Therefore, the value of 5.5 μ_B signifies a high-spin Mn(II) centre, with little, if any coupling to the Cr centre.

Variable-temperature magnetic susceptibility measurements were also performed on a polycrystalline sample of **3-18**. The measurement was conducted using a SQUID magnetometer in the temperature range 2–320 K and in an applied field of 0.01 Torr, the results of which are highlighted in Fig. 3.10. The data are similar to those obtained for the Mn–Mg complex **3-16**, in that they are indicative of a $S = 5/2$ ground state, with the $\chi_M T$ value decreasing gradually as a function of temperature in a Curie-Weiss fashion to ~3 K, and then more rapidly due to Zeeman

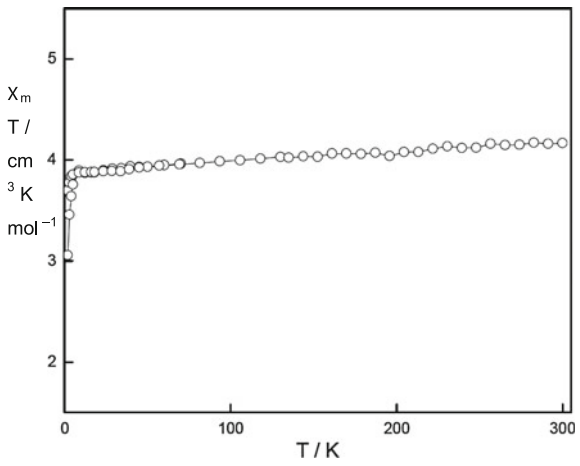

Fig. 3.10 Plot of $\chi_M T$ versus T for **3-18**. The *solid line* is a guide to the eye

depopulation. The results are reminiscent of a non-interacting high-spin Mn(II) centre, and show no indication of coupling to another metal centre.

Calculations using the theory methods CASSCF and CASPT2, were also performed on complex **3-18**, to further support the lack of a metal–metal interaction. The ground state of the complex was calculated to be a sextet, with the dominant configuration being $(1ML)^2(3d_{Cr})^2(2ML)^2(3d^a_{Mn})^1(3d^b_{Mn})^1(3d^c_{Mn})^1(3d^d_{Mn})^1(3d^e_{Mn})^1$ (Fig. 3.11). The calculations indicate the presence of five singly occupied, non-bonding 3*d* orbitals on the manganese centre, similar to the results for **3-16^{Me}**, in addition to three doubly occupied bonding orbitals on the chromium centre. The results are in agreement with the magnetic measurements and indicate effectively no bonding between the two metal centres.

By analysing the results from X-ray crystallography, magnetic measurements and calculations, in can be concluded that complex **3-18** is a mixed valence manganese(II)-chromium(0) heterobimetallic complex with effectively no metal–metal interaction, even though the solid state structure reveals the two metals to be in close proximity to one another. The complex was synthesised by the transfer of a "Ar†(Si^{i}Pr$_3$)NMn" group by the "inorganic Grignard reagent" **3-16**, onto a chromium centre derived from the complex **2-41**. The reaction is proposed to proceed through the initially targeted metal–metal bonded complex as a reaction intermediate, which undergoes an internal redox process to give **3-18**.

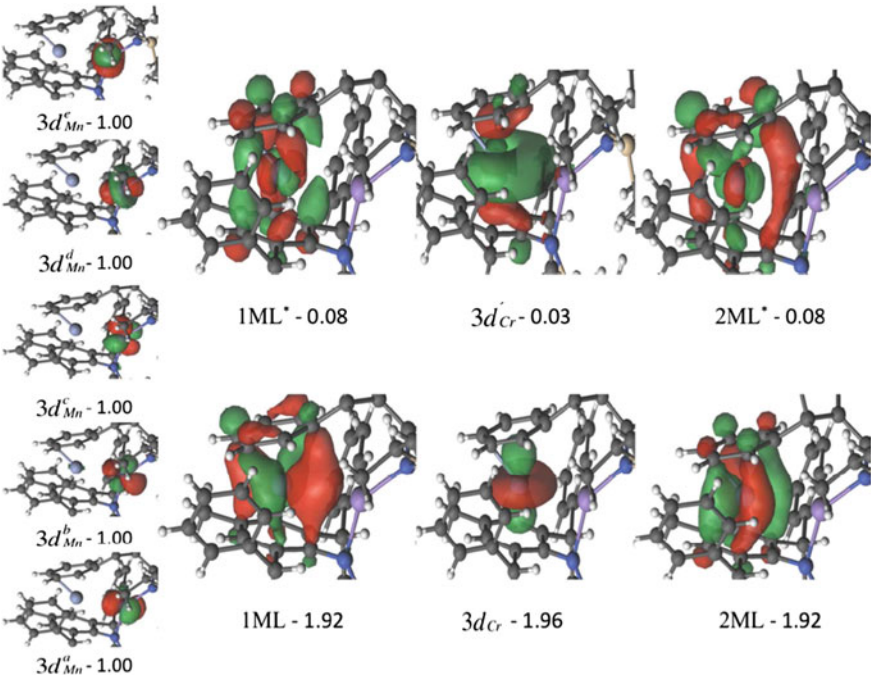

Fig. 3.11 Active orbitals and corresponding occupation numbers of the sextet ground state of **3-18**. The *grey-blue* atom (*left*) is Cr and the *purple* atom (*right*) is Mn. Iso-surface value 0.03 a.u

3.3.3.2 Reactivity of an Mn–Mg Bonded Complex Towards Small Organic Molecules and Gases

The reactivity of the manganese-magnesium heterobimetallic complex **3-16** towards a number of small organic molecules, as well as a range of different gases was also investigated. The results of these reactivity studies are outlined in Scheme 3.13.

In addition to the reactants shown in Scheme 3.13, toluene solutions of **3-16** were also reacted with the gases CO and O_2, under one atmosphere, at −80 °C. Both reactions resulted in colour changes, (from royal blue to red/brown on addition of CO, and to pale yellow on addition of O_2), but unfortunately, no product was isolated from either reaction.

When complex **3-16** was either dissolved in THF, or THF added to a solution of **3-16**, in a non-coordinating solvent such as toluene, a subtle but immediate colour change was observed, from royal blue to blue/purple. Crystals of this blue/purple product were grown from pentane, and characterised by X-ray crystallography (Fig. 3.12).

A crystal structure determination revealed the complex to be a THF adduct of the Mn–Mg complex **3-16** (viz. [Ar†(Si^{i}Pr$_3$)NMnMg(THF)(^{Mes}Nacnac)], **3-19**), where a molecule of THF is coordinating to the magnesium centre. The addition of THF increases the coordination number of the magnesium, from three in **3-16** to four in **3-19**, resulting in a change of the metal geometry from trigonal to distorted tetrahedral. The coordination of THF [along with other donor molecules such as

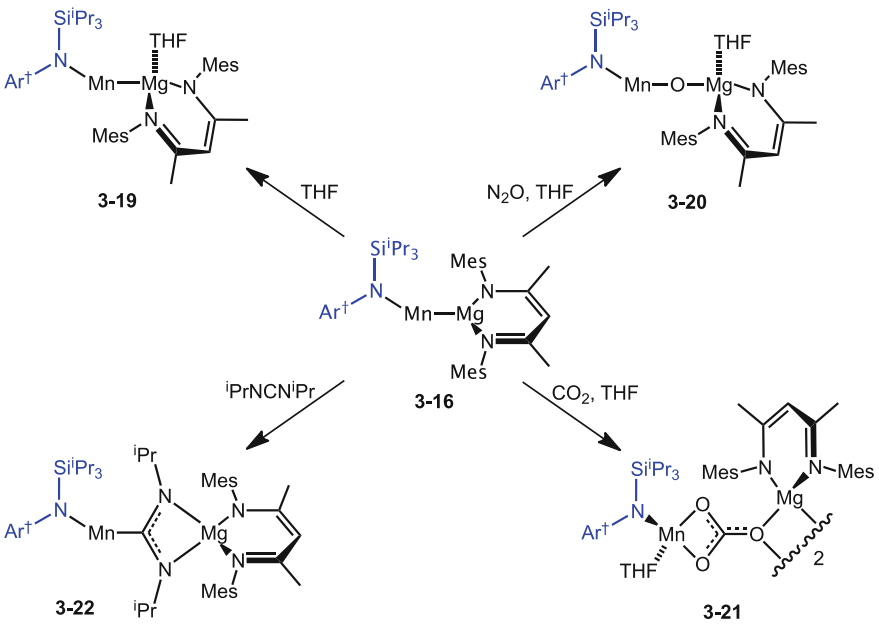

Scheme 3.13 Reactions of **3-16** with a selection of gases and organic substrates

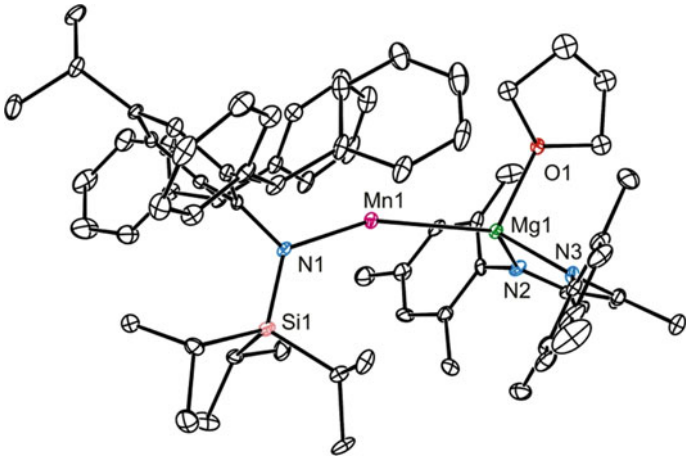

Fig. 3.12 Thermal ellipsoid plot (25 % probability surface) of the molecular structure of **3-19**. Hydrogen atoms have been omitted for clarity. Selected bond lengths (Å) and angles (°): Mn(1)-Mg(1) 2.921(2), Mn(1)-N(1) 2.041(5), Mg(1)-O(1) 2.10(2), Mg(1)-N(2) 2.071(5), Mg(1)-N(3) 2.082(2), N(1)-Mn(1)-Mg(1) 157.94(14) Mn(1)-Mg(1)-O(1) 111.6(5)

4-dimethylaminopyridine (DMAP)] to the three-coordinate (^{Mes}Nacnac) Mg unit, has previously been reported, for example with the coordination of THF to the magnesium(I) complex **1-08**, to give the tetrahedral magnesium complex [{(^{Mes}Nacnac)Mg(THF)}$_2$] [32].

The coordination of THF to the magnesium centre in **3-19** has also resulted in an elongation of the Mn–Mg bond by 0.1 Å [from 2.8244(13) Å in **3-16** to 2.921(2) Å in **3-19**], due to the increase in the coordination number of the magnesium. Rather surprisingly, even when **3-16** is dissolved in THF, the manganese centre remains two-coordinate, and THF free. This is likely due to the large steric demands of the Ar*(Si^{i}Pr$_3$)N$^-$ and ^{Mes}Nacnac ligands, disfavouring the coordination of a second molecule of THF. Complex **3-19** exhibits a solution state magnetic moment of 5.3 μ_B, which is the same as the THF free complex **3-16**, indicating little, if any, change to the Mn centre's electronics due to the coordination of THF.

The reactivity of complex **3-16** towards the oxidizing agent N_2O was also tested. When a toluene solution of **3-16** was exposed to one atmosphere of N_2O at −80 °C, an immediate colour change was observed from royal blue to pale yellow. After workup, including the addition of THF to aid crystallisation, colourless crystals of [Ar†(Si^{i}Pr$_3$)NMnOMg(THF)(^{Mes}Nacnac)] **3-20** were isolated in good yield (Fig. 3.13).

The reaction between complex **3-16** and N_2O has resulted in oxidation of the Mn(0) centre in the starting material, to Mn(II) in the oxo-bridged complex **3-20**, with a molecule of THF coordinated to the magnesium centre. Multiple attempts to isolate X-ray quality crystals of the THF free form of complex **3-20** were carried out, but unfortunately were unsuccessful. Complex **3-20** possesses a two-coordinate, non-linear manganese(II) centre [N–Mn–O = 163.85(8)°], with no strong

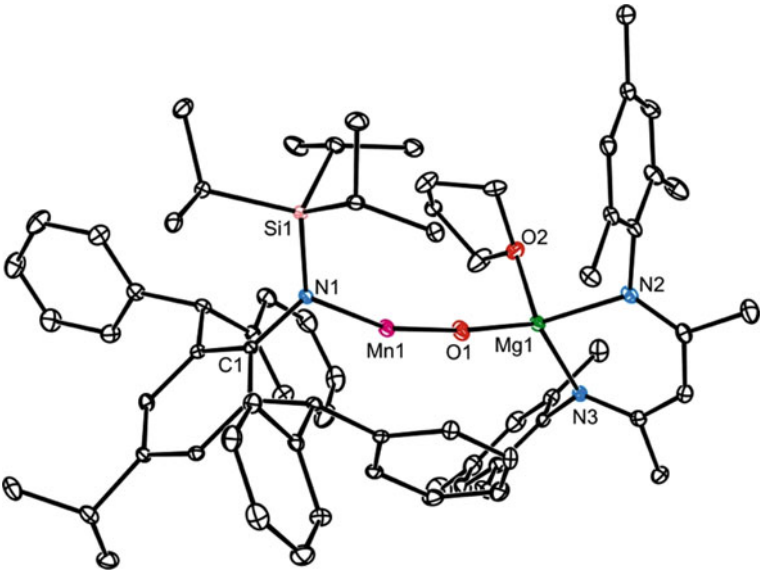

Fig. 3.13 Thermal ellipsoid plot (25 % probability surface) of the molecular structure of **3-20**. Hydrogen atoms have been omitted for clarity. Selected bond lengths (Å) and angles (°): Mn(1)-O(1) 1.7986(16), Mg(1)-O(1) 1.8490(18), Mn(1)-N(1) 2.0009(18), Mg(1)-O(2) 2.0755(19), Mg(1)-N(2) 2.048(2), Mg(1)-N(3) 2.055(2), N(1)-Mn(1)-O(1) 163.85(8), Mn(1)-O(1)-Mg(1) 172.80(11)

interactions between the flanking phenyl groups of the ligand [closest Mn···C_{phenyl} = 3.047(2)°]. The two-coordinate manganese oxide complex **3-20** is unprecedented. Reactions between low oxidation state manganese complexes and oxidizing agents such as N_2O, usually give dioxo-bridged structures, such as the dioxo-bridged [{(^{Dipp}Nacnac)Mn(μ-O)}$_2$] **3-03** and [{(Piso)Mn(μ-O)}$_2$] **3-09** [6, 12].

It is worth noting that from the reaction between **3-16** and N_2O, a crystal of [{Ar†(Si^{i}Pr$_3$)NMn}$_2$(μ-O)], a second two-coordinate oxo-bridged Mn(II) complex, was isolated on multiple occasions, suggesting that it is a by-product of the reaction. However, due to the very low yield of this complex (<2 %), no further analysis has been performed on it (see Sect. 7.2 for the molecular structure).

A toluene solution of **3-16** was also exposed to one atmosphere of CO_2 at −80 °C, which, similar to the addition of N_2O, resulted in an immediate colour change from royal blue to pale yellow. After workup, including the addition of THF to aid crystallisation, a small number of colourless crystals of [{Ar†(Si^{i}Pr$_3$)NMn(THF)(μ-CO_3)Mg(^{Mes}Nacnac)}$_2$] **3-21** were isolated (Fig. 3.14).

Complex **3-21** is an example of a manganese-magnesium carbonate compound, where the CO_3^{2-} units are bridging the metal centres. The complex is dimeric in the solid state, dimerising through the Mg-O units to give a central Mg_2O_2 four membered ring. The dimerization results in the magnesium centres possessing tetrahedral geometries, and therefore no Mg coordinated THF is present, even though THF was added to the reaction mixture. In contrast, the two manganese

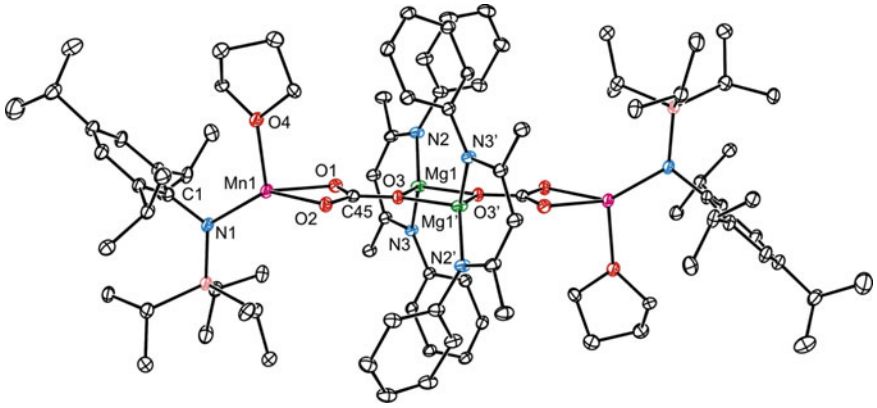

Fig. 3.14 Thermal ellipsoid plot (25 % probability surface) of the molecular structure of **3-21**. Hydrogen atoms have been omitted for clarity. Selected bond lengths (Å) and angles (°): Mn(1)-N (1) 1.997(4), Mn(1)-O(1) 2.165(3), Mn(1)-O(2) 2.140(3), Mn(1)-O(4) 2.127(3), Mg(1)-N(2) 2.027 (4), Mg(1)-N(3) 2.020(3), Mg(1)-O(3) 1.988(3), Mg(1)-O(3') 2.018(3), Mg(1)-Mg(1′) 3.124(3), O(1)-C(45) 1.300(5), O(2)-C(45) 1.252(5), C(45)-O(3) 1.293(5), O(1)-Mn(I)-O(2) 61.74(12), O(3)-Mg(1)-O(3') 77.53(13), Mg(1)-O(3)-Mg(1′) 102.47(13)

centres do possess a coordinating THF molecule, resulting in four coordinate manganese centres, also with distorted tetrahedral geometries.

The reaction of complex **3-16** with CO_2 has resulted in an oxidation of the Mn(0) centre to Mn(II), and consequently a reduction of CO_2. The mechanism of the reaction is likely similar to the reaction between CO_2 and the magnesium(I) dimer **1-04**, which yielded the related magnesium carbonate complex [(^{Dipp}Nacnac)Mg}$_2$(μ-CO_3)] **1-12** (as discussed in Sect. 1.4) [33]. That is, one equivalent of CO_2 initially reacts with the **3-16**, resulting in a two electron reduction of the gas, releasing a molecule of CO and forming the oxo-bridged structure [{Ar†(Si^{i}Pr$_3$)NMnOMg(^{Mes}Nacnac)}$_2$] **3-20a** (**3-20a** is essentially the same as the isolated structure **3-20**, but without a coordinating THF). The oxo-bridged complex **3-20** then reacts with a second equivalent of CO_2 to give the carbonate, presumably followed by dimerization (Scheme 3.14).

Unfortunately, due to the very low yields of complex **3-21** (<5 %), as well as difficulties isolating the complex cleanly, no further analysis of the compound has been performed.

Finally, to probe the reactivity of **3-16** towards small unsaturated organic molecules, one equivalent of N,N′-diisopropylcarbodiimide was added to a toluene solution of **3-16** at −80 °C. On warming to ambient temperature a colour change from royal blue to yellow was observed. After workup and subsequent crystallisation from pentane, large yellow crystals of [{Ar†(Si^{i}Pr$_3$)NMn{μ-C(N^{i}Pr)$_2$}Mg(^{Mes}Nacnac)}$_2$] **3-22** were isolated in good yield (Fig. 3.15).

The reaction of complex **3-16** and N,N′-diisopropylcarbodiimide, resulted in a two-electron reduction of the substrate, and its insertion into the metal–metal bond.

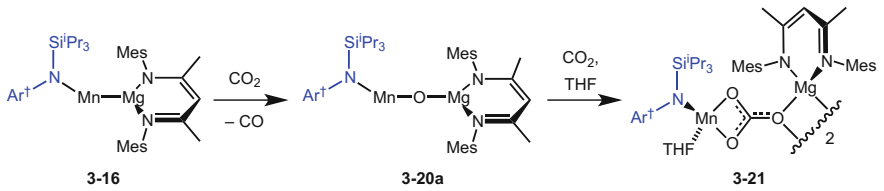

Scheme 3.14 Proposed synthesis of complex **3-21**

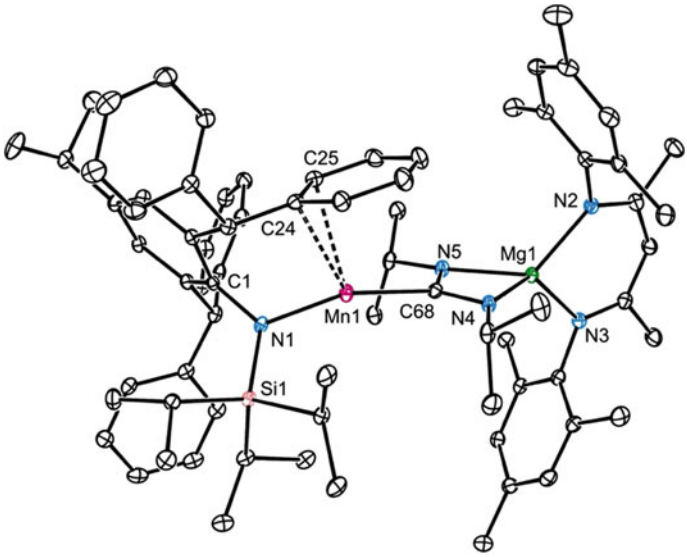

Fig. 3.15 Thermal ellipsoid plot (25 % probability surface) of the molecular structure of **3-22**. Hydrogen atoms have been omitted for clarity. Selected bond lengths (Å) and angles (°): Mn(1)-N (1) 1.981(2), Mn(1)-C(68) 2.131(3), Mn(1)-C(24) 2.851(3), Mn(1)-C(25) 2.617(3), Mg(1)-N(5) 2.038(2), Mg(1)-N(3) 2.050(2), Mg(1)-N(2) 2.057(2), Mg(1)-N(4) 2.060(2), N(4)-C(68) 1.348(3), N(5)-C(68) 1.348(3), N(1)-Mn(1)-C(68) 155.30(9), N(3)-Mg(1)-N(2) 91.83(9), N(5)-Mg(1)-N(4) 66.56(9), N(5)-C(68)-N(4) 113.1(2)

The two nitrogen atoms of the NCN unit are coordinated to the magnesium centre, resulting in a four-coordinate tetrahedral magnesium atom. The central carbon of the NCN unit is bonded to the manganese centre, resulting in an oxidation of the metal from 0 to +2. The manganese centre exhibits a fairly strong interaction with one of the flanking phenyl rings of the Ar† substituent [closest interaction Mn–C25 = 2.617(3) Å], which is highlighted in Fig. 3.15. Therefore the manganese(II) centre is pseudo two-coordinate with a bent N–Mn–C angle of 155.30(9)°.

The two electron reduction and insertion of a carbodiimide into a metal–metal bond is once again analogous to the reactivity of the magnesium(I) dimer **1-04**, where addition of N,N′-dicyclohexylcarbodiimide to a solution of the dimer resulted in the reductive insertion product [{(^{Dipp}Nacnac)Mg}$_2${μ-C(NCy)$_2$}] **1-13** [34].

As magnesium(I) dimers are becoming increasingly popular in the reduction of organic and inorganic substrates, the similar reactivity of complex **3-16** makes it a possible alternative.

3.4 Conclusion

In conclusion, a range of unprecedented low oxidation state manganese complexes have been isolated by utilizing the kinetic stabilising properties of two extremely bulky amido ligands. These include the first example of a two-coordinate manganese(I) dimer **3-15**, as well as the manganese-magnesium heterobimetallic complex **3-16**, which possesses a two coordinate manganese(0) centre. All complexes were characterised using a range of analytical techniques, including X-ray crystallography, SQUID and EPR spectroscopy, as well as ab initio calculations. The reactivity of complex **3-16** as an "inorganic Grignard reagent" was investigated, in the preparation of the asymmetrical manganese(I) dimer **3-17**, and the mixed valance chromium(0)-manganese(II) heterobimetallic complex **3-18**. Further reactivity of complex **3-16** towards a range of gases and small organic molecules was investigated, with mixed success.

3.5 Experimental

General methods. All manipulations were carried out using standard Schlenk and glove box techniques under an atmosphere of high purity dinitrogen. THF, hexane, cyclohexane, methylcyclohexane and toluene were distilled over molten potassium, while diethyl ether and pentane were distilled over sodium/potassium alloy (1:1). ^{1}H NMR spectra were recorded on either Bruker AvanceIII 400 or Varian Inova 500 spectrometers and were referenced to the resonances of the solvent used, or external $SiMe_4$. Mass spectra were recorded on an Agilent Techonlogies 5975D inert MSD with a solid state probe or obtained from the EPSRC National Mass Spectrometric Service at Swansea University. IR spectra were recorded using a Perkin-Elmer RX1 FT-IR spectrometer as Nujol mulls between NaCl plates or recorded as solid samples using an Agilent Cary 630 attenuated total reflectance (ATR) spectrometer. Microanalyses were carried out by the Science Centre, London Metropolitan University. A reproducible microanalysis could not be obtained for **3-17**, as the compound contained hexane of crystallization which could not be completely removed by placing the sample under reduced pressure for several hours. Moreover, recrystallized samples of the compound were consistently contaminated by small amounts (<5 % as determined by ^{1}H NMR spectroscopy) of free amine, Ar*(Si^{i}Pr$_3$)NH. The complexes [{Ar*(SiMe$_3$)NCr(μ-Cl)(THF)}$_2$] **2-41**, [{Ar*(SiMe$_3$)NMn(μ-Br)(THF)}$_2$] **2-43** and [{Ar†(Si^{i}Pr$_3$)NMn(μ-Br)(THF)}$_2$] **2-45** were prepared as discussed in Chap. 2 and [{(^{Mes}Nacnac)Mg}$_2$] **1-08** according to the literature method [32]. All other reagents were used as received.

Preparation 1 of [{Ar*(SiMe$_3$)NMn}$_2$], 3-15. To a suspension of [{Ar*(SiMe$_3$)NMn(μ-Br)(THF)}$_2$] **2-43** (0.200 g, 0.139 mmol) in cyclohexane (10 mL), was added a suspension of [{(^{Mes}Nacnac)Mg}$_2$] **1-08** (0.110 g, 0.153 mmol) in cyclohexane (10 mL) at 10 °C over 5 min. The reaction mixture turned from pale yellow to dark red after approximately 2 min. The reaction was slowly warmed to room temperature and stirred for a further 12 h, whereupon volatiles were removed in vacuo. The residue was extracted toluene (20 mL), and the extract concentrated (ca. 5 mL) and slowly cooled to −30 °C overnight to give **3-15** as dark red crystals (0.110 g, 70 %).

Preparation 2 of [{Ar*(SiMe$_3$)NMn}$_2$], 3-15. To a suspension of [{Ar*(SiMe$_3$)NMn(μ-Br)(THF)}$_2$] **2-43** (0.200 g, 0.139 mmol) in cyclohexane (10 mL), was added a suspension of KC_8 (0.041 g, 0.306 mmol) in cyclohexane (10 mL) at room temperature. The reaction mixture was stirred for 4 days, whereupon volatiles were removed in vacuo. The residue was extracted toluene (20 mL), and the extract concentrated (ca. 5 mL) and slowly cooled to −30 °C overnight to give **3-15** as dark red crystals (0.015 g, 10 %). Mp: 230–232 °C; ^{1}H NMR (499 MHz, C_6D_6, 298 K): δ = 1.49 (br.), 2.06 (br.), 2.35 (br.), 11.01 (br.), 13.07 (br.); IR υ/cm^{-1} (Nujol): 1596(m), 1492(m), 1237(s), 1207(m), 1132(m), 1074(m), 1031(m), 911(m), 899(s), 879(m), 847(s), 828(s), 752(m), 721(m), 699(s), 603(m), 558(m); UV-Vis (toluene) [λ_{max}, nm (ε, M^{-1} cm^{-1})]: 493 (1223); MS/EI *m/z* (%): 1128.5 ([M − 2H]$^+$, <1), 511.3 (Ar*N(H)SiMe$_3^+$, 100), 439.2 (Ar*NH$_2^+$, 28), 167.0 (Ph$_2$CH$^+$, 19); μ_{eff} (Evans, C_6D_6, 298 K): 3.4 μ_B; anal. calc. for $C_{72}H_{72}Mn_2N_2O_2Si_2$: C 76.43 %, H 6.41 %, N 2.48 %, found: C 76.33 %, H 6.35 %, N 2.53 %.

Preparation of [Ar†(Si^{i}Pr$_3$)NMnMg(^{Mes}Nacnac)], 3-16. To a suspension of [{Ar†(Si^{i}Pr$_3$)NMn(THF)(μ-Br)}$_2$] **3-45** (0.442 g, 0.266 mmol) in cyclohexane (30 mL), was added a suspension of [{^{Mes}Nacnac)Mg}$_2$] **1-08** (0.400 g, 0.559 mmol) in cyclohexane (15 mL) at room temperature. The reaction mixture turned an intense blue colour approximately 2 min after addition. The reaction was stirred for a further 2 h, whereupon volatiles were removed from the filtrate in vacuo. The residue was extracted with pentane (15 mL), the extract filtered and volatiles removed in vacuo to give **3-16** as a blue solid (0.390 g, 71 %). N.B. X-ray quality crystals of **3-16** were obtained by crystallizing this solid from hexane. Mp: 79–81 °C; ^{1}H NMR (499 MHz, C_6D_6, 298 K): δ = −1.16 (br.), 2.63 (br.), 4.36 (br.), 7.30 (br.); IR υ/cm^{-1} (Nujol): 1524(m), 1398(s), 1260(s), 1231(m), 1197(m), 1146(m), 1091(s), 1018(s), 856(m), 799(s), 721(m), 700(s), 604(m); UV-Vis (toluene) [λ_{max}, nm (ε, M^{-1} cm^{-1})]: 556 (1023), 588 (1101); MS/CI *m/z* (%): 624.4 (Ar†N(H)Si^{i}Pr$_3$ + H$^+$, 100), 580.3 (Ar†N(H)Si^{i}Pr$_3^+$ − ^{i}Pr, 16), 335.2 (^{Mes}NacnacH + H$^+$, 26), 167.0 (Ph$_2$CH$^+$, 7); μ_{eff} (Evans, C_6D_6, 298 K): 5.3 μ_B; anal. calc. for $C_{67}H_{81}MgMnN_3Si$: C 77.70 %, H 7.88 %, N 4.06 %, found: C 77.81 %, H 7.90 %, N 3.98 %.

Preparation of [Ar†(Si^{i}Pr$_3$)NMnMnN(SiMe$_3$)Ar*], 3-17. To a solution of [{Ar†(Si^{i}Pr$_3$)N}MnMg(^{Mes}Nacnac)] **3-16** (0.200 g, 0.193 mmol) in toluene (15 mL), was added a solution of [{Ar*(SiMe$_3$)NMn(THF)(μ-Br)}$_2$] **2-43** (0.152 g, 0.106 mmol) in toluene (15 mL) at room temperature. The reaction was stirred for a further 24 h at room temperature, whereupon volatiles were removed in vacuo. The

residue was extracted with warm hexane (15 mL), the extract filtered and concentrated (ca. 5 mL) then slowly cooled to 5 °C overnight to give **3-17** as red/purple crystals (0.118 g, 49 %). Mp: 195–198 °C; ^{1}H NMR (499 MHz, C_6D_6, 298 K): δ = 4.03 (br.), 7.03 (br.), 12.57 (br.), 14.04 (br.); IR υ/cm^{-1} (Nujol): 1598 (m), 1492(s), 1260(s), 1230(s), 1074(s), 1031(s), 919(m), 901(m), 860(m), 832(m), 810(m), 760(m), 744(m), 738(m), 717(m), 699(s), 652(m), 629(m), 603(m); UV-Vis (toluene) [λ_{max}, nm (ε, M^{-1} cm^{-1})]: 494 (1947); MS/EI *m/z* (%): 623.4 ($Ar^{\dagger}N(H)Si^{i}Pr_3^+$, 49), 580.4 ($Ar^{\dagger}N(H)Si^{i}Pr_3^+ - {}^{i}Pr$, 100), 511.3 ($Ar^*N(H)SiMe_3^+$, 51), 467.3 ($Ar^{\dagger}NH_2^+$, 8), 439.2 ($Ar^*NH_2^+$, 95), 167.0 ($Ph_2CH^+$, 87); μ_{eff} (Evans, C_6D_6, 298 K): 3.4 μ_B.

Preparation of [CrMn{N(Si^{i}Pr$_3$)Ar†}{N(SiMe$_3$)Ar*}], 3-18. To a suspension of [{Ar*(SiMe$_3$)NCr(THF)(μ-Cl)}$_2$] **2-41** (0.155 g, 0.116 mmol) in methylcyclohexane (20 mL), was added a solution of [{$Ar^{\dagger}$(Si^{i}Pr$_3$)N}MnMg(^{Mes}Nacnac)] **3-16** (0.200 g, 0.193 mmol) in methylcyclohexane (10 mL) at −80 °C over 5 min. The reaction mixture was warmed to room temperature, where it was stirred for a further 16 h, to give a dark yellow solution. Volatiles were removed in vacuo, the residue was extracted with pentane (15 mL), the extract filtered, and left to stand at room temperature overnight to give **3-18** as a small dark yellow crystals (0.048 g, 20 %). N.B. X-ray quality crystals were obtained by recrystallizing these small crystals from hexane. Mp: 230–232 °C; ^{1}H NMR (400 MHz, C_6D_6, 298 K): δ = 2.49 (br.), 3.64 (br.), 5.46 (br.), 8.77 (br.), 10,04 (br.), 13.30 (br.); IR ν/cm^{-1} (Nujol): 1598(m), 1492(m), 1446(s), 1383(s), 1255(m), 1233(s), 1195(m), 1121(m), 1077(m), 1031(m), 997(m), 981(m), 924(m), 909(s), 892(s), 856(m), 829(s), 786(m), 762(m), 747(m), 718(s), 697(s); UV-Vis (toluene) [λ_{max}, nm (ε, M^{-1} cm^{-1})]: 375 (6677); MS/EI *m/z* (%): 623.4 ($Ar^{\dagger}(Si^{i}Pr_3)NH^+$, 4), 580.3 ($Ar^{\dagger}(Si^{i}Pr_3)NH^+ - {}^{i}Pr$, 7), 511.3 ($Ar^*N(H)SiMe_3^+$, 100), 467.3 ($Ar^{\dagger}NH_2^+$, 17), 439.2 ($Ar^*NH_2^+$, 46), 167.0 ($Ph_2CH^+$, 48), 73.0 ($Me_3Si^+$, 18); μ_{eff} (Evan's, C_6D_6, 298 K): 5.5 μ_B; anal. calc. for $C_{80}H_{88}CrMnN_2Si_2$: C 77.45 %, H 7.15 %, N 2.26 %, found: C 77.46 %, H 7.53 %, N 2.27 %.

Preparation of [Ar†(Si^{i}Pr$_3$)NMnMg(THF)(^{Mes}Nacnac)], 3-19. Blue crystals of [$Ar^{\dagger}$(Si^{i}Pr$_3$)NMnMg(^{Mes}Nacnac)] **3-16** (0.200 g, 0.193 mmol) were dissolved in THF (25 mL) and stirred for 5 min. Volatiles were removed in vacuo, the residue was dissolved in the minimum volume of pentane (ca. 15 mL) and slowly cooled to −30 °C overnight, to yield **3-19** as green/blue crystals (0. 185 g, 87 %). Mp: 147–151 °C; ^{1}H NMR (499 MHz, C_6D_6, 298 K): −0.87 (br.), 2.22 (br.), 4.62 (br.) 7.15 (br.); IR υ/cm^{-1} (Nujol): 1599(m), 1515(m), 1492(m), 1446(s), 1429(s), 1389(s), 1257(m), 1229(m), 1195(m), 1145(m), 1125(m), 1073(m), 1030(m), 1015(m), 918 (m), 856(m), 831(m), 811(m), 758(m), 743(m), 717(m), 698(s); μ_{eff} (Evans, C_6D_6, 298 K): 5.3 μ_B; anal. calc. for $C_{74}H_{95}MgMnN_5Si$: C 76.98 %, H 8.10 %, N 3.79 %, found: C 76.69 %, H 78.87 %, N 3.69 %.

Preparation of [Ar†(Si^{i}Pr$_3$)NMnOMg(THF)(^{Mes}Nacnac)], 3-20. To the headspace of a Schlenk flask, containing a solution of [$Ar^{\dagger}$(Si^{i}Pr$_3$)NMnMg (^{Mes}Nacnac)] **3-16** (0.200 g, 0.193 mmol) in a mixture of toluene (15 mL) and THF (1 mL) cooled to −80 °C, was added N_2O (5.11 mL, 0.212 mmol) via a gas tight syringe. The reaction mixture was allowed to warm to room temperature, then

stirred for a further 60 min, whereupon volatiles were removed in vacuo. The residue was dissolved in pentane (10 mL), and the extract left overnight at room temperature to give **3-20** as large colourless crystals (0.155 g, 71 %). Mp: 155–158 °C; ^{1}H NMR (499 MHz, C_6D_6, 298 K): 2.00 (br.), 4.92 (br.), 7.23 (br.), 17.80 (br.); IR υ/cm^{-1} (Nujol): 1549(m), 1518(m), 1492(m), 1449(s), 1430(s), 1396(s), 1258(m), 1229(m), 1196(m), 1146(m), 1030(m), 900(m), 881(m), 857(s), 815(s), 759(m), 738(m), 723(m), 698(s); MS/EI *m/z* (%): 623.4 ($Ar^{\dagger}N(H)Si^iPr_3^+$, 52), 580.4 ($Ar^{\dagger}N(H)Si^iPr_3^+ - {}^i$Pr, 100), 467.2 ($Ar^{\dagger}NH_2^+$, 6), 334.2 (^{Mes}NacnacH$^+$, 12), 167.0 (Ph_2CH^+, 53); μ_{eff} (Evans, C_6D_6, 298 K): 5.9 μ_B; anal. calc. for $C_{74}H_{95}MgMnN_5Si$: C 75.88 %, H 7.98 %, N 3.74 %, found: C 75.67 %, H 8.17 %, N 3.76 %.

Preparation of [Ar†(Si^{i}Pr$_3$)NMn(μ-CO$_3$)Mg(^{Mes}Nacnac)], 3-21. To the headspace of a Schlenk flask containing a solution of [Ar†(Si^{i}Pr$_3$)NMnMg(^{Mes}Nacnac)] **3-16** (0.200 g, 0.193 mmol), in toluene (15 mL), was added one atmosphere of CO_2 at −80 °C. The reaction mixture was allowed to warm to room temperature, then stirred for a further 2 h, whereupon volatiles were removed in vacuo. The residue was dissolved in the minimum volume of pentane (ca. 5 mL), spiked with 2 drops of THF, and left overnight at ambient temperature, to give **3-22** as small colourless crystals (<2 %).

Preparation of [Ar†(Si^{i}Pr$_3$)NMn{μ-C(N^{i}Pr)$_2$}Mg(^{Mes}Nacnac)], 3-22. To a solution of [Ar†(Si^{i}Pr$_3$)NMnMg(^{Mes}Nacnac)] **3-16** (0.200 g, 0.193 mmol) in toluene (15 mL), was added N,N′-diisopropylcarbodiimide (0.027 g, 0.213 mmol) slowly at −80 °C. The reaction mixture was allowed to warm to room temperature, then stirred for a further 2 h, whereupon volatiles were removed in vacuo. The residue was dissolved in the minimum volume of pentane (ca. 5 mL), and left overnight at ambient temperature, to give **3-22** as large yellow crystals. (0.190 g, 85 %). Mp: 155–158 °C; ^{1}H NMR (499 MHz, C_6D_6, 298 K): 1.36 (br.), 2.22 (br.), 7.04 (br.); IR υ/cm^{-1} (Nujol): 1599(m), 1546(m), 1524(s), 1492(m), 1314(s), 1260(s), 1224(m), 1214(m), 1196(s), 1030(m), 1014(m), 891(m), 856(s), 848(s), 799(s), 757(m), 725(m), 700(s), 664(m); MS/EI *m/z* (%): 623.4 ($Ar^{\dagger}N(H)Si^iPr_3^+$, 42), 580.4 ($Ar^{\dagger}N(H)Si^iPr_3^+ - {}^i$Pr, 100), 334.2 (^{Mes}NacnacH$^+$, 17), 167.0 (Ph_2CH^+, 40); μ_{eff} (Evans, C_6D_6, 298 K): 5.1 μ_B; anal. calc. for $C_{74}H_{95}MgMnN_5Si$: C 76.49 %, H 8.24 %, N 6.03 %, found: C 76.32 %, H 8.30 %, N 6.12 %.

References

1. Selected recent reviews: (a) J.P. Krogman, C.M. Thomas, Chem. Commun. **50**, 5115 (2014); (b) B.G. Cooper, J.W. Napoline, C.M. Thomas, Catal. Rev.: Sci. Eng. **54**, 1 (2012); (c) F.A. Cotton, C.A. Murillo, R.A. Walton, *Multiple Bonds Between Metal Atoms*, 3rd edn. (Springer Science and Business Media, New York, 2005); (d) J.P. Collman, R. Boulatov, Angew. Chem. Int. Ed. **41**, 3948 (2002); (e) L.H. Gade, Angew. Chem. Int. Ed. **39**, 2658 (2000)
2. N.V.S. Harisomayajula, A.K. Nair, Y.-C. Tsai, Chem Commun. **50**, 3391 (2014) and references therein
3. D.M. Roundhill, *Photochemistry and Photophysics of Metal Complexes* (Plenum Press, New York, 1994)

4. As determined from a survey of the Cambridge Crystallographic Database, March (2015)
5. D.R. Lynam, J.W. Roos, G.D. Pfeifer, B.F. Fort, T.G. Pullin, Neurotoxicology **20**, 145 (1999)
6. J. Chai, H. Zhu, A.C. Stuckl, H.W. Roesky, J. Magull, A. Bencini, A. Caneschi, D. Gatteschi, J. Am. Chem. Soc. **127**, 9201 (2005)
7. R. Bianchi, G. Gervasio, D. Marabello, Inorg. Chem. **39**, 2360 (2000) and references therein
8. (a) R.D. Adams, O.-S. Kwon, M.D. Smith, Inorg. Chem. **40**, 5322 (2001); (b) R.D. Adams, O.-S. Kwon, M.D. Smith, Inorg. Chem. **41**, 5525 (2002)
9. L. Sorace, C. Golze, D. Gatteschi, A. Bencini, H.W. Roesky, J. Chai, A.C. Stuckl, Inorg. Chem. **45**, 395 (2006)
10. D.-Y. Lu, J.-S.K. Yu, T.-S. Kuo, G.-H. Lee, Y.-C. Tsai, Angew. Chem. Int. Ed. **50**, 7611 (2011)
11. Y.-C. Tsai, J.-K. Hwang, Y.-M. Lin, D.-Y. Lu, J.-S.K. Yu, Chem. Commun. 4125 (2007)
12. L. Fohlmeister, S. Liu, C. Schulten, B. Moubaraki, A. Stasch, J.D. Cashion, K.S. Murray, L. Gagliardi, C. Jones, Angew. Chem. Int. Ed. **51**, 8294 (2012)
13. (a) C. Jones, P.C. Junk, J.A. Platts, D. Rathmann, A. Stasch, Dalton Trans. 2497 (2005); (b) G. Jin, C. Jones, P.C. Junk, A. Stasch, W.D. Woodul, New J. Chem. **32**, 835 (2008)
14. C. Jones, P.C. Junk, J.A. Platts, A. Stasch, J. Am. Chem. Soc. **128**, 2206 (2006)
15. (a) D. Heitmann, C. Jones, P.C. Junk, K.-A. Lippert, A. Stasch, Dalton Trans. 187 (2007); (b) I.V. Basalov, D.M. Lyubov, G.K. Fukin, A.V. Cherkasov, A.A. Trifonov, Organometallics **32**, 1507 (2013)
16. D. Heitmann, C. Jones, D.P. Mills, A. Stasch, Dalton Trans. **2010**, 39 (1877)
17. L. Fohlmeister, Ph.D. Thesis, Monash University, (2013)
18. C. Ni, B.D. Ellis, J.C. Fettinger, G.J. Long, P.P. Power, Chem. Commun. 1014 (2008)
19. W. Huang, F. Dulong, T. Wu, S.I. Khan, J.T. Miller, T. Cantat, P.L. Diaconescu, Nat. Commun. **4**, 1448 (2013)
20. G.B. Nikiforov, P. Credson, S. Gambarotta, I. Korobkov, P.H.M. Budzelaar, Organometallics **26**, 48 (2007)
21. (a) A.W. Duff, K. Jonas, R. Goddard, H.-J. Kraus, C. Kruger, J. Am. Chem. Soc. **105**, 5479 (1983); (b) K. Angermund, K.H. Claus, R. Goddard, C. Kruger, Angew. Chem. Int. Ed. **24**, 237 (1985); (c) Y.-C. Tsai, P.-Y. Wang, K.-M. Lin, S.-A. Chen, J.-M. Chen, Chem. Commun. 205 (2008)
22. (a) W.M. Lamanna, W.B. Gleason, D. Britton, Organometallics **6**, 1583 (1987); (b) Y.-C. Tsai, P.-Y. Wang, S.-A. Chen, J.-M. Chen, J. Am. Chem. Soc. **129**, 8066 (2007); (c) W.H. Monillas, G.P.A. Yap, K.H. Theopold, Angew. Chem. Int. Ed. **46**, 6692 (2007)
23. J.L. Priego, L.H. Doerrer, L.H. Rees, M.L.H. Green, Chem. Commun. 779 (2000)
24. B. Cordero, V. Gómez, A.E. Platero-Prats, M. Revés, J. Echeverría, E. Cremades, F. Barragán, S. Alvarez, Dalton Trans. 2832 (2008)
25. W.A. Chomitz, S.F. Mickenberg, J. Arnold, Inorg. Chem. **47**, 373 (2008)
26. W.A. Chomitz, J. Arnold, Dalton Trans. 1714 (2009)
27. K. Weidenhammer, W.A. Herrmann, M.L. Ziegler, Z. Anorg, Allg. Chem. **457**, 183 (1979)
28. (a) D.F. Evans, J. Chem. Soc. 2003 (1959); b) E.M. Schbert, J. Chem. Educ. **69**, 62 (1992)
29. M.P. Blake, N. Kaltsoyannis, P. Mountford, Chem. Commun. **49**, 3315 (2013). and references therein
30. L. Pauling, *Nature of the Chemical Bond*. (Cornell University Press, 1960)
31. D. Seyferth, Organometallics **21**, 2800 (2002) and references therein
32. S.J. Bonyhady, C. Jones, S. Nembenna, A. Stasch, A. Edwards, G.J. McIntyre, Chem. Eur. J. **16**, 938 (2010)
33. R. Lalrempuia, A. Stasch, C. Jones, Chem. Sci. **4**, 4383 (2013)
34. S.J. Bonyhady, C. Jones, S. Nembenna, A. Stasch, A. Edwards, G.J. McIntyre, Chem. Eur. J. **16**, 938 (2010)

Chapter 4
Preparation of Low Oxidation State Group 12 Metal Complexes Stabilised by Bulky Amide Ligands

4.1 Introduction

The synthesis and isolation of stable molecular compounds bearing metal–metal bonds involving group 12 metals (Zn, Cd, Hg) has proven a significant synthetic challenge. For many years, the only bonding interactions between two group 12 metals existed in mercury salt-like compounds, which possess a $[Hg_2]^{2+}$ ion [1]. In the 1960s, a number of groups reported evidence for the related $[Zn_2]^{2+}$ and $[Cd_2]^{2+}$ ions in $Zn/ZnCl_2$ glasses and aluminium chloride melts [2]. However, it wasn't until 1986 that one of these ions was isolated in a stable compound (viz. $[Cd_2][AlCl_4]_2$) [3]. It therefore appeared that group 12 metal–metal bonds could only be isolated as ionic salts, and neutral molecular compounds were thought only to be transient species, existing for fractions of a second [1, 4].

Over the past couple of decades, this proposal has been disproven. By using bulky ligands, kinetic stabilisation of group 12 metal(I) dimers possessing metal–metal σ bonds has been made possible. This type of compound is the primary focus for this chapter.

4.1.1 The First Molecular Compounds Possessing Group 12 Metal–Metal Bonds

The first stable molecular compound containing a cadmium–cadmium bond was $[\{(Tp^{Me})Cd\}_2]$ **4-01** (Tp^{Me} = hydrotris(3,5-dimethylpyrazolyl)borate), reported by Reger and Mason in 1993 [5]. The complex was stabilised by bulky tridentate tris(pyrazolyl)-borate ligands, which when possessing a B-H backbone, are monoanionic. The complex was synthesised by treatment of $CdCl_2$ with two equivalents of

J. Hicks, *Preparation, Characterisation and Reactivity of Low Oxidation State d-Block Metal Complexes Stabilised by Extremely Bulky Amide Ligands*, Springer Theses,
DOI 10.1007/978-981-10-2905-9_4

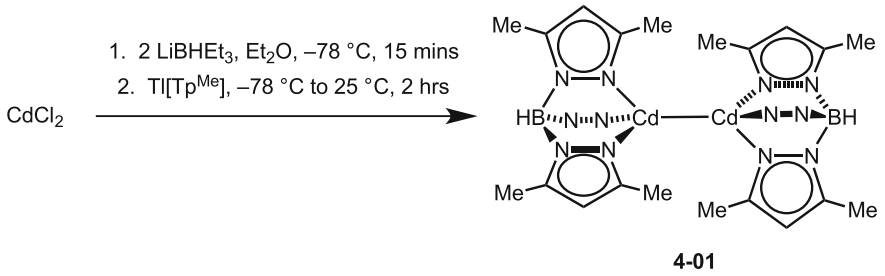

Scheme 4.1 Preparation of **4-01**, the first stable molecular compound to contain a Cd–Cd bond. One pyrazolyl ring from each ligand have been omitted for clarity

lithium triethylborohydride in diethyl ether, followed by the addition of $Tl[Tp^{Me}]$ (Scheme 4.1). Workup of the reaction mixture led to the isolation of **4-01** as a white solid in moderate yields (44 %).

Unfortunately, X-ray quality crystals of **4-01** could not be obtained, therefore a crystallographic analysis was not be performed on the complex. Despite this, the complex was analysed by a number of other spectroscopic techniques, which supported the presence of the Cd–Cd bonded structure. The most characteristic of these is the ^{113}Cd NMR spectrum of the complex, which shows one sharp singlet at 298.6 ppm with two small satellites. Cadmium has two naturally occurring isotopes that are NMR active, ^{111}Cd and ^{113}Cd, both of which have a spin of ½, and both have similar natural abundances, between 12 and 13 %. The satellites in the ^{113}Cd NMR spectrum of **4-01** are observed due to ^{113}Cd–^{111}Cd coupling, which because of the extremely large coupling constant (20,600 Hz), suggests the presence of a strong Cd–Cd bond. The ^{1}H NMR spectrum is also consistent with the proposed complex, and no unassigned resonances were observed, discounting the possibility of a cadmium hydride. Furthermore, accurate mass spectroscopy performed on the compound revealed a mass ion peak consistent with the proposed structure.

In 1999, Apeloig and co-workers reported the metal–metal bonded mercury(I) dimer $[\{(Me_3SiMe_2Si)_3SiHg\}_2]$ **4-02**, which was the first example of a molecular complex bearing a mercury–mercury σ bond [6]. At the time, over 50 other compounds containing mercury–mercury bonds had been crystallographically characterised, but the majority of these had ionic and/or oligomeric structures. For example, Hg_2Cl_2 in its crystalline state, each mercury atom coordinates to six chlorine atoms, two close and four more distant [4b]. The closest example of a molecular complex containing a mercury–mercury σ bond before then was the tetranuclear complex $[\{(np_3)CoHg\}_2]$ (np_3 = $N(CH_2CH_2PPh_2)_3$), which the authors described as a $[Hg_2]^{2+}$ bridge between two cobalt centres [7].

Complex **4-02** was synthesised by heating a mixture of $(Me_3SiMe_2Si)_3SiH$ **4-03** and $[^tBu_2Hg]$ **4-04**, in a 2:1 ratio at 120 °C for 4 h (Scheme 4.2). Workup and subsequent crystallisation of the reaction mixture from pentane afforded good yields of **4-02** as red crystals. The mercury(I) complex was found to be remarkably stable

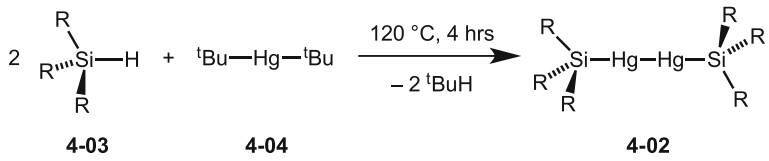

4-03 4-04 4-02

Scheme 4.2 Preparation of **4-02**, the first compound to possess a Hg–Hg σ-bond. R = Me_3SiMe_2Si

in the solid state, even when exposed to air. However, solutions of **4-02** in diethyl ether or hydrocarbon solvents were found to be particularly light sensitive.

Complex **4-02** was crystallographically characterised, showing it to be a linear mercury(I) dimer (Si–Hg-Hg = 180.0°), with a Hg–Hg bond length of 2.6569(8) Å. The bond is considerably longer than the Hg–Hg distance in ionic complexes bearing a $[Hg_2]^{2+}$ ion, such as $[(C_6Me_6)_2Hg][AlCl_4]_2$ (2.515(1) Å) [8], and also longer than oligomeric compounds such as Hg_2F_2, Hg_2Cl_2 and Hg_2Br_2 (2.508(1) Å, 2.526(6) Å and 2.490(10) Å respectively) [9]. However, it is comparable to that in the tetranuclear complex $[\{(np_3)CoHg\}_2]$ (2.6569(1) Å) [7].

Irradiation of a hexane solution of **4-02** with UV light led selectively to the formation of the Si–Si coupled product $[\{(Me_3SiMe_2Si)Si\}_2]$. A later publication from the group also found the compound to react with lithium metal in THF, to give elemental mercury and the first polysilyllithium compound $[\{(Me_3SiMe_2Si)SiLi(THF)_3\}]$ [10].

4.1.2 Isolation of the First Zinc(I) Dimer

The isolation of the cadmium(I) dimer **4-01** and the molecular σ bonded mercury(I) dimer **4-02** were remarkable synthetic achievements, however they were rather overshadowed in 2004, with the landmark discovery of a zinc(I) dimer by Carmona and co-workers [11]. Decamethyldizincocene [Cp*ZnZnCp*] **4-05** (Cp* = η^5-C_5Me_5) was the first example of a stable complex to contain both a zinc–zinc bond, and zinc in the formal oxidation state of +1. Complex **4-05** was synthesised by the addition of diethyl zinc to a solution of [Cp*Zn(η^1-C_5Me_5)] **4-06** in diethyl ethyl at −10 °C, resulting in a colour change from colourless to yellow (Scheme 4.3). After stirring for a further 2 h at −10 °C, workup followed by crystallisation of the reaction mixture gave **4-05** as a white crystalline solid. In comparison, the analogous reaction between the less sterically demanding zincocene [CpZn(η^1-C_5H_5)] (Cp = η^5-C_5H_5) with diethyl zinc at 60 °C gives the half-sandwich complex [CpZnEt] in essentially quantitative yields [12]. In the reaction yielding **4-05**, the analogous half-sandwich complex [Cp*ZnEt] **4-07** is always present as a by-product. However, the reaction conditions stated above have been optimised to keep this by-product at a minimum.

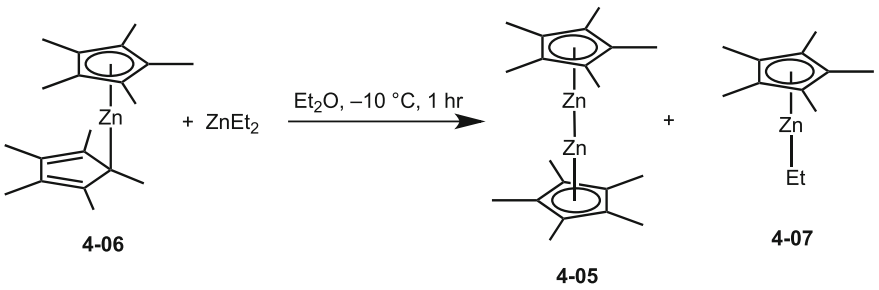

Scheme 4.3 Preparation of **4-05**, the first zinc(I) dimer

Compound **4-05** was found to be exceedingly reactive towards oxygen and moisture, both in solution and in the solid state. As a crystalline solid, **4-05** was found to spontaneously combust when exposed to air, but when kept under an argon atmosphere, it appeared to be indefinitely stable. ^{1}H NMR and ^{13}C NMR spectra for the compound both show one sharp methyl resonance, indicative of a symmetric structure in solution on the NMR timescale. Furthermore, the ^{1}H NMR spectrum shows no unassignable resonances, which could relate to a zinc hydride.

Complex **4-05** was crystallographically characterised. The molecular structure of **4-05** shows two "Cp*Zn" units, which are connected by a metal–metal bond. The complex was found to have a near linear structure (Cp^*_{centr}–Zn–Zn = 177.1°) with a Zn–Zn bond length of 2.305(±3) Å. This Zn–Zn distance is considerably shorter than twice Pauling's single-bond metallic radius of the metal (2.50 Å) [13], which therefore strongly indicates a Zn–Zn bonding interaction.

Preliminary reactivity studies of compound **4-05** were reported in the original publication, i.e. reacting the compound with the isocyanide CNXyl (Xyl = 2,6-dimethylphenyl) and *tert*-butanol (Scheme 4.4). The reaction between **4-05** and CNXyl led to the formation of the half-sandwich iminoacyl species [Cp*ZnC(η^1-C_5Me_5)NXyl] **4-08** and the precipitation of zinc metal, whereas the reaction with *tert*-butanol led to the formation of a zinc butoxy polymer, zinc metal and protonated Cp*H.

Since then, numerous groups from around the world have extensively studied the reactivity of **4-05** [14]. By compiling the results from these studies, it becomes clear

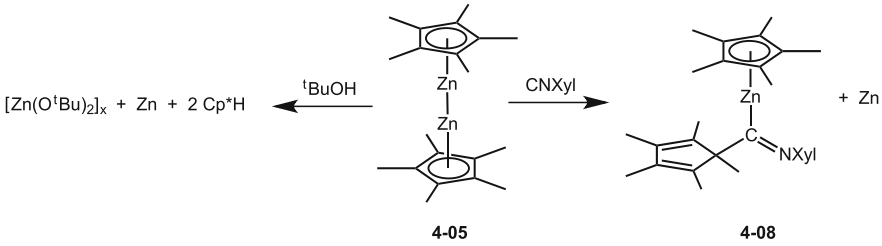

Scheme 4.4 Preliminary reactivity studies performed on **4-05**

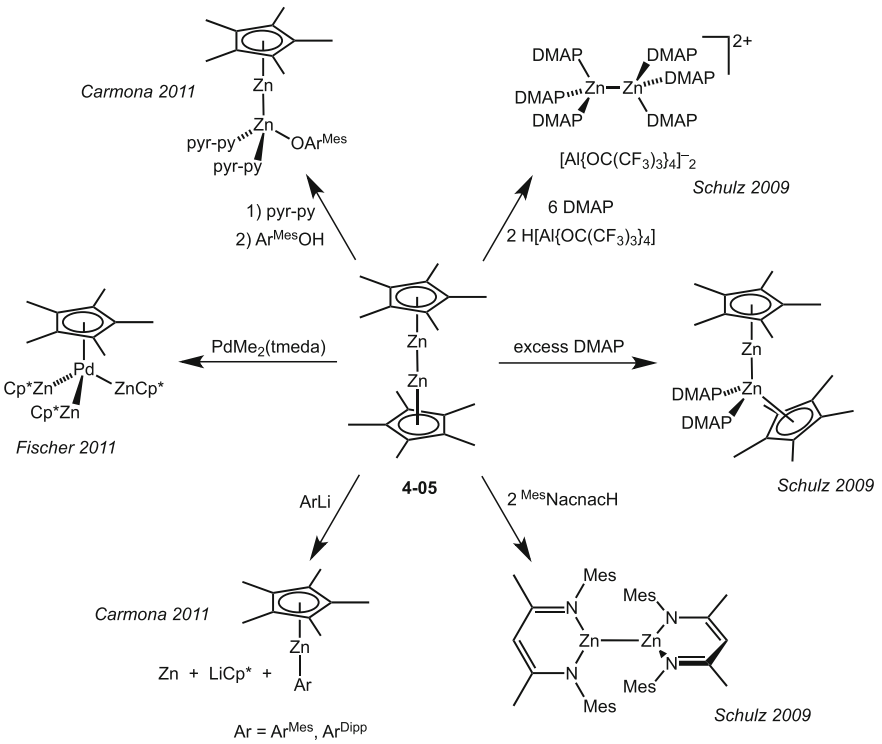

Scheme 4.5 A brief overview into the reactivity of **4-05**. Ar^{Mes} = 2,6-Mes_2-C_6H_3; Ar^{Dipp} = 2,6-$Dipp_2$-C_6H_3

that **4-05** generally reacts in one of two ways, by cleavage of the Zn–Zn bond, forming Zn(II) molecular complexes or polymers, or by ligand exchange, keeping the $[Zn_2]^{2+}$ motif intact. Coordination of strong donor ligands, such as DMAP (DMAP = dimethylaminopyridine) to the Zn_2 core has also been seen. A brief overview into some of this work by the groups of Schulz [15], Fischer [16] and Carmona [17] is outlined in Scheme 4.5. In recent years, the catalytic properties of **4-05** have also been investigated, where it has been shown to catalyse the hydroamination of alkynes [18].

4.1.3 Other Metal–Metal Bonded Zinc(I) Compounds

Since the pioneering work of Carmona and co-workers in 2004, there are now more than 30 other molecular complexes possessing Zn–Zn bonds that have been structurally characterised [14]. A good proportion of these were synthesised by ligand exchange reactions of **4-05**, however a fair number have been synthesised by the reductions of zinc(II) precursor complexes.

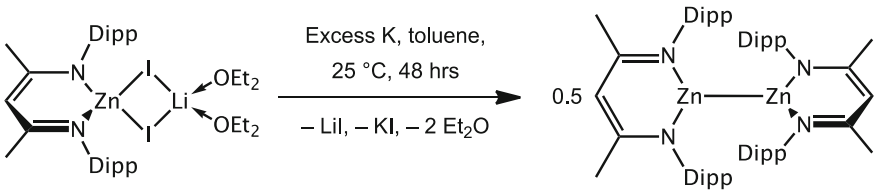

4-10 **4-09**

Scheme 4.6 Preparation of **4-09**

The β-diketiminato zinc(I) dimer [{(^{Dipp}Nacnac)Zn}$_2$] **4-09** was reported by Robinson and co-workers a year after decamethyldizincocene, which was the second molecular complex to possess a zinc–zinc bond [19]. The complex was synthesised by the reduction of the β-diketiminato zinc(II) diiodide lithiate complex [{(^{Dipp}Nacnac)Zn(μ-I)$_2$Li(OEt$_2$)$_2$] **4-10** with potassium metal in toluene over two days. Workup and subsequent crystallisation of the reaction mixture gave **4-09** as colourless crystals. It is worth noting that the related, less bulky [{(^{Mes}Nacnac)Zn}$_2$] complex cannot be accessed by this route, but was later found accessible by ligand substitution of **4-05** [15c] (Scheme 4.6).

Complex **4-09** is a metal–metal bonded zinc(I) dimer, which is kinetically stabilised by two bulky chelating β-diketiminate ligands. The complex was found to be highly air and moisture sensitive, but unlike **4-05** does not spontaneously combust when exposed to air. Compound **4-09** was crystallographically characterised. The molecular structure of **4-09** shows two Zn–Zn bonded "(^{Dipp}Nacnac)Zn" motifs, with the zinc centre sitting slightly out of the plane of the ligand. The complex is essentially isostructural to the previously reported Mn(I) dimer [{(^{Dipp}Nacnac)Mn}$_2$] **3-01** [20], in that the two ligands are arranged in a nearly orthogonal orientation, minimising the steric clashes between the flanking aryl groups. The two Zn centres in complex **4-09** are three-coordinate, which occupy distorted trigonal geometries. The Zn–Zn bond length is 2.3586(7) Å, which is 0.05 Å longer than that in **4-05**, possibly due to the greater steric demands of the ^{Dipp}Nacnac ligands, causing extra strain within the complex.

DFT calculations (B3LYP/DZP^{++} and BP86/DZP^{++}) were performed on a sterically reduced model of **4-09** (viz. [($C_3H_5N_2Zn)_2$] **4-09a**) to further probe the nature of the Zn–Zn bond [19]. The calculated frontier molecular orbitals of **4-09a** show a HOMO consistent with a zinc–zinc σ bond, formed from the overlap of the 4 s orbitals, whereas the LUMO is purely ligand based. The natural bond orbital (NBO) analysis shows that the natural charge of the zinc atoms are +0.85, consistent with the formal oxidation state of +1. The Zn–Zn bond was also calculated to have a dissociation energy of 65.2 kcal/mol, which is in good agreement with that calculated for **4-05** (67.7 kcal/mol) [21].

In 2007, Fedushkin and co-workers prepared the Zn–Zn bonded complex [{(^{Dipp}bian)Zn}$_2$] **4-11**, (^{Dipp}bian = 1,2-bis-[(Dipp)imino]acenaphthene), supported by two bulky radical anionic ligands [22]. The complex was found to be isolable by

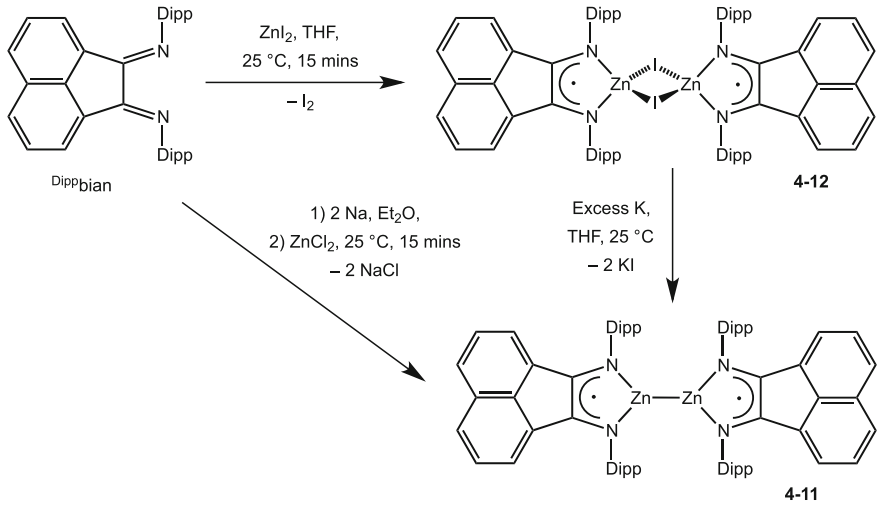

Scheme 4.7 Preparation of **4-11** by two different synthetic pathways

two different synthetic routes; by either the reduction of the dimeric zinc(II) iodide complex [{(^{Dipp}bian)Zn(μ-I)}$_2$] **4-12** with K in THF, or by the direct reaction between $ZnCl_2$ and Na_2[^{Dipp}bian], which was prepared in situ by the reduction of ^{Dipp}bian with sodium in diethyl ether (Scheme 4.7). Workup, followed by crystallisation of the reaction mixture from either route gives **4-11** in good yields. In contrast to the zinc(I) dimers **4-05** and **4-09**, which are both colourless complexes, **4-11** is intense gold-red in solution and crystallises from diethyl ether as very dark red, almost black crystals, due to the radical nature of the ligands.

Compound **4-11** was crystallographically characterised, revealing a zinc(I) dimer possessing a metal–metal bond. The complex is similar to the β-diketiminato zinc(I) dimer **4-09**, in that the two zinc atoms occupy distorted trigonal geometries, from the coordination of a bidentate N,N′ donor ligand and a metal–metal bond. However in **4-09**, the ligands are orthogonal to each other, whereas in **4-11** the ligands are closer to planar (the dihedral angle between two planes C_2N_2Zn is ca. 42°). This twist was proposed to be the effect of steric repulsion between the flanking aryl groups on the opposing ligands. The Zn–Zn bond length is 2.3321(2) Å, which is slightly longer than that in Carmona's zinc(I) dimer **4-05** but slightly shorter than that in **4-09**.

To probe whether **4-11** remains dimeric in solution, EPR (electron paramagnetic resonance) spectroscopy was performed on a solution of the complex in toluene. As expected, the biradical complex showed a broad unresolved EPR signal at room temperature. However, when the solution was cooled to 130 K, the compound exhibited a half-field signal ($\Delta m_s = 2$) characteristic of a biradical species in toluene. The zero-field splitting parameters of the signal (D = 6.39 mT, E = 1.01 mT) allowed the unpaired electron separation to be calculated (7.57 Å), which is in

perfect agreement with the solid state structure, therefore supporting that the complex is dimeric in solution.

Later in 2007, Tsai and co-workers reported a further example of a zinc–zinc bond in the dianionic complex $[\{\mu\text{-}\eta^2\text{-}Me_2Si(DippN)_2Zn\}_2]^{2-}$ **4-13**, which is stabilised by bidentate amido ligands [23]. The compound was synthesised by the reduction of the dinuclear zinc(II) precursor complex $[\{\kappa^2\text{-}Me_2Si(DippN)_2Zn\}_2]$ **4-14**, in which the ligands bridge the two-coordinate metal centres, with KC_8 in toluene (Scheme 4.8). Workup and subsequent crystallisation of the reaction mixture gave **4-13** as colourless blocks.

Crystallographic analysis of **4-13** revealed a dramatic change in the ligand's coordination mode, from bridging in **4-14**, to chelating in **4-13**, forming two four-membered Zn–N–Si–N rings, which are connected by an unsupported zinc–zinc bond. The dizinc unit has undergone a two-electron reduction in the reaction, which results in a dianionic complex. Two potassium counterions balance the charge of the complex, which coordinate to two flanking aryl rings, one from each ligand in an η^6 fashion, to give a sandwich type motif. These interactions keep the complex rigid, and consequently the two Zn–N–Si–N rings are almost coplanar (torsion angle = 10.8°). The Zn–Zn bond length in **4-13** is 2.3695(17) Å, which is 0.07 Å longer than in decamethyldizincocene **4-05**, but similar to that in **4-09** (2.3586(7) Å) [19], therefore implying a substantial zinc–zinc bonding interaction.

In a second reduction of **4-14**, performed with KC_8 in THF, but in the presence of cryptand [2.2.2] (crypt-222), a variation of the zinc(I) complex was isolated (viz. $[\{\mu\text{-}\eta^2\text{-}Me_2Si(DippN)_2Zn\}_2][K\text{-crypt-222}]_2$ **4-13a**). In **4-13a**, the potassium cations

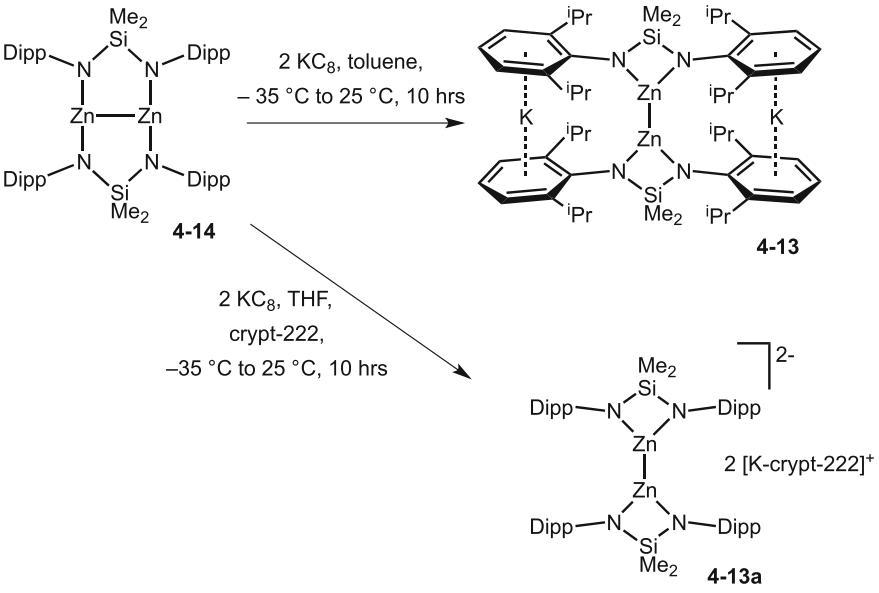

Scheme 4.8 Preparation of **4-13** and **4-13a**. crypt-222 = cryptand [2.2.2]

are encaged within the cryptand [2.2.2] ligands, resulting in a charge-separated structure. The absence of sandwiched potassium ions in the dianionic complex has dramatically increased the torsion angle between the two Zn–N–Si–N planes (torsion angle = 50.6°), to minimise steric buttressing between the flanking aryl groups. Surprisingly, this structural change has had little effect on the Zn–Zn bond length (2.3634(11) Å), which is only marginally shorter than that in **4-13**. The similar Zn–Zn bond lengths in the two complexes, independent of the rotation of the metal–metal axis, signifies that the Zn–Zn bond is essentially a σ bond.

Calculations performed on the dianion of **4-13a**, found that the HOMO is localised mainly on the σ bonding region between the two metal centres. Further detailed NBO analysis of this bond indicates that it has very high s character (94.75 %), with slight p (2.59 %) and d character (2.66 %). This is consistent with calculations performed on decamethylzincocene **4-05** and the β-diketiminato zinc (I) dimer **4-09**, which also calculated the Zn–Zn bond to be high in s character.

The handfull of zinc(I) complexes discussed above are just a select few of the zinc–zinc bonded complexes that have been reported to date. Many others have since been published, including Zn_2^{2+} units stabilised by Tp^{Me} [24], aryloxy [17, 25] diiminophosphinate [26], α-diimine [27], *N*-heterocyclic carbenes [28], bis(iminodi(phenyl)phosphorano)methane [29] and aminotroponiminate [30] ligands, as well as some Zn_2^{2+} units coordinated to transition metals [31]. However, in all of these complexes, at least one of the zinc centres is stabilised by either a bidentate (or higher dentate) ligand, or multiple monodentate ligands. This results in zinc(I) centres that are three-coordinate or higher. So far, only one two-coordinate zinc(I) dimer has been reported, this is the terphenyl stabilised complex $[Ar^{Dipp}ZnZnAr^{Dipp}]$ **4-15**, which is discussed below [32].

4.1.3.1 A Homologous Series of Two-Coordinate Group 12 Metal–Metal Bonded Dimers

Between the years of 2006 and 2007, Power and co-workers reported a series of publications on the synthesis and structure of a homologous series of metal–metal bonded metal(I) dimers (viz. $[Ar^{Dipp}MMAr^{Dipp}]$, M = Zn **4-15** [32], Cd **4-16** [33], Hg, **4-17** [34]), all of which bear the same monodentate terphenyl ligand. Complexes **4-15** and **4-16** remain the only reported examples of neural two-coordinate zinc(I) and cadmium(I) dimers respectively, although one dianionic complex bearing a two-coordinate Cd–Cd motif has since been reported [35].

The three metal(I) dimers were synthesised via the reduction of their the appropriate terphenyl metal(II) iodide precursor complex, $[\{Ar^{Dipp}Zn(\mu\text{-}I)\}_2]$ **2-29**, $[\{Ar^{Dipp}Cd(\mu\text{-}I)\}_2]$ **2-31** and $[Ar^{Dipp}HgI]$ **2-32**, using a number of different reducing agents and reaction conditions. The reduction of the zinc iodide complex **2-29** was performed using one equivalent of sodium metal in diethyl ether (Scheme 4.9). Workup and crystallisation of the reaction mixture gave **4-15** as large colourless blocks in low yields. In contrast, the reduction of cadmium derivative **2-31** was performed using two equivalents of sodium hydride in THF, which after workup

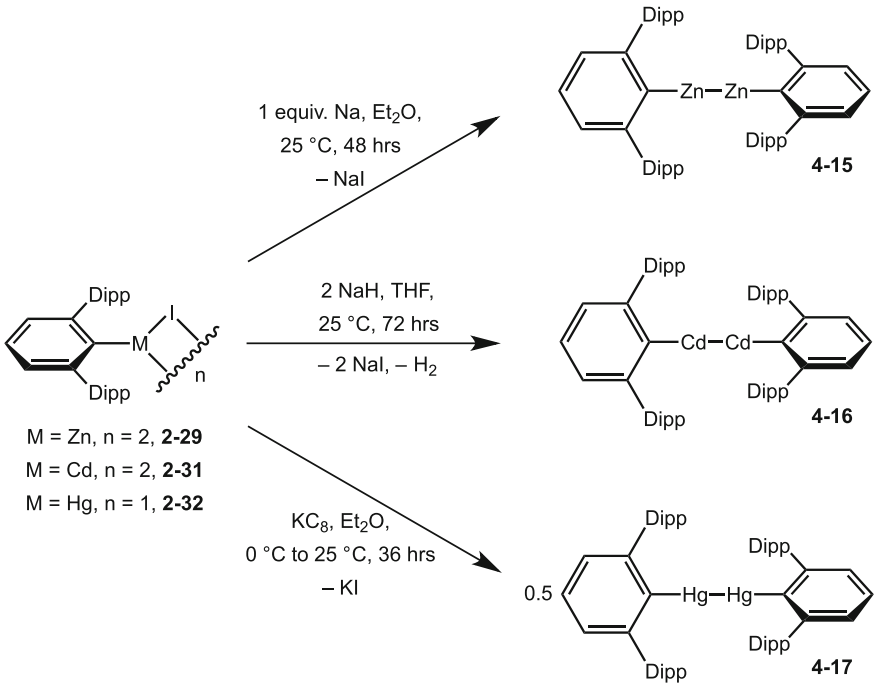

Scheme 4.9 Preparation of **4-15**–**4-17**, a series of homologous group 12 metal(I) dimers

and crystallisation of the reaction mixture gave **4-16** as colourless crystals in low yields. The reduction of the mercury iodide **2-32** was performed using a stoichiometric amount of KC_8 in diethyl ether, which after workup and crystallisation gave **4-17** also as colourless crystals in low yields (Scheme 4.9).

All three metal(I) dimers were crystallographically characterised, and were found to be essentially isostructual in the solid state. All three complexes possess two-coordinate metal centres, with an almost linear arrangement observed for the C-M-M-C unit, with little or no bending in the C-M-M angles (177.5° avg. for **4-15**; 177.5° for **4-16**; 180.0° for **4-17**). In all three complexes, the two bulky terphenyl ligands are essentially orthogonal to each other, minimising the steric repulsion between the flanking aryl groups. The Zn–Zn bond in **4-15** (2.3591(9) Å) is approximately 0.05 Å longer than that in Carmona's zinc(I) dimer **4-05**, but identical to that in the β-dikeminato complex **4-09**. The cadmium(I) dimer **4-16** was the first crystallographically characterised example of a neutral cadmium bonded structure, with a Cd–Cd bond (2.6257(5) Å) slightly longer than that in the ionic compound $[Cd_2][AlCl_4]_2$ (2.576(1) Å) [3]. The Hg–Hg bond in **4-17** (2.5738 (3) Å) is approximately 0.08 Å shorter than in the silylated derivative **4-02**, but is in the range of previously reported ionic complexes bearing mercury-mercury bonds (ca. 2.49–2.59 Å).

The most striking observation of the three metal–metal bond lengths comes when comparing them to each other (Zn–Zn 2.3591(9) Å; Cd–Cd 2.6257(5) Å; Hg–Hg 2.5738(3) Å), that is, the Hg–Hg bond in **4-17** is 0.05 Å shorter than the Cd–Cd bond in **4-16**. This observation is consistent with previous calculations reported for the $[Cd_2]^{2+}$ and $[Hg_2]^{2+}$ dications, using the relativistic Hartree-Fock-Slater one-electron equation, which showed an approximate 0.1 Å contraction in the M-M bond distance between $[Cd_2]^{2+}$ and $[Hg_2]^{2+}$ [36]. A similar contraction trend is also present in neighbouring group 11 compounds, which is confirmed by both theoretical calculations and structural data [37].

The contraction of the Hg–Hg bond in **4-17** compared with Cd–Cd bond in **4-16**, was explained to be due to a number of different reasons. First of all, since the 1970s, the covalent radius of mercury has consistently been calculated to be smaller than that of cadmium, which is also experimentally observed by a shorter Hg–C bond length in **4-17** (2.098(3) Å) than the related Cd–C bond length in **4-16** (2.138 (3) Å) [38]. This is due to relativistic and correlation effects, as well as lanthanide contraction. In addition, DFT calculations performed on the three metal(I) dimers **4-15–4-17**, using the B3LYP/ECP/6-31 g* level of theory, show a stronger Hg–Hg bonding energy in **4-17** (51.0 kcal/mol) than the Cd–Cd bonding energy in **4-16** (48.8 kcal/mol). One might expect the Hg–Hg bonding energy to be the lowest of the three because of the increase in the total Pauli repulsion, which is induced by the higher quantum number of the Hg electrons. However, an energy decomposition analysis of **4-17** clearly shows that the presence of relativistic effects stabilizes the electrostatic and orbital terms, ΔE_{el} and ΔE_{o} which overcomes the increase in the total Pauli repulsion term, ΔE_{p} resulting in a higher metal–metal bonding energy for the Hg–Hg bond compared with that of the Cd–Cd bond. A similar bonding energy trend has also been seen for the metal(I) salts M_2X_2 (M = group 12 metal, X = halogen) [39].

Further frontier orbital calculation on the zinc(I) dimer **4-15** found that the HOMO is mainly localised in the Zn–Zn σ bonding region, with some additional Zn–C σ bonding character [32]. The LUMO and LUMO+1 consist of two almost degenerate orbitals of p symmetry, which are localized mostly on the central Zn_2 unit. The calculations show that the Zn–Zn bond is formed from the overlap of mainly $4p_z$ orbitals in the HOMO, thus leaving two empty orthogonal p_x and p_y orbitals to form the π symmetric LUMOs. The 4s orbitals of the zinc centres are mainly involved in bonding to the coordinating carbon atoms of the ligands. This is in contrast to decamethyldizincoene **4-05** and the β-diketiminato zinc(I) dimer **4-09**, in which the Zn–Zn σ bonds are formed by the overlap of the 4s orbitals [19, 21]. Similar bonding models were calculated for the homologous cadmium and mercury complexes **4-16** and **4-17**, but with decreasing p and increasing s character to the metal–metal σ bond upon descending the group [33, 34].

4.1.3.2 Other Recently Reported Low Oxidation State Group 12 Metal Complexes

Over the past year, a number of unprecedented complexes bearing group 12 metal–metal bonds have been reported. One of these is the σ-aromatic zinc cluster $[Zn_3Cp^*_3]^+$ **4-18** reported by Frenking, Fischer and co-workers earlier this year [40]. The cationic cluster was synthesised by the reaction between decamethylzincocene **4-05** and $[ZnCp^*][BAr^F_4]$ (Ar^F = 3,5-$(F_3C)_2$–C_6H_3), which was subsequently generated in situ by the reaction between $ZnCp^*_2$ and $[H(Et_2O)_2][BAr^F_4]$ (Scheme 4.10).

Complex **4-18** was found to be highly air and moisture sensitive, both in solution and in the solid state. Moreover, solutions of **4-05** decompose fairly rapidly at room temperature, and once crystalline the compound cannot be redissolved without approximately 60 % decomposition. ^{1}H NMR spectroscopy performed on the decomposition solutions are consistent with the formation of decamethyldizincocene **4-05**, $[Cp^*_2Zn]$ **4-06** and BAr^F_3, the latter suggesting the migration of an Ar^F group from the $[BAr^F_4]^-$ ion may be involved in the decomposition pathway.

Complex **4-18** is formally a mixed valence zinc cluster, bearing one zinc(II) and two zinc(I) centres arranged in a triangle. Although, due to delocalisation of electrons around the Zn_3 core, the three zinc centres are essentially equivalent. The complex is formed by the donation of electrons from the Zn–Zn sigma bond in decamethyldizincocene **4-05**, into the formally empty 4s orbital of the $[Cp^*Zn]^+$ cation, resulting in a three-centred two-electron (3c2e) bond. This bonding model can be compared to the side-on coordination of H_2 to an unsaturated transitional metal complex, which also results in a 3c2e bond. Remarkably, the complex was calculated to possess σ-aromaticity around the three zinc atoms, resulting in a considerable stabilisation energy contribution to the complex.

Complex **4-18** was crystallographically characterised, revealing the three zinc centres to be arranged in a near perfect equilateral triangle (Zn–Zn–Zn angles = 61.1°, 59.2 and 59.7°). The slight distortion was found to be due to weak intermolecular interactions. The Zn–Zn bond distances are almost identical (2.430 Å

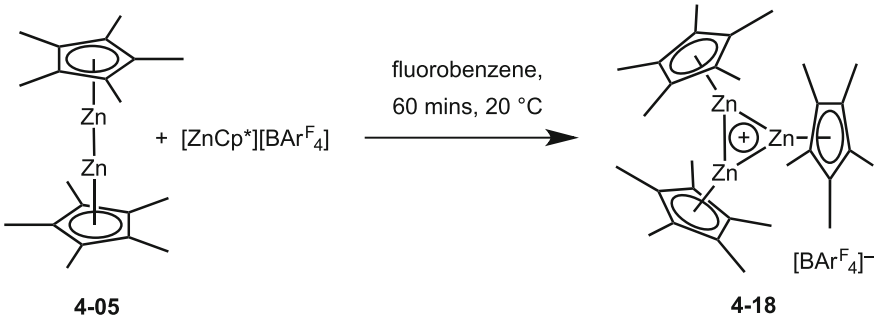

Scheme 4.10 Preparation of the trinuclear cationic zinc complex **4-18**

avg.), and are slightly longer than the two-centred, two electron σ bonds in typical zinc(I) dimers, due to an average decrease in electron density per Zn–Zn bond.

The Zn–Hg–Zn bonded complex [{(^{Dipp}Nacnac)Zn}$_2$Hg] **4-19** was another unprecedented group 12 complex reported earlier this year, by Mountford and co-workers [41]. The complex possesses the same β-diketiminate ligands that were used in the isolation of the zinc(I) dimer [{(^{Dipp}Nacnac)Zn}$_2$] **4-09** [19]. However, whereas complex **4-09** was prepared by a potassium reduction of the β-diketiminato zinc(II) diiodide lithiate complex [{(^{Dipp}Nacnac)Zn(μ-I)$_2$Li(OEt$_2$)$_2$] **4-10**, complex **4-19** was synthesised by the reduction of β-diketiminato zinc(II) iodide complex [(^{Dipp}Nacnac)ZnI] **4-20** with potassium mercury amalgam (Scheme 4.11). Workup and subsequent crystallisation of the reaction mixture gave **4-19** as orange crystals in good yield.

Complex **4-19** bears a novel Zn–Hg–Zn bonding motif, and furthermore, represents the first molecular complex to possess a bond between two different group 12 metals. The formation of complex **4-19** was proposed to proceed via a transient "(^{Dipp}Nacnac)Zn" radical intermediate, which is intercepted by the large excess of Hg in the reaction mixture before it can dimerise. Other mercury bridged species have been isolated from the reductions of transition metal complexes with alkali metal mercury amalgams, e.g. [{Cp*Mo(η^2-C$_2$H$_2$)(N^{t}Bu)}$_2$Hg], in which a similar mechanism was proposed [42].

A crystallographic analysis of complex **4-19** revealed a two-coordinate linear mercury centre (Zn–Hg–Zn = 180.0°), which is coordinated to two "(^{Dipp}Nacnac)Zn" units. The "(^{Dipp}Nacnac)Zn" moieties are significantly distorted, with the two N–Zn–Hg angles differing by more than 40° (153.4° and 111.9°) and Zn–N distances differing by >0.03 Å (1.9643(19) and 2.002(2) Å). The Zn–Hg bond lengths within the complex are 2.4846(3) Å, but as **4-19** is the first crystallographically characterised complex to possess a Zn–Hg bond, there is no direct structural precedent for this to be compared with. It is however within the sum of the covalent radii of the two elements (2.54 Å) [43], and close to the value estimated (2.466 Å) by additive extrapolation from Robinson's [{(^{Dipp}Nacnac)Zn}$_2$] **4-09** (three-coordinate Zn–Zn = 2.3586(7) Å) [19] and Power's [{(Ar^{Dipp})Hg}$_2$] **4-17** (two-coordinate Hg–Hg = 2.5738(3) Å) [34].

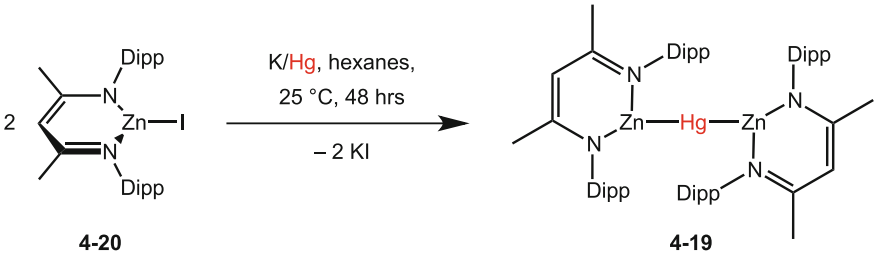

4-20 **4-19**

Scheme 4.11 Preparation of **4-19**

To further investigate the bonding and oxidation states of the metals in complex **4-19**, extensive DFT calculations, in conjunction with Quantum Theory of Atoms in Molecules (QTAIM) analysis were carried out on the complex, along with a number of related model compounds. Two metal-based MO's were calculated for complex **4-19**, the HOMO and HOMO-7. The HOMO has mainly Zn character (56 % 4s, 24 % 4p) and just 7 % Hg (6s) character, whereas the HOMO-7, has mainly Hg character (69 %) and only 12 % Zn character. Neither of these MOs are suggestive of strong bonds between the metal atoms. However, further QTAIM analysis supports the existence of Zn–Hg bonds in finding bond paths, with values that are characteristic of homo- and hetero-nuclear metal–metal bonded compounds in general. Moreover, data from these experiments are indicative of Zn–Hg formal single bonds.

As complex **4-19** possesses three metal centres and only two anionic ligands, as well as the fact Zn and Hg having similar electronegativities (Zn 1.65 and Hg 2.00 by the Pauling scale) [13], there are two possible ways to view the complex in terms of oxidation states, Zn(I)–Hg(0)–Zn(I) or Zn(0)–Hg(II)–Zn(0). To decipher which was more correct, QTAIM atomic charges of the Zn and Hg atoms (Q(Zn) and Q(Hg)) were calculated within the complex, and compared to those for [(^{Dipp}Nacnac)ZnI] **4-20** and the radical intermediate [(^{Dipp}Nacnac)Zn]. The Q(Zn) for the radical intermediate [(^{Dipp}Nacnac)Zn] was calculated to be +0.585, which increases to +0.934 upon formal oxidation to **4-20**, with 0.428 electrons being transferred to the iodine (Q(I) = −0.428). In contrast, the Q(Zn) increases by only 0.08 from the Zn(I) radical intermediate to the Zn–Hg–Zn complex **4-19**, showing that less than 0.07 electrons are transferred per "(^{Dipp}Nacnac)Zn" fragment upon coordination to Hg (Q(Hg) = −0.139). Therefore complex **4-19** is best described as a Zn(I)–Hg(0)–Zn(I) system with only a small degree of charge transfer from Zn(I) to Hg(0) upon Zn–Hg bond formation. This is also in good agreement with the calculated MOs.

Preliminary reactivity studies indicate that complex **4-18** does indeed react as if it were a source of Zn(I) (Scheme 4.12). The reaction between **4-18** and one equivalent of iodine gives [(^{Dipp}Nacnac)ZnI] **4-20** and mercury metal in quantitative yields. The reaction between the compound and one equivalent of FpI (Fp = CpFe$(CO)_2$) leads to a 1:1 mixture of **4-20** and [(^{Dipp}Nacnac)ZnFp] **4-21**, once again eliminating mercury metal, whereas the same reaction using two equivalents of FpI gives **4-20** and $HgFp_2$ in a 2:1 ratio. In addition, the reaction between one equivalent of Fp_2 and complex **4-19** leads to the formation of elemental mercury and compound **4-21** in quantitate yields.

One last zinc(I) complex that was reported earlier this year, was by Cui, Hu and co-workers, which challenged our understanding of low oxidation state group 12 chemistry [44]. This was the formally Zn(I) anionic cubic cluster $K_{1.4}Na_{10.6}[Zn_8(HTz)_4(Tz)_8]$ **4-22** (Tz = tetrazole dianion, CN_4^{2-}). The complex was synthesized by the reaction between $Zn(ClO_4)_2.6H_2O$, $K[C(CN)_3]$, NaN_3 and NH_4F in DMF, which were heated in a sealed Teflon-lined stainless steel autoclave vessel at 155 °C for 4 days. Slow cooling of the reaction mixture led to the isolation of **4-22** as colourless crystals (26 % yield).

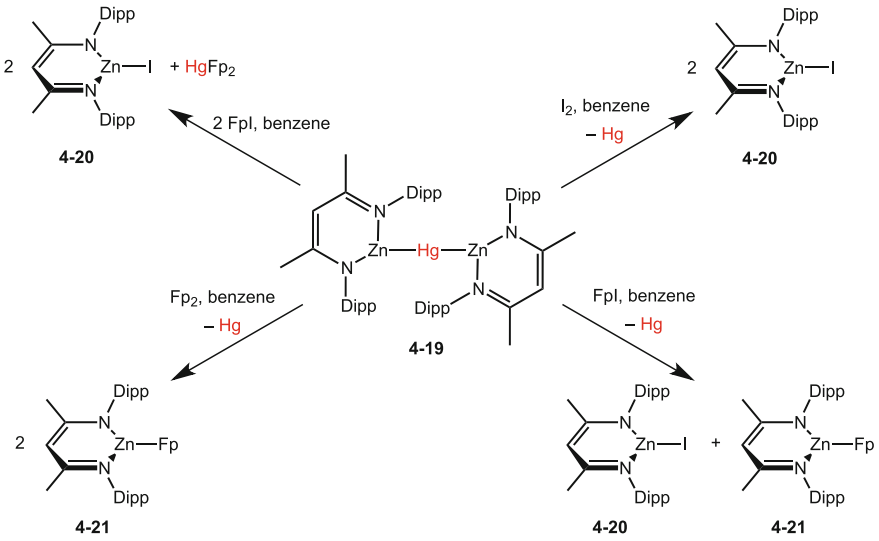

Scheme 4.12 Preliminary reactivity studies performed on **4-19**

A crystallographic analysis of **4-22** revealed a Zn_8 cube, surrounded by 12 tetrazole ligands, one bridging each edge of the cube (Fig. 4.1). Four of these ligands are monoanionic, identifiable by a H on the carbon atom, whereas the other eight are dianionic. This, combined with the 1.4 K^+ and 10.6 Na^+ cations surrounding the cube indicate that the central Zn_8 unit possesses an 8+ charge, and

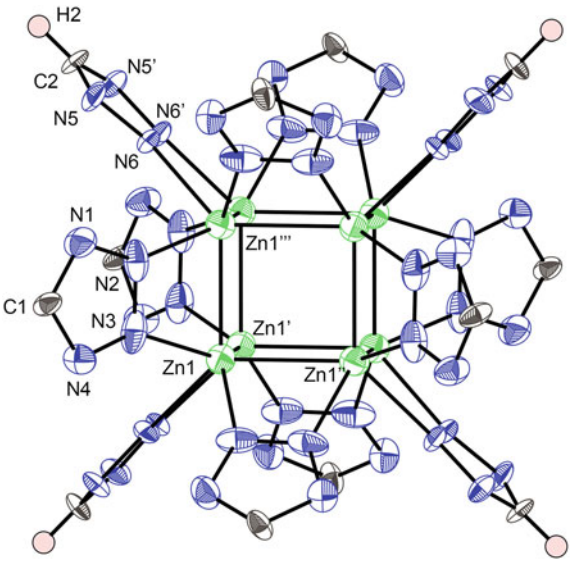

Fig. 4.1 The molecular structure of the $[Zn_8(HTz)_4(Tz)_8]^{12-}$ ion of **4-22**

therefore the complex is formally a zinc(I) complex. Each zinc(I) centre is six-coordinate, coordinating to three other zinc atoms in addition to three ligands (two dianionic and one monoanionic). The complex possesses two different Zn–Zn bond lengths, those that are bridged by a monoanionic ligand (2.292(2) Å) and those bridged by a dianionic ligand (2.4810(8) Å). These two bond lengths represent the shortest and longest formal Zn–Zn bonds reported to date [45].

Low oxidation state zinc complexes are in general highly air and moisture sensitive compounds, as significant energy gains usually result from the oxidation of the zinc centres to the more thermodynamically favourable Zn(II). Remarkably, compound **4-22** does not appear to be air or moisture sensitive, as samples that were left exposed to air for more than half a year did not show signs of decomposition. Moreover, the compound was prepared in air, using wet solvents and hydrated starting materials. The compound also shows remarkable thermal stability, unexpected for a complex which nitrogen contributes >35 % of the overall mass. Although it does undergo explosive combustion at temperatures above 300 °C.

The unprecedented stability of compound **4-22** was calculated to be due to a number of factors, including mixing of the Zn 4p and 3d orbitals, as well as exceptionally strong ligand to metal interactions. The Zn–Zn bonding in the central Zn_8 cube is also a considerable factor, as it was found to possess cubic aromaticity. The eight Zn(I) centres each possess one 4s electron, which are delocalized around the Zn_8 cube in one of four bonding orbitals, leaving four antibonding orbitals empty. This leads to a considerable stabilization effect of the overall complex.

4.2 Research Outline

As discussed in Chap. 2, eleven bulky amido group 12 metal(II) halide complexes of the general structure $[\{Ar(SiR_3)NMX(THF)_n\}_m]$ (M = Zn, Cd or Hg; X = Br or I; Ar = Ar* or Ar†; R = Me, Ph or ^{i}Pr; n = 0–1; m = 1–2) have been prepared as potential precursors for low coordinate, low oxidation state group 12 chemistry. As terphenyls are the only monodentate ligand class so far to stabilise neural two-coordinate zinc(I) and cadmium(I) metal–metal bonded dimers, the initial aim was to reduce these complexes in an attempt to isolate two-coordinate amido derivatives.

Secondly, as discussed in Chap. 3, the extremely bulky $Ar^\dagger(Si^iPr_3)N^-$ ligands were found to be sufficiently bulky to prevent the dimerization of two "$Ar^\dagger(Si^iPr_3)$NMn" fragments. Consequently, these fragments were further reduced by the magnesium(I) reducing agent $[\{(^{Mes}Nacnac)Mg\}_2]$ **1-08** to give the Mn–Mg bonded complex $[Ar^\dagger(Si^iPr_3)NMn\text{-}Mg(^{Mes}Nacnac)]$ **3-16**. As a number of amido group 12 metal(II) halide complexes, bearing the same extremely bulky $Ar^\dagger(Si^iPr_3)N^-$ ligand have been synthesized, similar complexes possessing group 12 metal-magnesium bonds (i.e. $[Ar^\dagger(Si^iPr_3)NM–Mg(^{Mes}Nacnac)]$ M = a group 12 metal) were also targeted, with the goal of studying their structure and reactivity.

4.3 Results and Discussion

4.3.1 *Preparation and Characterisation of a Homologous Series of Group 12 Metal(I) Dimers*

Initially, the reduction of the least bulky amido zinc(II) bromide complex [Ar*(SiMe$_3$)NZnBr(THF)] **2-51** was attempted using sodium, potassium and KC_8 in both toluene and diethyl ether. However, in every case, decomposition of the starting material was observed by the precipitation of zinc metal, and the ^{1}H NMR spectrum of the reaction mixture showed the free amine Ar*(SiMe$_3$)NH as the only identifiable product. When the magnesium(I) reducing agent [{(^{Mes}Nacnac)Mg}$_2$] **1-08** was added to a toluene solution of **2-51** at −80 °C, the reaction mixture turned bright orange. However, whilst slowly warming the reaction mixture to room temperature, the orange colour disappeared at ca. −40 °C, followed by precipitation of metallic zinc. ^{1}H NMR spectroscopy performed on the reaction mixture at room temperature, showed the formation of the free amine Ar*(SiMe$_3$)NH and [{(^{Mes}Nacnac)Mg(μ-Br)}$_2$] **1-21-Br** as the only two identifiable products. Multiple attempts to isolate the orange product were made, including layering the reaction mixture with pentane at −80 °C, and concentrating the reaction mixture at −50 °C in an attempt to grow crystals. Unfortunately all attempts were unsuccessful.

The reaction between the related amido zinc bromide complex [Ar†(SiMe$_3$)NZnBr(THF)] **2-52** (which varies from **2-51** by just the substituent in the *para* position of the central ligand ring) and stoichiometric amounts of the magnesium(I) reducing agent **1-08** was initially expected to give a similar result. However, upon warming the reaction mixture to room temperature, no precipitation of metallic zinc was seen, even after stirring the reaction mixture for several hours. Workup and subsequent crystallization of the reaction mixture gave the amido zinc(I) dimer complex [{Ar†(SiMe$_3$)NZn}$_2$] **4-23** as colourless crystals in good yield (Scheme 4.13). The reason why this small change in the *para* substituent of the ligand has such a large effect on the overall stabilization properties of that ligand is currently unknown, although similar effects have been observed in terphenyl stabilized complexes [46].

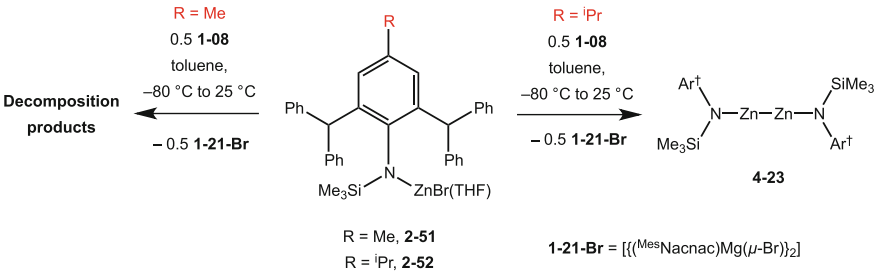

Scheme 4.13 Reactions between the related amido zinc(II) bromide complexes **2-51** and **2-52** with the magnesium(I) reducing agent **1-08**

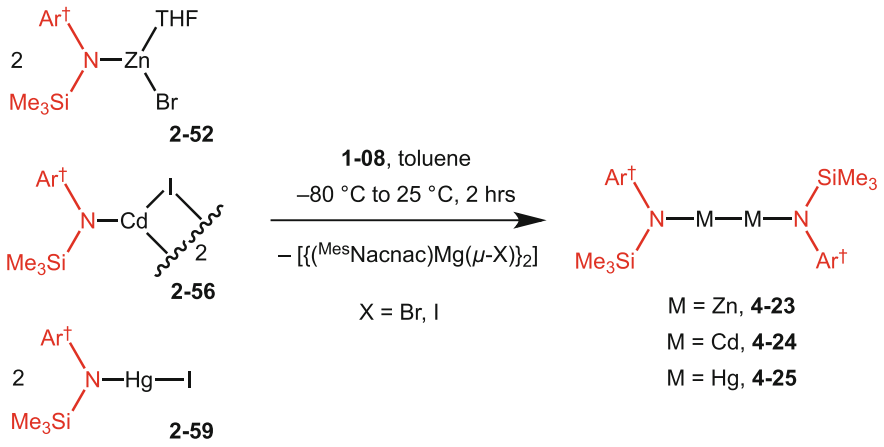

Scheme 4.14 Preparation of **4-23**–**4-25**, a homologous series of amido group 12 metal(I) dimers

As the $Ar^{\dagger}(SiMe_3)N^{-}$ ligand was shown to be capable of stabilising a metal–metal bonded zinc(I) dimer, the reduction of the two heavier amido metal(II) halide precursor complexes $[\{Ar^{\dagger}(SiMe_3)NCd(\mu\text{-}I)\}_2]$ **2-56** and $[Ar^{\dagger}(SiMe_3)NHgI]$ **2-59**, which both bear the same $Ar^{\dagger}(SiMe_3)N^{-}$ ligand, were also carried out. Stoichiometric amounts of the magnesium(I) reducing agent **1-08** were added to toluene solutions of **2-56** and **2-59** at −80 °C (Scheme 4.14). Both reaction mixtures were allowed to warm to room temperature and stir for a further two hours, in which time no precipitation of elemental metal was observed. Workup and subsequent crystallisation of both reaction mixtures led to the isolation of the two amido metal(I) dimers $[\{Ar^{\dagger}(SiMe_3)NCd\}_2]$ **4-24** and $[\{Ar^{\dagger}(SiMe_3)NHg\}_2]$ **4-25** as colourless crystals in good yields.

The three metal–metal bonded dimers **4-23**–**4-25** are the first examples of neutral group 12 metal(I) dimers stabilised by monodentate amido ligands, although one dianionic cadmium complex has previously been reported [35]. Complexes **4-23** and **4-24** are also only the second examples of two-coordinate Zn(I) and Cd(I) metal–metal bonded dimers, the first being the terphenyl complexes **4-15** and **4-16**. Complexes **4-23** and **4-24** are highly air and moisture sensitive, quickly decomposing when exposed to air in solution and in the solid state. In contrast, the mercury(I) dimer **4-25** is stable in air for several days in the solid state, but slowly decomposes when a solution of it is exposed to air.

The ^{1}H, ^{13}C and ^{29}Si NMR spectra for the dimers **4-23**–**4-25** are all consistent with their proposed structures, although they are not overly informative, as they display spectral patterns similar to those of the amido metal(II) halide precursors. More information can be gained from the ^{113}Cd and ^{199}Hg NMR spectra of **4-24** and **4-25** respectively (Fig. 4.2). The ^{113}Cd NMR spectrum of **4-24** exhibits a single resonance at 270.6 ppm, which is flanked by ^{111}Cd satellites, due to ^{113}Cd-^{111}Cd coupling. The observation of these satellites is consistent with other Cd–Cd bonded complexes, such as $[\{(Tp^{Me})Cd\}_2]$ **4-01** and the terphenyl cadmium dimer **4-16**.

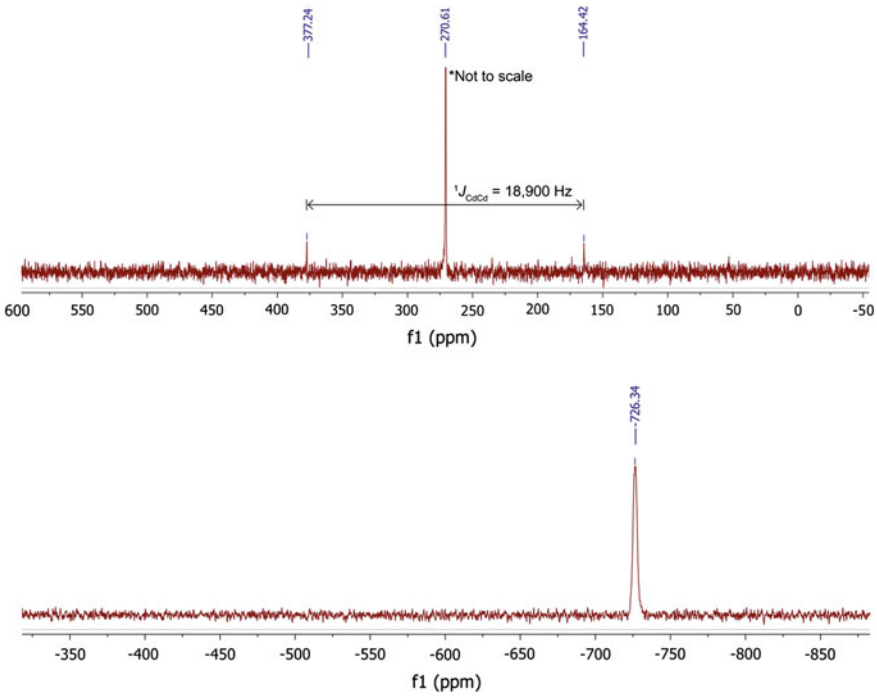

Fig. 4.2 ^{113}Cd NMR spectrum of **4-24** (*top*) and ^{199}Hg NMR spectrum of **4-25** (*bottom*)

The ^{113}Cd-^{111}Cd coupling constant was calculated to be 18,900 Hz, which is more than double that in the terphenyl complex **4-16** (8,650 Hz) [33], but slightly less than that in **4-01** (20,646 Hz) [5]. This high coupling constant suggests a stronger and/or higher s-character Cd–Cd bond in **4-24** than in the related terphenyl complex. The ^{199}Hg NMR spectrum for **4-25** shows a broad but single resonance at −726.3 ppm, which is considerably upfield relative to that for the terphenyl complex **4-17** (150.5 ppm) [34].

To gain further structural information on the three amido metal(I) dimers **4-23**–**4-25**, the three complexes were crystallographically characterised, and their molecular structures depicted in Fig. 4.3. The three dimers were found to be isomorphous, all crystallising in the same space group with very similar unit cell parameters. Compounds **4-23**–**4-25** represent only the second crystallographically characterised series of homologous group 12 metal(I) dimers. The three complexes were found to have two-coordinate metal centres with near linear geometries (N–M–M: 174.26(5)° **4-23**, 172.77(5)° **4-24**, 176.44(8)° **4-25**). The metal–metal distances in the three complexes (**4-23** 2.3520(6) Å, **4-24** 2.5785(6) Å, **4-25** 2.5394 (5) Å) are all slightly shorter than in the related terphenyl dimer, but as was the case in that series, the Hg–Hg bond in **4-25** is shorter than the Cd–Cd bond in **4-24**. Interestingly though, in the terphenyl series a shorter C-Hg bond was observed in

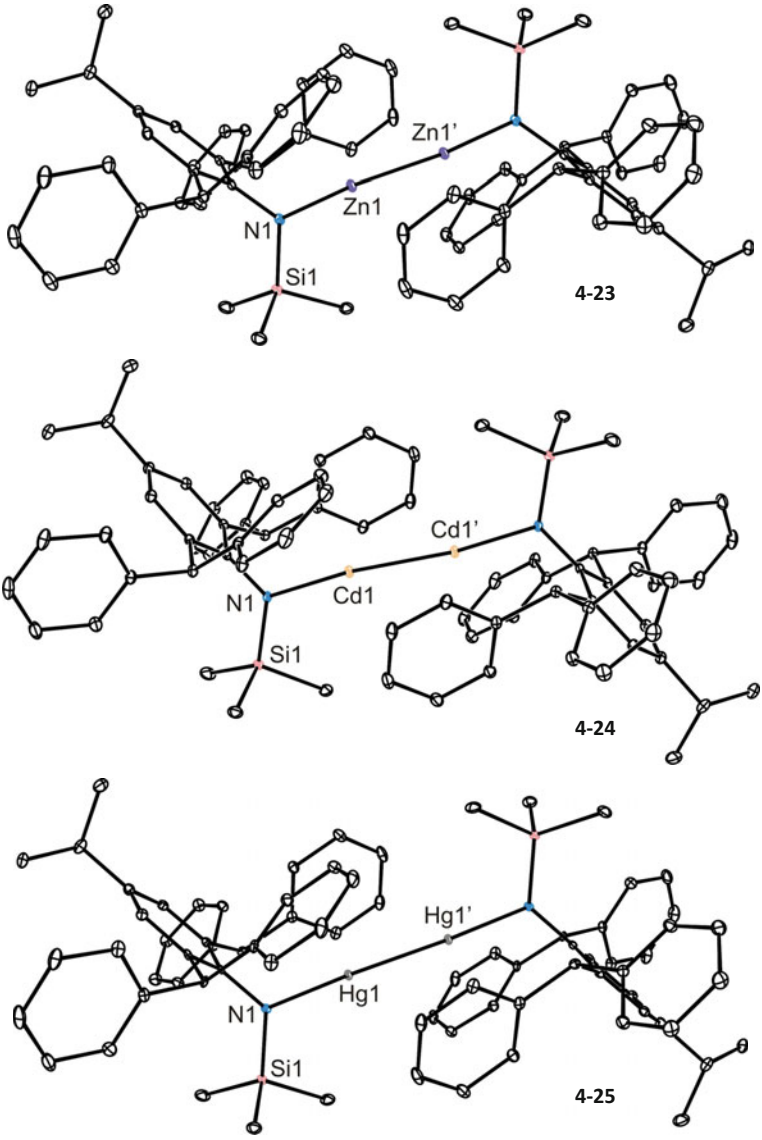

Fig. 4.3 Thermal ellipsoid plots (25 % probability surface) of the molecular structures of **4-23** (*top*), **4-24** (*middle*) and **4-25** (*bottom*). Hydrogen atoms have been omitted for clarity. Selected interatomic distances (Å) and angles (°) for complexes **4-23**–**4-25** is found in Table 4.1

4-17 than the associated C–Cd bond in **4-16**, suggestive of a smaller atomic radii for mercury than for cadmium. This was not observed in the amido series, as the N–Cd and N–Hg bond lengths in **4-24** and **4-25** are identical (N–M = 2.0988(16) Å, **4-24**; 2.099(3) Å, **4-25**) within experimental error.

Table 4.1 Selected interatomic distances (Å) and angles (°) for **4-23**–**4-25**

	4–23 (Zn)	4–24 (Cd)	4–25 (Hg)
M–M	2.3520(6)	2.5785(6)	2.5394(5)
N–M	1.8976(16)	2.0988(16)	2.099(3)
Closest $C_{phenyl}\cdots M$	3.077(3)	3.088(3)	3.155(5)
N–M–M	174.26(5)	172.77(5)	176.44(8)

To investigate the electronic structure of the three metal(I) dimers **4-23**–**4-25**, DFT calculations using B3LYP and B3PW91 levels of theory were carried out on the complexes in the gas phase. The geometries of all three complexes optimized to be close to those in the solid-state structures, with good agreement between the calculated and experimentally obtained metal–metal bond lengths (calculated M-M bond lengths = 2.312 Å for **2-23**, 2.582 Å for **2-24**, 2.555 Å for **2-25**). It is worth noting that the calculated bond lengths also follow the same trend as experimentally observed, i.e. a longer Cd–Cd bond in **4-24** than the Hg–Hg bond in **4-25**.

The HOMO of **4-23** was calculated to consist of a metal–metal σ bond, along with some ligand bonding interactions, whereas the LUMO was found to possess significant σ-antibonding character (Fig. 4.4). A Wiberg bond index (WBI) of 0.87 was calculated for the zinc–zinc bond, indicative of a single bond. This bond was found to high in s character (89.81 %), with small contributions from p (8.79 %) and d (1.41 %) orbitals. This is in good agreement with other zinc–zinc σ bonded complexes, such as decamethyldizincocene **4-05** and the β-diketminato zinc(I) dimer **4-09**, whose zinc–zinc σ bonds were also found to be high in s character [19, 21]. However, this is contrast to the two-coordinate terphenyl zinc(I) dimer **4-16**, which was calculated to have high p character to its Zn–Zn bond [32].

The calculated HOMO and LUMO of **4-24** and **4-25**, were found to be almost identical to that in **4-23**, that is the HOMO is shows a metal–metal σ bond, and the LUMO consistent with a metal–metal antibonding interaction (see Appendix 7.2 for diagrams). Complexes **4-24** and **4-25** were both calculated to possess metal–metal

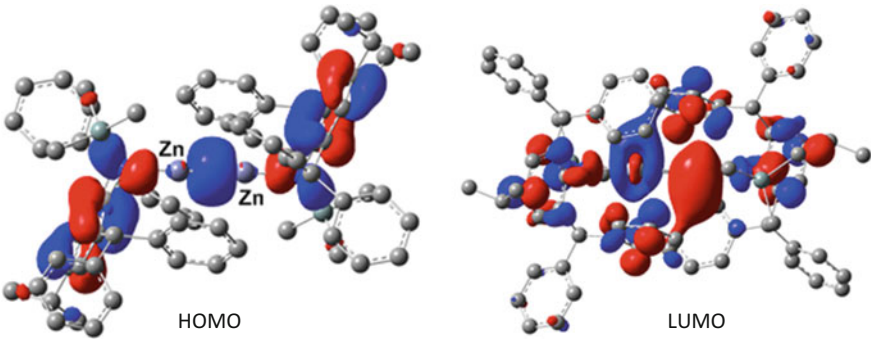

Fig. 4.4 Selected calculated frontier orbitals for **4-23**. HOMO (*left*) and LUMO (*right*). Iso-surface value 0.03 a.u

single bonds, with calculated WBI values of 0.90 and 0.72 respectfully. The Cd–Cd bond was found to be high in s character (86.54 %), but with slightly higher p (11.93 %) and d (1.54 %) orbital contributions compared with the Zn–Zn bond. The Hg–Hg bond in **4-25** also possesses high s character (89.40 %), low p (2.86 %), but significantly higher d orbital contribution (7.73 %) compared to the lighter group 12 metals. Therefore the Zn–Zn, Cd–Cd and Hg–Hg bonds in compounds **4-23**–**4-25** are all single σ bonds, formed mainly from the overlap of the metal's s orbitals.

4.3.2 *Preparation and Characterisation of a Two-Coordinate Zinc(0) Heterobimetallic Complex with an Unsupported Zn–Mg Bond*

As discussed in Chapter 3, the reaction between $[\{Ar^{\dagger}(Si^{i}Pr_3)NMn(\mu\text{-}Br)(THF)\}_2]$ **2-45** and two equivalents of the magnesium(I) reducing agent **1-08** gave the unprecedented Mn–Mg bonded complex $[\{Ar^{\dagger}(Si^{i}Pr_3)NMnMg(^{Mes}Nacnac)]$ **3-16**. The reaction was proposed to proceed via a transient "$Ar^{\dagger}(Si^{i}Pr_3)NMn$" fragment, which due to extreme bulk of the ligand, is incapable of dimerising. As zinc and manganese have similar atomic radii, and the amido zinc(II) bromide complex $[Ar^{\dagger}(Si^{i}Pr_3)NZnBr]$ **2-55** bears the same extremely bulky $Ar^{\dagger}(Si^{i}Pr_3)N^{-}$ ligand as **2-45**, a similar reaction was proposed to give the analogous heterobimetallic Zn–Mg bonded complex. With that in mind, a toluene of solution of **2-55** was slowly added to an excess of the magnesium(I) reducing agent **1-08** (1.1 equivalents, 1:2.2 ratio between Zn and Mg) at −80 °C (Scheme 4.15). The reaction mixture was slowly warmed to room temperature where it was stirred for a further 12 h. Workup and subsequent crystallization of the reaction mixture from pentane

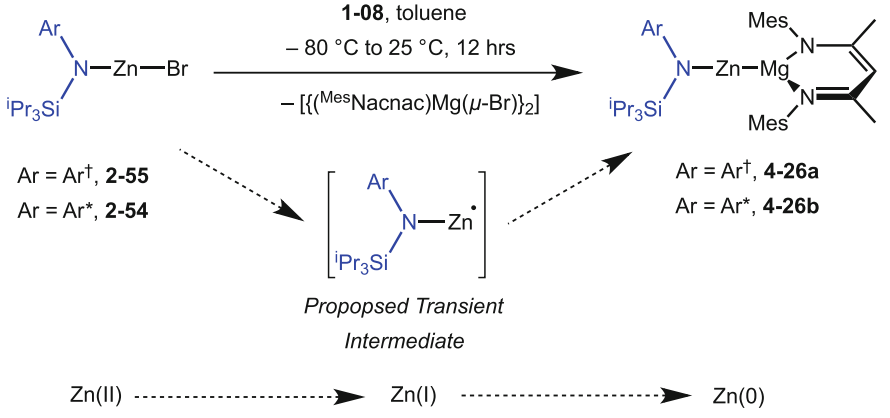

Scheme 4.15 Preparation of the two Zn–Mg bonded complexes **4-26a** and **4-26b**

gave the proposed Zn–Mg bonded heterobimetallic complex [{Ar†(Si^{i}Pr$_3$)NZnMg(^{Mes}Nacnac)] **4-26a** as colourless crystals. However, these crystals were repeatedly found to be contaminated with Ar†(Si^{i}Pr$_3$)NH (~20–30 %), therefore multiple recrystallizations were required to obtain a product of acceptable purity. A similar reaction between [Ar*(Si^{i}Pr$_3$)NZnBr] **2-54** and **1-08** gave the analogous Zn–Mg bonded complex [{Ar*(Si^{i}Pr$_3$)NZnMg(^{Mes}Nacnac)] **4-26b** (Scheme 4.15), which after a single crystallization from pentane gave the product in good yields and high purity (>98 %). Therefore all further reactivity studies were performed on **4-26b** because of the simpler purification step.

The two reactions to give the Zn–Mg bonded complexes **4-26a** and **4-26b** were repeated using half an equivalent of the magnesium(I) reducing agent **1-08** (1:1 ratio of Zn and Mg), which is correct ratio to form a zinc(I) dimer. However, neither reaction led to the formation of a zinc(I) dimer, just the isolation of the appropriate Zn–Mg bonded complex and unreacted amido zinc bromide in an approximate 1:1 ratio. This suggests that the formation of the two Zn–Mg bonded complexes proceeds via a similar mechanism proposed for the related Mn–Mg bonded complex **3-16**. That is, initially forming a transient "Ar(Si^{i}Pr$_3$)NZn" fragment (Ar = Ar* or Ar†), which due to its size is incapable of dimerising at room temperature. Therefore, the transient species is further reduced by the magnesium(I) reducing agent to give the Zn–Mg bonded complexes **4-26a** and **4-26.**

The two zinc-magnesium heterobimetallic complexes **4-26a** and **4-26b** are highly air and moisture sensitive compounds, both in solution and in the solid state. However, both compounds are surprisingly thermally stable, decomposing at temperatures >190 °C in the solid state. In addition, toluene solutions of the two complexes can be heated to reflux for several hours without decomposition.

To investigate the solid-state structures of **4-26a** and **4-26b**, both complexes were crystallographically characterised, and their molecular structures are depicted in Fig. 4.5. Compounds **4-26a** and **4-26b** are essentially isostructual, varying only by the alkyl group on the backbone of the ligand. The two compounds are unprecedented examples of zinc–magnesium heterobimetallic complexes with unsupported Zn–Mg bonds, and furthermore are the first molecular complexes to contain zinc–magnesium bonds. The zinc centre in both compounds is two-coordinate, with a near linear geometry (N–Zn–Mg = 171.2° **4-26a**; 168.9° **4-26b**), and does not exhibit any close contacts with the flanking phenyl rings (closest $C_{phenyl}\cdots$Zn = 3.249 Å **4-26a**; 3.280 Å **4-26b**). The magnesium centre on the other hand is three-coordinate, occupying a distorted trigonal planar geometry. The Zn–Mg bond lengths (2.6082 (14) Å **4-26a**; 2.5775(9) Å **4-26b**) lie almost exactly in between the metal–metal bond lengths of the amido zinc(I) dimer **4-23** (Zn–Zn = 2.3520(6) Å) and of the magnesium(I) dimer **1-08** (Mg–Mg = 2.808(1) Å) [47], and are also within the sum of the covalent radii of the two elements (2.63 Å) [43]. Due to the difference in electronegativities of the two metals, zinc being the most electronegative of the two (Zn 1.65, Mg 1.31 by the Pauling scale) [13], formal oxidation states of zinc(0)-magnesium(II) can be assigned to the two complexes.

To investigate the electronic structure of the Zn–Mg bonded complexes, DFT calculations using B3LYP and B3PW91 levels of theory were carried out on

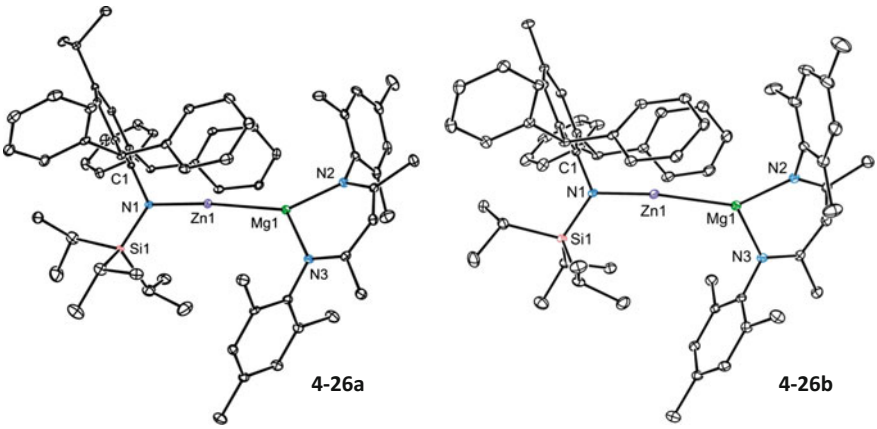

Fig. 4.5 Thermal ellipsoid plots (25 % probability surface) of the molecular structures of **4-26a** (*left*) and **4-26b** (*right*). Hydrogen atoms have been omitted for clarity. Selected bond lengths (Å) and angles (°): **4-26a**; Zn(1)–Mg(1) 2.6082(14), Zn(1)–N(1) 1.941(3), Mg(1)–N(2) 2.054(3), Mg(1)–N(3) 2.046(3), N(1)–Zn(1)–Mg(1) 171.20(9), N(2)–Mg(1)–N(3) 92.50(13): **4-26b**; Zn(1)–Mg(1) 2.5775(9), Zn(1)–N(1) 1.9342(19), Mg(1)–N(2) 2.045(2), Mg(1)–N(3) 2.034(2), N(1)–Zn(1)–Mg(1) 168.88(6), N(2)–Mg(1)–N(3) 93.89(9)

complex **4-26b** in the gas phase. The geometries of the calculated complex optimized to be close to those in the solid-state structure, with good agreement between the metal–metal bond lengths (calculated Zn–Mg = 2.582 Å). Analysis of the calculated MOs of **4-26b** found the HOMO to possess significant Zn–Mg σ bond character, whereas the LUMO is reminiscent of a π^* antibonding orbital, which is purely ligand based (Fig. 4.6). The Zn–Mg σ bond was calculated to be high in s character (Zn 91.1 % and Mg 81.6 % s contribution), which largely originates from

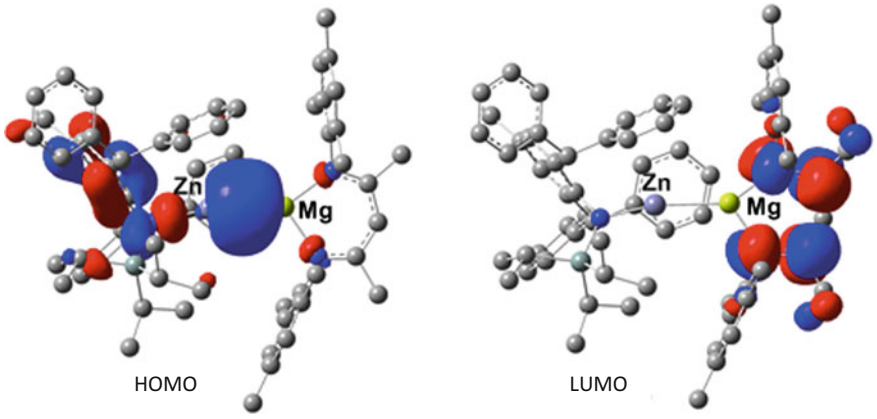

Fig. 4.6 Selected calculated frontier orbitals for **4-26b**. HOMO (*left*) and LUMO (*right*). Iso-surface value 0.03 a.u

the 4s and 3s orbitals on the Zn and Mg respectively. Lower energy MOs were consistent with the zinc centre possessing five fully occupied essentially non-bonding 3d orbitals.

As previously mentioned, Zn and Mg have different electronegativities (Zn 1.65 and Mg 1.31 by the Pauling scale) [13], resulting in **4-26b** being a formal Zn(0)Mg (II) complex. However, as the difference in these electronegativities is not great, the Zn–Mg bond should not be heavily polarised and consequently should possess significant covalent character. Indeed this is the case, and an only slightly polarised covalent bond is calculated between the two metal centres. In addition, the Zn–Mg bond was calculated to have a Wiberg Bond Index (WBI) value of 0.78, which is slightly lower than expected for a fully covalent bond (likely due to a small electrostatic contribution) but is still indicative of a Zn–Mg bond that is high in covalent character. To add further support, atomic natural charges were also calculated for the N–Zn–Mg unit (N −1.47, Zn +0.36, Mg +1.07), which found the Zn and Mg both to be positive. These charges are also in agreement with the complex's Zn(0) Mg(II) formal oxidation state, as the magnesium was calculated to be more positively charged than the zinc metal centre.

4.3.3 *Attempts to Synthesise Two-Coordinate Cadmium(0) or Mercury(0) Heterobimetallic Complexes with Unsupported M–Mg Bonds*

As previously discussed in Sect. 4.3.1, the three group 12 metal(I) dimers **4-23**–**4-25** are prepared by the reduction of their corresponding amido group 12 metal(II) halide complexes with the magnesium(I) reducing agent **1-08**. It is therefore possible that these reactions could proceed via a group 12 metal–magnesium bonded intermediate (Scheme 4.16), similar to complexes **4-26a** and **4-26b**. These intermediates could

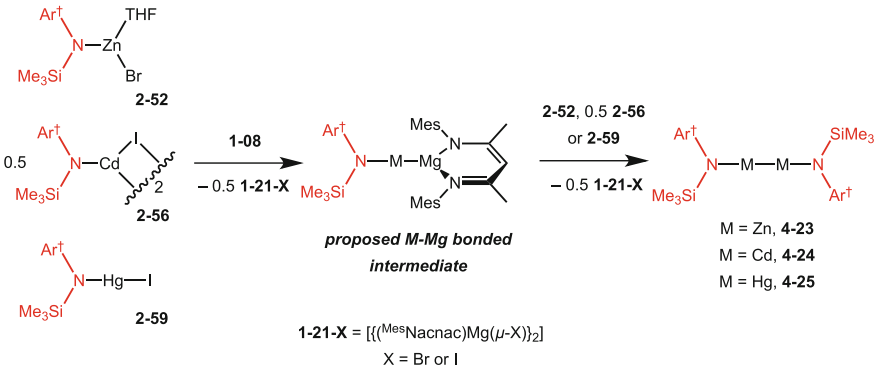

Scheme 4.16 Proposed synthetic pathway to the metal(I) dimers **4-23**–**4-25**

then react with a further equivalent of the amido group 12 metal(II) halide to give the appropriate group 12 metal(I) dimer.

In an attempt to trap the proposed M–Mg bonded intermediates, toluene solutions of the appropriate amido metal(II) halides were added to an excess of the magnesium(I) dimer **1-08** (1:2.5 group 12 metal to Mg ratio) at −80 °C. The idea behind this was that the excess magnesium(I) dimer would react with all of the amido metal(II) halide, therefore trapping the M–Mg bonded intermediate. Unfortunately this was not the case, and ^{1}H NMR spectroscopy performed on all three reaction mixtures revealed that the amido metal(I) dimer **4-23**–**4-25** were the only products synthesised in every case, along with approximately 1.5 equivalents of unreacted **1-08**. A similar result was observed when the reactions were repeated using a larger excess of the reducing agent (i.e. 20 equivalents). These observations suggests that either the proposed M–Mg bonded intermediates are not being formed in these reactions, (i.e. the magnesium(I) dimer reduces the amido metal(II) halides to form transient radical intermediates "Ar†(SiMe$_3$)NM" that quickly dimerise), or the M–Mg bonded intermediates reacts with the amido metal(II) halide complexes much faster than the magnesium(I) reducing agent. Either way, isolation of a M–Mg bonded complex is unlikely from any of these reactions.

The two Zn–Mg bonded complexes **4-26a** and **4-26b**, along with the related Mn–Mg bonded complex **3-16**, were all isolated because of the extreme steric bulk of the amide ligand, preventing two transient "Ar(Si^{i}Pr$_3$)NM" fragments from dimerising. As attempts to trap a M–Mg bonded complex bearing a smaller amide ligand have proven unsuccessful, it is thought that these extremely bulky ligands are needed for their isolation. As the amido mercury iodide complex [Ar*(Si^{i}Pr$_3$)NHgI] **2-61** bears the same amido ligand used to isolate the Zn–Mg complex **4-26b**, it seemed reasonable that this complex could be a precursor to a Hg–Mg bonded complex. Accordingly, a toluene solution of the amido mercury(II) iodide complex **2-61** was added to a solution of 1.1 equivalents of the magnesium(I) reducing agent **1-08** (1:2.2 ratio between Hg and Mg) at −80 °C. The reaction mixture was slowly warmed to room temperature where it was stirred for a further 30 min. Workup and subsequent crystallisation of the reaction mixture gave the amido mercury(I) dimer [{Ar*(Si^{i}Pr$_3$)NHg}$_2$] **4-27** as pale yellow crystals (Scheme 4.17). Repeating the reaction using a large excess of the magnesium(I) reducing agent (i.e. 20 equivalents) also led to isolation of the mercury(I) dimer **4-27** as the only product.

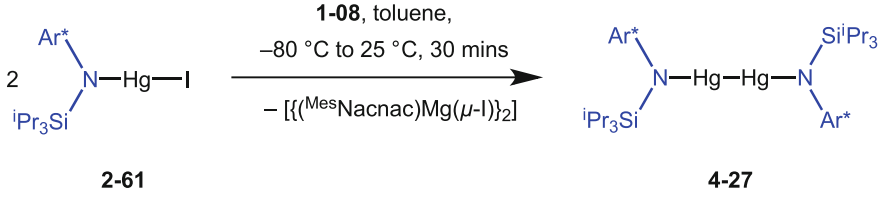

2-61 **4-27**

Scheme 4.17 Preparation of **4-27**

The isolation of the mercury(I) dimer **4-27** from the reduction of **2-61** with **1-08**, suggests that the extremely bulky Ar*(Si^{i}Pr$_3$)N$^-$ ligands that were used to prevent the dimerization of two transient "Ar*(Si^{i}Pr$_3$)NZn" fragments, are not bulky enough to prevent the dimerization of two "Ar*(Si^{i}Pr$_3$)NHg" fragments. This is likely due to the larger atomic radii of mercury compared with zinc, resulting in a longer metal–metal bond. It is therefore apparent that a larger ligand would need to be developed in order to possibly isolate a Hg–Mg bonded complex. Unfortunately, as explained in Chap. 2, an amido cadmium(II) halide precursor complex bearing the extremely bulky Ar*(Si^{i}Pr$_3$)N$^-$ ligand could not be isolated, to investigate whether it would prevent the dimerization of two "Ar*(Si^{i}Pr$_3$)NCd" fragments. However, as Cd–Cd bonds have been shown to be longer than the Hg–Hg bonds (as seen in the two homologous series of group 12 metal(I) dimers), it seems unlikely that two "Ar*(Si^{i}Pr$_3$)NCd" fragments would not also dimerise.

The amido mercury(I) dimer **4-27** was crystallographically characterised, and its molecular structure depicted in Fig. 4.7. The complex is essentially isostructural to the previously discussed amido mercury(I) dimer **4-25**, with two-coordinate linear mercury centres (N–Hg–Hg = 176.7°) but with a slightly longer Hg–Hg bond (2.5811(10) Å compared with 2.5394(5) Å in **4-25**). The longer metal–metal bond in **4-27** is likely due to the increase in ligand size.

In a final attempt to synthesise a Cd–Mg or Hg–Mg bonded complex, reductions of the related amido cadmium and mercury iodide complexes [Ar*(SiPh$_3$)NMI] (M = Cd **2-57** or Hg **2-60**), both bearing the extremely bulky Ar*(SiPh$_3$)N$^-$ ligand were carried out. However, when either complex was reacted with 0.5, 1.0 or 20 equivalents of the magnesium(I) reducing agent **1-08**, decomposition of the starting material was observed, by the almost instantaneous formation of cadmium or mercury metal. ^{1}H NMR spectroscopy performed on all reaction solutions showed

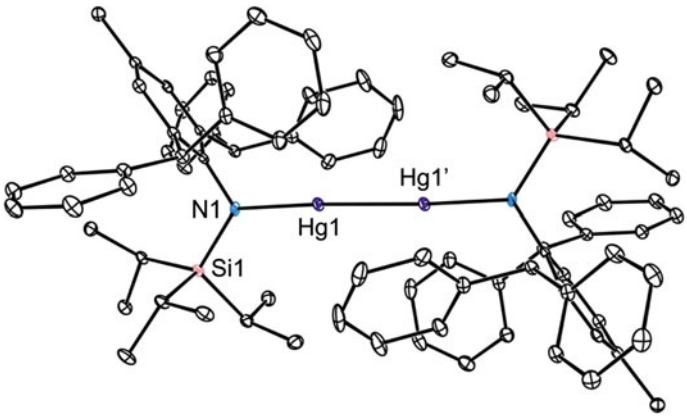

Fig. 4.7 Thermal ellipsoid plot (25 % probability surface) of the molecular structures of **4-27**. Hydrogen atoms have been omitted for clarity. Selected bond lengths (Å) and angles (°): Hg(1)–Hg(1′) 2.5811(10), N(1)–Hg(1) 2.068, N(1)–Hg(1)–Hg(1′) 176.67(9), Si(1)–N(1)–Hg(1) 125.03(17)

that the bulky amide Ar*($SiPh_3$)NH was the only identifiable product in every case. It is therefore apparent that the extremely bulky amide ligand Ar*($SiPh_3$)N^- does not provide the kinetic stabilisation required to isolate a low oxidation state cadmium or mercury compound.

4.3.4 *Reactivity of a Two-Coordinate Zinc(0) Heterobimetallic Complex with an Unsupported Zn–Mg Bond*

As previously discussed in Chap. 3, the reactivity of the Mn–Mg bonded complex **3-16** towards other metal halides was investigated. The complex was found to act as "inorganic Grignard reagent", by transfer of the "Ar†(Si^iPr_3)NMn" fragment onto other metal centres, creating new metal–metal bonds. As **4-26b** is essentially isostructual to **3-16**, it was proposed that it could also act as an "inorganic Grignard reagent", but by the transfer of an "Ar*(Si^iPr_3)NZn" fragment onto different metal centres, possibly creating new metal–metal bonds.

With that in mind, a 1:1 mixture of **4-26b** and the amido zinc(II) bromide precursor complex [Ar*(Si^iPr_3)NZnBr] **2-45** was dissolved in cyclohexane and stirred for one week at room temperature. This resulted in no reaction, and complete recovery of the starting materials was obtained. This was not unexpected, as the reaction between **2-54** and half an equivalent of the magnesium(I) reducing agent **1-08** gave **4-26b** and unreacted **2-54** in an approximate 1:1 ratio. However, when the reaction was repeated, and the reaction mixture heated to 70 °C for 12 h, complete consumption of the starting materials was observed by ^{1}H NMR spectroscopy, and the precipitation of [{(^{Mes}Nacnac)Mg(μ-Br)}$_2$] **1-21-Br** was seen. Workup, followed by crystallisation of the reaction mixture gave the zinc(I) dimer [{Ar*(Si^iPr_3)NZn}$_2$] **2-28** as small colourless crystals in good yields (Scheme 4.18). It is worth noting that this is in contrast with manganese chemistry, where heating a similar mixture of the Mn–Mg bonded complex **3-16** and [{Ar(Si^iPr_3)NMn(THF)(μ-Br)}$_2$] **2-45** led to complete decomposition of the starting materials. It was later found that **2-28** can also be isolated by heating a 2:1 mixture of **2-45** and **1-08** in cyclohexane for 12 h, generating the Zn–Mg bonded complex **4-26b** in situ.

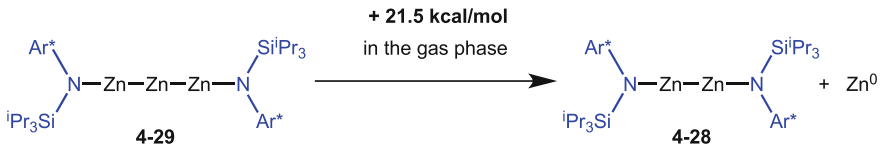

Scheme 4.18 Preparation of **4-28**

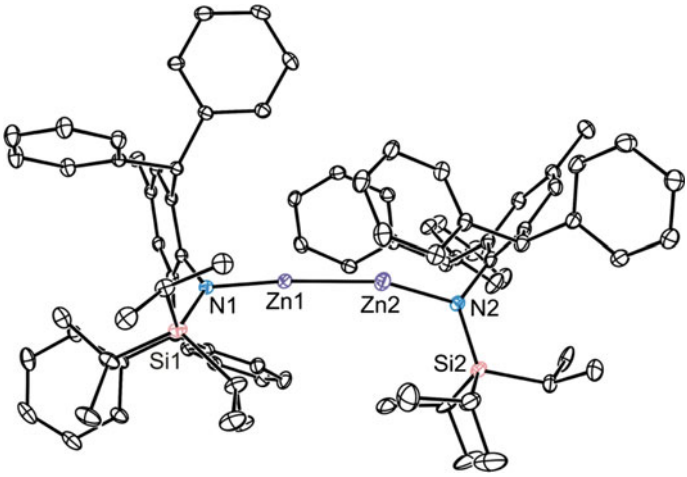

Fig. 4.8 Thermal ellipsoid plot (25 % probability surface) of the molecular structure of **4-28**. Hydrogen atoms have been omitted for clarity. Selected bond lengths (Å) and angles (°): Zn(1)–Zn (2) 2.4291(12), Zn(1)–N(1) 1.915(4), Zn(2)–N(2) 1.945(4), N(1)–Zn(1)–Zn(2) 174.40(13), Zn(1)–Zn(2)–N(2) 164.07(15)

Complex **4-28** was crystallographically characterised, and its molecular structure depicted in Fig. 4.8. Complex **4-28** is a two-coordinate amido zinc(I) dimer, bearing two extremely bulky Ar*(Si^iPr_3)N^- ligands. The solid state structure resembles that of the related zinc(I) dimer [{$Ar^\dagger(SiMe_3)NZn\}_2$] **4-23**, but due to the increase in steric bulk of the amido ligands in **4-28**, the complex is considerably more strained. As a result, the Zn–Zn bond length has increased by 0.07 Å, from 2.3520(6) Å in **4-23** to 2.4291(12) Å in **4-28**. In addition, complex **4-23** possesses two equivalent zinc centres with near linear geometries (N–Zn–Zn 174.3°), whereas **4-28** does not possess any symmetry in the solid state, and the two N–Zn–Zn angles are considerably different (N–Zn–Zn = 174.4° and 164.1°). The strain within the complex provides a good explanation as to why the dimerization of two "Ar*(Si^iPr_3)NZn" fragments does not occur at room temperature.

In the reaction between the Zn–Mg bonded complex **4-26b** and the amido zinc(II) bromide **2-54**, compound **4-26b** transfers a "Ar*(Si^iPr_3)NZn" unit onto the second zinc centre, creating a new zinc–zinc bond. Therefore, the Zn–Mg bonded complex **4-26b** is acting as an "inorganic Grignard reagent", showing similar reactivity to the Mn–Mg bonded complex **3-16**. As with **3-16**, we wanted to further explore the reactivity of **4-26b** towards other metal halides, to target a number of low coordinate heterobimetallic complexes with unsupported zinc-metal bonds. Accordingly, complex **4-26b** was reacted with numerous amido transition metal(II) halide complexes, including [Ar*($SiMe_3$)NM(THF)(μ-X)] (M = Cr, Mn or Fe; X = Cl or Br) **2-41**, **2-43** and **2-46**. Unfortunately, even after multiple attempts, whilst changing the reaction conditions and solvents used, no heterobimetallic

compound was isolated from any reaction. Instead, these reactions typically led to decomposition of the starting materials, or intractable mixtures of products. Two amido group 14 metal chlorides (viz. [Ar*($SiMe_3$)NMCl] M = Ge or Sn) were also reacted with the Zn–Mg bonded complex **4-26b**, however these too typically led to complex mixtures of products (observed by ^{1}H NMR spectroscopy). Although, one reaction between **4-26b** and [Ar*($SiMe_3$)NGeCl], performed in toluene at room temperature, did lead to the isolation of the desired Zn–Ge bonded complex [Ar*(Si^iPr_3)NZnGeN($SiMe_3$)Ar*] as blue crystals. These crystals were crystallographically characterised (see Sect. 7.2 for X-ray analysis), but due to the extremely low yield (<5 %), and problems resynthesizing the product, no further characterisation has been performed on the compound.

4.3.4.1 Preparation and Characterisation of a Homologous Series of Mixed-Valence Group 12 Metal Trimetallic Complexes

With the relatively unsuccessful preparation of Zn–M heterobimetallic compounds, our attention returned to group 12. As we have already shown (in the reaction between **4-26b** and the amido zinc(II) bromide **2-54**), transfer of a single "Ar*(Si^iPr_3)NZn" unit onto a second zinc centre, creating a new Zn–Zn bond is possible. Therefore we wondered if it were possible to react two equivalents of the Zn–Mg bonded complex **4-26b** with a zinc dihalide, to consequently transfer two "Ar*(Si^iPr_3)NZn" units onto the same metal centre? To investigate this proposal, two equivalents of **4-26b** were added to a suspension of $ZnBr_2$ in benzene at room temperature. The reaction mixture was stirred for 12 h at room temperature, resulting in a considerable amount of zinc metal precipitation. ^{1}H NMR spectroscopic analysis of the reaction solution revealed that the major reaction product (>80 %) was the amido zinc(II) bromide complex [Ar*(Si^iPr_3)NZnBr] **2-54**, suggesting that the Zn–Mg bonded complex had simply reduced the $ZnBr_2$ to Zn(0) metal. However, closer examination of the ^{1}H NMR spectrum revealed that a new product had been synthesised, albeit in low yields (>20 %). Remarkably, fractional crystallisation of this reaction mixture from pentane led to the isolation of proposed trimetallic zinc complex [{Ar*(Si^iPr_3)NZn}$_2$Zn] **4-29** as colourless crystals. Furthermore, reacting two equivalents of the Zn–Mg bonded complex **4-26b** with CdI_2 and $HgCl_2$ in similar reactions, gave the analogous trimetallic complexes [{Ar*(Si^iPr_3)NZn}$_2$M] (M = Cd **4-30**; Hg **4-31**) also as colourless crystals in low yields (Scheme 4.19). It is worthy of mention that the reaction between two equivalents of **4-26b** and Hg_2Cl_2 was also carried out, with aim of isolating the tetrametallic complex [{Ar*(Si^iPr_3)NZnHg}$_2$]. However, this led to a complex mixture of products, with the trimetallic complex **4-31**, the mercury(I) dimer **4-27**, [Ar*(Si^iPr_3)NZnCl] and Ar*(Si^iPr_3)NH being the only identifiable products.

Optimisation of the reaction conditions found that all three trimetallic complexes **4-29**–**4-31** were synthesised in their highest yields when the starting materials were reacted in an exact 2:1 ratio, and the solubility of the group 12 metal dihalide was

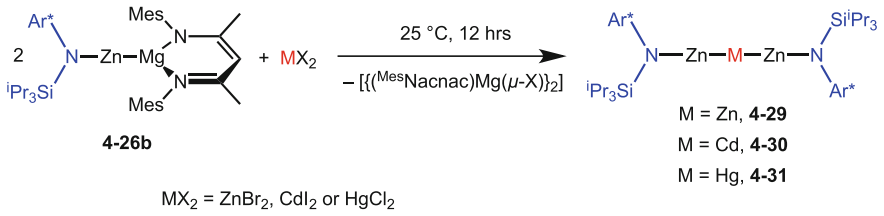

Scheme 4.19 Preparation of complexes **4-29**–**4-31**, a series of group 12 metal trimetallic complexes

kept to a minimum (as group 12 metal dihalides were found to react with the products). Therefore **4-29** and **4-30** are synthesised in their highest yields (44 and 60 % respectively) by reacting exactly two equivalents of **4-26b** with one equivalent of either $ZnBr_2$ or CdI_2, in a mixture of cyclohexane and diethyl ether (40:1) at room temperature. As $HgCl_2$ has a much higher solubility in organic solvents than $ZnBr_2$ or CdI_2, compound **4-31** is synthesised in its highest yields (34 %) by adding two equivalents of **4-26b** as a hexane solution to a suspension of $HgCl_2$ at −80 °C, followed by slow warming of the reaction mixture to room temperature overnight.

The three trimetallic complexes **4-29**–**4-31** are highly air and moisture sensitive. Furthermore, complexes **4-29**–**4-31** slowly decompose both in solution and in the solid state at room temperature to deposit Zn, Cd or Hg metal respectively. The ^{1}H, ^{13}C and ^{29}Si NMR spectra for trimetallic compounds, although consistent with their proposed structures, are not overly informative, as they all display similar spectral patterns. The ^{113}Cd NMR spectrum for complex **4-30** shows one sharp singlet at δ 688.6 ppm, consistent with the one Cd environment within the complex. Unfortunately, the ^{199}Hg NMR spectrum for **4-31** did not reveal an observable resonance, even after multiple 12 h scans over a large ppm range (δ −2000 to +1500 ppm). This is in agreement with the related β-diketiminate stabilised ZnHgZn bonded species **4-19**, which the authors reported it to be ^{199}Hg NMR silent also [41].

The three trimetallic complexes were crystallographically characterised, and their molecular structures are depicted in Fig. 4.9. Similar to the metal(I) dimers, the trimetallic species, **4-29**–**4-31** are isomorphous, all crystallising with similar unit cell parameters, but with a single molecule of pentane in the asymmetric unit (ASU). The three complexes all contain near linear chains (N–M–M: 170.8° **4-29**, 172.0° **4-30**, 171.3° **4-31**; M–M–M 180.0° **4-29**–**4-31**) of three two-coordinate metal centres. As far as we are aware, such a bonding arrangement in molecular compounds is unknown for any metal in the periodic table. Moreover, **4-30** incorporates the first structurally characterised examples of Zn–Cd bonds. The length of the Zn–Zn bonds in **4-29** (3.3840(12) Å) are in between those in the two amido zinc(I) dimers **4-23** and **4-28** (2.3520(6) Å and 2.4291(12) Å respectively). The Zn–M bond lengths in the heterotrimetallic compounds (2.487(2) Å **4-30**; 2.476(5) Å **4-31**) are the same, within experimental error, and are comparable to the

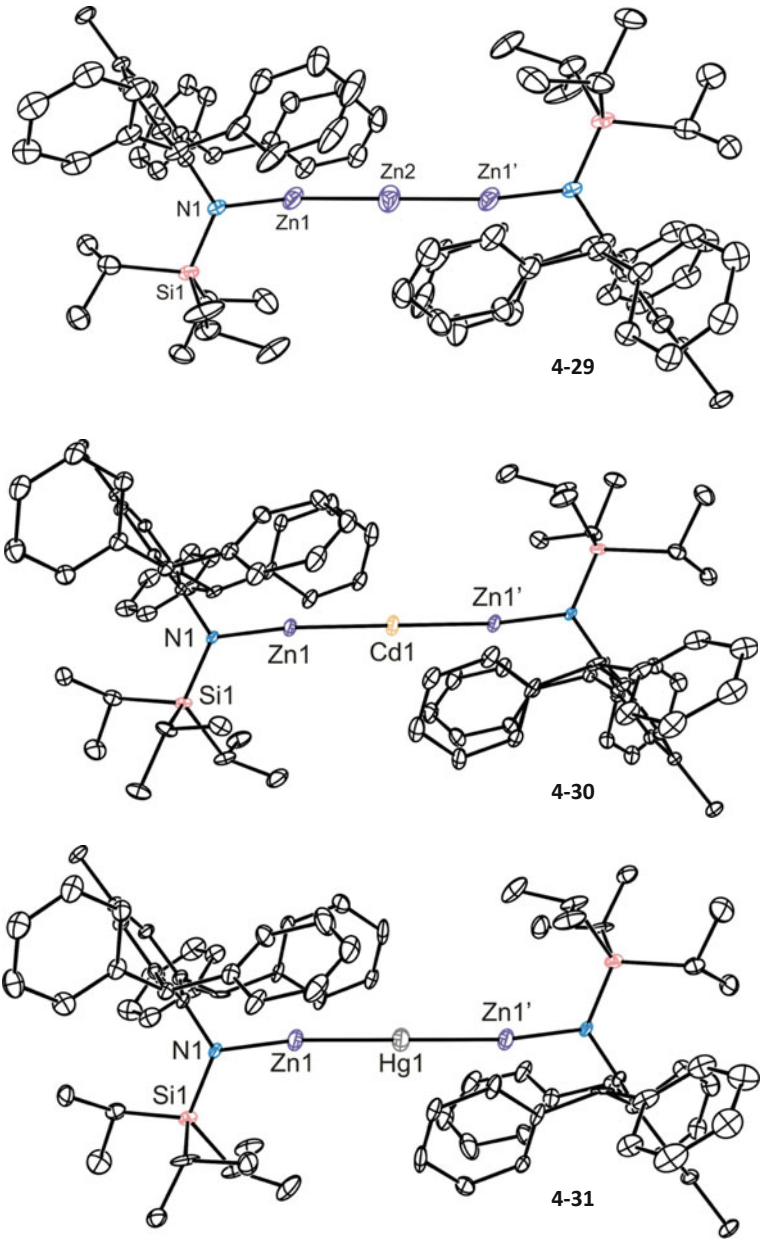

Fig. 4.9 Thermal ellipsoid plots (25 % probability surface) of the molecular structures of **4-29** (*top*), **4-30** (*middle*) and **4-31** (*bottom*). Hydrogen atoms have been omitted for clarity. Selected interatomic distances (Å) and angles (°) for complexes **4-29**–**4-31** is found in Table 4.2

Table 4.2 Selected interatomic distances (Å) and angles (°) for **4-29**–**4-31**

	4–29 (Zn)	4–30 (Cd)	4–31 (Hg)
Zn–M	2.3840(12)	2.487(2)	2.476(5)
N–Zn	1.901(5)	1.884(14)	1.90(3)
Closest $C_{phenyl}\cdots M$	3.073(13)	3.098(9)	3.055(16)
N–Zn–M	170.81(15)	172.0(4)	171.3(9)
Zn–M–Zn	180.00(5)	180.00(9)	180.000(1)

Zn–Hg bonds in the related β-diketiminate stabilised ZnHgZn bonded species **4-19** (2.4846(3) Å) [41]. It is evident from the structures of **4-29**–**4-31** that they are kinetically stabilised by the extreme bulk of the amide ligands, as four phenyl groups from which, enshroud the M_3 chains, without coordinating to them (all $M\cdots C_{Ph}$ distances >3.05 Å).

Complex **4-29** is an unprecedented example of a mixed valence tri-zinc cluster bearing a linear chain of two-coordinate zinc centres. Formal oxidation states can be assigned to the complex as Zn(I)–Zn(0)–Zn(I), due to the coordination of the two monoanionic amide ligands, one to each of the outer zinc centres. The central zinc atom is two-coordinate, and is coordinated to the two outer Zn atoms by two Zn–Zn bonds. The compound can be loosely be compared with the σ-aromatic trimetallic zinc complex $[(Cp^*Zn)_3][BAr^F_4]$ **4-18**, but that complex is cationic, with the three Zn atoms forming a three-membered ring, surrounded by three anionic ligands [40]. The Zn–Cd–Zn bonded complex **4-30** is also unprecedented, as it is the first molecular complex to contain Zn–Cd bonds. As cadmium has a slightly higher electronegativity than zinc (Zn 1.65 and Cd 1.69 by the Pauling scale) [13], similar formal oxidation states can be assigned to that complex, i.e. Zn(I)–Cd(0)–Zn(I). The Zn–Hg–Zn bonded complex **4-31** is however, comparable to the β-diketiminate stabilised ZnHgZn bonded species **4-19**, reported by Mountford and co-workers earlier this year. The two complexes possess a similar Zn–Hg–Zn unit, with a central two-coordinate mercury centre coordinated to two zinc centres. However, as complex **4-19** is stabilised by chelating β-diketiminate ligands, the two zinc centres are three-coordinate, whereas in **4-31** all three metal centres are two-coordinate. Similar to **4-19**, formal oxidation states can be assigned to complex **4-31** as Zn(I)–Hg(0)–Zn(I), due to the higher electronegativity of mercury compared to zinc (Zn 1.65 and Hg 2.00 by the Pauling scale) [13].

To further investigate the electronic structure of the Zn_3 complex **4-29**, DFT calculations using B3LYP and B3PW91 levels of theory were carried out on the complex in the gas phase. The geometries of the calculated complex optimized to be close to those in the solid-state structure, but with a slight underestimation of the Zn–Zn bond length (calculated Zn–Zn = 2.361 Å). It is worth noting that in 2007, Fernández, Frenking and co-workers also performed calculations on model complexes containing two-coordinate zinc atom strings capped by Cp* ligands (viz. $[Cp^*Zn_nCp^*]$ n = 2–5) [48]. The trizinc model complex [Cp*ZnZnZnCp*] was calculated to have Zn–Zn bond lengths (2.340 Å) similar to those experimentally

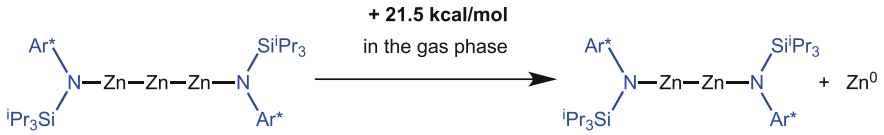

Scheme 4.20 Ejection of a Zn atom from **4-29** in the gas phase

obtained for **4-29**. However, they concluded that these model complexes with Zn chains of 3 or more would likely not be stable, as a considerable energy gain for the ejection of a Zn(0) atom was calculated. In comparison, calculations performed on **4-29** found a small energy requirement for the ejection of Zn(0) of +21.5 kcal/mol (Scheme 4.20). However, this value is for the ejection of a Zn atom in the gas phase. When the energy of vaporization of zinc metal is taken into account (31.2 kcal/mol), the disproportionation of **4-29** to Zn(s) and LZnZnL (L = Ar* (Si^{i}Pr$_3$)N$^-$) will clearly be exergonic. The compound is likely kinetically stabilized towards disproportionation by its bulky amide groups.

Analysis of the calculated MOs of **4-29** found the HOMO to have significant Zn–Zn σ bonding character, with σ bonding interactions either side of the central Zn atom (Fig. 4.10). The LUMO on the other hand is mostly based on the central Zn, and is representative of an empty p orbital.

Further examination of the two Zn–Zn σ bonds found them to possess considerable p character. This is because the central Zn is essentially sp hybridised (49.90 % s and 49.92 % p character). The two outer Zn centres are electronically similar to those calculated for the amido zinc(I) dimer **4-23**, that is high in s character (93.21 %) with a small contribution from the p and d orbitals (5.57 % p and 1.23 % d character). A Wiberg bond index of 0.68 was calculated for the two Zn–Zn bonds. This value is slightly low for a fully covalent bond (likely due to electrostatic contributions), but is still indicative of a Zn–Zn single bond that is high in covalent character. Finally natural charges for the Zn_3 core were calculated to be Zn(+0.50)–Zn(+0.18)–Zn(+0.50). These clearly show a significant decrease of

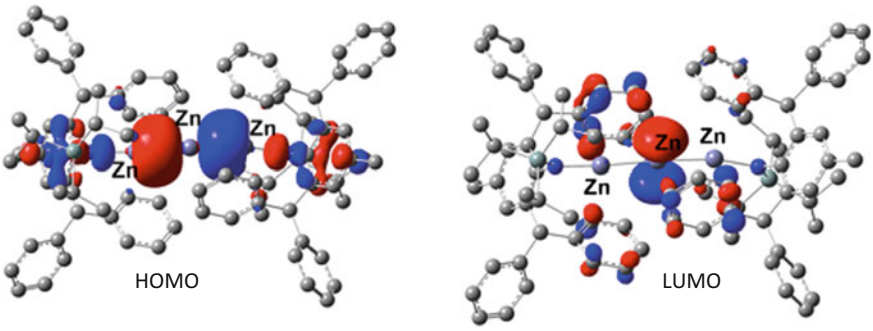

Fig. 4.10 Selected calculated frontier orbitals for **4-26b**. HOMO (*left*) and LUMO (*right*). Iso-surface value 0.03 a.u

positive charge for the central zinc atom in comparison to the outer two, which is in good agreement with the formal oxidation states Zn(I)–Zn(0)–Zn(I).

The three trimetallic species were synthesised by reactions of the appropriate metal(II) dihalide with two equivalents of the Zn–Mg bonded complex **4-26b**. In all three reactions, the Zn–Mg bonded complex **4-26b** is acting as an "inorganic Grignard reagent" in the transfer of two "Ar*(Si^{i}Pr$_3$)NZn" units onto a central metal centre. As it is unlikely that the transfer of the two "Ar*(Si^{i}Pr$_3$)NZn" units happens simultaneously, it was proposed that the reactions proceed via a mono substituted intermediate, i.e. [Ar*(Si^{i}Pr$_3$)NZnMX] (M = Zn, Cd, Hg; X = Cl, Br, I), which then reacts with a further equivalent of **4-26b** to give the trimetallic species **4-29**–**4-31**. In an attempt to isolate these mono substituted intermediates, 1:1 reactions between **4-26b** and the metal(II) dihalides $ZnBr_2$, CdI_2 and $HgCl_2$ were carried out. Unfortunately, "over-reduction" of the metal(II) dihalide was observed in every case, to give quantitative yields of the appropriate amido zinc(II) halide [Ar*(Si^{i}Pr$_3$)NZnX] and the formation of the appropriate group 12 metal. This suggests that these mono substituted intermediates are not stable, and therefore are only transient species in the reaction mixture, which react with a further equivalent of **4-26b** to give the trimetallic complexes before decomposing. This could also explain why the formation of metal is seen in the preparation of all three trimetallic complexes, which increases towards the end of the reaction. As the reaction proceeds, the relative concentration of the starting material **4-26b** decreases, and therefore the mono substituted intermediates have a greater chance to decompose.

In a final attempt to isolate a mono substituted product, the related base stabilised zinc(II) dibromide complex [$ZnBr_2$(tmeda)] (tmeda = tetramethylethylenediamine) was reacted with **4-26b** in a 1:1 ratio, in the hope that the coordinated tmeda would stabilize the mono substituted product. Indeed this turned out to be the case, and the tmeda stabilized mono substituted product [Ar*(Si^{i}Pr$_3$)NZnZnBr(tmeda)] **4-32** was isolated as large colourless crystals in good yields (Scheme 4.21).

Complex **4-32** is an asymmetrical metal–metal bonded zinc(I) dimer, bearing a single bulky monoanionic amide ligand coordinated to one Zn centre, and a bromide to the other. Furthermore, compound **4-32** is the first example of zinc(I) halide complex. The complex is highly air and moisture sensitive, but surprisingly thermally stable, only decomposing at temperatures >200 °C in the solid state.

Compound **4-32** was crystallographically characterised, and its molecular structure is depicted in Fig. 4.11. The molecular structure clearly shows two inequivalent zinc centres in two different geometries. One zinc centre (Zn1) is two-coordinate and near linear (N–Zn–Zn = 172.7°), coordinated to the bulky

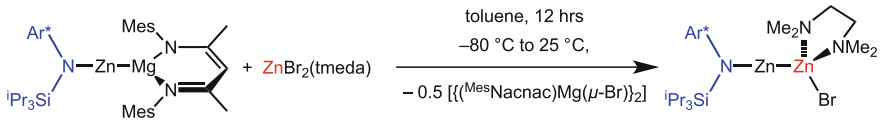

4-26b **4-32**

Scheme 4.21 Preparation of **4-32**

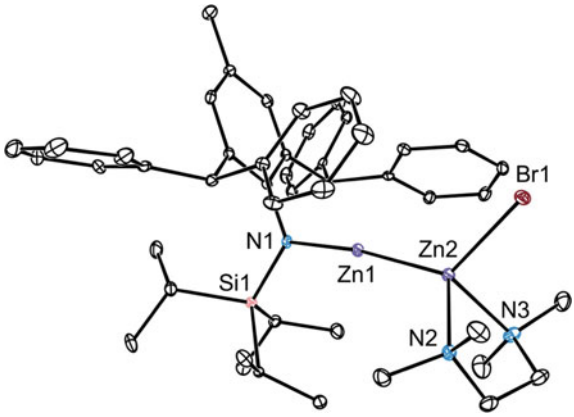

Fig. 4.11 Thermal ellipsoid plot (25 % probability surface) of the molecular structure of **4-32**. Hydrogen atoms have been omitted for clarity. Selected bond lengths (Å) and angles (°): Zn(1)–Zn (2) 2.3751(6), Zn(2)–Br(1) 2.4322(5), N(1)–Zn(1) 1.929(3), Zn(2)–N(2) 2.171(3), Zn(2)–N(3) 2.205(3), N(1)–Zn(1)–Zn(2) 172.73(8), Zn(1)–Zn(2)–Br(1) 124.74(2), N(2)–Zn(2)–N(3) 83.48(11)

amide ligand and the other zinc centre. The second zinc centre (Zn2) is four-coordinate, possessing a distorted tetrahedral geometry. A bromide, a chelating molecule of tmeda and the other zinc centre occupy its four coordination sites. The Zn–Zn bond distance in **4-32** (2.3751(6) Å) is within the expected range of a zinc(I) dimer, and furthermore is comparable to the Zn–Zn distances in the Zn_3 complex **4-29** (2.3840(12) Å).

The reduction of **4-32** was attempted using stoichiometric amounts of the magnesium(I) dimer **1-08** in toluene at −80 °C, in efforts to isolate a complex containing a chain of four metal–metal bonded zinc atoms, i.e. [{Ar*(Si^iPr_3)NZnZn(tmeda)}$_2$]. However almost instantly after the addition of **1-08**, metal precipitation was observed, and Ar*(Si^iPr_3)NH, [{(^{Mes}Nacnac)Mg(μ-Br)}$_2$] **1-21-Br** and tmeda were the only identifiable products as determined by an ^{1}H NMR spectroscopic analysis of the reaction solution.

The zinc(I) bromide complex **4-32** could be a useful starting material for the synthesis of other metal–metal bonded zinc(I) complexes. Having a bromide coordinated to a Zn_2^{2+} unit allows simple ligand substitution via salt metathesis reactions, or even the coordination of other metal complex fragments.

4.4 Conclusion

A number of bulky amido group 12 metal(II) halide complexes have been reduced with the magnesium(I) reducing agent **1-08** with varying outcomes. The three related group 12 complexes **2-52**, **2-56** and **2-59**, which all bear the same

$Ar^{\dagger}(SiMe_3)N^{-}$ ligand, were reduced to give a homologous series of two-coordinate group 12 metal(I) dimers (viz. $[\{Ar^{\dagger}(SiMe_3)NM\}_2]$ M = Zn, Cd or Hg, **4-23**–**4-25**). Moreover, the bulkier amido zinc(II) bromide complexes **2-54** and **2-55** were reduced to give the unprecedented heterobimetallic two-coordinate Zn(0)Mg(II) complexes **4-26a** and **4-26b** respectively, due to the increase in ligand bulk. The reduction of the analogous mercury(II) iodide complex **2-61** under the same reaction conditions did not give a Hg–Mg bonded complex, but instead the mercury(I) dimer **4-27**, due to the larger atomic radii of mercury compared with zinc.

The Zn–Mg bonded complex **4-26b** was found to act as an "inorganic Grignard reagent", by transfer of an "$Ar^*(Si^iPr_3)NZn$" fragment onto other metal centres creating new metal–metal bonds. This previously unseen reactivity led to the isolation of the 3 unprecedented group 12 metal trimetallic complexes **4-29**–**4-31**, which possess strings of two-coordinate metal atoms. All complexes were analysed by X-ray crystallography, multinuclear NMR spectroscopy as well as other techniques, including DFT calculations.

4.5 Experimental

General methods. All manipulations were carried out using standard Schlenk and glove box techniques under an atmosphere of high purity dinitrogen. THF, hexane, cyclohexane and toluene were distilled over molten potassium, while diethyl ether and pentane were distilled over sodium/potassium alloy (1:1). ^{1}H NMR spectra were recorded on either Bruker AvanceIII 400 or Varian Inova 500 spectrometers and were referenced to the resonances of the solvent used, or external $SiMe_4$. Mass spectra were recorded on an Agilent Techonlogies 5975D inert MSD with a solid state probe or obtained from the EPSRC National Mass Spectrometric Service at Swansea University. IR spectra were recorded using a Perkin-Elmer RX1 FT-IR spectrometer as Nujol mulls between NaCl plates or recorded as solid samples using an Agilent Cary 630 attenuated total reflectance (ATR) spectrometer. Microanalyses were carried out by the Science Centre, London Metropolitan University. A reproducible microanalysis for **4-31** could not be obtained, as the complex constantly crystallizes with small amounts (≈5 %) of the impurity $[Ar^*(Si^iPr_3)NZnCl]$. The amido metal(II) halide complexes **2-52**, **2-54**, **2-55**, **2-56**, **2-59** and **2-61** were prepared as discussed in Chap. 2, whereas $[\{(^{Mes}Nacnac)Mg\}_2]$ **1-08** and $[ZnBr_2(tmeda)]$ were prepared according to the literature method [47, 49] All other reagents were used as received.

Preparation of $[\{Ar^{\dagger}(SiMe_3)NZn\}_2]$, 4-23. To a solution of $[\{Ar^{\dagger}(SiMe_3)NZnBr(THF)]$ **2-52** (0.200 g, 0.264 mmol) in toluene (10 mL) was added a solution of $[\{(^{Mes}Nacnac)Mg\}_2]$ **1-08** (0.104 g, 0.145 mmol) in toluene (10 mL) at −80 °C over 5 min. The reaction was slowly warmed to room temperature and stirred for a further 4 h, whereupon volatiles were removed in vacuo. The residue was extracted with toluene (25 mL), concentrated (ca. 5 mL) and slowly cooled to 5 °C overnight to give **4-23** as colourless crystals (0.120 g, 75 %). Mp.: 240–242 °C (decomp. on

melting); ^{1}H NMR (499 MHz, C_6D_6, 298 K): δ = 0.27 (s, 18H, $Si(CH_3)_3$), 1.02 (d, $^{3}J_{HH}$ = 6.9 Hz, 12H, $CH(CH_3)_2$), 2.55 (sept., $^{3}J_{HH}$ = 6.9 Hz, 2H, $CH(CH_3)_2$), 6.30 (s, 4H, Ph_2CH), 6.95–7.29 (m, 44H, ArH); $^{13}C\{^{1}H\}$ NMR (75 MHz, C_6D_6): δ = 4.2 ($Si(CH_3)_3$), 24.3 ($CH(CH_3)_2$), 33.8 ($CH(CH_3)_2$), 52.7 (Ph_2CH), 126.5, 127.2 127.4, 128.6, 128.6, 129.6, 130.0, 130.2, 130.4, 141.3, 141.4, 145.6, 145.8, 146.1 (Ar–C); $^{29}Si\{^{1}H\}$ NMR (80 MHz, C_6D_6): δ = −2.96 (s); IR υ/cm^{-1} (Nujol): 1599 (m), 1492(m), 1436(m), 1258(m), 1243(s), 1229(s), 1159(m), 1124(m), 1074(m), 1031(m), 922(s), 908(s), 865(s), 841(s), 823(s), 746(s), 699(s), 670(s); MS/EI *m/z* (%): 602.4 ($Ar^{\dagger}(SiMe_3)NZn^{+}$, 59), 539.4 ($Ar^{\dagger}N(H)SiMe_3^{+}$, 100), 466.4 ($Ar^{\dagger}NH^{+}$, 12), 167.1 ($Ph_2CH^{+}$, 41); anal. calc. for $C_{76}H_{80}N_2Si_2Zn_2$: C 75.54 %, H 6.67 %, N 2.32 %, found: C 75.41 %, H 6.52 %, N 2.33 %.

Preparation of [{Ar†(SiMe3)NCd}2], 4-24. To a solution of [{$Ar^{\dagger}(SiMe_3)NCd(\mu\text{-}I)\}_2$] **2-56** (0.300 g, 0.193 mmol) in benzene (20 mL) was quickly added a solution of [{(^{Mes}Nacnac)Mg}$_2$] **1-08** (0.166 g, 0.231 mmol) in benzene (10 mL) at room temperature. The reaction was stirred for a further 2 h, whereupon volatiles were removed in vacuo. The off white residual was washed with pentane (2 × 10 mL), then extracted with toluene (25 mL), the extract concentrated (ca. 5 mL) and slowly cooled to 5 °C overnight to give **4-24** as colourless crystals (0.195 g, 78 %). Mp: 247–250 °C; ^{1}H NMR (499 MHz, C_6D_6, 298 K): δ = 0.37 (s, 18H, $Si(CH_3)_3$), 0.99 (d, $^{3}J_{HH}$ = 6.9 Hz, 12H, $CH(CH_3)_2$), 2.53 (sept., $^{3}J_{HH}$ = 6.9 Hz, 2H, $CH(CH_3)_2$), 6.41 (s, 4H, Ph_2CH), 6.94–7.30 (m, 44H, ArH); $^{13}C\{^{1}H\}$ NMR (75 MHz, C_6D_6): δ = 4.6 ($Si(CH_3)_3$), 24.4 ($CH(CH_3)_2$), 33.8 (CH ($CH_3)_2$), 52.7 (Ph_2CH), 126.5, 126.9, 127.1, 128.6, 129.9, 130.0, 130.4, 140.7, 140.8, 145.4, 145.9, 148.8 (Ar–C); $^{29}Si\{^{1}H\}$ NMR (80 MHz, C_6D_6): δ = −5.1 (s); $^{113}Cd\{^{1}H\}$ NMR (89 MHz, C_6D_6): δ = 270.6 ($^{1}J_{CdCd}$ = 18,900 Hz); IR υ/cm^{-1} (Nujol): 1596(m), 1490(m), 1465(m), 1435(m), 1256(m), 1240(m), 1127(m), 1073 (m), 1030(m), 933(s), 911(m), 862(m), 821(s), 746(m), 735(m), 698(s), 667(s); MS/EI m/z (%): 652.4 ($Ar^{\dagger}(SiMe_3)NCd^{+}$, 1), 539.5 ($Ar^{\dagger}N(H)SiMe_3^{+}$, 100), 466.4 ($Ar^{\dagger}NH^{+}$, 39), 167.2 ($Ph_2CH^{+}$, 71), 73.2 ($Me_3Si^{+}$, 72); anal. calc. for $C_{76}H_{80}Cd_2N_2Si_2$: C 70.08 %, H 6.19 %, N 2.15 %, found: C 69.88 %, H 6.23 %, N 2.31 %.

Preparation of [{Ar†(SiMe3)NHg}2], 4-25. To a solution of [$Ar^{\dagger}(SiMe_3)NHgI$] **2-59** (0.300 g, 0.346 mmol) in benzene (20 mL) was slowly added a solution of [{(^{Mes}Nacnac)Mg}$_2$] (0.136 g, 0.190 mmol) in benzene (10 mL) over 10 min at room temperature. The reaction was stirred for a further 2 h at room temperature, whereupon volatiles were removed in vacuo. The off white residual was washed with pentane (2 × 10 mL), then extracted with toluene (25 mL), the extract concentrated (ca. 5 mL) and slowly cooled to 5 °C overnight to give **4-25** as colourless crystals (0.180 g, 70 %). Mp: 259–261 °C; ^{1}H NMR (499 MHz, C_6D_6, 298 K): δ = 0.35 (s, 18H, $Si(CH_3)_3$), 1.01 (d, $^{3}J_{HH}$ = 6.9 Hz, 12H, $CH(CH_3)_2$), 2.56 (sept., $^{3}J_{HH}$ = 6.9 Hz, 2H, $CH(CH_3)_2$), 6.48 (s, 4H, Ph_2CH), 6.95–7.31 (m, 44H, ArH); $^{13}C\{^{1}H\}$ NMR (75 MHz, C_6D_6): δ = 4.2 ($Si(CH_3)_3$), 24.4 ($CH(CH_3)_2$), 33.8 (CH ($CH_3)_2$), 52.4 (Ph_2CH), 126.5, 127.1, 128.6, 129.5, 130.3, 141.7, 142.4, 145.1, 145.9, 146.9 (Ar–C); $^{29}Si\{^{1}H\}$ NMR (80 MHz, C_6D_6): δ = −1.8 (s); $^{199}Hg\{^{1}H\}$ NMR (72 MHz, C_6D_6): δ = −726.3 (br. s); IR υ/cm^{-1} (Nujol): 1598(m), 1520(m),

1492(m), 1435(s), 1243(s), 1198(m), 1127(m), 1030(m), 926(s), 855(m), 828(s), 747(s), 698(s), 671(s); MS/EI m/z (%): 740.4 ($Ar^{\dagger}(SiMe_3)NHg^+$, <1), 539.4 ($Ar^{\dagger}N(H)SiMe_3^+$, 30), ($Ar^{\dagger}N(H)SiMe_2^+$, 96), 167.1 ($Ph_2CH^+$, 100), 73.1 ($Me_3Si^+$, 27); anal. calc. for $C_{76}H_{80}Hg_2N_2Si_2$: C 61.73 %, H 5.45 %, N 1.89 %, found: C 61.65 %, H 5.39 %, N 1.83 %.

Preparation of [$Ar^{\dagger}(Si^iPr_3)$NZnMg(^{Mes}Nacnac)], 4-26a. To a suspension of [{(^{Mes}Nacnac)Mg}$_2$] **1-08** (0.168 g, 0.234 mmol) in toluene (15 mL) was added a solution of [$Ar^{\dagger}(Si^iPr_3)$NZnBr] **2-55** (0.200 g, 0.260 mmol) in toluene (15 mL) at −80 °C over 5 min. The reaction mixture was slowly warmed to room temperature, where it stirred for a further 12 h. Volatiles were removed in vacuo, the residue extracted with toluene (20 mL), the extract filtered and volatiles removed from the filtrate in vacuo to give an off white solid. The solid was washed twice with ice cold pentane (2 × 10 mL) to give **4-26a** as a white powder (0.180 g, 74 %). N.B. X-ray quality crystals of **4-26a** were obtained by crystallizing this solid from warm pentane. Mp: 199–202 °C; ^{1}H NMR (499 MHz, C_6D_6, 298 K): δ = 0.96 (d, $^3J_{HH}$ = 6.5 Hz, 6H, ArCH(CH_3)$_2$), 1.17 (br. d, 18H, Si{CH(CH_3)$_2$}$_3$), 1.36 (br. sept., 3H, Si{CH(CH_3)$_2$}$_3$), 1.50 (s, 6H, NCCH_3), 2.07 (s, 12H, o-CH_3), 2.20 (s, 6H, p-CH_3), 2.50 (sept, $^3J_{HH}$ = 6.5 Hz, 1H, ArCH(CH_3)$_2$), 4.86 (s, 1H, NCCH), 6.56 (s, 2H, Ph_2CH), 6.80–7.38 (m, 26H, ArH); ^{13}C{^{1}H} NMR (75 MHz, C_6D_6): δ = 15.4 (Si{CH(CH_3)$_2$}$_3$), 19.4 (o-CH_3), 20.1 (Si{CH(CH_3)$_2$}$_3$), 21.0 (p-CH_3), 23.4 (NCCH_3), 24.2 (ArCH(CH_3)$_2$), 33.6 (ArCH(CH_3)$_2$), 51.8 ($CHPh_2$), 96.3 (NCCH), 125.6, 126.1, 127.6, 128.3, 128.6, 129.0, 129.8, 130.1, 130.5, 130.8, 131.4, 134.0, 139.3, 140.6, 145.1, 146.2, 148.3, 148.6, 168.7 (Ar–C), 168.7 (NCCH_3); ^{29}Si{^{1}H} NMR (80 MHz, C_6D_6): δ = −0.6 (s); IR υ/cm^{-1} (Nujol): 1599 (m), 1522(m), 1493(m), 1447(s), 1431(s), 1380(s), 1253(m), 1229(m), 1199(m), 1146(m), 1121(m), 1076(m), 1030(m), 1018(m), 915(m), 901(m), 860(m), 761(m), 748(m), 701(s), 687(s); MS/EI m/z (%): 623.4 ($Ar^{\dagger}N(H)Si^iPr_3^+$, 54), 580.3 ($Ar^{\dagger}N(H)Si^iPr_3^+$–^{i}Pr, 100), 467.3 ($Ar^{\dagger}NH_2^+$, 7), 334.2 (^{Mes}NacnacH$^+$, 38), 167.0 (Ph_2CH^+, 31); anal. calc. for $C_{67}H_{81}MgN_3SiZn$: C 76.92 %, H 7.80 %, N 4.02 %, found: C 76.64 %, H 7.88 %, N 3.91 %.

Preparation of [$Ar^*(Si^iPr_3)$NZnMg(^{Mes}Nacnac)], 4-26b. To a suspension of [{(^{Mes}Nacnac)Mg}$_2$] **1-08** (0.213 g, 0.297 mmol) in cyclohexane (15 mL) was added a solution of [Ar*(Si^iPr_3)NZnBr] **2-54** (0.200 g, 0.270 mmol) in cyclohexane (15 mL) at room temperature over 5 min. The reaction mixture was stirred for a further 16 h, whereupon volatiles were removed in vacuo. The residue was extracted with pentane (20 mL), the extract filtered and volatiles removed from the filrate in vacuo to give **4-26b** as an off white solid (0.205 g, 75 %). N.B. X-ray quality crystals of **4-26b** were obtained by crystallizing this solid from a concentrated solution of warm pentane. Mp: 193–196 °C; ^{1}H NMR (499 MHz, C_6D_6, 298 K): δ = 1.16 (br. d, 18H, CH(CH_3)$_2$), 1.25 (br. sept., 3H, CH(CH_3)$_2$), 1.52 (s, 6H, NCCH_3), 1.86 (s, 3H, Ar*-CH_3), 2.08 (s, 12H, o-CH_3), 2.20 (s, 6H, p-CH_3), 4.86 (s, 1H, NCCH), 6.59 (s, 2H, Ph_2CH), 6.79–7.39 (m, 26H, ArH); ^{13}C{^{1}H} NMR (75 MHz, C_6D_6): δ = 15.4 (Si{CH(CH_3)$_2$}$_3$), 19.6 (o-CH_3), 20.1 (Si{CH(CH_3)$_2$}$_3$), 21.0 (p-CH_3), 21.1 (ArCH_3), 23.5 (NCCH_3), 51.2 ($CHPh_2$), 95.8 (NCCH_3), 125.5, 126.1, 128.2, 128.7, 129.8, 130.6, 130.8, 131.0, 131.5, 133.7,

140.4, 145.5, 146.2, 148.4, 148.7 (Ar–C), 168.4 ($NCCH_3$); $^{29}Si\{^1H\}$ NMR (80 MHz, C_6D_6): δ = −0.42 (s); IR υ/cm^{-1} (Nujol): 1597(m), 1517(m), 1493(m), 1253(s), 1233(s), 1198(s), 1146(m), 1126(m), 1075(m), 1019(m), 914(m), 897(s), 879(s), 858(s), 831(m), 814(m), 758(s), 723(s), 701(s); MS/EI m/z (%): 595.5 (Ar*N(H)Si^{i}Pr$_3^+$, 35), 552.5 (Ar*N(H)Si^{i}Pr$_2^+$, 100), 334.3 (^{Mes}NacnacH$^+$, 9), 167.1 (Ph_2CH^+, 93); anal. calc. for $C_{65}H_{77}MgN_3SiZn$: C 76.68 %, H 7.62 %, N 4.13 %, found: C 76.49 %, H 7.49 %, N 4.18 %.

Preparation of [{Ar*(Si^{i}Pr$_3$)NHg}$_2$], 4-27. To a solution of [Ar*(Si^{i}Pr$_3$)NHgI] **2-61** (0.200 g, 0.217 mmol) in toluene (20 mL) was slowly added a solution of [{(^{Mes}Nacnac)Mg}$_2$] **1-08** (0.085 g, 0.119 mmol) in toluene (10 mL) at −80 °C over 5 min. The reaction mixture was slowly warmed to room temperature and stirred for a further 2 h, whereupon volatiles were removed in vacuo. The off white residue was extracted with pentane (25 mL), the extract concentrated (ca. 5 mL) and slowly cooled to 5 °C overnight to give **4-27** as colourless crystals (0.085 g, 49 %). ^1H NMR (499 MHz, C_6D_6, 298 K): δ = 1.22 (d, $^3J_{HH}$ = 7.5 Hz, 36H, CH(CH_3)$_2$), 1.31 (sept., $^3J_{HH}$ = 7.5 Hz, 6H, CH(CH_3)$_2$), 1.94 (s, 6H, ArCH_3), 6.71 (s, 4H, Ph_2CH), 7.02–7.37 (m, 44H, ArH); $^{13}C\{^1H\}$ NMR (75 MHz, C_6D_6): δ = 15.3 (CH(CH_3)$_2$), 19.9 (CH(CH_3)$_2$), 21.0 (ArCH_3), 50.9 (Ph_2CH), 126.5, 127.1, 128.6, 129.2, 130.1, 130.4, 130.6, 131.3, 141.9, 145.7, 146.2, 147.4 (Ar–C); $^{29}Si\{^1H\}$ NMR (80 MHz, C_6D_6): δ = 4.4 (s); $^{199}Hg\{^1H\}$ NMR (72 MHz, C_6D_6): δ = −773.3 (br. s). MS/EI m/z (%): 595.5 (Ar*N(H)Si^{i}Pr$_3^+$, 32), 552.5 (Ar*N(H)Si^{i}Pr$_2^+$, 76), 167.2 (Ph_2CH^+, 100).

Preparation A of [{Ar*(Si^{i}Pr$_3$)NZn}$_2$], 4-28. To a suspension of [{(^{Mes}Nacnac)Mg}$_2$] **1-08** (0.145 g, 0.203 mmol) in cyclohexane (20 mL) was added a solution of [Ar*(Si^{i}Pr$_3$)NZnBr] **2-54** (0.300 g, 0.405 mmol) in cyclohexane (20 mL) over 5 min. The reaction mixture was stirred at ambient temperature for 2 h, before being heated to 70 °C. The reaction mixture was stirred for a further 12 h at 70 °C, whereupon volatiles were removed in vacuo. The residue was extracted with pentane (20 mL), the extract filtered, the filtrate concentrated in vacuo (ca. 3 mL) and slowly cooled to 5 °C overnight to give **4-28** as small colourless crystals (0.155 g, 58 %).

Preparation B of [{Ar*(Si^{i}Pr$_3$)NZn}$_2$], 4-28. To a solution of [Ar*(Si^{i}Pr$_3$)NZn–Mg(^{Mes}Nacnac)] **4-26b** (0.200 g, 0.196 mmol) in cyclohexane (15 mL) was added a solution of [Ar*(Si^{i}Pr$_3$)NZnBr] **2-54** (0.160 g, 0.216 mmol) in cyclohexane (15 mL) at ambient temperature, before being heated to 70 °C. The reaction mixture was stirred for a further 12 h at 70 °C, whereupon volatiles were removed in vacuo. The residue was extracted with pentane (20 mL), the extract filtered, the filtrate concentrated in vacuo (ca. 3 mL) and slowly cooled to 5 °C overnight to give **4-28** as small colourless crystals (0.180 g, 70 %). Mp: 240–243 °C (200–210 °C decomp.); ^1H NMR (499 MHz, C_6D_6, 298 K): δ = 1.34 (d, $^3J_{HH}$ = 7.4 Hz, 36H, CH(CH_3)$_2$), 1.55 (sept., $^3J_{HH}$ = 7.4 Hz, 6H, CH(CH_3)$_2$), 1.93 (s, 6H, ArCH_3), 6.41 (s, 4H, Ph_2CH), 6.85–7.35 (m, 44H, ArH); $^{13}C\{^1H\}$ NMR (75 MHz, C_6D_6): δ = 15.6 (Si{CH(CH_3)$_2$}$_3$), 20.2 (Si{CH(CH_3)$_2$}$_3$), 21.2 (ArCH_3), 52.4 ($CHPh_2$), 126.6, 127.1, 128.8, 129.5, 129.6, 130.1, 130.5, 130.8, 141.9, 145.7, 146.6, 148.2 (Ar–C); $^{29}Si\{^1H\}$ NMR (80 MHz, C_6D_6): δ = −0.1 (s); IR υ/cm^{-1} (Nujol): 1596

(m), 1491(m), 1430(s), 1230(s), 1208(m), 1129(m), 1072(m), 1030(m), 913(m), 896(m), 877(s), 835(m), 760(m), 740(s), 698(s); MS/EI m/z (%): 658.5 (Ar*(Si^iPr_3)NZn$^+$, 2), 595.5 (Ar*N(H)$Si^iPr_3^+$, 36), 552.5 (Ar*N(H)$Si^iPr_2^+$, 80), 167.2 (Ph_2CH^+, 100); anal. calc. for $C_{84}H_{96}N_2Si_2Zn_2$: C 76.40 %, H 7.33 %, N 2.12 %, found: C 76.29 %, H 7.40 %, N 2.15 %.

Preparation of [{Ar*(Si^{i}Pr$_3$)NZn}$_2$Zn], 4-29. To a suspension of $ZnBr_2$ (0.022 g, 0.098 mmol) in cyclohexane (10 mL) was added a solution of [Ar*(Si^iPr_3)NZnMg(^{Mes}Nacnac)] **4-26b** (0.200 g, 0.196 mmol) in a mixture of cyclohexane (10 mL) and diethyl ether (0.5 mL) at atmospheric temperature. The reaction mixture was stirred for a further 12 h at room temperature, whereupon volatiles were removed in vacuo. The residue was extracted with pentane (20 mL), the extract filtered, the filtrate concentrated in vacuo (ca. 5 mL) and left to stand for 1 h at room temperature to give **4-29** as small colourless crystals (0.060 g, 44 %). NB. If the extracted solution is left to crystallise for much longer than 1 h, small amounts of the impurity [Ar*(Si^iPr_3)NZnBr] **2-54** crystallise with the product. Mp: 238–242 °C (decomp. 51–59 °C); ^{1}H NMR (499 MHz, C_6D_6, 298 K): δ = 1.34 (d, $^3J_{HH}$ = 7.4 Hz, 36H, $CH(CH_3)_2$), 1.55 (sept., $^3J_{HH}$ = 7.4 Hz, 6H, $CH(CH_3)_2$), 1.93 (s, 6H, $ArCH_3$), 6.41 (s, 4H, Ph_2CH), 6.85–7.35 (m, 44H, ArH); ^{13}C{^{1}H} NMR (75 MHz, C_6D_6): δ = 15.6 (Si{$CH(CH_3)_2$}$_3$), 20.2 (Si{$CH(CH_3)_2$}$_3$), 21.2 ($ArCH_3$), 52.4 ($CHPh_2$), 126.6, 127.1, 128.6, 128.8, 129.5, 129.6, 130.1, 130.5, 130.8, 141.9, 145.7, 146.6, 148.2 (Ar–C); ^{29}Si{^{1}H} NMR (80 MHz, C_6D_6): δ = −0.1 (s); IR υ/cm^{-1} (Nujol): 1597(m), 1492(m), 1434(s), 1233(s), 1209(m), 1129(m), 1073(m), 1031(m), 996(m), 913(m), 897(s), 878(s), 834(s), 818(m), 757 (m), 736(s), 697(s); MS/EI m/z (%): 595.6 (Ar*N(H)$Si^iPr_3^+$, 30), 552.5 (Ar*N(H)$Si^iPr_2^+$, 91), 439.4 (Ar*NH_2, 13); 167.2 (Ph_2CH^+, 100); anal. calc. for $C_{84}H_{96}N_2Si_2Zn_3$: C 72.79 %, H 6.98 %, N 2.02 %, found: C 72.67 %, H 6.67 %, N 2.05 %.

Preparation of [{Ar*(Si^{i}Pr$_3$)NZn}$_2$Cd], 4-30. To a suspension of CdI_2 (0.036 g, 0.098 mmol) in cyclohexane (10 mL) was added a solution of [Ar*(Si^iPr_3)NZnMg(^{Mes}Nacnac)] **4-26b** (0.200 g, 0.196 mmol) in a mixture of cyclohexane (10 mL) and diethyl ether (0.5 mL) at room temperature. The reaction mixture was stirred for a further 12 h at room temperature, whereupon volatiles were removed in vacuo. The residue was extracted with pentane (20 mL), the extract filtered, the filtrate concentrated in vacuo (ca. 5 mL) and left to stand for 1 h at room temperature to give **4-30** as small colourless crystals (0.085 g, 60 %). NB. If the extracted solution is left to crystallise for much longer than 1 h, small amounts of the impurity [Ar*(Si^iPr_3)NZnI] crystallise with the product. Mp: >260 °C (decomp. 61–76 °C); ^{1}H NMR (499 MHz, C_6D_6, 298 K): δ = 1.35 (d, $^3J_{HH}$ = 7.3 Hz, 36H, $CH(CH_3)_2$), 1.56 (sept., $^3J_{HH}$ = 7.4 Hz, 6H, $CH(CH_3)_2$), 1.94 (s, 6H, $ArCH_3$), 6.46 (s, 4H, Ph_2CH), 6.86–7.35 (m, 44H, ArH); ^{13}C{^{1}H} NMR (75 MHz, C_6D_6): δ = 15.5 (Si{$CH(CH_3)_2$}$_3$), 20.3 (Si{$CH(CH_3)_2$}$_3$), 21.2 ($ArCH_3$), 52.4 ($CHPh_2$), 126.5, 127.0, 128.6, 128.8, 128.9, 129.6, 130.4, 130.5, 130.8, 131.7, 141.9, 145.7, 146.8, 148.0 (Ar–C); ^{29}Si{^{1}H} NMR (80 MHz, C_6D_6): δ = −0.2 (s); ^{113}Cd{^{1}H} NMR (89 MHz, C_6D_6): δ = 688.6 (s); IR υ/cm^{-1} (Nujol): 1597(m), 1492(m), 1433(m), 1234(s), 1209(m), 1130(m), 1073(m), 1031(m),

997(m), 913(m), 896(s), 878(s), 834(s), 818(m), 758(m), 736(s), 698(s); MS/EI m/z (%): 595.6 (Ar*N(H)Si^{i}Pr$_3^+$, 35), 552.5 (Ar*N(H)Si^{i}Pr$_2^+$, 93), 439.3 (Ar*NH$_2$, 53); 167.2 (Ph$_2$CH$^+$, 100); anal. calc. for $C_{84}H_{96}CdN_2Si_2Zn_2$: C 70.40 %, H 6.75 %, N 1.95 %, found: C 70.32 %, H 6.77 %, N 2.01 %.

Preparation of [{Ar*(Si^{i}Pr$_3$)NZn}$_2$Hg], 4-31. To a suspension of $HgCl_2$ (0.027 g, 0.099 mmol) in hexane (10 mL) was added a solution of [Ar*(Si^{i}Pr$_3$)NZnMg(^{Mes}Nacnac)] **4-26b** (0.200 g, 0.196 mmol) in hexane (10 mL) at −80 °C over 5 min. The reaction mixture was slowly warmed to room temperature, where it was stirred for a further 12 h, producing a white precipitate. This white solid was isolated via filtration, extracted with toluene, the extract filtered and volatiles removed from the filtrate in vacuo to give **4-31** as an off white powder (0.050 g, 34 %). NB. X-ray quality crystals were grown from slow diffusion of pentane into a concentrated toluene solution of [{Ar*(Si^{i}Pr$_3$)NZn}$_2$Hg]. Mp: >260 °C (94–98 °C decomp.); ^{1}H NMR (499 MHz, C_6D_6, 298 K): δ = 1.34 (d, $^3J_{HH}$ = 7.4 Hz, 36H, CH(CH$_3$)$_2$), 1.55 (sept., $^3J_{HH}$ = 7.4 Hz, 6H, CH(CH$_3$)$_2$), 1.95 (s, 6H, ArCH$_3$), 6.50 (s, 4H, Ph$_2$CH), 6.81–7.34 (m, 44H, ArH); ^{13}C{^{1}H} NMR (75 MHz, C_6D_6): δ = 15.6 (Si{CH(CH$_3$)$_2$}$_3$), 20.4 (Si{CH(CH$_3$)$_2$}$_3$), 21.2 (ArCH$_3$), 52.4 (CHPh$_2$), 126.6, 128.6, 128.8, 128.9, 129.6, 130.1, 130.4, 130.6, 142.1, 144.9, 145.7, 146.5 (Ar–C); ^{29}Si{^{1}H} NMR (80 MHz, C_6D_6): δ = -0.3 (s); IR υ/cm^{-1} (Nujol): 1598 (m), 1544(m), 1523(m), 1492(m), 1444(s), 1398(s), 1233(m), 1201(m), 1129(m), 1075(m), 1030(m), 1013(m), 914(m), 879(s), 854(m), 833(m), 811(m), 760(m), 743 (m), 698(s), 650(s); MS/EI m/z (%): 595.5 (Ar*N(H)Si^{i}Pr$_3^+$, 36), 552.5 (Ar*N(H) Si^{i}Pr$_2^+$, 100), 439.3 (Ar*NH$_2^+$, 27); 167.2 (Ph$_2$CH$^+$, 95).

Preparation of [{Ar*(Si^{i}Pr$_3$)NZnZnBr(tmeda)], 4-32. To a solution of [ZnBr$_2$(tmeda)] (0.060 g, 0.177 mmol) in toluene (15 mL) was added a solution of [Ar*(Si^{i}Pr$_3$)NZnMg(^{Mes}Nacnac)] **4-26b** (0.200 g, 0.196 mmol) in toluene (15 mL) at −80 °C over 5 min. The reaction mixture was slowly warmed to room temperature and stirred for a further 12 h, whereupon volatiles were removed from the filtrate in vacuo. The residue was extracted with pentane (20 mL), the extract filtered, the filtrate concentrated in vacuo (ca. 10 mL) and slowly cooled to 5 °C overnight to give **4-32** as large colourless crystals (0.140 g, 86 %). Mp: 208–210 °C (decomp. on melting); ^{1}H NMR (499 MHz, C_6D_6, 298 K): δ = 1.34 (d, $^3J_{HH}$ = 7.4 Hz, 18H, CH(CH$_3$)$_2$), 1.65 (sept., $^3J_{HH}$ = 7.4 Hz, 3H, CH(CH$_3$)$_2$), 1.66 (br., 12H, TMEDA), 1.92 (s, 3H, ArCH$_3$), 2.05 (br., 6H, TMEDA), 6.64 (s, 2H, Ph$_2$CH), 6.92–7.40 (m, 22H, ArH); ^{13}C{^{1}H} NMR (75 MHz, C_6D_6): δ = 15.6 (Si {CH(CH$_3$)$_2$}$_3$), 20.1 (Si{CH(CH$_3$)$_2$}$_3$), 21.2 (ArCH$_3$), 47.9 (TMEDA), 51.8 (CHPh$_2$), 56.5 (TMEDA), 126.2, 128.6, 129.6, 130.0, 130.1, 130.3, 130.7, 141.2, 146.3, 147.1, 148.2 (Ar–C); ^{29}Si{^{1}H} NMR (80 MHz, C_6D_6): δ = 0.2 (s); IR υ/cm^{-1} (Nujol): 1596(m), 1523(m), 1493(m), 1448(s), 1256(m), 1236(s), 1204(m), 1125(m), 1027(m), 1006(m), 950(m), 914(m), 899(m), 881(s), 856(m), 834(m), 811 (m), 792(s), 753(s), 728(s), 701(s); MS/EI m/z (%): 739.5 (Ar*(Si^{i}Pr$_3$)NZnBr$^+$, 5), 696.4 (Ar*(Si^{i}Pr$_2$)NZnBr$^+$, 50), 595.6 (Ar*N(H)Si^{i}Pr$_3^+$, 14), 552.5 (Ar*N(H) Si^{i}Pr$_2^+$, 42), 167.2 (Ph$_2$CH$^+$, 100); anal. calc. for $C_{48}H_{64}BrN_3SiZn_2$: C 62.54 %, H 7.00 %, N 4.56 %, found: C 62.49 %, H 7.11 %, N 4.64 %.

References

1. C.E. Holloway, M. Melník, J. Organomet. Chem. **495**, 1 (1995)
2. (a) J.D Corbett, W.J Burkhard, L.F. Druding, J. Am. Chem. Soc. **83**, 76 (1961); (b) J.D. Corbett, Inorg. Chem. **1**, 700 (1962); (c) R.A. Potts, R.D. Barnes, J.D. Corbett, Inorg. Chem. 7, 2558 (1968); (d) D.H Kerridge, S.A. Tariq, J. Chem. Soc. A 1122 (1967)
3. (a) R. Faggiani, R.J. Gillespie, J.E. Vekris, J. Chem. Soc., Chem. Commun. 517 (1986); (b) T. Staffel, G.Z. Meyer, Anorg. Allg. Chem. **548**, 45 (1987)
4. (a) Wardell, J.L., *Comprehensive Organometallic Chemistry*. (Pergamon, Oxford, 1982), vol. 2, p. 864; (b) K. Brodersen, H.-U. Hummel, *Comprehensive Coordination Chemistry*. (Pergamon, Oxford, 1987), p. 1050
5. D.L. Reger, S.S. Mason, J. Am. Chem. Soc. **115**, 10406 (1993)
6. D. Bravo-Zhivotovskii, M. Yuzefovich, M. Bendikov, K.W. Klinkhammer, Y. Apeloig, Angew. Chem. Int. Ed. **38**, 1100 (1999)
7. C. A. Ghilardi, S. Midollini, S. Moneti, J. Chem. Soc., Chem. Commun. **865** (1981)
8. W. Frank, B. Dincher, Z. Naturforsch. B **42**, 828 (1987)
9. (a) E. Dorm, Chem. Commun. **466** (1971); (b) H. Stammreich, T.T. Sans, J. Mol. Struct. **1**, 55 (1967)
10. Y. Apeloig, M. Yuzefovich, M. Bendikov, D. Bravo-Zhivotovskii, D. Blaser, R. Boese, Angew. Chem. Int. Ed. **40**, 3016 (2001)
11. I. Resa, E. Carmona, E. Gutierrez-Puebla, A. Monge, Science **305**, 1136 (2004)
12. J.T.B.H. Jastrzebski, J. Boersma, G. van Koten, W.J.J. Smeets, A.L. Spek, Recl. Trav. Chim. Pays-Bas **107**, 263 (1988)
13. L. Pauling, *The Nature of the Chemical Bond*, 3rd edn. (Cornell University Press, Ithaca, 1960), Chap. 7
14. T. Li, S. Schulz, P.W. Roesky, Chem. Soc. Rev. **41**, 3759 (2012), and references therein
15. (a) D. Schuchmann, U. Westphal, S. Schulz, U. Flörke, D. Bläser, R. Boese, Angew. Chem., Int. Ed. **48**, 807 (2009); (b) S. Schulz, D. Schuchmann, I. Krossing, D. Himmel, D. Bläser, R. Boese, Angew. Chem., Int. Ed., **48**, 5748 (2009); (c) S. Schulz, T. Eisenmann, D. Bläser and R. Boese, Z. Anorg. Allg. Chem. **635**, 995 (2009)
16. T. Bollermann, K. Freitag, C. Gemel, R.W. Seidel, R.A. Fischer, Organometallics **30**, 4123 (2011)
17. M. Carrasco, R. Peloso, I. Resa, A. Rodríguez, L. Sánchez, E. Álvarez, C. Maya, R. Andreu, J.J. Calvente, A. Galindo, E. Carmona, Inorg. Chem. **50**, 6361 (2011)
18. A. Lühl, H. Pada Nayek, S. Blechert, P.W. Roesky, Chem. Commun. **47**, 8280 (2011)
19. Wang, B. Quillian, P. Wei, H. Wang, X.-J. Yang, Y. Xie, R. B. King, P.V.R. Schleyer, H.F. Schaefer III, G.H. Robinson, J. Am. Chem. Soc. **127**, 11944 (2005)
20. J. Chai, H. Zhu, A.C. Stuckl, H.W. Roesky, J. Magull, A. Bencini, A. Caneschi, D. Gatteschi, J. Am. Chem. Soc. **127**, 9201 (2005)
21. Z.-Z. Xie, W.-H. Fang, Chem. Phys. Lett. **404**, 212 (2005)
22. I.L. Fedushkin, A.A. Skatova, S.Y. Ketkov, O.V. Eremenko, A.V. Piskunov, G.K. Fukin, Angew. Chem. Int. Ed. **46**, 4302 (2007)
23. Y.-C. Tsai, J.-K. Hwang, Y.-M. Lin, D.-Y. Lu, J.-S. K. Yu, Chem. Commun. **40**, 4125 (2007)
24. S. Gondzik, D. Blaser, C. Wolper, S. Schulz, Chem. Eur. J. **16**, 13599 (2010)
25. M. Carrasco, R. Peloso, A. Rodríguez, E. Álvarez, C. Maya, E. Carmona, Chem. Eur. J. **16**, 9754 (2010)
26. A. Stasch, Chem. Eur. J. **18**, 15105 (2012)
27. (a) X.-J. Yang, J. Yu, Y. Liu, Y. Xie, H. F. Schaefer, Y. Liang, B. Wu, Chem. Commun. 2363 (2007); (b) J. Yu, X.-J. Yang, Y. Liu, Z. Pu, Q.-S. Li, Y. Xie, H. F. Schaefer, B. Wu, Organometallics **27**, 5800 (2008); (c) P. Yang, X.-J. Yang, J. Yu, Y. Liu, C. Zhang, Y.-H. Deng, B. Wu, Dalton Trans. 5773 (2009); (d) Y. Liu, S. Li, X.-J. Yang, P. Yang, J. Gao, Y. Xia, B. Wu, Organometallics **28**, 5270 (2009); (e) J. Gao, S. Li, Y. Zhao, B. Wu, X.-J. Yang, Organometallics **31**, 2978 (2012)

28. P. Jochmann, D.W. Stephan, Chem. Eur. J. **20**, 8370 (2014)
29. S. Schulz, S. Gondzik, D. Schuchmann, U. Westphal, A. Dobrzycki, R. Boese, S. Harder, Chem. Commun. **46**, 7757 (2010)
30. H.P. Nayek, A. Luhl, S. Schulz, R. Koppe, P.W. Roesky, Chem. Eur. J. **17**, 1773 (2011)
31. T. Bollermann, K. Freitag, C. Gemel, R.W. Seidel, M. von Hopffgarten, G. Frenking, R.A. Fischer, Angew. Chem. Int. Ed. **50**, 772 (2011)
32. Z. Zhu, R.J. Wright, M.M. Olmstead, E. Rivard, M. Brynda, P.P. Power, Angew. Chem. Int. Ed. **45**, 5807 (2006)
33. Z. Zhu, R.C. Fischer, J.C. Fettinger, E. Rivard, M. Brynda, P.P. Power, J. Am. Chem. Soc. **128**, 15068 (2006)
34. Z. Zhu, M. Brynda, R.J. Wright, R.C. Fischer, W.A. Merrill, E. Rivard, R. Wolf, J.C. Fettinger, M.M. Olmstead, P.P. Power, J. Am. Chem. Soc. **129**, 10847 (2007)
35. D.-Y. Lu, J.-S.K. Yu, T.-S. Kuo, G.-H. Lee, Y.-C. Tsai, Angew. Chem. Int. Ed. **50**, 7611 (2011)
36. T. Ziegler, J.G. Snijders, E.J. Baerends, J. Chem. Phys. **74**, 1271 (1981)
37. (a) P. Schwerdtfeger, M. Dolg, W.H.E Schwarz, G.A Bowmaker, P.D.W Boyd, J. Chem. Phys. **91**, 1762 1989; (b) P. Schwerdtfeger, P.D. W. Boyd, A.K. Burrell, W.T. Robinson, M. Taylor, J. Inorg. Chem. **29**, 3593 (1990); (c) A. Bayler, A. Schier, G.A. Bowmaker, H. Schmidbaur, J. Am. Chem. Soc., **118**, 7006 (1996)
38. (a) J.P. Desclaux, At. Data Nucl. Data Tables, **i2**, 311 (1973); (b) P. Pyykkö, Chem. Rev. **88**, 563 (1988)
39. (a) P. Schwerdtfeger, P.D. W. Boyd, S. Brienne, J.S. McFeaters, M. Dolg, M.-S. Liao, W.H. E. Schwarz, Inorg. Chim. Acta **213**, 233 (1993); (b) M. Kaupp, H.-G. von Schnering, Inorg. Chem. **33**, 4179 (1994)
40. K. Freitag, C. Gemel, P. Jerabek, M.I. Oppel, R.W. Seidel, G. Frenking, H. Banh, K. Dilchert, R.A. Fischer, Angew Chem., Int. Ed. **54**, 1 (2015)
41. M.P. Blake, N. Kaltsoyannis, P. Mountford, Chem. Commun. **51**, 5743 (2015)
42. M.L.H. Green, P.C. Konidaris, P. Mountford, J. Chem. Soc., Dalton Trans. 2851 (1994)
43. B. Cordero, V. Gómez, A.E. Platero-Prats, M. Revés, J. Echeverría, E. Cremades, F. Barragán, S. Alvarez, Dalton Trans. 2832 (2008)
44. P. Cui, H.-S. Hu, B. Zhao, J.T. Miller, P. Cheng, J. Li, Nat. Commun. **6**, 6331 (2015)
45. As determined from a survey of the Cambridge Crystallographic Database, May, 2015
46. R. Wolf, C. Ni, T. Nguyen, M. Brynda, G.J. Long, A.D. Sutton, R.C. Fischer, J.C. Fettinger, M. Hellman, L. Pu, P.P. Power, Inorg. Chem. **46**, 11277 (2007)
47. S.J. Bonyhady, C. Jones, S. Nembenna, A. Stasch, A. Edwards, G.J. McIntyre, Chem. Eur. J. **16**, 938 (2010)
48. A. Velazquez, I. Fernández, G. Frenking, G. Merino, Organometallics **26**, 4731 (2007)
49. G.E. Coates, D. Ridley, J. Chem. Soc. 166 (1964)

Chapter 5
Preparation of Low Oxidation State Cobalt Complexes Stabilised by a Bulky Amide Ligand

5.1 Introduction

Due to their highly reactive nature, low oxidation state carbonyl-free cobalt complexes have previously been found effective in many areas of chemistry, from the catalytic hydrogenation of CO_2 [1], to C–C bond activations of small molecules [2]. While most low oxidation state carbonyl free cobalt complexes are stabilised by multidentate anionic ligands, more coordinatively unsaturated complexes incorporating bulky lower-dentate ligands have proved more reactive in their further chemistry [3]. This type of complex is the primary focus of this chapter.

5.1.1 Low Oxidation State Cobalt Complexes Stabilised by Bulky Bidentate Monoanionic Ligands

One of the first quasi-low coordinate cobalt(I) species, was the toluene capped β-diketiminate complex [(^{Xyl}Nacnac)Co(η^6-toluene)] **5-01** (^{Xyl}Nacnac = [(XylNCMe)$_2$CH]$^-$, Xyl = 2,6-Me$_2$-C$_6$H$_3$) reported by Warren and co-workers in 2004 [4]. The complex was synthesised by reduction of the four-coordinate cobalt(II) iodide complex [(^{Xyl}Nacnac)CoI(lut)] **5-02** (lut = 2,4-lutidine) with magnesium powder in toluene (Scheme 5.1). After workup and subsequent crystallisation, complex **5-01** was isolated as air sensitive red crystals in good yields.

Compound **5-01** was crystallography characterised, which showed the Co centre to have an η^6 coordination to a molecule of toluene (Co–C = 2.207(6) Å to 2.288(5) Å), which results in an 18 electron cobalt complex. This is in contrast to the related rhodium(I) compounds [(^{Xyl}Nacnac)Rh(η^4-benzene)] and [{(^{Xyl}Nacnac)Rh}$_2$(η^4-toluene)], which both favour η^4 coordination to the solvent molecule [5]. As both of these rhodium complexes are low spin, the η^4 coordination of toluene and benzene is favoured due to the stability of 16 electron Rh complexes.

J. Hicks, *Preparation, Characterisation and Reactivity of Low Oxidation State d-Block Metal Complexes Stabilised by Extremely Bulky Amide Ligands*, Springer Theses,
DOI 10.1007/978-981-10-2905-9_5

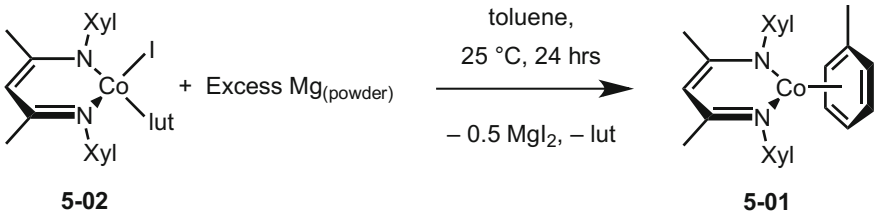

Scheme 5.1 Preparation of **5-01**

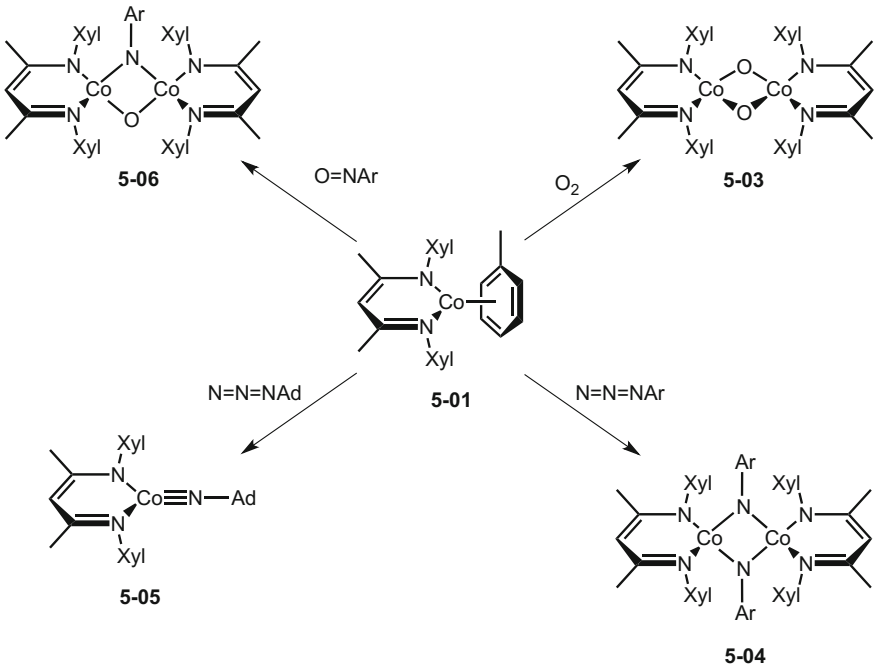

Scheme 5.2 Overview of the reactivity of **5-01**. Ar = 3,5-dimethylphenyl, Ad = 1-adamantyl

Compound **5-01** is paramagnetic in solution, exhibiting an effective magnetic moment of 2.7 μ_B, just slightly less than expected spin only value for a d^8 high-spin centre (μ_{so} = 2.83 μ_B), but indicative of a high-spin Co(I) complex.

The reactivity of compound **5-01** towards O_2, two organic azides and a substituted nitrosobenzene was investigated, the results of which are outlined in Scheme 5.2. When a diethyl ether solution of **5-01** was treated with 1.5 equivalents of O_2 at room temperature, an immediate colour change from red to violet was observed, signalling the formation of the dioxo-bridged cobalt(III) complex [{(^{Xyl}Nacnac)Co(μ-O)}$_2$] **5-03**. Compound **5-03** was crystallographically characterised, revealing positional disorder of the bridging oxygen atoms. The dominant orientation of 86 % occupancy,

consisted of the oxygen atoms laying near planar with the two "(^{Xyl}Nacnac)Co" central rings (22.2° and 23.0° twist angles between the N–Co–N and O–Co–O' planes), resulting in the cobalt centres occupying distorted square planar geometries. The minor orientation consisted of the oxygen atoms laying essentially perpendicular to the two Co-Nacnac planes, resulting in the metal centres occupying distorted tetrahedral geometries. Isolating both Co geometries in the same crystal suggests that there is very little energy difference between the two structures, with the square planar orientation slightly favoured. The Co–O bond lengths in the square planar orientation (1.784(3) and 1.793(4) Å) are comparable to those in related "diamond core" structures $M_2(\mu\text{-}O)_2$ (M = Fe–Cu) [6], however the Co–O bond lengths of the tetrahedral orientation are considerably longer.

Diethyl ether solutions of complex **5-01** were also treated with the two organic azides, 1-azidoadamantane and 3,5-dimethylphenylazide at room temperature. No obvious colour change was observed in either reaction, although effervescence of N_2 was observed. After workup and subsequent crystallisation, moderate yields of the cobalt(III) imido complexes [{(^{Xyl}Nacnac)Co(μ-NAr)}$_2$] **5-04** (Ar = 3,5–Me_2–C_6H_3) and [(^{Xyl}Nacnac)CoNAd] **5-05** (Ad = 1-adamantyl) were isolated as red crystalline solids. Similar to the reaction with O_2, the two reactions have resulted in oxidation of the Co centre to Co(III), and consequently a two electron reduction of the azide. The two products have differing structures in the solid state, as determined by X-ray crystallography. Complex **5-04** is dimeric, with two cobalt centres bridged by two approximately equivalent imido ligands (Co–N = 1.983(3) Å and 1.988(3) Å). The bridging N atoms are essentially orthogonal to the (^{Xyl}Nacnac)Co plane, resulting in the two Co centres possessing tetrahedral geometries. In contrast, complex **5-05** is monomeric in the solid state, with a three-coordinate cobalt(III) core, which occupies a distorted trigonal geometry. The Co–NAd bond is extremely short (1.624(4) Å), shorter than any other first row transition metal terminal imide reported at the time. Moreover, the complex is diamagnetic in solution at room temperature, suggestive of a low-spin cobalt(III) centre. DFT calculations were performed on the complex, supporting the presence of low-spin d^6 Co(III) centre, which is stabilised by $1\sigma2\pi$-donation from the imido ligand, leading to the Co–N bond possessing considerable multiple bonding character.

Finally, a diethyl ether solution of **5-01** was reacted with 3,5-dimethylnitrosobenzene. After workup and crystallisation, a low yield of the red crystalline product [{(^{Xyl}Nacnac)Co}$_2$(μ-NAr)(μ-O)] **5-06** was isolated. The addition of the nitrosobenzene to **5-01** resulted in the four electron reductive cleavage of the O=N bond of the substrate. Consequently, the two cobalt centres have been oxidised from Co(I) to Co(III). Complex **5-06** was crystallographically characterised, showing the cobalt centres to occupy geometries in between square planar and tetrahedral, with the opposing (^{Xyl}Nacnac)Co fragments nearly orthogonal to each other (89.2° twist angle). The complex was found to be paramagnetic in solution, with an effective magnetic moment of 4.9 μ_B at room temperature, indicative of a high spin cobalt complex.

In 2009, Holland and co-workers expanded the work on low oxidation state cobalt complexes, stabilised by β-diketiminate ligands, by reductions of the bulkier

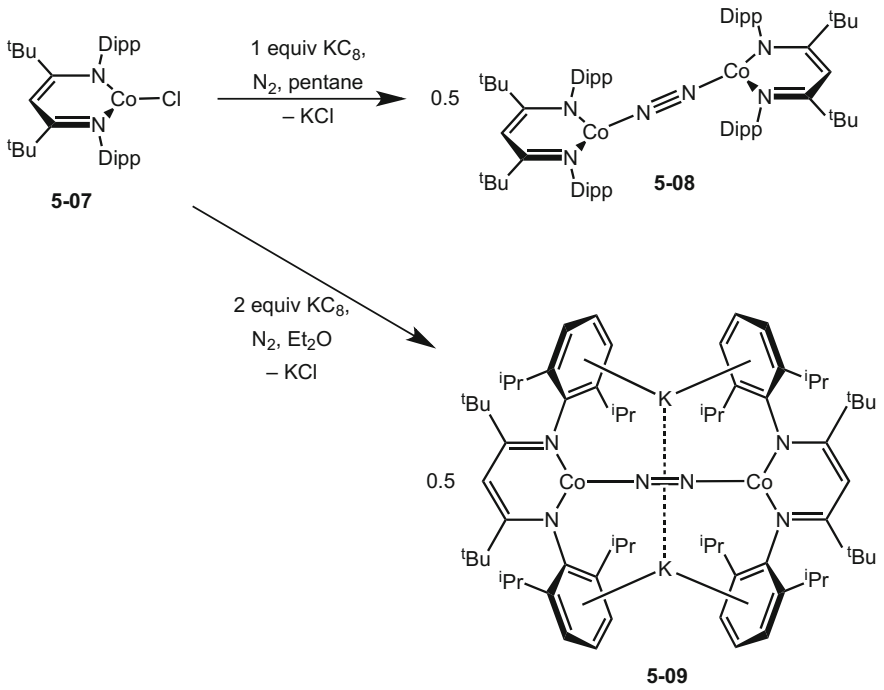

Scheme 5.3 Preparation of **5-08** and **5-09**

β-diketiminato cobalt(II) chloride precursor complex [(^{tBu}Nacnac)CoCl] **5-07** (^{tBu}Nacnac = [(DippNC^{t}Bu)$_2$CH]$^-$) with KC_8 [7]. Depending on the stoichiometry of KC_8 used in the reaction, two different products could be isolated. When the reduction of **5-07** was performed in pentane, using one equivalent of KC_8 under a N_2 atmosphere, [(^{tBu}Nacnac)Co$\}_2(\mu$-$N_2)$] **5-08** was isolated in moderate yields as dark brown crystals (Scheme 5.3). However, when the reduction of **5-07** was performed in diethyl ether, using two equivalents of KC_8 under a N_2 atmosphere, [(^{tBu}Nacnac)Co(μ-K)$\}_2(\mu$-$N_2)$] **5-09** was isolated in moderate yields as a dark purple solid (Scheme 5.3).

Both products were crystallographically characterised. Complex **5-08** is a three-coordinate cobalt(I) dimer, with a molecule of dinitrogen bridging in an end-on fashion between the two metal centres. From the molecular structure of **5-08**, a small elongation of the N–N triple bond was observed (N–N = 1.1390(15) Å compared with 1.098 Å in free N_2), which was further supported by Raman spectroscopy. This lengthening of the N–N triple bond is greater than in the analogous nickel(I) compound [(^{tBu}Nacnac)Ni$\}_2(\mu$-$N_2)$] (1.120(4) Å) [7], but not as great as in the analogous iron(I) compound [(^{tBu}Nacnac)Fe$\}_2(\mu$-$N_2)$] (1.189(4) Å) [8]. This is due to a greater donation of electron density into the N–N π* antibonding orbitals in the iron complex compared with the other two.

The formally cobalt(0) complex **5-09** has a similar structure to **5-08**, in that it is a cobalt dimer with a bridging molecule of dinitrogen. However, complex **5-09** has the addition of two potassium cations, each coordinating to one flanking phenyl ring of each ligand, and also to the dinitrogen bridge. This cobalt(0) complex shows a significant increase in the activation of the dinitrogen bridge (N–N = 1.220(2) Å) compared with **5-08**, which was also supported by Raman spectroscopy, i.e. a shift of the N–N absorbance of >730 cm^{-1} to lower wavenumbers compared with N_2 gas. DFT calculations were performed on a simplified model of **5-09**, which suggest that the significant increase in the N–N bond length is due to both the lower oxidation state of the metal and the coordination of the K^+ cations. The lower oxidation state of the metal means that more electrons are available for backing into the N–N π* orbitals, whilst coordination of the K^+ cation increases the overall electron transfer to the N_2 unit. The resulting activation of the N–N bond in complex **5-09** is comparable to that of the analogous iron(0) compound $[(^{tBu}Nacnac)Fe(\mu\text{-}K)\}_2(\mu\text{-}N_2)]$ (1.241(7) Å) [8].

In 2011, the same group reported on the reduction of the same *β*-diketiminato cobalt(II) chloride precursor complex **5-07**, once again with KC_8, but this time in THF under an argon atmosphere [9]. The reaction led to the isolation of the mononuclear cobalt(I) complex $[(^{tBu}Nacnac)Co(THF)]$ **5-10**, which possesses a molecule of THF coordinating to the metal centre. Crystallographic analysis of **5-10** showed the metal to occupy a three-coordinate trigonal geometry, with no strong interactions from the ligand's flanking phenyl rings.

Dissolution of compound **5-10**, in non-polar solvents such as toluene, under an argon atmosphere, favours the dissociation of THF to give the monomeric cobalt(I) complex $[(^{tBu}Nacnac)Co]$ **5-11**, with no additional donor molecules coordinating to the metal centre (Scheme 5.4). The reaction was found to be reversible, and dissolution of compound **5-11** in THF, leads to essentially quantitative yields of **5-10**. Analysis of **5-11** by X-ray crystallography showed the *β*-diketiminate ligand to be stabilising the metal centre in an unusual N,η^6-arene bonding motif, rather than the typical N,N′ coordination, presumably to increase the number of valence electrons on the metal ($12e^-$ vs. $16e^-$). This unusual ligand coordination results in the cobalt centre occupying a bent one-legged piano stool geometry (N–Co-centroid = 148°), in what the authors call a "masked two-coordinate complex". Both complexes **5-10** and **5-11** are paramagnetic in solution, and exhibit solution state effective magnetic moments of 3.23 and 3.07 μ_B respectively, indicating that both are high-spin cobalt (I) complexes.

The reactivity of complex **5-11** towards neutral donor molecules was explored. Solutions of complex **5-11** were independently treated with pyridine (Py), triphenylphosphine and one atmosphere of CO gas, which resulted in all three reactions yielding their respective adducts (Scheme 5.5). The introduction of pyridine or PPh_3 to **5-11** resulted in a single donor molecule coordinated to the metal centre (viz. $[(^{tBu}Nacnac)Co(Py)]$ **5-12** and $[(^{tBu}Nacnac)Co(PPh_3)]$ **5-13**). In contrast, the reaction between **5-11** and one atmosphere of CO favoured the coordination of two CO molecules to give $[(^{tBu}Nacnac)Co(CO)_2]$ **5-14**. All three reactions result in a change of the ligand's coordination mode, from N,η^6-arene to N,N′ chelating,

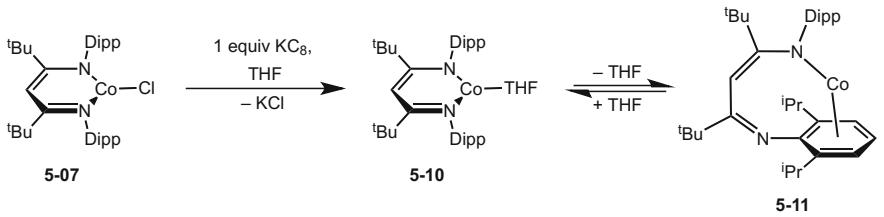

Scheme 5.4 Preparation of the three-coordinate cobalt(I) complex **5-10** and the "masked two-coordinate" cobalt(I) complex **5-11**

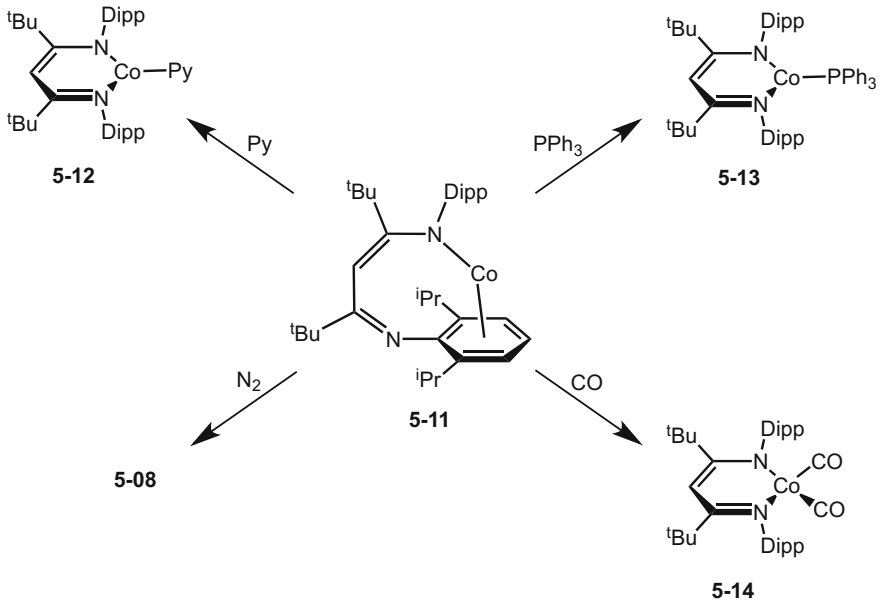

Scheme 5.5 Reactivity of the "masked two-coordinate" cobalt(I) complex **5-11** with neutral donor molecules

described in the publication as "slipping", yielding three-coordinate metal centres in **5-12** and **5-13**, and a four-coordinate metal centre in **5-14**. It is also worth noting that exposure of a toluene solution of **5-11**, to an atmosphere of N_2 gas, leads to almost quantitate yields of the nitrogen bridged complex **5-08**.

The reactivity of compound **5-11** was also tested towards fluorobenzene. Five equivalents of fluorobenzene were added to a solution of **5-11** in deuterated cyclohexane and the mixture heated to 60 °C for 18 h (Scheme 5.6). This led to complete consumption of the starting material and the formation of two new products. The products were identified as [(^{tBu}Nacnac)CoPh] **5-15** and [{(^{tBu}Nacnac)Co(μ-F)}$_2$] **5-16**, by a combination of ^{1}H NMR spectroscopy and

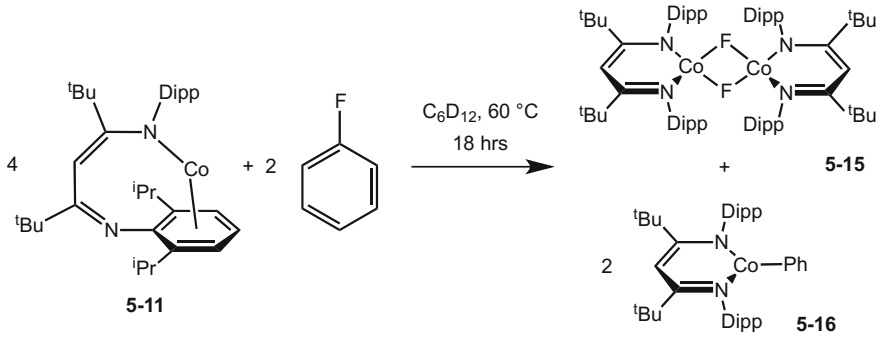

Scheme 5.6 C–F activation of fluorobenzene by complex **5-11**

X-ray crystallography. Each compound accounted for approximately 50 % of the cobalt in the reaction, showing that **5-11** is capable of C–F bond activation.

In 2009, the Jones group investigated the stabilising properties of bulky amidinate and guanidinate ligands towards low oxidation state cobalt complexes, prepared via the reductions of the cobalt(II) chloride complexes [{(Piso)Co(μ-Cl)}$_2$] **5-17a**, [{(Giso)Co(μ-Cl)}$_2$] **5-17b** and [{(Priso)Co(μ-Cl)}$_2$] **5-17c** (Piso, Giso and Priso = [(DippN)$_2$CR]$^-$, R = ^{t}Bu, Piso; NCy$_2$, Giso; N^{i}Pr$_2$, Priso) [10]. The reductions of all three amidinato- or guanidinato cobalt(II) chloride complexes were attempted using a number of different reducing agents and solvents. The reductions of complexes **5-17a**–**5-17c** were initially carried out by stirring toluene solutions of the complexes over a potassium mirror at room temperature, which in every case produced a colour change from green to red. After workup and crystallisation, the three analogous toluene capped cobalt(I) complexes [(Piso)Co(η^6-toluene)] **5-18a**, [(Giso)Co(η^6-toluene)] **5-18b** and [(Priso)Co(η^6-toluene)] **5-18c** were isolated in good yields (Scheme 5.7).

The reductions of complexes **5-17a**–**5-17c** were also attempted in cyclohexane, once again over a potassium mirror, which for complexes **5-17a** and **5-17b** produced a colour change from green to red. After workup and crystallisation, red crystals of the dimeric cobalt(I) complexes [{Co(μ-Piso)}$_2$] **5-19a** and [{Co(μ-Giso)}$_2$] **5-19b** were isolated in moderate yields (Scheme 5.7). No product was isolated from the reduction of **5-17c** under these conditions. It is worth mentioning that all reactions were carried out under an atmosphere of dinitrogen, however a dinitrogen coordinated product was not obtained from any reaction, showing contrasting reactivity to the β-diketiminate cobalt(I) complexes.

All five cobalt(I) complexes **5-18a**–**5-18c** and **5-19a**–**5-19b** were crystallographically characterised. The molecular structures of **5-18a**–**5-18c** showed them to be essentially isostructual, with the amidinate or guanidinate ligand coordinating to the metal centre in the expected N,N′ chelating bonding mode, with a further η^6 coordination to a molecule of toluene. These three complexes are comparable to β-diketiminate cobalt(I) complex **5-01**, which shows similar metal coordination. Similar to **5-01**, all three complexes **5-18a**–**5-18c** are paramagnetic in solution

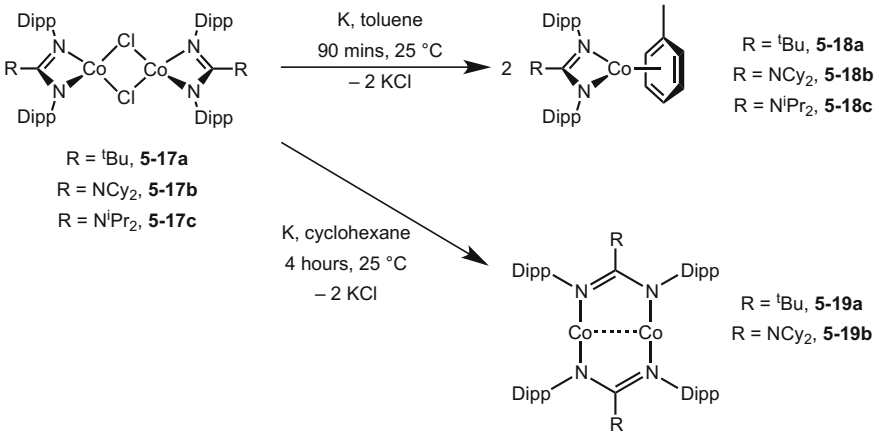

Scheme 5.7 Preparation of the toluene capped cobalt(I) complexes **5-18a–c** and the cobalt(I) dimers **5-19a** and **5-19b**

(μ_{eff} = 3.09–3.22 μ_B), indicative of a $S = 1$ spin state in each case. Therefore complexes **5-18a**–**5-18c** all possess high-spin cobalt(I) centres.

The solid-state structures of **5-19a** and **5-19b** show the two complexes to be amidinate and guanidinate bridged dimers, with essentially planar L_2Co_2 cores. No analogous β-diketiminate complexes have been reported to date, but the structures of the two compounds are comparable to the chromium and molybdenum quintuple bonded complexes [$Cr_2(\mu$-Pipiso$)_2$] **1-02** and [$Mo_2(\mu$-Piso$)_2$] **1-03** (previously discussed in Sect. 1.3). The two cobalt centres in both **5-19a** and **5-19b** are three-coordinate, with T-shaped coordination geometries, but with a number of close contacts to the isopropyl hydrogen atoms on the flanking aryl rings (closest C–H···Co = 2.62 Å in **5-19a** and 2.30 Å in **5-19b**). The Co–Co interactions in complexes **5-19a** and **5-19b** are exceptionally short (2.1404(10) Å in **5-19a** and 2.1345(7) Å in **5-19b**), implying a degree of multiple bonding between the metal centres. Calculations were carried out on the two dimers, in an attempt to further understand the bonding between the two cobalt centres. However, due to the wave-functions of both model complexes possessing highly multiconfigurational character, accurate bond orders could not be assigned.

Complexes **5-19a** and **5-19b** were found to be paramagnetic in solution, exhibiting effective magnetic moments of 5.25 and 5.10 μ_B respectively, characteristic of high-spin cobalt(I) centres. Interestingly, the data obtained from a solid-state variable-temperature magnetic susceptibility measurement on **5-19a**, could either indicate a single $S = 2$ ground state for the dimer, or two-non high-spin d^8 centres, each with spin of $S = 1$. Attempts to distinguish which spin state the complex possesses unfortunately proved unsuccessful.

The reactivity of the amidinate and guanidinate cobalt(I) complexes towards O_2, CO and 1-azoadamantane was investigated. When a toluene solution of **5-18c** was exposed to a small volume of air, the dioxobridged cobalt(III) compound [{(Priso)

Co(μ-O)}$_2$] **5-20** was isolated as purple-red crystals, although in very low yields (Scheme 5.8). Compound **5-20** is a square-planar cobalt(III) dimer, with bridging oxides. The structure resembles that of the related β-diketiminate cobalt(III) complex **5-03**, isolated from the reaction of toluene capped cobalt(I) complex **5-01** with O_2 [4].

The reaction of **5-18b** with 1-azoadamantane in hexane, gave the three-coordinate cobalt(III) complex [(Giso)CoNAd] **5-21** (Scheme 5.8). The Co–NAd bond is exceptionally short (1.621(3) Å) [4], due to considerable multiple bond character. The complex resembles the β-diketiminate complex **5-05**, which is also a three-coordinate cobalt(III) complex with an extremely short Co–N bond.

The reactivity of **5-19a** towards CO was also investigated. Exposure of a toluene solution of **5-19a** to one atmosphere of CO, gives the CO insertion product [(PisoCO)Co(CO)$_3$] **5-22** (Scheme 5.8), where three molecules of CO have coordinated to the metal centre, and a fourth has inserted into one of the N–Co bonds. This reactivity is in contrast to the β-diketiminate cobalt(I) complex **5-01**, which when reacted with CO, only simple coordination to the metal centre was observed [4]. This difference in reactivity is likely due to the relative ring strain between the two complexes, which in complex **5-22**, results in a more stable five membered ring.

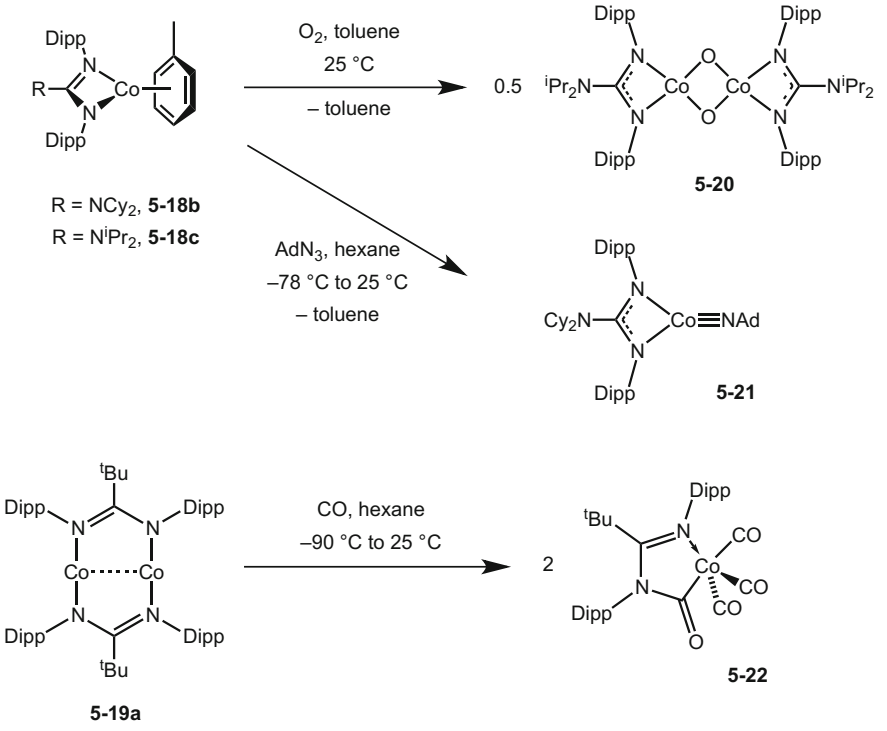

Scheme 5.8 Reactivity of the amidinato- and guanidinato cobalt(I) complexes **5-18b**, **5-18c** and **5-19a**

5.1.2 *Low Oxidation State Cobalt Complexes Stabilised by Bulky Monodentate Monoanionic Ligands*

In 2008, Power and co-workers published the synthesis and structure of two first-row transition metal(I) dimers, bearing the Ar^{Dipp} (Ar^{Dipp} = 2,6-$Dipp_2$-C_6H_3) terphenyl ligand, for comparisons with the related Cr–Cr quintuple bonded complex $[(Ar^{Dipp}Cr)_2]$ **1-01** [11]. One of these complexes was the terphenyl cobalt(I) dimer $[(Ar^{Dipp}Co)_2]$ **5-23**, prepared in low yields by the reduction of $[\{Li(OEt_2)_2Ar^{Dipp}CoI_2\}_2]$ [12] with KC_8 in THF (Scheme 5.9).

Complex **5-23** was crystallographically characterised, revealing a number of structural differences between it and the related chromium(I) dimer **1-01**. Firstly, the two metal centres in **5-23** are nearly 1.0 Å further apart than in the chromium analogue (2.8033(5) Å in **5-23**; 1.8351(4) Å in **1-01**) [13], indicating a much weaker metal–metal interaction. In addition, strong η^6-arene interactions between the Co centres and one of the neighbouring ligand's flanking aryl groups have replaced the weaker η^1 interactions between the chromium and the neighbouring ligand's *ipso*-carbon.

Unexpectedly for a low coordinate cobalt(I) dimer, compound **5-23** shows very little paramagnetic behaviour, with all resonances from ^{1}H NMR spectroscopy appearing in the region between δ 0 and 10 ppm. This suggests either strong antiferromagnetic coupling between the two high-spin metal centres, or that the complex is low-spin. For there to be strong antiferromagnetic coupling between the two d^8 cobalt centres, pairing of two electrons from each cobalt centre is required, essentially creating a double bond between the metal centres. However, the long Co–Co separation in the complex, does not support the existence of a double bond, therefore it is likely that the complex is low-spin.

The authors turned to calculations on the model complex [MeCo(η^6-C_6H_6)] [14] in an attempt to explain the low-spin nature of **5-23**. The calculations predicted a high-spin S = 1 configuration for the model complex with a linear Me–Co-centroid motif. However, when the Me–Co-centroid angle is bent to 135°, a bending of 45° from linearity, electron pairing is induced and the configuration becomes low-spin. The C–Co-centroid angle in **5-23** is 143.7°, a bending of 36.3° from linearity, which could be enough to induce the low-spin configuration.

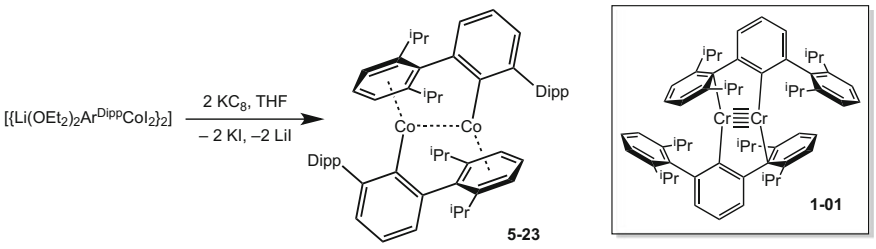

Scheme 5.9 Preparation of **5-23**

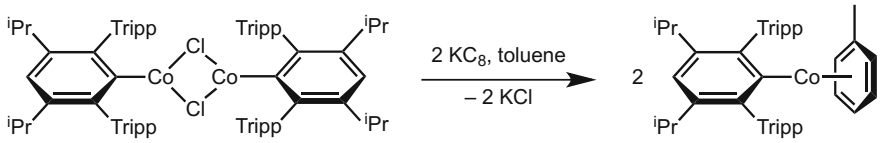

2-28 **5-24**

Scheme 5.10 Preparation of **5-24**

Towards the end of 2008, the group authored a second report on the reduction of the bulkier terphenyl cobalt(II) chloride precursor complex [{3,5-$^{i}Pr_2$-Ar^{Tripp}Co(μ-Cl)}$_2$] **2-28** (Ar^{Tripp} = 2,6-$Tripp_2$-C_6H_3) with KC_8 in toluene [15]. After workup and subsequent crystallisation, the mononuclear cobalt(I) complex [3,5-$^{i}Pr_2$-Ar^{Tripp}Co(η^6-toluene)] **5-24** was isolated in good yields as bright green crystals (Scheme 5.10).

Crystallographic analysis of **5-24** found the cobalt(I) complex to be monomeric in the solid state, with η^6 coordination of a molecule of toluene to the metal centre. This structure is in contrast to the previously discussed terphenyl cobalt(I) complex **5-23**, likely due to a combination of ligand bulk and the reaction solvent. The structure is also in contrast to the related manganese(I) compound [{3,5-$^{i}Pr_2$-Ar^{Tripp}Mn}$_2$(μ-η^6:η^6-toluene)] **3-11**, which is dimeric in the solid state, with a "3,5-$^{i}Pr_2$-Ar^{Tripp}Mn" unit coordinating to each side of a bridging toluene molecule [16].

Unlike complex **5-23**, complex **5-24** is paramagnetic, exhibiting a solid-state effective magnetic moment of 3.37 μ_B at 298 K, indicating a high-spin Co(I) centre with a spin state of $S = 1$. This is in good agreement with calculations performed on the model complex [MeCo(η^6-C_6H_6)], as the central C–Co-centroid unit is only slightly bent at 167.6(2)°, not great enough to induce electron pairing [14].

The reactivity of compound **5-24** towards CO and NO was investigated. When a diethyl ether solution of **5-24** was exposed to an excess of dry CO gas at atmospheric pressure, a colour change from green to red was observed after stirring for approximately 10 min at room temperature. Workup and subsequent crystallisation gave a low yield of the CO inserted product [[3,5-$^{i}Pr_2$-Ar^{Tripp}C(O)Co(CO)] **5-25** as red crystals. Crystallographic analysis of the complex showed the coordination of one molecule of CO to the metal centre, while a second CO has inserted into the C–Co bond (Scheme 5.11). The metal centre is further stabilised by an η^6 coordination to one of the ligand's flanking aryl groups. The reaction between complex **5-24** and CO is similar to that of the amidinato cobalt(I) dimer **5-19a**, in which a molecule of CO inserted into the Co–N bond of the ligand [10].

Exposure of a diethyl ether solution of **5-24** to one atmosphere of NO at room temperature afforded low yields of the double insertion product [[3,5-$^{i}Pr_2$-Ar^{Tripp}N(O)NOCo(NO)$_2$] **5-26** as reddish-brown crystals. The reaction resulted in two molecules of NO inserting into the C–Co bond and coupling together, forming a new N–N bond. Two further molecules of NO have terminally coordinated to the

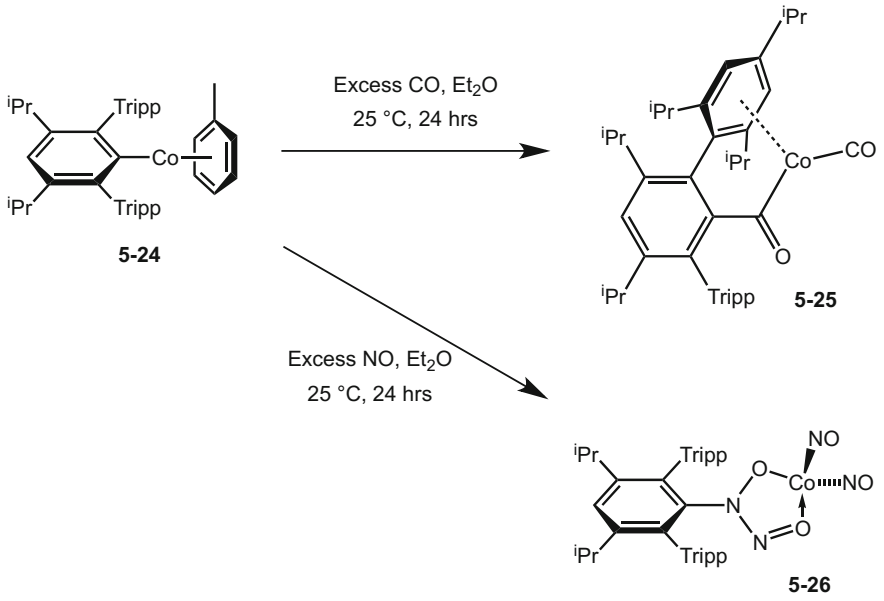

Scheme 5.11 Reactions of **5-24** with CO and NO

metal centre, resulting in a tetrahedral cobalt geometry. Insertion of two molecules of NO into early transition metal–carbon bonds is known, for complexes such as $[(\eta^5\text{-}C_5H_5)_2Zr(CH_2Ph)_2]$ [17] and WMe_6 [18]. However double insertion into late transition metal–carbon bonds is rare.

In a follow up paper published in 2012, the same group reported the synthesis and characterisation of the two related cobalt(I) complexes, [3,5-$^{i}Pr_2$-$Ar^{Tripp}Co(\eta^6$-$C_6H_6)$] **2-27** and [3,5-$^{i}Pr_2$-$Ar^{Tripp}Co(\eta^6$-$C_6H_5F)$] **5-28**, with η^6 coordination of the cobalt centre to a molecule of benzene and fluorobenzene respectively [19]. The two complexes were synthesised by reduction of the terphenyl cobalt(II) chloride **2-28** with KC_8 in THF, in the presence of the appropriate arene (Scheme 5.12). The reduction of **2-28** was also performed in the presence of bulkier arenes, such as mesitylene, hexamethylbenzene, tertbutylbenzene and 1,3,5-triisopropylbenzene, but no product was isolated for any reaction. This was proposed to be because of the instability of the products, due to steric repulsion between the substituents on the arene and the isopropyl groups on the flanking aryl rings of the terphenyl ligand.

The η^6 coordination of fluorobenzene to the Co(I) centre in **5-28**, is in contrast to the β-diketiminate cobalt(I) complex **5-11**, which does not coordinate to fluorobenzene, but instead activates the C–F bond within the molecule [9]. Although, the C–F activated product K[3,5-$^{i}Pr_2$-$Ar^{Tripp}Co(F)(C_6F_5)$] **5-29** can be obtained by the reduction of **2-28** with KC_8 in THF, in the presence of C_6F_6 (Scheme 5.12). The mechanism for the reaction is currently unknown, and therefore it is not clear whether the KC_8 or cobalt centre initially activates the C–F bond.

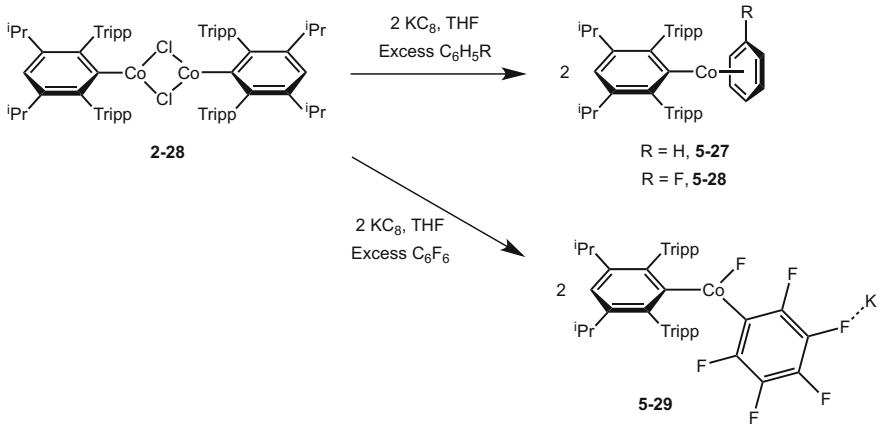

Scheme 5.12 Preparations of **5-27**–**5-29**

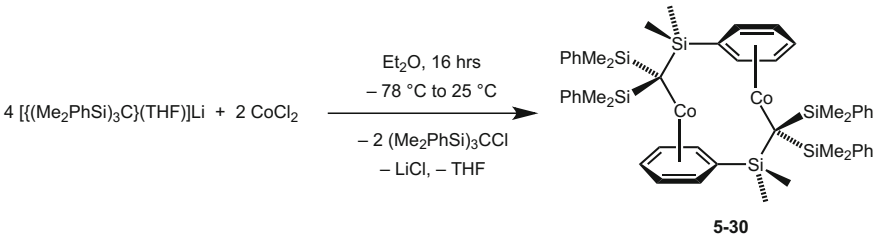

Scheme 5.13 Preparation of **5-30**

The latest cobalt(I) complex to be stabilised by bulky monodentate ligands is the dimeric alkyl cobalt complex [{$(Me_2PhSi)_3CCo\}_2$] **5-30** reported in 2014, once again by Power and co-workers [20]. Unusually, the low oxidation state complex was synthesised by reacting the lithium salt of the ligand [{$(Me_2PhSi)_3C\}$(THF)]Li with $CoCl_2$ in a 2:1 ratio (Scheme 5.13), in which the [{$(Me_2PhSi)_3C\}$(THF)]Li is acting as both a pre-ligand and a reducing agent. After workup and subsequent crystallisation, **5-30** was isolated as a green crystalline solid in low yields.

Crystallographic analysis of **5-30** revealed the complex to dimeric in the solid state. Each cobalt(I) centre coordinated to the alkyl carbon of one ligand, and further coordinated in a η^6 fashion to a flanking phenyl ring of the neighbouring "$(Me_2PhSi)_3CCo$" unit. The Co···Co distance in **5-30** (4.3480(7) Å) is much longer than a normal Co–Co single bond (2.46 Å) [21] and more than twice the van der Waals radius for cobalt metal (4.00 Å) [22], thus suggesting little, if any interaction is present between the two metal centres.

Solid-state variable temperature magnetic susceptibility measurements were performed on complex **5-30**, which gave an effective magnetic moment of 2.63 μ_B

per cobalt centre at room temperature, indicative of high-spin cobalt centres. The complex that is in good agreement with the theoretical calculations performed the model complex [MeCo(η^6-C_6H_6)] [14], as it is high-spin, with near linear geometry of the C–Co-centroid units (173.7° avg.).

5.1.3 *Other Relevant Low Coordinate, Low Oxidation State Cobalt Complexes*

Along with the bulky mono- and bidentate anionic ligands, a number of other ligand types have also been successfully used for the stabilisation of low coordinate, low oxidation state cobalt complexes, including NHCs (N-heterocyclic carbenes), CAACs (cyclic alkyl amino carbenes) and radical anionic α-diimine ligands.

In 2013, Yang and co-workers performed reductions of the previously reported [(^{Dipp}DAB)$CoCl_2$] [23] **5-31** (^{Dipp}DAB = {(DippNC(CH_3)}$_2$) under a variety of different conditions, to isolate a range of different products [24]. When a diethyl ether solution of complex **5-31** was reacted with exactly one equivalent of potassium metal at room temperature over 3 days, the cobalt(II) dimer [{(^{Dipp}DAB)Co(μ-Cl)}$_2$] **5-32** was isolated in moderate yields (Scheme 5.14). Interestingly, the one electron reduction of the complex has resulted in a reduction of the ^{Dipp}DAB ligand, and not of the cobalt centre, therefore complex **5-32** is a cobalt(II) complex bearing two radical mono-anionic α-diimine ligands.

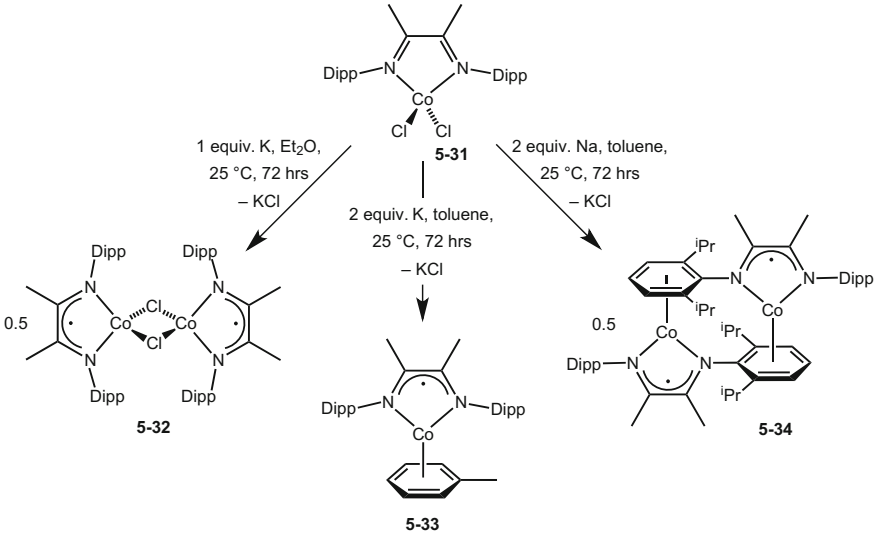

Scheme 5.14 Preparations of **5-32**–**5-34** from the reduction of **5-31**

The reduction of complex **5-31** in toluene, using two equivalents of potassium metal, yields the toluene capped cobalt(I) complex [(^{Dipp}DAB)Co(η^6-toluene)] **5-33** in moderate yields. Using two equivalents of potassium metal has resulted in a one electron reduction of both the ligand and the metal centre, yielding the cobalt(I) complex **5-33**, stabilised by a radical mono-anionic α-diimine ligand. In addition, the reduction of **5-31** with two equivalents of sodium metal in diethyl ether, yields a third reduction product, the cobalt(I) dimer [{(^{Dipp}DAB)Co}$_2$] **5-34**. Similar to **5-33**, complex **5-34** has undergone two single electron reductions (per cobalt centre), one of the ligand and one of the metal centre, yielding a dimeric cobalt(I) complex, stabilised by radical mono-anionic α-diimine ligands.

All three reduction products were crystallographically characterised, which revealed the reduction of the ligand in all three compounds, as made clear by a considerable shortening of the C–C bond length in the backbone of the ligand (from 1.497(9) Å in **5-31** [23], to 1.413(4)–1.435(6) Å in **5-32**–**5-34**) [24]. The structure of the toluene capped cobalt(I) complex **5-33** closely resembles that of the aforementioned β-diketiminato cobalt(I) complex **5-01** and the amidinato- and guanidinato cobalt(I) complexes **5-18a-c**. That is, all five complexes possess a N,N′ chelating anionic bidentate ligand, with a further η^6 coordination to a molecule of toluene.

Complex **5-34** is a cobalt(I) dimer, with η^6 coordination to one of the flanking aryl groups of the neighbouring (^{Dipp}DAB)Co fragment. The Co···Co separation in the complex is 4.062(1) Å, too long to imply any significant Co–Co bonding interaction as it is more than double the van der Waals radius for cobalt (4.00 Å) [22]. No equivalent structure has yet been reported with the related amidinate, guanidinate or β-diketiminate ligand classes, but the structure can be compared to those of the terphenyl stabilised cobalt(I) dimer **5-23** and the alkyl cobalt(I) dimer **5-30**. Complexes **5-23**, **5-30** and **5-34** all possess similar structures, in that they are all dimeric cobalt(I) complexes, with η^6 coordination of the metal centre to a flanking aryl group of the adjacent cobalt(I) unit. However, the structure of complex **5-34** more strongly resembles that of **5-30**, as the metal centres are a similar distance apart (2.8033(5) Å in **5-23,** 4.3480(7) Å in **5-30** and 4.062(1) Å in **5-34**) [11, 20].

Both **5-33** and **5-34** are paramagnetic compounds, which exhibit effective magnetic moments of 3.31 μ_B and 3.25 μ_B (per monomer) respectively in the solid state at 298 K. As expected, both of these values are above the spin only value for a high-spin cobalt(I) centre, due to the paramagnetic nature of the radical ligand, nevertheless both values are indicative of high-spin Co complexes.

In 2012, Deng and co-workers reported the synthesis and isolation of the three-coordinate cobalt(I) complex [(IMes)$_2$CoCl] **5-35** (IMes = 1,3-dimesitylimidazol-2-ylidene), synthesised from the reaction between [(PPh$_3$)$_3$CoCl] **5-36** and two equivalents of IMes (Scheme 5.15) [25]. The three-coordinate complex **5-35** was further reacted with the halide extracting reagent NaBPh$_4$, to yield the first two-coordinate cobalt(I) compound [(IMes)$_2$CoCl][BPh$_4$] **5-37** as a cationic complex (Scheme 5.15).

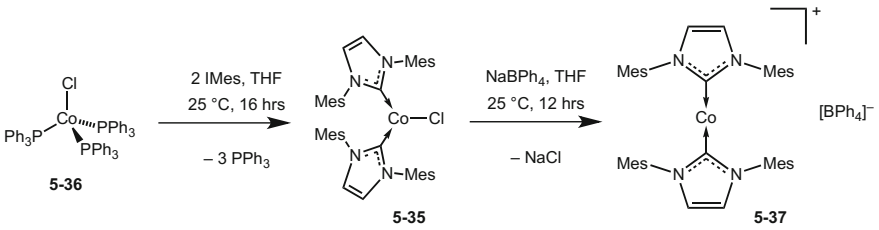

Scheme 5.15 Preparation of **5-37** though **5-35**

Complexes **5-35** and **5-37** were crystallographically characterised. Analysis of the molecular structure of complex **5-35** found the cobalt centre to occupy a distorted tetrahedral geometry, with C–Co–C and C–Co–Cl angles of 129.6° and 115.2° (avg.) respectively. The cationic complex **5-37** was found to have an essentially linear two-coordinate cobalt centre (C–Co–C = 178.57(7)°), with no close interactions between the metal centre and the flanking aryl groups.

Both cobalt(I) complexes **5-35** and **5-37** were found to be paramagnetic, exhibiting effective magnetic moments of 4.4 μ_B and 4.1 μ_B respectively in solution at room temperature. These values are much higher than the spin only value for a high-spin d^8 centre (2.83 μ_B), which the authors explained was due to orbital angular momentum contributions in the complexes [25].

The reaction of complex **5-35** towards a sodium mercury amalgam was also reported, initially targeting the first two-coordinate cobalt(0) complex [$(IMes)_2Co$]. Unfortunately, the target complex was not isolated, as a doubly ligand C–H activated cobalt(II) complex was instead synthesised, likely because of the highly reactive nature of a two-coordinate cobalt(0) centre [25].

The first two two-coordinate cobalt(0) complexes were actually reported almost simultaneously, both using similar CAAC ligands by the groups of Bertrand and H. Roesky in 2014 [26, 27]. Bertrand's route to the two-coordinate cobalt(0) complex involved halide extraction of the three-coordinate cobalt(I) complex [$(Et_2$-CAAC$)_2$CoCl] **5-38** (Et_2-CAAC = :C(CEt_2)(CH_2)(CMe_2)NDipp) with Na $BAr^F{}_4$ (Ar^F = 3,5-$(F_3C)_2C_6H_3$), to give the two-coordinate cobalt(I) cationic complex [$(Et_2$-CAAC$)_2$Co][$BAr^F{}_4$] **5-39**. Complex **5-39** was then reduced using a sodium mercury amalgam in diethyl ether to give [$(Et_2$-CAAC$)_2$Co] **5-40** as dark green crystals (Scheme 5.16). Roesky's route on the other hand, involved the direct reduction of the three-coordinate cobalt(I) precursor complex [$(Me_2$-CAAC$)_2$CoCl] **5-41** (Me_2-CAAC = :C(CH_2)(CMe_2)$_2$N-Dipp) with KC_8 in THF, to give the two-coordinate cobalt(0) complex [$(Me_2$-CAAC$)_2$Co] **5-42** in high yields (Scheme 5.17).

All five compounds **5-38**–**5-42** were crystallographically characterised. The structure of the two neural cobalt(I) complexes **5-38** and **5-41** closely resemble that of the related NHC analogous complex **3-35**, in that all three complexes possess a three-coordinate cobalt(I) centre, occupying a distorted trigonal geometry. The cationic cobalt(I) complex **5-39** also closely resembles the analogous NHC complex

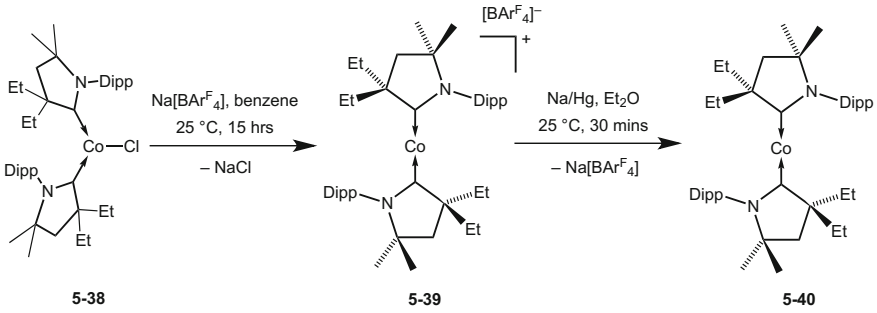

Scheme 5.16 Bertrand's preparation of the two-coordinate cobalt(0) complex **5-40**

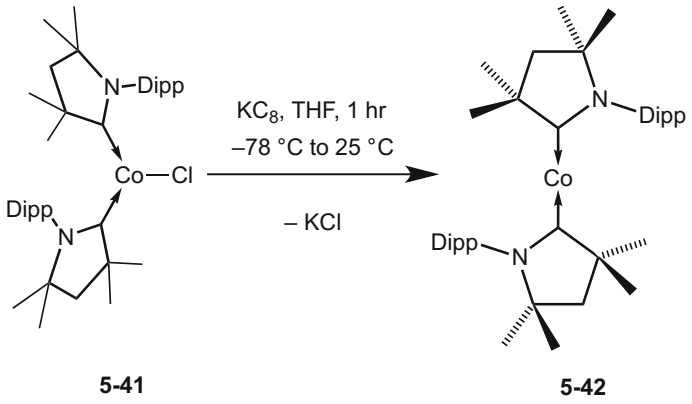

Scheme 5.17 Roesky's preparation of the two-coordinate cobalt(0) complex **5-42**

5-37, in that both structures bear two-coordinate cationic cobalt(I) centres in essentially linear geometries (C–Co–C = 168.35(9)° in **5-39**). All three cobalt(I) complexes are paramagnetic in solution, indicative of high spin cobalt(I) complexes. Solution state effective magnetic moments of 2.9 μ_B and 3.2 μ_B were calculated for complexes **5-38** and **5-39** respectively, however no effective magnetic moment was reported for **5-41**.

The two cobalt(0) complexes **5-40** and **5-42** were revealed to have very similar structures. Both cobalt centres were found to be two-coordinate with slightly bent geometries (C–Co–C = 169.52(5) in **5-40** and 170.12(8)° in **5-42**), with no strong interactions between the metal centre and the ligand in either structure.

Complexes **5-40** and **5-42** were analysed by EPR spectroscopy, both giving broad unresolved resonances in the X-band experiments, due to their near linear geometry. However both spectra were well fitted to a $S = ½$ spin state, expected for a d^9 cobalt(0) complex. Further reactivity of the two two-coordinate cobalt(0) complexes has yet to be reported.

5.2 Research Outline

As discussed in Chap. 2, the two bulky amido cobalt(II) chloride complexes [{Ar*($SiPh_3$)NCo(μ-Cl)(THF)}$_2$] **2-48** and [{Ar*($SiPh_3$)NCo(μ-Cl)}$_2$] **2-49** have been prepared as potential precursors for low coordinate, low oxidation state cobalt complexes. As there are currently no low coordinate, low oxidation state cobalt complexes stabilized by monodentate amide ligands, the initial goal of this chapter was to reduce these two precursor complexes in the hope to obtain examples of such compounds. In addition, even though a number of other bulky monodentate ligands have proven successful in the isolation of low coordinate cobalt(I) species, a neutral two-coordinate cobalt(I) complex has yet to be reported. Therefore, the second objective of this chapter was to target a two-coordinate cobalt(I) complex, by utilizing the stabilizing properties of the extremely bulky amide ligand.

5.3 Results and Discussion

5.3.1 Preparation and Characterisation of Two Low Coordinate Amido Cobalt(I) Complexes

At the outset of this study, the reduction of the amido cobalt(II) chloride precursor complex [{Ar*($SiPh_3$)NCo(μ-Cl)(THF)}$_2$] **2-48** was attempted using activated magnesium metal in both THF and diethyl ether. After stirring for five days at room temperature, almost complete recovery of the starting material **2-48** was obtained. Heating the THF reaction mixture to 60 °C overnight, led to slow decomposition of the starting material. In addition, the reduction of **2-48** was also attempted by stirring toluene and THF solutions of the complex over both sodium and potassium mirrors. In all cases, "over-reduction" of the precursor complex was observed, resulting in the formation cobalt metal and the protonated amine Ar*($SiPh_3$)NH as the only isolable products. In contrast, when the reduction of **2-48** was performed using 2.2 equivalents of KC_8 in benzene, the reaction solution changed from yellow/brown to intense green over several days. Filtration, followed by concentration of the filtrate, gave the benzene capped amido cobalt(I) complex [{Ar*($SiPh_3$)NCo(η^6-benzene)] **5-43** as bright green crystals in good yields (Scheme 5.18). It was later realized that **5-43** can also be synthesized by replacing KC_8 with the magnesium(I) reducing agent [{(^{Mes}Nacnac)Mg}$_2$] **1-08**. However, on multiple occasions, the product was found to be contaminated with small amounts the by-product [{(^{Mes}Nacnac)Co(μ-Cl)}$_2$], presumably formed by a trans-metallation side reaction. The reaction between the THF free precursor complex [{Ar*($SiPh_3$)NCo(μ-Cl)}$_2$] **2-49** and 2.2 equivalents of KC_8 in benzene also gives **5-43**, but in slightly lower yields.

When the reduction of **2-48** was repeated in THF, a colour change from dull green to bright green was observed after stirring for several hours at room

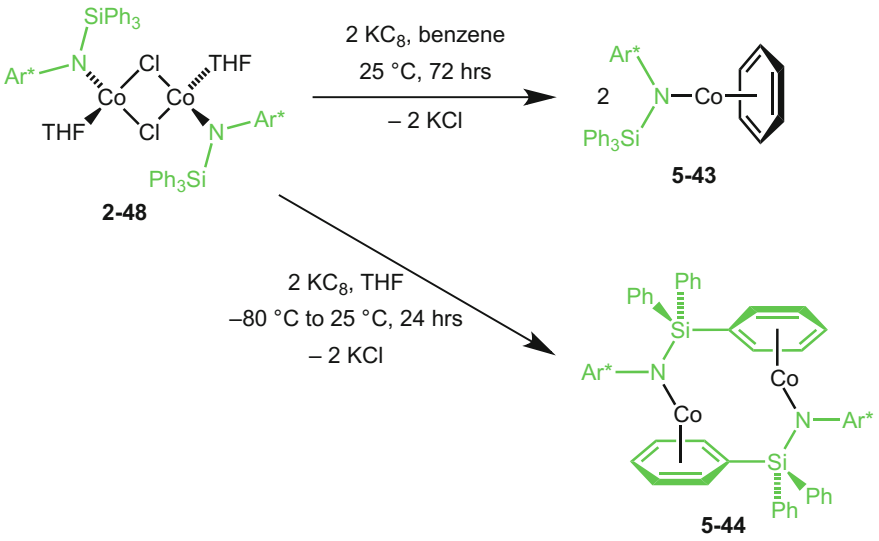

Scheme 5.18 Preparation of the cobalt(I) complexes **5-43** and **5-44**

temperature. Workup, followed by crystallization of the crude reaction solution from diethyl ether, gave the cobalt(I) dimer [{Ar*($SiPh_3$)NCo}$_2$] **5-44** as small green needle crystals in moderate yields (Scheme 5.18).

Complex **5-43** is an amido cobalt(I) compound, with an η^6 coordination of the cobalt centre to a molecule of benzene. The complex is similar to that of the β-diketiminato cobalt(I) complex **5-01** [4], the three amidinato- and guanidinato cobalt(I) complexes **5-18a–c** [10], and the two mononuclear terphenyl cobalt(I) complexes **5-24** and **5-27** [15, 19], as all possess an η^6 coordination of the cobalt centre to either a molecule of benzene or toluene. The complex can also be compared to Holland's "masked two-coordinate" complex **5-11**, as both complexes contain a N–Co-η^6-arene bonding motif [9].

Complex **5-44** is a cobalt(I) dimer, with η^6 coordination of the metal centres to a flanking phenyl group from a second "Ar*($SiPh_3$)NCo" unit. The complex can be compared to the previously reported terphenyl cobalt(I) dimer **5-23** [11], the alkyl cobalt(I) dimer **5-30** [20], and the cobalt(I) dimer stabilised by mono-anionic α-diimine ligands **5-34** [23], as all four complexes are cobalt(I) dimers with similar bonding motifs.

Interestingly, in the formation of the cobalt(I) dimer **5-44**, the η^6 coordination of a flanking phenyl group from a second "Ar*($SiPh_3$)NCo" motif is preferred over coordination to THF. This is in contrast with the reduction of the β-diketiminate cobalt(II) chloride complex **5-07**, which gave the mononuclear THF coordinated cobalt(I) complex **5-10** using similar reaction conditions [9]. However, the isolation of the terphenyl cobalt(I) dimer **5-23** was also achieved by reduction of a cobalt(II) precursor in THF [11]. Also worth noting is that both reductions were carried out

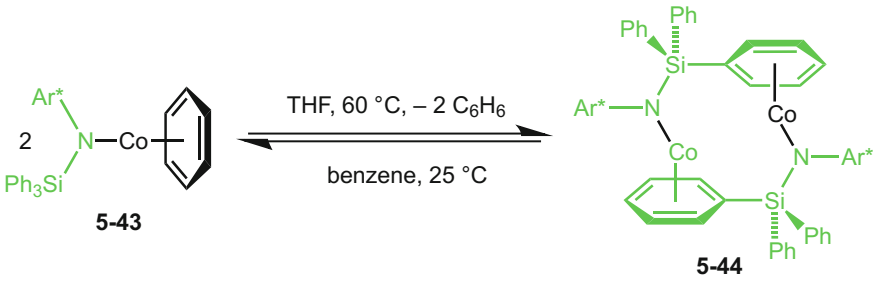

Scheme 5.19 The reversible conversion between complexes **5-43** and **5-44**

under an atmosphere of high purity dinitrogen, and no dinitrogen coordinated product was obtained from either reaction. This is once again in contrast with the reductions of the β-diketiminate cobalt(II) chloride complex **5-07**, but similar to the reductions of the amidinate and guanidinate cobalt(II) precursor complexes **5-17a–c** [10].

It was later found that the benzene capped complex **5-43** can be converted to dimer **5-44**, by dissolution of **5-43** in THF at 60 °C (Scheme 5.19). The reaction proceeds with a colour change from bright green to deep orange at 60 °C. Upon on cooling the reaction mixture to room temperature, it returns to a bright green solution. This reaction is reversible, and dissolution of **5-44** in benzene at room temperature, leads to the rapid regeneration of **5-43** (Scheme 5.19).

To compare the solid state structures of **5-43** and **5-44** with the previously reported cobalt(I) complexes, both complexes were crystallographically characterised (Figs. 5.1 and 5.2). The molecular structure of **5-43** shows the cobalt centre to a possess a one legged piano stool geometry, similar to that in the benzene capped terphenyl cobalt(I) complex **5-27** [19]. The N–Co distance (1.9166(19) Å) is similar to that in the precursor complex **2-48** (1.932(6) Å) [28], and the N centre is planar, with the sum of its angles equalling 359.9°. The Co-centroid distance in **5-43** (1.647 (3) Å) is similar to that in the related terphenyl complex **5-27** (1.634(2) Å), but with a N–Co-centroid angle of 166.3°, compared with the linear C–Co-centroid angle in complex **5-27** [19].

The molecular structure of **5-44** show it to be dimeric in the solid state, with each Co centre coordinated in an η^6 fashion to one of the phenyl rings of the $SiPh_3$ group on the opposing "Ar*($SiPh_3$)NCo" motif. The two N–Co bond lengths within the complex are identical (1.913(3) Å), and are the same as in **5-43** (1.9166(19) Å) within error. The Co···Co separation in complex **5-44** (3.6331(7) Å) is in the range of the two dimeric cobalt(I) complexes **5-23** (2.8033(5) Å) [11] and **5-30** (4.3480(7) Å) [20]. However, as it is well outside the covalent radii of two high-spin cobalt centres (3.00 Å) [29], it is clearly too large to imply any significant interaction between the two metal centres. Interestingly, the N–Co-centroid angles (159.2° mean) are almost exactly between the equivalent C–Co-centroid angles in the related low-spin complex **5-23** (143.7°) [11] and high-spin complex **5-30** (173.7°) [20].

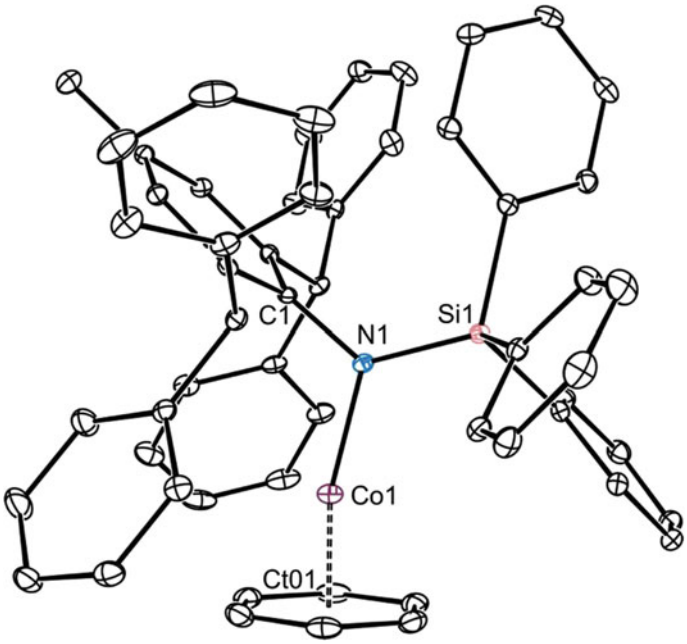

Fig. 5.1 Thermal ellipsoid plot (25 % probability surface) of the molecular structure of **5-43**. Hydrogen atoms have been omitted for clarity. Selected bond lengths (Å) and angles (°): Co(1)–N (1) 1.9166(19), Co(1)–Ct(01) 1.647(3), N(1)–Si(1) 1.711(2), N(1)–C(1) 1.433(3), N(1)–Co(1)–Ct (01) 166.31(11)

Theoretical calculations suggest that the low-spin configuration of **5-23** is due to a bending of the C–Co-centroid unit, which induces electron pairing [14]. Therefore, are the N–Co-centroid angles of 159.2° in **5-44** enough to induce electron pairing? To investigate the spin states of **5-43** and **5-44**, solution state magnetic studies were undertaken on the two complexes via the Evans method [30].

Compounds **5-43** and **5-44** were both found to be paramagnetic in solution, exhibiting solution state effective magnetic moments of 2.8 μ_B and 3.9 μ_B (2.8 μ_B per Co centre) respectively at room temperature. Both values are indicative of high-spin d^8 cobalt(I) centres, and are consistent with the spin only value for a non-interacting high-spin d^8 complex (μ_{so} = 2.83 μ_B). Furthermore, the measured magnetic moment of **5-44** remains essentially constant over the temperature range of 65–55 °C, suggesting that there is minimal magnetic communication between the two metal centres. The magnetic moment of **5-43** falls in the range of the previously reported mononuclear arene capped cobalt(I) complexes **5-18a**–**c**, **5-24**, **5-27** and **5-28** (2.35 to 3.37 μ_B) [15, 19], whereas that for **5-44** is comparable to the high-spin alkyl dimer **2-30** (2.63 μ_B) [20]. Therefore the N–Co-centroid angles of 159.2° in **5-44** are apparently not acute enough to induce a low spin complex.

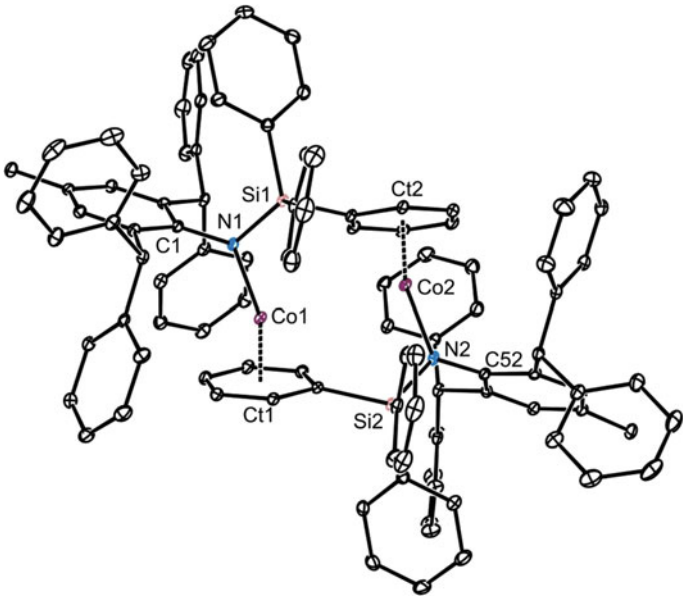

Fig. 5.2 Thermal ellipsoid plot (25 % probability surface) of the molecular structure of **5-44**. Hydrogen atoms have been omitted for clarity. Selected bond lengths (Å) and angles (°): Co(1)–N(1) 1.913(3), Co(2)–N(2) 1.913(3), Co(1)–Ct(1) 1.635(4), Co(2)–Ct(2) 1.634(4), Co(1)···Co(2) 3.6331(7), N(1)–Co(1)–Ct(1) 159.23(14), N(2)–Co(2)–Ct(2) 159.14(14)

5.3.2 Reactivity of the Two Amido Cobalt(I) Complexes

Both Holland, with the "masked two-coordinate" cobalt(I) complex **5-11**, and Power, with the KC_8 reduction of the terphenyl cobalt chloride complex **2-28** have shown that activation of C–F bonds is possible with low coordinate cobalt complexes [9, 19]. As the amido benzene capped cobalt(I) complex **5-43** is comparable to **5-11**, it seemed reasonable that it could also activate C–F bonds. With that in mind, crystals of **5-43** were suspended in dry fluorobenzene and stirred overnight at room temperature. Due to the extremely low solubility of **5-43** in that solvent at room temperature, almost complete recovery of the starting material was obtained. However, when the reaction was repeated and heated to 60 °C, complete dissolution of **5-43** was observed, resulting in a dark orange solution. On cooling to room temperature, bright green crystals of the cobalt(I) dimer **5-44** were grown from the reaction mixture in good yields (Scheme 5.20). A similar reaction was observed when **5-43** was dissolved in dry hexafluorobenzene at 60 °C. Also worth noting is that heating a solution of **5-44** in hexafluorobenzene to 60 °C for 3 days, resulted in almost complete recovery of the starting material.

The dissolution of **5-43** in either fluorobenzene or hexafluorobenzene favours the loss of benzene and dimerization of two "Ar*($SiPh_3$)NCo" fragments to yield **5-44**. This lack of reactivity towards fluorobenzene is in contrast to both the β-diketiminate

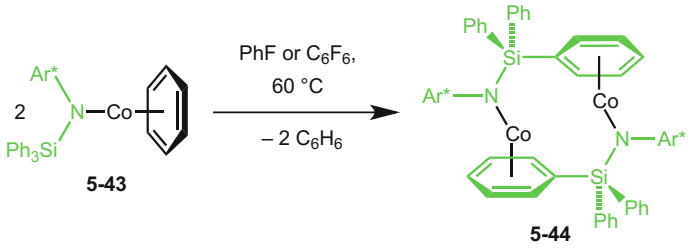

Scheme 5.20 Conversion of **5-43** to **5-44** by dissolution in fluorobenzene or hexafluorobenzene

and terphenyl cobalt(I) complexes **5-11** and **5-24** respectively, the first of which activates the C–F bond whereas the second coordinates in an η^6 fashion to a fluorobenzene molecule [9, 19].

As previously discussed, Power isolated the hexafluorobenzene C–F activated product **5-29**, by reduction of the terphenyl cobalt(II) chloride complex **2-28** with KC_8 in THF, in the presence of C_6F_6 [19]. With that in mind, KC_8 (2.2 equiv.) was added to a THF solution of the amido cobalt(II) chloride precursor complex **2-48** containing hexafluorobenzene (50 equiv.) at –80 °C. After warming the reaction mixture to room temperature and stirring overnight, the cobalt(I) dimer **5-44** was once again the only product isolated.

With the lack of reactivity towards C–F bonded molecules, reactivity studies of **5-43** moved on to two-electron donor molecules, in an attempt to exchange the η^6 coordination of benzene for a monodentate donor ligand, thus yielding a neutral two-coordinate cobalt(I) complex. A number of strong σ-donor ligands were tested, including phosphines, pyridines and NHC's.

The addition of triphenylphosphine to a benzene solution of **5-43** led to no reaction, even after heating to 60 °C overnight. It was proposed that the large size of PPh_3 made the coordination of it to the metal centre unfavorable. In contrast, the addition of the smaller trimethylphophine to a benzene solution of **5-43**, produced an immediate colour change from green to brown, and the formation of a brown insoluble sticky product. Due to the product's extremely poor solubility in solvents such as hexane, benzene and THF, no further data on this compound were obtained. The addition of pyridine to a benzene solution of **5-43** also led to no reaction, even after heating to 60 °C overnight, whereas the addition of DMAP (DMAP = 4-dimethylaminopyridine) to a benzene solution of **5-43** gave an intractable mixture of products.

Various NHC's were also investigated in attempts to substitute the benzene ligand, including IMes, IPr (IPr = :C{N(Dipp)CH}$_2$), TMC (TMC = :C{N(Me)C(Me)}$_2$) and IPriMe (IPriMe = :C{N(^{i}Pr)C(Me)}$_2$). The two most stericly hindering NHC's, IPr and IMes did not react with **5-43** even after prolonged heating to 60 °C, likely due to their large bulk disfavoring coordination to the metal centre. In contrast, TMC reacted immediately on addition, to give a dark orange/yellow solution. However seconds later, signs of decomposition were observed by elemental metal

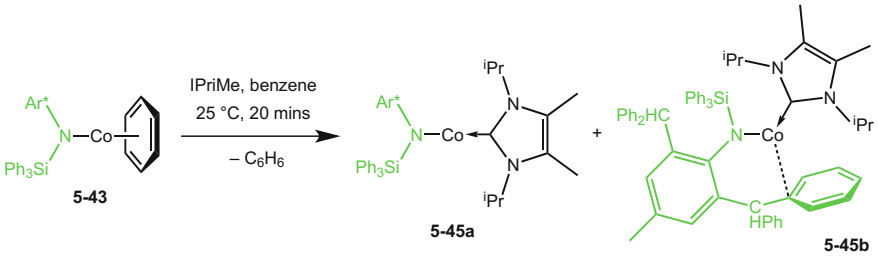

Scheme 5.21 Preparation of **5-45**, showing the two isolated isomers **5-45a** and **5-45b**

precipitating from the reaction mixture, suggesting that the product is not stable at least at room temperature.

When 1.1 equivalents of the slightly bulkier IPriMe was added to a benzene solution of **5-43**, an instant colour change from green to orange/yellow was observed, which persisted at room temperature for several days. Workup, followed by crystallization of the reaction mixture from diethyl ether led to the isolation of the two-coordinate cobalt(I) complex [Ar*($SiPh_3$)NCo(IPriMe)] **5-45a** as yellow crystals (Scheme 5.21). Interestingly, when the reaction mixture is crystallised from pentane, red crystals of a higher coordinate isomer of **5-45** were isolated (viz. **5-45b**), which possessed an intermolecular cobalt-arene interaction.

Both isomers of **5-45** were crystallographically characterised (Fig. 5.3). It is worthy of mention that a small number of crystals of the charge separated species $[Ar^*(SiPh_3)N]^-[Co(IPriMe)_3]^+$ were isolated from one reaction, presumably formed by excess IPriMe reacting with **5-45** (see Appendix 7.2 for the molecular structure). The molecular structure of **5-45a**, the isomer crystallised from diethyl ether, shows a two-coordinate cobalt centre with a near linear N–Co–C fragment (173.2°). The N–Co bond length (1.889(2) Å) is not surprisingly shorter than in the higher coordinate isomer **5-45b** (1.979(3) Å) and also shorter than in the two η^6 coordinated cobalt(I) complexes **5-43** and **5-44**. The Co-C distance in **5-45a** (1.962(3) Å) is similar to those in other IPriMe complexes of cobalt, such as in $[CoPh_2(IPriMe)_2]$ (1.962 Å avg.) [31], but expectedly shorter than the equivalent bond in the higher coordinate isomer **5-45b** (2.009(4) Å).

The N–Co–C unit in the higher coordinate isomer **5-45b** is considerably bent (140.2°), due to a close interaction between the cobalt centre and an *ipso*-carbon of one flanking phenyl from the amide ligand ($C\cdots C_{ipso}$ = 2.103(3) Å). It is apparent that such an interaction is avoided in the two-coordinate isomer **5-45a**, as the compound packs in the crystal lattice with relatively close intermolecular contacts between the *p*-methyl group on the amide ligand of one molecule and the Co centre of another (closest methyl proton···Co distance: 3.27 Å). In addition, the structure of **5-45a** incorporates a diethyl ether molecule of crystallisation in the lattice, while the structure of **5-45b** incorporates a pentane molecule. This difference could also affect the crystal packing of the two isomeric forms of **5-45**.

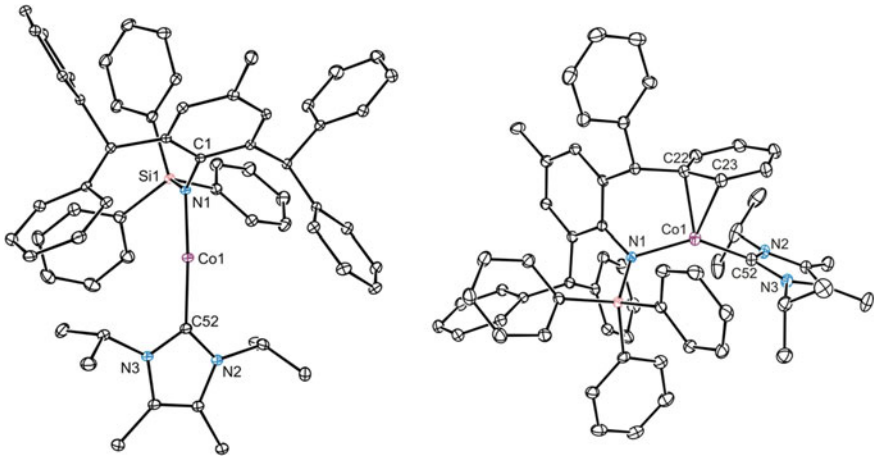

Fig. 5.3 Thermal ellipsoid plots (25 % probability surface) of the molecular structures of **5-45a** (*left*) and **5-45b** (*right*). Hydrogen atoms have been omitted for clarity. Selected bond lengths (Å) and angles (°) for **5-45a**: Co(1)–N(1) 1.889(2), Co(1)–C(52) 1.962(3), C(52)–N(2) 1.363(3), C(52)–N(3) 1.359(4), N(1)–Co(1)-C(52) 173.18(10). Selected bond lengths (Å) and angles (°) for **5-45b**: Co(1)–N(1) 1.979(3), Co(1)–C(52) 2.009(4), Co(1)–C(22) 2.103(3), Co(1)–C(22) 2.13(4), C(52)–N(2) 1.357(5), C(52)–N(3) 1.360(5), N(1)–Co(1)-C(52) 140.16(13)

Dissolving crystals of both isotopes of **5-45** in C_6D_6 results in similar dark orange/yellow solutions. ^{1}H NMR spectroscopy studies of the two solutions gave identical spectra, with 10 clear hydrogen resonances over a wide ppm range (δ −100 to +83 ppm, 12 different hydrogen environments are expected for **5-45**, but likely due to overlapping of broad peaks in the ^{1}H NMR, only 10 are seen). The observation of such a low number of resonances suggests that the complex exists in solution as its symmetrical two-coordinate form, as many more are expected for the higher coordinate **5-45b**. Compound **5-45** is therefore the first example of neural two-coordinate cobalt(I) complex.

Compound **5-45** was found to possess a solution state magnetic moment of 2.6 μ_B (determined by the Evans method) at room temperature [30], which is indicative of a high-spin cobalt(I) centre. The value is considerably lower than the two-coordinate cationic complexes **5-37** and **5-39** (3.2–4.1 μ_B) [25, 26], as the cationic complexes were proposed to have enhanced effective magnetic moments due to spin-orbit coupling contributions.

5.4 Conclusion

In summary, a series of low coordinate cobalt(I) complexes, bearing an extremely bulky amido ligand have been synthesised. These include the benzene capped complex **5-43**, which readily loses its benzene ligand in solution to give the dimeric

cobalt(I) complex **5-44**. The benzene ligand of **5-43** can also be displaced by the NHC IPriMe, to yield the first neural two-coordinate cobalt(I) complex **5-45**. Complex **5-45** can be crystallised as two distinct structural isomers, **5-45a**, which possesses a two-coordinate near linear cobalt centre and **5-45b**, which possesses a higher coordinate cobalt centre due to an intramolecular arene interaction. All synthesised complexes were found to possess high-spin cobalt(I) centres in solution, with the dimeric complex **5-44** appearing to have no detectable magnetic communication between the two metal centres.

5.5 Experimental

General methods. All manipulations were carried out using standard Schlenk and glove box techniques under an atmosphere of high purity dinitrogen. THF, benzene and toluene were distilled over molten potassium, while diethyl ether and pentane were distilled over sodium/potassium alloy (1:1). Fluorobenzene was distilled over CaH_2. ^1H NMR spectra were recorded on a Varian Inova 500 spectrometer and were referenced to the resonances of the solvent used, or external $SiMe_4$. Mass spectra were recorded on an Agilent Techonlogies 5975D inert MSD with a solid state probe or obtained from the EPSRC National Mass Spectrometric Service at Swansea University. IR spectra were recorded as solid samples using an Agilent Cary 630 attenuated total reflectance (ATR) spectrometer. Microanalyses were carried out by the Science Centre, London Metropolitan University. A reproducible microanalysis for **5-45** could not be obtained as the compound contained variable amounts of either diethyl ether or pentane of crystallization, which could not be completely removed from the sample by vacuum drying the compound at room temperature for several hours. The starting materials [{Ar*($SiPh_3$)NCo(μ-Cl)(THF)}$_2$] **2-48** and [{Ar*($SiPh_3$)NCo(μ-Cl)}$_2$] **2-49** were prepared as discussed in Chap. 2. The starting materials [{(^{Mes}Nacnac)Mg}$_2$] [32] **1-08** and IPriMe [33] were prepared according to the literature method.

Preparation 1 of [Ar*($SiPh_3$)NCo(η^6-benzene)], 5-43. To a suspension of KC_8 (0.086 g, 0.637 mmol) in benzene (25 mL) was added a solution of [{Ar*($SiPh_3$)NCo(μ-Cl)(THF)}$_2$] **2-48** (0.500 g, 0.290 mmol) in benzene (25 mL) at ambient temperature. The reaction mixture was stirred for 72 h, producing a colour change from yellow/brown to intense green. The reaction mixture was filtered, concentrated (ca. 10 mL) and slowly cooled to 5 °C overnight to give **5-43** as green crystals (0.365 g, 75 %).

Preparation 2 of [Ar*($SiPh_3$)NCo(η^6-benzene)], 5-43. To a solution of [{Ar*($SiPh_3$)NCo(μ-Cl)(THF)}$_2$] **2-48** (0.500 g, 0.290 mmol) in toluene (25 mL) was added a solution of [{(^{Mes}Nacnac)Mg}$_2$] **1-08** (0.228 g, 0.318 mmol) in toluene (25 mL) at –80 °C over 5 min. The reaction was slowly warmed to ambient temperature, producing a colour change from yellow/brown to intense green. The reaction mixture was stirred for a further 2 h at ambient temperature, whereupon volatiles were removed from the filtrate *in vacuo*. The residue was extracted with

ice cold toluene (25 mL), filtered and volatiles once again removed from the filtrate *in vacuo* to give a green solid. This solid was then dissolved in the minimum volume of hot benzene (ca. 10 mL) and slowly cooled to 5 °C overnight to give **5-43** as green crystals (0.320 g, 66 %). Mp: 117–119 °C (decomp. on melting); ^{1}H NMR (499 MHz, C_6D_6, 298 K): δ = 3.40 (br.), 5.07, 6.40, 6.66, 7.11, 8.54, 11.59, 13.22, 19.63 (br.), 21.37, 23.55; IR υ/cm^{-1} (Nujol): 1597(m), 1492(m), 1437(m), 1426(s), 1257(m), 1231(s), 1210(m), 1130(m), 1100(s), 1076(m), 1030(m), 922(m), 904(m), 832(m), 804(m), 761(s), 739(m), 697(s), 675(s); UV-Vis (benzene) [λ_{max}, nm (ε, m^{-1} cm^{-1})]: 612 (304); MS/EI *m/z* (%): 697.3 (Ar*N(H)SiPh$_3^+$, 97), 439.2 (Ar*NH$_2^+$, 36), 259.0 (Ph$_3$Si$^+$, 100), 167.0 (Ph$_2$CH$^+$, 10); μ_{eff} (Evan's, C_6D_6, 298 K): 2.8 μ_B; anal. calc. for $C_{57}H_{48}CoNSi$: C 82.09 %, H 5.80 %, N 1.68 %, found: C 81.91 %, H 5.92 %, N 1.71 %.

Preparation 1 of [{Ar*(SiPh$_3$)NCo}$_2$], 5-44. To a suspension of KC_8 (0.086 g, 0.637 mmol) in THF (25 mL) was added a solution of [{Ar*(SiPh$_3$)NCo(THF)(μ-Cl)}$_2$] **2-48** (0.500 g, 0.290 mmol) in THF (25 mL) at –80 °C. The reaction mixture was allowed to slowly warm to ambient temperature where it was stirred for a further 24 h. Volatiles were removed *in vacuo*, the residue extracted with diethyl ether (25 mL), filtered, concentrated (ca. 10 mL) and slowly cooled to 5 °C overnight to give **5-44** as small green crystals (0.280 g, 64 %).

Preparation 2 of [{Ar*(SiPh$_3$)NCo}$_2$], 5-44. [Ar*(SiPh$_3$)NCo(η^6-benzene)] **5-43** (0.200 g, 0.240 mmol) was suspended in fluorobenzene (10 mL) and heated at 60 °C for 5 min whereupon it dissolved to give a dark orange solution. The reaction mixture was slowly cooled to 5 °C overnight to give **5-44** as small green crystals (0.135 g, 74 %). Mp: 215–218 °C (decomp. on melting); ^{1}H NMR (499 MHz, d^8-THF, 298 K): δ = –31.33 (br.), –16.61 (br.), –10.53 (br.), –4.44 (br.), 7.24 (br.), 9.71 (br.), 11.68 (br.), 12.91 (br.), 14.14 (br.), 19.05 (br.), 19.85 (br.), 22.56 (br.), 29.14 (br.), 44.01 (br.), 45.46 (br.), 46.65 (br.), 48.37 (br.), 56.49 (br.), 88.11 (br.), 109.72 (br.); IR υ/cm^{-1} (Nujol): 1595(m), 1492(s), 1437(s), 1426(s), 1255(m), 1228 (s), 1213(s), 1154(m), 1132(m), 1101(s), 1089(s), 1029(m), 924(m), 915(m), 853 (m) 831(m), 803(s), 742(s), 696(s), 673(s), 663(m); UV-Vis (THF) [λ_{max}, nm (ε, m^{-1} cm^{-1})]: 355 (3046); MS/EI *m/z* (%): 755.3 (Ar*(SiPh$_3$)NCo$^+$, 99), 697.3 (Ar*N(H)SiPh$_3^+$, 100), 439.2 (Ar*NH$_2^+$, 9), 259.0 (Ph$_3$Si$^+$, 64), 167.0 (Ph$_2$CH$^+$, 4); μ_{eff} (Evan's, d^8-THF, 298 K): 3.9 μ_B (per dimer); anal. calc. for $C_{57}H_{48}CoNSi$: C 81.03 %, H 5.60 %, N 1.85 %, found: C 80.93 %, H 5.71 %, N 1.92 %.

Preparation of [{Ar*(SiPh$_3$)NCo(IPriMe)], 5-45. To a solution of [{Ar*(SiPh$_3$)NCo(η^6-benzene)] **5-43** (0.200 g, 0.240 mmol) in benzene (15 mL) was added a solution of IPriMe (0.048 g, 0.264 mmol) in benzene (15 mL) at ambient temperature over 5 min, resulting in an immediate colour change from green to dark orange. The reaction mixture was stirred for a further 20 min, whereupon volatiles were removed *in vacuo*. The residue was extracted with diethyl ether (25 mL), the extract filtered, concentrated (ca. 10 mL) and slowly cooled to 5 °C overnight to give **5-45a** as yellow crystals (0.050 g, 22 %). The residue was also be extracted with pentane (25 mL), the extract filtered, concentrated (ca. 10 mL) and slowly cooled to 5 °C overnight to give **5-45b** as orange-red crystals (0.045 g, 20 %). Mp: 119–122 °C (decomp. on melting); ^{1}H NMR (499 MHz, C_6D_6, 298 K):

δ = –99.47 (br.), –46.10 (br.), –18.64 (br.), 12.79 (br.), 13.81 (br.), 15.55 (br.), 19.92 (br.), 26.04 (br.), 34.40 (br.), 82.75 (br.); IR υ/cm^{-1} (Nujol): 1598(m), 1492 (m), 1444(m), 1426(m), 1364(m), 1259(s), 1097(s), 1015(s), 921(m), 880(m), 855 (m), 797(s), 741(m), 697(s); MS/EI *m/z* (%): 697.6 ($Ar^*N(H)SiPh_3^+$, 64), 619.5 ($Ar^*N(H)SiPh_2^+$, 28), 438.3 (Ar^*NH^+, 22), 259.0 (Ph_3Si^+, 100), 181.1 (NHC $+H^+$, 26), 167.

References

1. M.J. Jeletic, M.T. Mock, A.M. Appel, J.C. Lineham, J. Am. Chem. Soc. **135**, 11533 (2013)
2. H. Xu, P.G. Williard, W.H. Bernskoetter, Organometallics **31**, 1588 (2012)
3. (a) S.S. Rozenel, R. Padilla, J. Arnold, Inorg. Chem. **52**, 11544 (2013); (b) A.C. Bowman, C. Milsmann, C.C.H. Atienza, E. Lobkovsky, K. Wieghardt, P.J. Chirik, J. Am. Chem. Soc. **132**, 1676 (2010); (c) W.A. Chomitz, S.F. Mickenberg, J. Arnold, Inorg. Chem. **47**, 373 (2008); (d) W.A. Chomitz, J. Arnold, Chem. Commun. 3648 (2008); (e) A.R Fout, F. Basuli, H. J. Fan, J. Tomaszewski, J.C. Huffman, M.H. Baik, D.J. Mindiola, Angew. Chem., Int. Ed. **45**, 3291 (2006)
4. X. Dai, P. Kapoor, T.H. Warren, J. Am. Chem. Soc. **126**, 4798 (2004)
5. P.H.M. Budzelaar, N.N.P. Moonen, R. de Gelder, J.M.M. Smits, A.W. Gal, Chem. Eur. J. **6**, 2740 (2000)
6. (a) L. Que, W.B. Tolman, Angew. Chem., Int. Ed. **41**, 1114 (2002) and references therein; (b) P.L. Larsen, T.J. Parolin, D.R. Powell, M.P. Hendrich, A.S. Borovik Angew. Chem., Int. Ed. **42**, 85 (2003)
7. S. Pfirrmann, C. Limberg, C. Herwig, R. Stosser, B. Ziemer, Angew. Chem., Int., Ed. **48**, 3357 (2009)
8. J.M. Smith, R.J. Lachicotte, K.A. Pittard, T.R. Cundari, G. Lukat-Rodgers, K.R. Rodgers, P. L. Holland, J. Am. Chem. Soc. **123**, 9222 (2001)
9. T.R. Dugan, X. Sun, E.V. Rybak-Akimova, O. Olatunji-Ojo, T.R. Cundari, P.L. Holland, J. Am. Chem. Soc. **133**, 12418 (2011)
10. C. Jones, C. Schulten, R.P. Rose, A. Stasch, S. Aldridge, W.D. Woodul, K.S. Murray, B. Moubaraki, M. Brynda, G. La Macchia, L. Gagliardi, Angew. Chem. Int. Ed. **48**, 7406 (2009)
11. T. Nguyen, W.A. Merrill, C. Ni, H. Lei, J.C. Fettinger, B.D. Ellis, G.J. Long, M. Brynda, P. P. Power, Angew. Chem. Int. Ed. **47**, 9115 (2008)
12. A.D. Sutton, T. Ngyuen, J.C. Fettinger, M.M. Olmstead, G.J. Long, P.P. Power, Inorg. Chem. **46**, 4809 (2007)
13. T. Nguyen, A.D. Sutton, M. Brynda, J.C. Fettinger, G.J. Long, P.P. Power, Science **310**, 844 (2005)
14. G. La Macchia, L. Gagliardi, P.P. Power, M. Brynda, J. Am. Chem. Soc. **130**, 5104 (2008)
15. H. Lei, B.D. Ellis, C. Ni, F. Grandjean, G.J. Long, P.P. Power, Inorg. Chem. **47**, 10205 (2008)
16. C. Ni, B.D. Ellis, J.C. Fettinger, G.J. Long, P.P. Power, Chem. Commun. 1014 (2008)
17. G. Fochi, C. Floriani, A. Chiesi-Villa, C. Guastini, J. Chem. Soc., Dalton Trans. 445 (1986)
18. S.R. Fletcher, A.C. Skapski, J. Organomet. Chem. **59**, 299 (1973)
19. H. Lei, J.C. Fettinger, P.P. Power, Inorg. Chem. **2012**, 51 (1821)
20. P. Zhao, Z. Brown, J.C. Fettinger, F. Grandjean, G.J. Long, P.P. Power, Organometallics **2014**, 33 (1917)
21. L. Pauling, Proc. Natl. Acad. Sci. U.S.A. **73**, 4290 (1976)
22. Atomic Radii of the Elements, *CRC Handbook of Chemistry and Physics*, 94th ed. by W.M. Haynes (CRC Press/Taylor and Francis, Boca Raton, FL, 2014), internet version

23. V. Rosa, P.J. Gonzalez, T. Aviles, P.T. Gomes, R. Welter, A.C. Rizzi, M.C.G. Passeggi, C.D. Brondino, Eur. J. Inorg. Chem. 4761 (2006)
24. X.-J. Yang, X. Fan, Y. Zhao, X. Wang, B. Liu, J.-H. Su, Q. Dong, M. Xu, B. Wu, Organometallics **32**, 6945 (2013)
25. Z. Mo, D. Chen, X. Leng, L. Deng, Organometallics **31**, 7040 (2012)
26. G. Ung, J. Rittle, M. Soleilhavoup, G. Bertrand, J.C. Peters, Angew. Chem. Int. Ed. **53**, 8427 (2014)
27. K.C. Mondal, S. Roy, S. De, P. Parameswaren, B. Dittrich, F. Ehret, W. Kaim, H.W. Roesky, Chem. Eur. J. **20**, 11646 (2014)
28. See Chapter 2.3 for further details
29. B. Cordero, V. Gómez, A.E. Platero-Prats, M. Revés, J. Echeverría, E. Cremades, F. Barragán, S. Alvarez, Dalton Trans. 2832 (2008)
30. (a) D.F. Evans, J. Chem. Soc. 1959, 2003; (b) E.M. Schbert, J. Chem. Educ. **69**, 62 (1992)
31. L. Deng, E. Bill, K. Wieghardt, R.H. Holm, J. Am. Chem. Soc. **131**, 11213 (2009)
32. S.J. Bonyhady, C. Jones, S. Nembenna, A. Stasch, A. Edwards, G.J. McIntyre, Chem. Eur. J. **16**, 938 (2010)
33. N. Kuhn, T. Kratz, Synthesis **56** (1993)

Chapter 6
Preparation of Molybdenum Aminogermylene and Aminogermylyne Complexes

6.1 Introduction

Transition metal carbyne complexes are organometallic compounds that contain a transition-metal carbon triple bond. Since their discovery in 1973 [1], this fundamental compound class has been extensively studied, due to their numerous synthetic, catalytic and analytical applications [2]. In recent years, considerable efforts have been made to extend this work to the preparation of heavier group 14 analogues, i.e. transition metal tetrelynes $L_nM{\equiv}ER$ (E = Si, Ge, Sn or Pb; M = a transition metal; L = a ligand, R = an organic group) to investigate their further chemistry. However, unlike their lighter carbon analogues, bulky substituents are required to kinetically stabilise the reactive M≡E core. The synthesis and reactivity of these transition metal tetrelyne complexes is the primary focus for this chapter.

6.1.1 Previously Reported Transition Metal Tetrelyne Complexes

The first report of a transition metal tetrelyne complex was by Tilley and co-workers in 1992, with the isolation of the base stabilised silylyne complex $[(Me_3P)_2(Cp^*)RuSi\{S(4\text{-}Me\text{-}C_6H_4)\}(bipy)][OTf]_2$ **6-01** ($Cp^* = C_5Me_5$; bipy = 2,2′-bipyridine; Tf = triflate) [3]. However, as the silicon centre in this complex is four-coordinate, occupying a distorted tetrahedral geometry, it cannot be considered as a "true" silylyne complex.

J. Hicks, *Preparation, Characterisation and Reactivity of Low Oxidation State d-Block Metal Complexes Stabilised by Extremely Bulky Amide Ligands*, Springer Theses,
DOI 10.1007/978-981-10-2905-9_6

6.1.1.1 Transition Metal Germylyne Complexes

The first "true" transition metal tetrelyne complex was reported by Simons and Power almost two decades ago, that is the molybdenum-germanium triply bonded complex $[(CO)_2(Cp)Mo{\equiv}GeAr^{Mes}]$ **6-02** [4]. The complex was synthesised by a salt metathesis reaction between the terphenyl germanium(II) chloride complex $[Ar^{Mes}GeCl]$ **6-03** and the molybdenum salt $Na[CpMo(CO)_3]$ **6-04** in THF at 50 °C (Scheme 6.1). During the reaction, a single molecule of CO is lost from the molybdenum centre allowing for the formation of the MoGe triple bond. After workup and crystallisation, complex **6-02** was isolated as air sensitive red crystals in low yields.

Complex **6-02** was crystallographically characterised, revealing a two coordinate germanium centre with near linear Mo–Ge–C geometry (172.2°). The Mo-Ge bond length was found to be remarkably short (2.271(1) Å), considerably shorter than previously reported MoGe singly bonded complexes, e.g. $[\{EtO(Ph)C\}(CO)_2CpMo\text{-}GePh_3]$ (2.658(2) Å) [5] and $[(\eta^3\text{-}C_6H_{11})(NO)CpMo\text{-}GePh_3]$ (2.604(2) Å) [6]. The short MoGe bond length, in addition to the near linear geometry of the germanium atom, is in good agreement with the proposed MoGe triple bonded model.

In 2000, the same group published a follow up paper, proposing that the formation of germylyne complex **6-02** goes through a singly bonded intermediate, i.e. $[Cp(CO)_3Mo\text{–}GeAr^{Mes}]$, before eliminating CO to form the MoGe triple bond [7]. In an attempt to isolate this intermediate, the bulkier terphenyl germanium chloride complex $[Ar^{Tripp}GeCl]$ **6-05** was reacted with the molybdenum salt complex **6-04**.2DME (DME = 1,2-dimethoxyethane), in the hope that the extra steric bulk from the ligand would stabilise the singly bonded intermediate. This was not the case, and the triply bonded complex $[Cp(CO)_2Mo{\equiv}GeAr^{Tripp}]$ **6-06** was isolated, even when the reaction mixture was maintained at 0 °C. Therefore, it appears that the MoGe singly bonded complex spontaneously undergoes CO elimination at temperatures ≤ 0 °C. Complex **6-06** was crystallographically characterised, and it was found to be essentially isostructural to the previously reported complex **6-02**, only differing by the size of the terphenyl ligand.

The bulky terphenyl germanium chloride complex **6-05** was reacted with the two analogous group 6 metal salts $Na[CpM(CO_3)]{\cdot}2DME$ (M = Cr or W) in toluene,

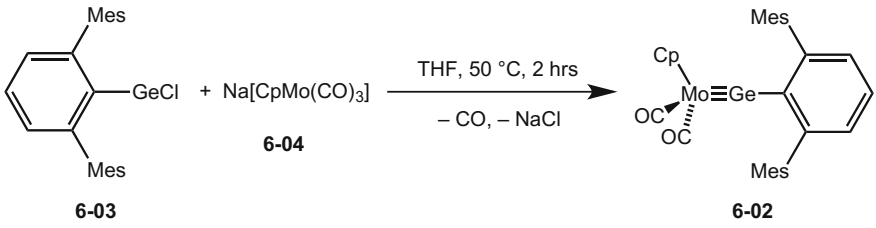

Scheme 6.1 Preparation of **6-02**, the first transition metal-tetrelyne complex

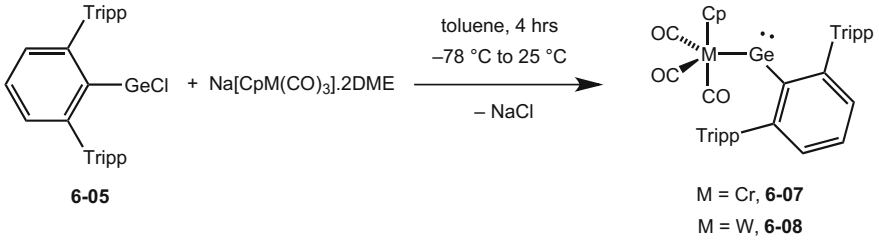

6-05

M = Cr, **6-07**

M = W, **6-08**

Scheme 6.2 Preparation of **6-07** and **6-08**, singly bonded transition metal-germylene compounds

maintaining the reaction temperature at, or below 25 °C. Contrastingly, workup of the two green reaction mixtures, followed by crystallisation from hexane, gave the singly bonded tricarbonyl complexes [$Cp(CO)_3M–GeAr^{Mes}$] (M = Cr, **6-07**; W, **6-08**) as green crystals in moderate yields (Scheme 6.2).

Both complexes **6-07** and **6-08** were crystallographically characterised, and they were found to be essentially isostructual, both maintaining the three carbonyl ligands from the starting materials. Both complexes were found to possess two-coordinate germanium centres with bent geometries (Cr–Ge–C = 117.9° in **6-07** and W–Ge–C = 114.7° in **6-08**), consistent with the presence of a stereochemically active lone pair on the group 14 element. In addition, the germanium-transition metal bond lengths in both complexes (Cr–Ge = 2.590(2) Å and W–Ge = 2.681(3) Å) are comparable to the sum of the covalent radii of the two elements (Cr and Ge = 2.50 Å; W and Ge = 2.61 Å) [8]. All of these structural characteristics support the formulation of the two singly bonded transition metal-germylene complexes.

The complexes **6-07** and **6-08** were found to eliminate CO to give the corresponding germylynes, albeit under more forcing conditions than required for the molybdenum analogue **6-06**. Heating a toluene solution of **6-07** to reflux for 15 min favours elimination of CO, and consequently the formation of the triply bonded [$Cp(CO)_2Cr{\equiv}GeAr^{Tripp}$] **6-09**, indicated by a colour change from green to red (Scheme 6.3). Irradiation of a hexane solution of **6-08** with UV light for 2 h favours

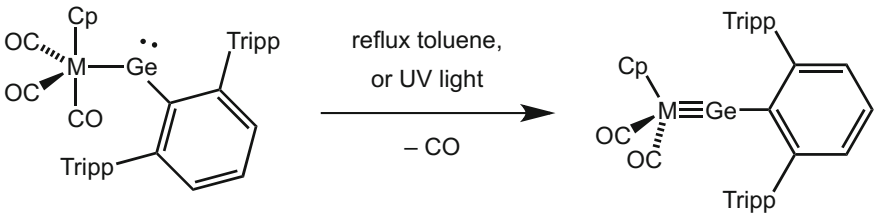

M = Cr, **6-07**

M = W, **6-08**

M = Cr, **6-09**

M = W, **6-10**

Scheme 6.3 Preparation of **6-09** and **6-10**

the elimination of CO for that compound, and the subsequent formation of [Cp$(CO)_2$W≡GeAr^{Tripp}] **6-10** (Scheme 6.3). It is not yet fully understood why the molybdenum analogue eliminates CO under much milder conditions than the other group 6 metals, but it is in agreement with other studies, which found molybdenum carbonyl complexes to be more reactive than analogous chromium or tungsten complexes [9].

Complex **6-09** was crystallographically characterised, but unfortunately a satisfactory X-ray diffraction data set could not be obtained for **6-10**, likely due to inclusion of disordered solvent molecules. However, a second tungsten-germylyne complex was also prepared and successfully structurally characterised (viz. [Cp$(CO)_2$W≡GeAr^{Mes}] **6-11**) for comparison with **6-08**. As the two tungsten complexes **6-10** and **6-11** vary only by the size of the terphenyl ligand, it was assumed that this would have little influence on the overall structure of the complex. Therefore the triply bonded complex **6-11** was directly compared with the singly bonded complex **6-08**.

As expected, the molecular structure of **6-09** showed a significant decrease in the chromium-germanium bond length of >0.4 Å (Cr–Ge = 2.166(4) Å), compared with the precursor complex **6-07**, indicative of an increase in bond order. Also the Cr–Ge–C angle significantly widened to almost linear in **6-09** (176.0°), from a highly bent geometry in **6-07**. Also worth noting is that a small shortening of the Ge-C bond is observed from **6-07** to **6-09** (i.e. 0.047 Å), due to the change in the hybridization of the Ge atom, owing to its change in geometry from bent to linear.

The molecular structure of the tungsten analogue **6-11** tells a similar story, with a W-Ge bond length of 2.2767(14) Å, with a shortening of >0.4 Å compared to the singly bonded precursor complex **6-08**. Moreover, the W–Ge–C angle has widened significantly from **6-08** to **6-11** (170.9°), and once again a small shortening of the Ge–C was observed, due to a change in hybridisation of the Ge centre.

A number of other transition metal-germylynes containing different ligands and transition metals have been reported by various groups [10]. However, with the exception of two transition metal-germylyne complexes, which dimerise in the solid state to give $L_nM{\equiv}Ge{-}Ge{\equiv}ML_n$ compounds (M = Mo, W) [10e], all contain bulky alkyl or aryl substituents on the germanium centre.

6.1.1.2 Transition Metal Stannylyne Complexes

In 2002, Power and co-workers published their findings on reactions between the three group 6 metal salt complexes Na[Cp$M(CO_3)$] (M = Cr, Mo, W) and two bulky terphenyl tin(II) chloride complexes [ArSnCl] (Ar = Ar^{Mes}, Ar^{Tripp}), i.e. analogous reactions to those which gave the germylyne complexes **6-02** and **6-06** [11]. However, in contrast to germanium, the reactions between all three group 6 salt complexes and both terphenyl tin chloride precursors yielded the singly bonded transition metal-stannylene complexes [Cp$(CO)_3$M–SnAr]. Unfortunately, none of the complexes were found to eliminate CO to give a transition metal-stannylyne complex.

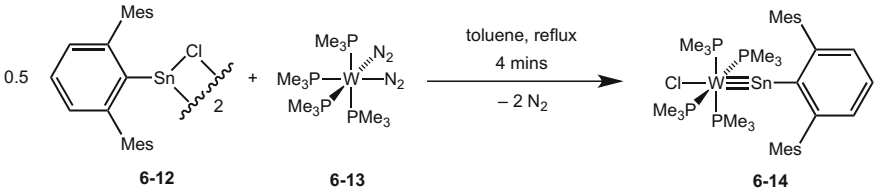

Scheme 6.4 Preparation of the first transition metal-stannylyne complex **6-14**

The first transition metal-stannylyne complex was reported the following year by Filippou and co-workers, with the oxidative addition reaction between the terphenyl tin chloride $[\{Ar^{Mes}Sn(\mu\text{-}Cl)\}_2]$ **6-12** and the neutral tungsten(0) complex *cis*-$[W(N_2)_2(PMe_3)_4]$ **6-13** in refluxing toluene (Scheme 6.4) [12]. The reaction mixture rapidly changed colour upon heating, from yellow-orange to dark red-brown, indicating the formation of the tungsten-stannylyne complex $[Cl(Me_3P)_4W{\equiv}SnAr^{Mes}]$ **6-14**. No intermediates could be detected by IR spectroscopy during the fast reaction, which was complete in just a few minutes.

Complex **6-14** was crystallographically characterised, revealing a two-coordinate tin centre with an essentially linear geometry (W–Sn–C = 178.2°). This is in contrast to the previously reported "distannyne" $[Ar^{Dipp}SnSnAr^{Dipp}]$, which has a *trans*-bent structure, with Sn-Sn-C angles of 125.2° [13]. The tungsten centre occupies a slightly distorted octahedral geometry, with the chloride ligand *trans* to the stannylyne ligand. The tungsten-tin bond length (2.4901(7) Å) was unsurprisingly found to be the shortest known at the time, shorter than a number of previously reported W-Sn single and double bonds (2.71–2.81 Å) [14].

Later in 2003, the same group reported a second tungsten-stannylyne complex (viz. *trans*-$[Cl(dppe)_2W{\equiv}SnAr^{Mes}]$ **6-15** (dppe = $\{Ph_2PCH_2\}_2$), prepared by a similar method used to access **6-14**, differing only by the phosphine groups coordinated to the tungsten [15]. Crystallographic analysis of **6-15** found it to possess a very similar structure to **6-14**, with an essentially linear tin centre (W–Sn–C = 175.9°) and a similar W-Sn bond length (2.504(1) Å).

DFT calculations, using the B3LYP/6-311G* level of theory, were performed on a simplified model of **6-15**, *trans*-$[Cl(PH_3)_4W{\equiv}SnMe]$ **6-15a** and the related carbyne complex *trans*-$[Cl(PH_3)_4W{\equiv}CMe]$ **6-15b** for comparison [15]. Both compounds were found to possess a C_s-symmetric minimum structure with a linear geometry at the Sn or C atom. The calculated MOs show that both W-Sn and W-C bonds are made up of a single σ bond, which is polarised towards the group 14 element, and two π bonds, which are polarised towards the tungsten. The polarisation of both the σ and π bonds is greater in the model stannylyne complex **6-15a**, than in the model carbyne complex **6-15b**, due to a larger difference in electronegativities of the two elements. Moreover, a comparison of the calculated partial charges in both complexes showed that the tungsten atom in **6-15a** is considerably more negatively charged than that in **6-15b**. In addition, the carbyne atom in **6-15b** was calculated to be essentially electro-neutral, whereas the Sn atom in

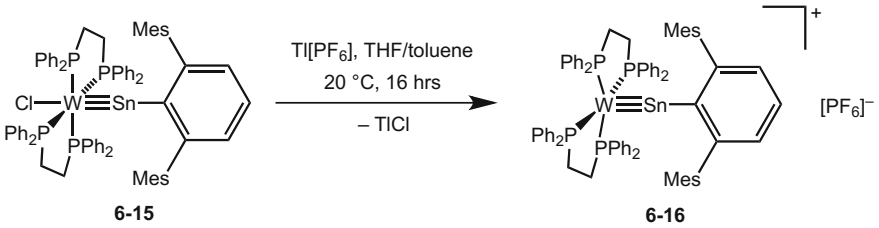

Scheme 6.5 Preparation of **6-16**

6-15a has a considerable positive charge, again due to the difference in electronegativies of the two elements.

In the same publication, compound **6-15** was reacted with the halide extraction reagent Tl[PF_6] in THF at room temperature (Scheme 6.5). Workup followed by crystallisation of the reaction mixture gave the cationic stannylyne complex [$(dppe)_2W{\equiv}SnAr^{Mes}$][$PF_6$] **6-16** as highly air sensitive green crystals in a 51 % yield.

A crystallographic analysis of **6-16** found the cationic complex to be well separated from the PF_6 anion (closest W···F and Sn···F distances >6.8 Å). The extraction of the chloride ligand has resulted in a decrease in coordination number of the tungsten metal centre, from six in **6-15** to five in **6-16**. The tungsten centre in **6-16** was found to possess a square pyramidal geometry, with the stannylyne ligand as the best π-acceptor group occupying the apical position. The W-Sn bond length in **6-16** (2.4641(7) Å) is slightly shorter than that in the neutral complex **6-15** (2.504 (1) Å), consistent with the lower coordination number of the tungsten atom. Structurally, the tin centre remains essentially unchanged, maintaining its near linear geometry (W–Sn–C = 178.8°).

Recently, Filippou and co-workers have reported a second cationic stannylyne complex *trans*-[$H(dmpe)_2Mn{\equiv}SnAr^{Mes}]^+$ **6-17** (dmpe = $\{Ph_2PCH_2\}_2$) [16], synthesised by the reaction of the same terphenyl tin chloride **6-12** with *trans*-[H $(dmpe)_2Mn(H_2)$], followed by halide extraction. Compound **6-17** is the first example of manganese-tetrelyne complex.

6.1.1.3 Transition Metal Plumbylyne Complexes

In 2004, Filippou and co-workers were also the first to report a stable transition metal-plumbylyne complex (viz. *trans*-[$Br(Me_3P)_4Mo{\equiv}PbAr^{Tripp}$] **6-18**) [17]. The complex was synthesised by the reaction between the bulky terphenyl lead(II) bromide complex [$\{Ar^{Tripp}Pb(\mu\text{-}Br)\}_2$] **6-19** and *cis*-[$Mo(N_2)_2(PMe_3)_4$] **6-20** (the molybdenum analogue of **6-13**), in toluene at room temperature (Scheme 6.6). Workup and subsequent fractional crystallisation of the reaction mixture gave the plumbylyne complex **6-18** as red-brown crystals.

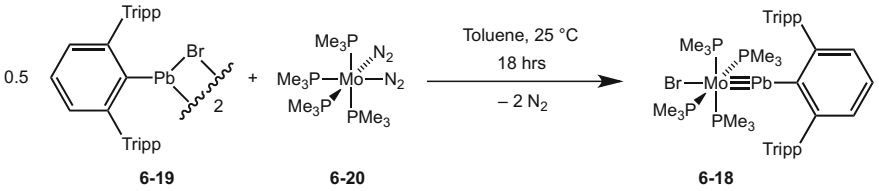

6-19 **6-20** **6-18**

Scheme 6.6 Preparation of **6-18**, the first transition metal plumbylyne complex

Due to the extremely large and diffuse orbitals of row 6 elements in general, multiple bonding is rare; complex **6-18** was the first example of a complex containing a row 6 main group element forming a triple bond. The complex was found to be highly air sensitive, but surprisingly thermally stable, decomposing only at temperatures above 194 °C in the solid state.

Complex **6-18** was crystallographically characterised, revealing a structure similar to its lighter analogues. The lead centre is two-coordinate, possessing an essentially linear geometry (177.8°), with a short Mo-Pb bond length of 2.5495(8) Å. The Mo-Pb bond length in **6-18** is much shorter than in previously reported single bonded complexes, e.g. [{$(CO)_3CpMo$}$_2$Pb] (Mo-Pb = 2.9845(7) Å) [18], where the lead atom is also two-coordinate, but with a bent geometry. The structure of **6-18** is in contrast with the previously reported "diplumbyne" [$Ar^{Tripp}PbPbAr^{Tripp}$], which possesses a *trans*-bent structure (Pb–Pb-C = 94.3°), and a Pb–Pb single bond (3.1881(1) Å) [19].

Calculations, using the BP86/LANL2DZ level of theory, were performed on a simplified model of complex **6-18** (*trans*-[$Br(H_3P)_4Mo{\equiv}PbPh$], **6-18a**) and the related carbyne complex (*trans*-[$Br(H_3P)_4Mo{\equiv}CPh$], **6-18b**), the results of which mirrored those for the stannylyne complex **6-15a**. That is, the structure of **6-18a** is best modelled as having a Mo-Pb triple bond with a C_{2v}-symmetric minima, resulting in a linear Pb geometry. The Mo-Pb bond in **6-18a** is more polarised than the Mo-C bond in **6-18b**, due to the molybdenum centre being considerably more negatively charged in **6-18a** than in **6-18b**.

Later in 2004, the group published a follow up paper on the synthesis and characterisation of the tungsten-plumbylyne analogues (viz. *trans*-[X$(Me_3P)_4W{\equiv}PbAr^{Tripp}$] (X = Br, **6-21-Br**; I, **6-21-I**) [20]. The complexes possess a very similar structure to that of **6-18**, with a Pb-W bond length of 2.5464(5) Å (for **6-21-Br**) and an essentially linear lead centre (W–Pb–C = 177.5°). Complex **6-21-Br** was further reacted with the halide extracting reagents M[BAr_4] (M = Li or Na, Ar = C_6F_5 or 3,5-$(CF_3)_2$-C_6H_3), in the presence of either phenylnitrile or PMe_3, to give the cationic tungsten-plumbylyne complexes, *trans*-[L$(Me_3P)_4W{\equiv}PbAr^{Tripp}$][$BAr_4$] (L = PhCN, Ar = 3,5-$(CF_3)_2$-$C_6H_3$, **6-22**; L = PMe_3, Ar = C_6F_5, **6-23**), in relatively good yields (Scheme 6.7).

The solid state structures of compounds **6-22** and **6-23** closely resemble those of the cationic tungsten-stannylyne **6-15**, but in that complex, the tungsten is five-coordinate, occupying a square-pyramidal geometry. The geometry of the tungsten

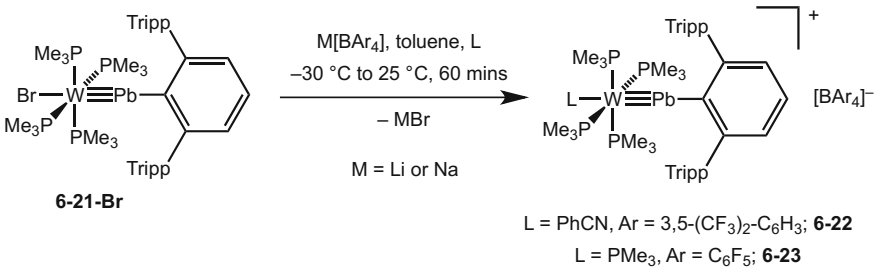

Scheme 6.7 Preparation of **6-22** and **6-23**

atoms in **6-22** and **6-23** is octahedral, due to the coordination of either a phenylnitrile or a PMe_3 ligand *trans* to the plumbylyne ligand. As in **6-16**, there are no close contacts between the anion and the metal centres in either complex. Compounds **6-22** and **6-23** possess two-coordinate, near linear lead centres (W–Pb–C = 171.7° for **6-22** and 177.5° for **6-23**), and W−Pb bond lengths (2.5520(6) Å for **6-22** and 2.5744(2) Å for **6-23**) comparable with those of the neutral complexes **6-18** and **6-21**.

In 2008, the same group reported their latest findings on a new method to prepare plumbylyne complexes, which was via activation of a Pb−N bond [21]. The reaction between the bulky terphenyl lead(II) amide $[\{Ar^{Tripp}Pb(\mu\text{-}NMe_2)\}_2]$ and $[(\eta^2\text{-}CH_2PMe_2)(H)(PMe_3)_4W]$ in toluene at 80 °C resulted in the activation of the Pb–N bond, and consequent formation of the tungsten-plumbylyne complex *trans*-$[H(Me_3P)_4W{\equiv}PbAr^{Tripp}]$ **6-24**. Complex **6-24** is essentially isostructual with the previously reported tungsten-plumbylyne **6-21**, only with a hydride ligand *trans* to the plumbylyne ligand instead of a bromide or iodide. The change was found to have little effect on the overall structure of the complex, but could show differences in further reactivity.

6.1.1.4 Transition Metal-Silylyne Complexes

The isolation of a transition metal-silylyne complex, the last in the series of metallo-tetrelynes, eluded organometallic chemists for many years. As mentioned at the start of this chapter, in 1992, Tilley and co-workers successfully isolated the base stabilised silylyne complex $[(Me_3P)_2(Cp^*)RuSi\{S(p\text{-tol})\}(bipy)][OTf]_2$ **6-01** (*p*-tol = 4-Me-C_6H_4), but due to the silicon centre being four-coordinate (Fig. 6.1), it cannot be considered as a "true" silylyne complex [3]. Tilley and co-workers came close again in 2003, with what they described as "A Transition-Metal Complex with Considerable Silylyne Character" [22]. The complex in question was $[Cp^*(dmpe)(H)MoSiMes][B(C_6F_5)_3]$ **6-25** (dmpe = 1,2-bis(dimethylphosphanyl) ethane). However, as the hydride ligand could not be accurately located, likely because it was bridging the two metal centres (Fig. 6.1), this cannot be considered as a "true" silylyne complex either.

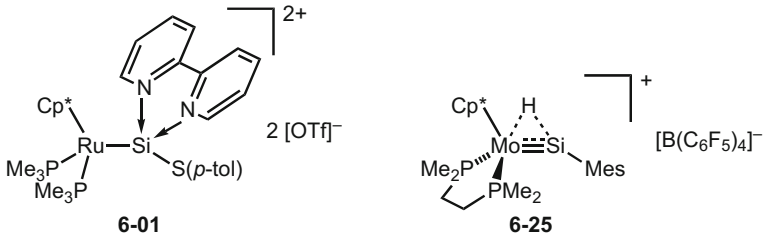

Fig. 6.1 Diagrammatic representations of the two transition metal-silicon bonded complexes, **6-01** and **6-25**, isolated by Tilley and co-workers that contain silylyne character. p-tol = 4-Me-C_6H_4, Tf = triflate

It wasn't until 2010, with the work of Filippou and co-workers, that a "true" silylyne was isolated [23]. The complex was synthesised by firstly heating a toluene solution of the NHC coordinated terphenyl silicon(II) chloride complex [Ar^{Tripp}SiCl (TMC)] **6-26** (TMC = :C{N(Me)C(Me)}$_2$) with Li[CpMo(CO)$_3$] **6-27** to 100 °C, to give rapid generation of the silylene complex [Cp(CO)$_2$Mo = Si(TMC)Ar^{Tripp}] **6-28** in moderate yields (Scheme 6.8). The silylene complex was subsequently treated with the carbene trapping reagent [B(4-Me-C_6H_4)$_3$] and heated at reflux in *o*-xylene for 10 min, which favored the removal of the NHC from the complex, and consequent formation of the silylyne [Cp(CO)$_2$Mo≡SiAr^{Tripp}] **6-29** (Scheme 6.8).

Both the silylene complex **6-28** and the silylyne complex **6-29** were crystallographically characterised. The molecular structure of **6-28** shows it to possess a three-coordinate silicon centre, with a Mo-Si double bond (2.3476(6) Å) in the range of previously reported molybdenum arylsilylene complexes (2.29–2.39 Å) [22, 24]. The Si-C_{NHC} bond length (1.943(2) Å) is comparable to that in other Si-TMC complexes, but importantly slightly longer than that in **6-26** (1.937(2) Å). The silicon centre has a trigonal pyramidal geometry (sum of the angles = 357.0°), but due to the steric demands of the large Ar^{Tripp} ligand, is severally distorted. The Mo−Si−C_{Ar} angle is considerably widened to 145.3°, whereas the C_{Ar}–Si–C_{NHC} angle is lowered to 100.4°, both of which should favour the rehybridization of silicon.

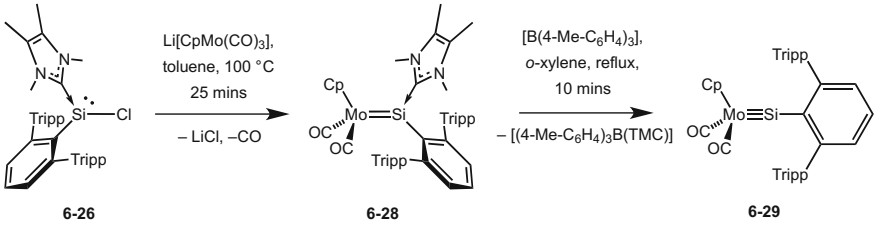

Scheme 6.8 Preparation of **6-29**, the first transition metal-silylyne complex, through the silylene **6-28**

The molecular structure of the silylyne **6-29** shows it to be essentially isostructual to the germanium analogue **6-06**, with a two-coordinate silicon centre occupying a near linear geometry (Mo–Si–C = 173.5°). The Mo−Si bond length is very short (2.2241(7) Å), 0.12 Å shorter than the double bond in the starting material **6-28**, but surprisingly not quite as short as Tilley's hydride bridged complex **6-25** (2.219(2) Å) [22].

In 2011, the group released a second publication outlining the reactivity of the silylyne complex **6-29** towards a range of nucleophiles and the reducing agent KC_8 [25]. The nucleophiles reacted with **6-29** by attack at the silicon centre, whereas the reaction of the complex with KC_8 led to C–C bond activation of the Ar^{Tripp} ligand in a silicon redox reaction. The results of these reactivity studies are outlined in Scheme 6.9.

In the group's most recent paper on silylyne chemistry, the synthesis of a second compound possessing a silylyne ligand in the chromium cationic complex Cp*$(CO)_2Cr{\equiv}Si(SIDipp)][BAr^F{}_4]$ **6-30** (SIDipp = :C{DippNCH$_2$}$_2$) was reported [26]. The complex was synthesised by halide extraction from the chromium-silylene complex [Cp*$(CO)_2$Cr = SiBr(SIDipp)] **6-31** with Na[$BAr^F{}_4$] at room temperature (Scheme 6.10). Workup followed by crystallisation of the reaction mixture gave **6-30** in high yields as dark red crystals. In contrast to the previously reported silylyne complex **6-29**, complex **6-31** possesses a bulky neutral NHC substituent coordinating to the metal centre, rather than an anionic terphenyl ligand.

Complex **6-30** was crystallographically characterised, and shown to possess a similar structure to **6-29**, in that it possesses a two-coordinate silicon centre with near linear geometry (Cr–Si–C = 169.8°). The chromium centre occupies a three-legged piano-stool geometry, similar to the molybdenum centre in **6-29**. The Cr–Si bond length was found to be very short (2.1220(9) Å) as prior

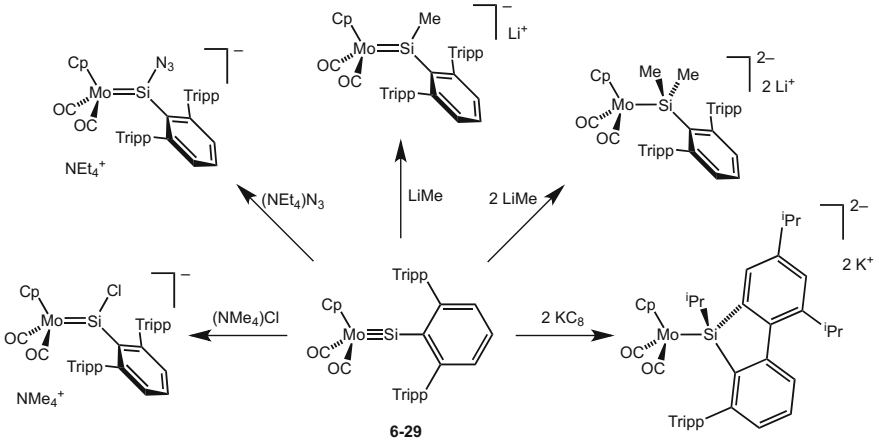

Scheme 6.9 Overview of the reactivity of the silylyne complex **6-29** towards a range of nucleophiles and KC_8

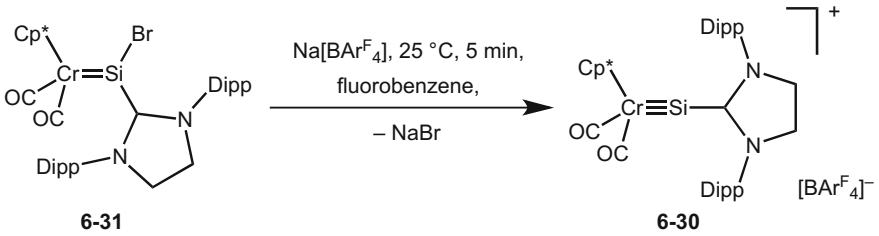

Scheme 6.10 Preparation of **6-30**

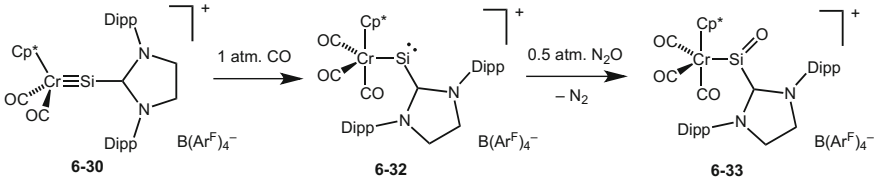

Scheme 6.11 Preparation of the first three-coordinate silanone complex **6-33**, through the chromium-silyene complex **6-32**

calculations had predicted, i.e. 0.05 Å shorter than the Cr–Si double bond in the starting material **6-31**.

The silylyne complex **6-30** was found to rapidly react with one atmosphere of CO in fluorobenzene at room temperature, to give the singly bonded silylene salt [Cp*$(CO)_3$Cr–Si(SIDipp)][BAr$^F_4$] **6-32** (Scheme 6.11). This reaction indicates that the formation of silylynes by CO elimination may not be favourable, as was seen in the case of germylynes and heavier analogues. This is one possible reason why a silylyne complex had not been isolated earlier. Remarkably, complex **6-32** further reacted with one equivalent of N_2O, yielding the so-called silanone complex [Cp*$(CO)_3$Cr–Si(O)(SIDipp)][B(Ar^F)$_4$] **6-33**, containing a terminal Si=O double bond. Complex **6-33** is unprecedented, and remains the only complex to possess a three-coordinate silicon centre with a formal Si=O double bond.

6.2 Research Outline

With the exception of two dimeric metallo-germylynes, which both contain a $L_nM{\equiv}Ge–Ge{\equiv}ML_n$ (M = Mo, W) bonding structure [10e], all reported transition metal tetrelyne complexes contain either a bulky alkyl, aryl or NHC substituent coordinating to the group 14 element. This results in all complexes possessing a similar $L_nM{\equiv}E–C$ (M = a transition metal, E = Si, Ge, Sn, Pb) bonding motif.

On the other hand, transition-metal carbyne complexes have been isolated with a many substituents bonded to the two-coordinate carbon atom. One interesting class of these are the transition-metal aminocarbynes, $L_nM{\equiv}C{-}NR_2$, where the triply bonded carbon atom possesses an NR_2 substituent. In these complexes, the amino substituents are often planar, as their bonding typically exhibits a significant contribution from their 2-azavinylidene canonical form, i.e. $L_n^-M{=}C{=}N^+R_2$. This causes transition-metal aminocarbyne complexes to show differing reactivity to those containing organocarbyne ligands.

As there are currently no heavier analogues of transition-metal aminocarbynes reported, i.e. transition-metal aminotetrelynes, and also because transition-metal tetrelyne complexes are currently a topic of considerable interest, we sought to prepare the first example of a transition-metal aminotetrelyne complex. As is the case with the previously reported organotetrelynes, it was proposed that an amino substituent of considerable steric bulk would be needed to stabilise such a complex. As the bulky amido ligands have been shown in previous chapters to have similar stabilising properties to terphenyls, it was proposed that these could stabilise a transition-metal aminotetrelyne complex. With that in mind, a range of bulky amido group 14 element chloride complexes, comprising of [Ar*($SiMe_3$)$NSiCl_3$] **6-34** [27], [Ar*($SiMe_3$)NSnCl] **6-35**, [{Ar*($SiMe_3$)NPb(μ-Cl)}$_2$] **6-36**, [Ar*(Mes)NGeCl] **6-37**, [Ar*(Ph)NGeCl] **6-38** and [Ar*($SiMe_3$)NGeCl] **6-39** were to be reacted with the molybdenum salt complex Na[CpMo$(CO)_3$] **6-04** in an attempt to isolate a molybdenum aminotetrelyne complex. If successful, the aminotetrelyne complex was to be investigated to see whether it possesses a significant contribution from its 2-azavinylidene canonical form, i.e. $L_n^-Mo{=}E{=}N^+R_2$.

6.3 Results and Discussion

6.3.1 Preparation of Two Molybdenum Aminogermylene Complexes

The 1:1 reactions of the six amido group 14 element chloride complexes **6-34–6-39**, with the molybdenum sodium salt complex Na[CpMo$(CO)_3$] **6-04** led to varying outcomes. The addition of **6-04** to a THF solution of the amido silicon trichloride complex [Ar*($SiMe_3$)$NSiCl_3$] **6-34** at room temperature, resulted in no reaction, even after stirring for 24 h. Heating the reaction mixture at reflux resulted in slow decomposition of the starting materials over the course of several days. In contrast, the addition of a THF solution **6-04** to toluene solutions of [Ar*($SiMe_3$)NSnCl] **6-35** and [{Ar*($SiMe_3$)NPb(μ-Cl)}$_2$] **6-36** at −80 °C, produced instant colour changes from pale yellow to dark red-brown. Upon warming both reaction mixtures to room temperature, decomposition of the starting materials was observed by the precipitation of elemental metal (at approx. −40 °C for tin and −70 °C for lead). ^{1}H NMR spectroscopy performed on the crude reaction mixtures (after warming to

room temperature) showed complete decomposition of the amido metal chloride complexes had occurred, to give the free amine Ar*($SiMe_3$)NH. Also worth mentioning, is that the addition of a THF solution of **6-04** to a toluene solution of [Ar*(Mes)NGeCl] **6-37** at −80 °C also produced an instant colour change, from pale yellow to orange. However this reaction led to an unidentifiable mixture of products.

When a THF solution of **6-04** was slowly added to a solution of [Ar*(Ph)NGeCl] **6-38** or [Ar*($SiMe_3$)NGeCl] **6-39** at −80 °C, an instant colour change from pale yellow to orange was observed. Both reaction mixtures were slowly warmed to room temperature and stirring for a further 4 h, whereupon workup and subsequent crystallisation led to the isolation of the two molybdenum aminogermylene complexes [$Cp(CO)_3Mo$–GeN(R)Ar*] (R = Ph, **6-40**; R = $SiMe_3$, **6-41**) as orange crystals in moderate yields (Scheme 6.12).

Complexes **6-40** and **6-41** are both thermally stable in the solid state, both decomposing at temperature >160 °C. It is worth noting that both complexes are resistant to CO elimination under ambient conditions, as complete recovery of the starting material can be obtained after a stirring solutions of either complex at room temperature for several days. This is in contrast to the implied intermediate in the synthesis of [$Cp(CO)_2Mo{\equiv}GeAr^{Tripp}$] **6-06**, i.e. [$Cp(CO)_3Mo$–$GeAr^{Tripp}$], which could not be isolated, as it spontaneously eliminates CO at temperatures $\leq$0 °C [7].

IR spectroscopy was performed on the two complexes (as Nujol mulls), which showed a series of strong CO stretching bands in the ranges 1972–1867 cm^{-1} for **6-40** and 1966–1830 cm^{-1} for **6-41**. This is comparable to other molybdenum-tetrelene complexes bearing the same "$Cp(CO)_3Mo$" unit, e.g. [$Cp(CO)_3Mo$–$SnAr^{Mes}$] (1960–1878 cm^{-1}) [11], which have been calculated to exhibit minimal donation from the filled transition metal based orbitals into the empty p orbital at the group 14 centre [28]. In addition, ^{13}C NMR spectroscopy performed on solutions of both complexes in C_6D_6 shows a broad resonance for the three carbonyls at 225.0 ppm for **6-40**, and 226.1 ppm for **6-41**. This is once again comparable to [$Cp(CO)_3Mo$–$SnAr^{Mes}$], which showed a broad resonance at 226.6 ppm.

To investigate the solid-state structure of the molybdenum-germylenes, complexes **6-40** and **6-41** were crystallographically characterised (Fig. 6.2). The two

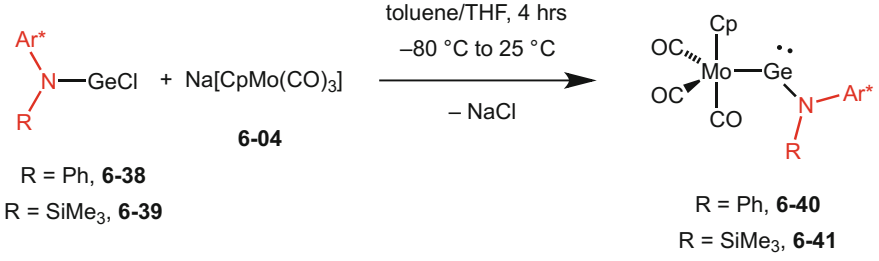

Scheme 6.12 Preparation of the molybdenum aminogermylene complexes **6-40** and **6-41**

complexes represent the first examples of two-coordinate molybdenum-germylene complexes, although one three coordinate example has recently been reported [29]. Complexes **6-40** and **6-41** are essentially isostructural, with Mo−Ge bond lengths (2.7100(4) Å for **6-40** and 2.7377(3) Å for **6-41**) comparable to the sum of the single bond covalent radii for the two elements (2.74 Å) [30]. The bond lengths are also comparable to the W–Ge bond in the related tungsten-germylene singly bonded complex $[Cp(CO)_3W–GeAr^{Tripp}]$ **6-08** (W–Ge = 2.681(3) Å) [7]. These comparisons suggest that there is little multiple bonding character between the germanium and molybdenum centres in the two complexes. It is also worth noting that in both complexes the coordinating nitrogen atom is planar (sum of angles = 360° for both **6-40** and **6-41**). However, as the N–Ge bond lengths (1.879(2) Å for **6-40** and 1.8871(18) Å for **6-41**) are longer than for the precursor complex **6-39** (1.855(3) Å) [27], and also close to the sum of the covalent radii of the two elements (1.91 Å) [30], it is unlikely that the bonds possess much, if any multiple bond character. The germanium centre in both complexes is two-coordinate, occupying a bent geometry (Mo–Ge–N = 115.9° for **6-40** and 118.8° for **6-41**). This strongly suggests the presence of a stereochemically active lone pair on the germanium centre in both complexes, as was calculated for the model complex $[Cp(CO)_3Mo–GeMe]$ [28]. In addition, there are no close interactions observed between the germanium centre and the flanking phenyl rings in either complex (closest $Ge\cdots C_{Phenyl}$ = 3.34 Å for **6-40**; 3.16 Å for **6-41**).

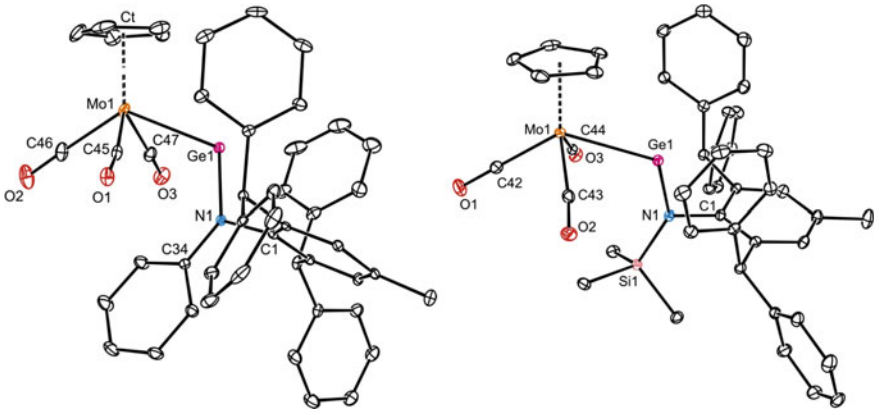

Fig. 6.2 Thermal ellipsoid plots (25 % probability surface) of the molecular structures of **6-40** (*left*) and **6-41** (*right*). Hydrogen atoms have been omitted for clarity. Selected bond lengths (Å) and angles (°) for **6-40**: Mo(1)-Ge(1) 2.7100(4), Ge(1)-N(1) 1.879(2), Mo(1)-Ct(1) 2.013(1), Mo−Ge−N 115.90(7), C(34)-N(1)-C(1) 112.6(2). Selected bond lengths (Å) and angles (°) for **6-41**: Mo(1)-Ge(1) 2.7377(3), Ge(1)-N(1) 1.8871(18), Mo(1)-Ct(1) 2.023(1), Mo−Ge−N 118.80(5), Si(1)-N(1)-C(1) 114.61(13)

In an attempt to further understand the electronic structure of the two molybdenum-germylene complexes, quantum chemical calculations (B3LYP/6-311G(d)/LANL2DZ and BP86/6-311G(d)/LANL2DZ) were performed on **6-41** in the gas phase. As **6-40** is essentially isostructural to **6-41**, we would expect the results for that complex to be similar. The calculated geometry of **6-41** optimized to be close to that in the solid-state structure, but with slight overestimations of the Ge–Mo (+0.076 Å) and Ge–N (+0.012 Å) bond lengths (calculated distances from the B3LYP calculations; Mo–Ge 2.814 Å, Ge–N 1.899 Å). Analysis of the frontier orbitals of **6-41** found an electronic structure similar to those of related germylenes, e.g. [$Cp(CO)_3Mo$–GeMe] [28] and **6-39** [27]. That is, the HOMO has significant Ge lone pair character, whereas the LUMO is consistent with an empty p orbital at the germanium centre (Fig. 6.3). Also worth noting is that the p-orbital lone pair of the N centre is associated with HOMO-6, which shows negligible interactions with the empty p-orbital on the germanium centre (Fig. 6.3).

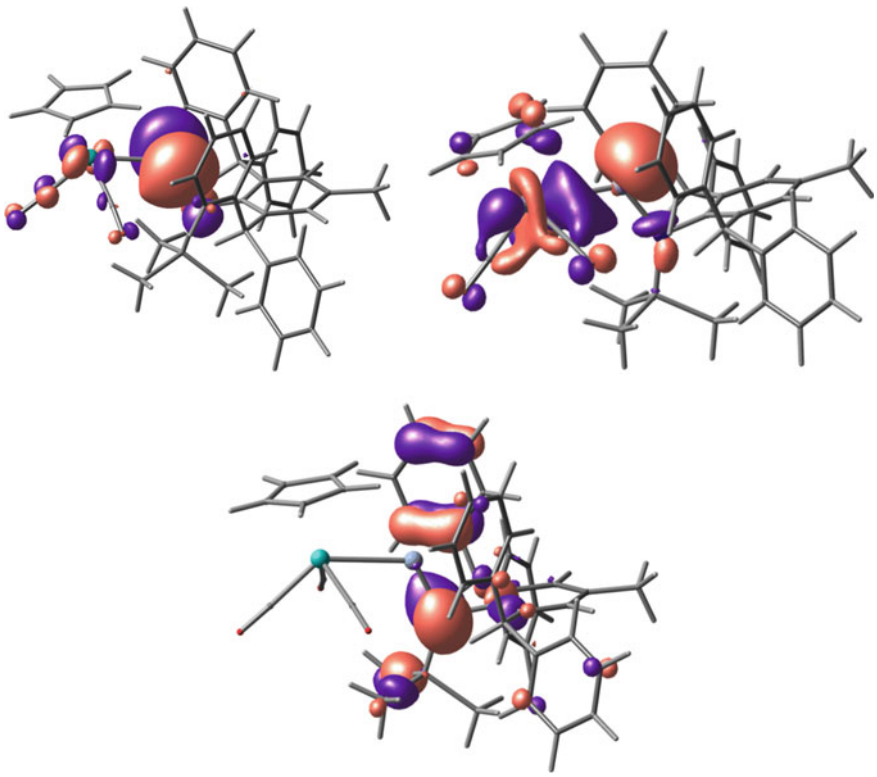

Fig. 6.3 Selected frontier orbitals calculated for **6-41**. LUMO (*top-left*), HOMO (*top-right*) and HOMO-6 (*bottom*). Iso-surface value 0.03 a.u.

6.3.2 *Preparation of a Molybdenum Aminogermylyne Complex*

Both aminogermylene compounds **6-40** and **6-41** were tested for CO elimination, in an attempt to form Mo-Ge triply bonded complexes. Power and co-workers induced CO elimination from their chromium- and tungsten germylene complexes **6-07** and **6-08**, by either refluxing in toluene or irradiating with UV light [7]. Therefore these two methods were tested here.

When a toluene solution of **6-40** was heated at reflux for 1 h, no obvious colour change was observed. ^{1}H NMR spectroscopy preformed on the reaction mixture revealed that no new product had formed, except for the generation of a small amount (≈10 %) of the free amine Ar*(Ph)NH, formed from the decomposition of the starting material. Refluxing the reaction mixture overnight led to almost complete decomposition of the starting material. A similar result was observed when irradiating a solution of the complex in C_6D_6 with UV light (λ = 254 nm) from a mercury vapour lamp. In contrast, refluxing a toluene solution of **6-41** for 1 h, resulted in the elimination of one molecule of CO from the starting material to cleanly form [$Cp(CO)_2Mo{\equiv}GeN(SiMe_3)Ar^*$] **6-42** in essentially quantitative yields (Scheme 6.13). Irradiation of a solution of **6-41** in C_6D_6 with UV light for 20 min also led to quantitative conversion to **6-42**.

Compound **6-42** is a thermally stable complex, decomposing at temperatures >220 °C in the solid state. IR spectroscopy performed on the complex (Nujol mull) shows two distinct carbonyl stretches at 1926 and 1853 cm^{-1}, in similar positions to those in the related terphenyl complex [$Cp(CO)_2Mo{\equiv}GeAr^{Mes}$] **6-02** (1930 and 1872 cm^{-1}). It might be thought that, if there was a significant bonding contribution from the heterovinylidene resonance form of **6-42**, i.e. [$Cp(CO)_2^-Mo{=}Ge{=}N^+(Ar^*)(SiMe_3)$], these bands might occur at lower wavenumbers. This is because the Mo centre of the heterovinylidene form should have a higher density than that in the germylyne form, i.e. [$Cp(CO)_2Mo{\equiv}GeN(Ar^*)(SiMe_3)$], thereby leading to a weakening of its C–O bonds relative to those in the germylyne form. This may well suggest that the germylyne resonance form of **6-42** predominates. Although generally higher frequency bands are seen for related complexes incorporating carbyne and aza-vinylidene ligands, due to those ligands being more π-acidic than the

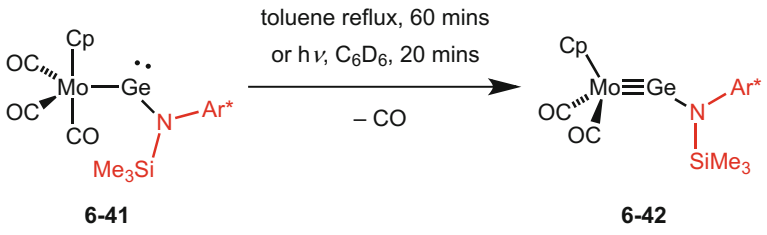

6-41 **6-42**

Scheme 6.13 Preparation of the molybdenum aminogermylyne complex **6-42**

tetrelynes, the trend to lower frequency CO stretching bands for azavinylidene complexes relative to carbyne complexes is well-established [31], e.g. [Cp$(CO)_2$Mo≡CXyl] (ν = 1992 and 1919 cm^{-1}) [32]. and [Cp$(CO)_2$Mo=C=N^+Et_2] (ν = 1952 and 1866 cm^{-1}) [33]. In addition, ^{13}C NMR spectroscopy performed on the complex shows one broad resonance for the two carbonyls, at 231.3 ppm. This is once again similar to the situation with the related terphenyl complex [Cp$(CO)_2$Mo≡GeAr^{Tripp}] **6-06** (231.4 ppm) [7].

To further investigate the bonding in complex **6-42**, its X-ray crystal structure was determined (Fig. 6.4). The molecular structure of **6-42** shows a Mo−Ge bond length of 2.2811(4) Å, which is a shortening of 0.45 Å from the starting complex **6-41**. The Mo−Ge bond length is only slightly longer than the Mo–Ge triple bonds in two related terphenyl germylyne complexes (2.271(1) Å, **6-02**; 2.272(8) Å, **6-06**). In fact, it is shorter than the majority of known molybdenum germylyne bonds, which range from 2.271 to 2.318 Å [4, 7, 10]. In addition, the Ge−Mo bond length in **6-42** is also shorter than that calculated for the model complex [Cp$(CO)_2$Mo≡GeMe] (2.309 Å) [28]. This is all in good agreement with the complex existing predominantly in its triply bonded germylyne form. However, as the angle of the two-coordinate germanium centre has significantly widened from the precursor complex (Mo–Ge–N = 118.8° in **6-41** to 155.8° in **6-42**), it is still a long

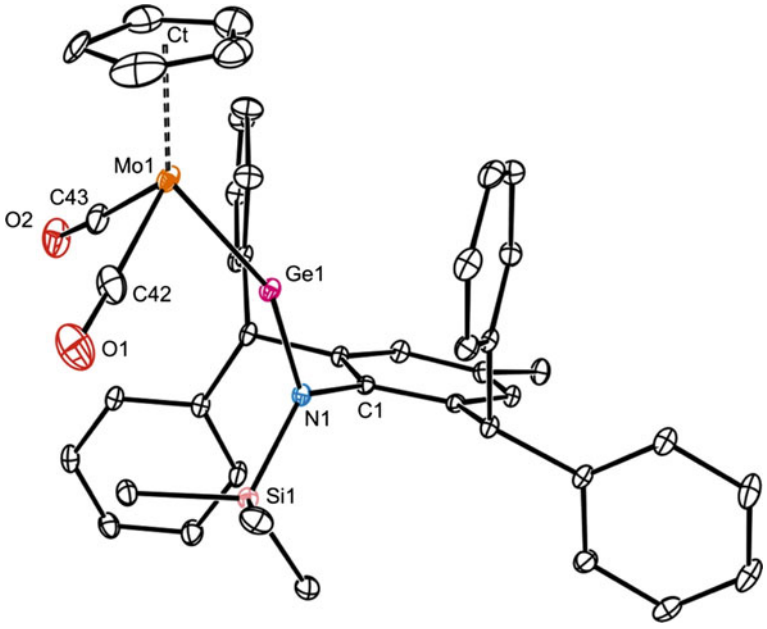

Fig. 6.4 Thermal ellipsoid plot (25 % probability surface) of the molecular structure of **6-42**. Hydrogen atoms have been omitted for clarity. Selected bond lengths (Å) and angles (°): Mo(1)-Ge(1) 2.2811(4), Ge(1)-N(1) 1.812(2), Mo(1)-Ct(1) 2.006(1), Mo(1)-Ge(1)-N(1) 155.81(8), Si(1)-N(1)-C(1) 124.5(2)

way from the linear geometry expected for these complexes. A bending of this degree should not allow for optimal σ and π-orbital overlap between the Mo and Ge centres. This distortion from linear is likely due to steric interactions between the bulky Ar* substituent and the $CpMo(CO)_2$ moiety. If the Mo–Ge–N angle in **6-42** was near linear, this buttressing would be significantly increased.

The Ge–N bond length in the complex is slightly shorter than that of the precursor complex [1.812(2) Å for **6-42** compared with 1.8871(18) Å for **6-41**], which could signify some multiple bond character, and thus a contribution from the [$Cp(CO)_2^-Mo{=}Ge{=}N^+(Ar^*)(SiMe_3)$] canonical form. However, once again for this to be optimal, the germanium centre would need to possess a linear geometry. The above discussion on the molecular structure of **6-42,** along with IR spectroscopy, suggests that the complex predominantly exists in its 'triply' bonded germylyne form, at least in the solid state.

To assign the extent of the multiple bonding in **6-42**, quantum chemical calculations (B3LYP/6-311G(d)/LANL2DZ and BP86/6-311G(d)/LANL2DZ) were carried out on the complex in the gas phase. The geometries of the model complex optimized to be close that seen in the solid-state structure (Fig. 6.4), but with slight over estimations of the Mo–Ge and Ge–N bond lengths (calculated distances from the B3LYP calculations; Mo–Ge 2.317 Å, Ge–N 1.844 Å). Analysis of the frontier orbitals of **6-42**, revealed the HOMO and HOMO-2 have character strongly reminiscent of orthogonal Mo–Ge π-bonds (Fig. 6.5), however the σ component seems to be distributed between several MO's. The HOMO-1 is a largely metal based orbital, whereas the LUMO is reminiscent of a Mo–Ge π^*-antibonding orbital (Fig. 6.5). Similar to **6-41**, none of the MO's of **6-42** suggest that any significant Ge–N π-bonding is present. These MO calculations are in agreement with the complex possessing a "triple" bond, with little Ge–N multiple bond character, even though the germanium centre is significantly bent.

In an attempt to quantify the Mo–Ge and Ge–N bond orders in the complex, Wiberg bond index (WBI) calculations (B3LYP/6-311G(d)/LANL2DZ) were carried out on **6-42** (and the singly bonded precursor complex **6-41** for comparison). The Mo–Ge WBI values calculated for complexes **6-41** and **6-42** are 0.50 and 1.50 respectively. Even though these values are half that expected for single and triply bonded complexes, they are in an exact a 1:3 ratio. It is worth noting that the WBIs are almost identical to those calculated for the model complexes [$Cp(CO)_3Mo$–GeMe] (0.50) and [$Cp(CO)_2Mo{\equiv}GeMe$] (1.46) using the same level of theory, the latter of which has a near linear Ge centre and a formal Mo–Ge triple bond [28]. The Ge-N WBI calculated for complexes **6-41** and **6-42** are 0.48 and 0.59 respectively. The latter clearly shows a small increase compared with the singly bonded precursor, which could signify a small amount of the [$Cp(CO)_2^-Mo{=}Ge{=}N^+(Ar^*)(SiMe_3)$] canonical form. However, a small increase in the equivalent Ge-C WBI was also calculated for the model complexes [$Cp(CO)_3Mo$–GeMe] and [$Cp(CO)_2Mo{\equiv}GeMe$], even though a similar canonical form cannot exist in the latter complex.

As was proposed for the model complexes [$Cp(CO)_3Mo$–GeMe] and [$Cp(CO)_2Mo{\equiv}GeMe$], the low WBI values for the Mo–Ge and Ge–N bonds in **6-41**

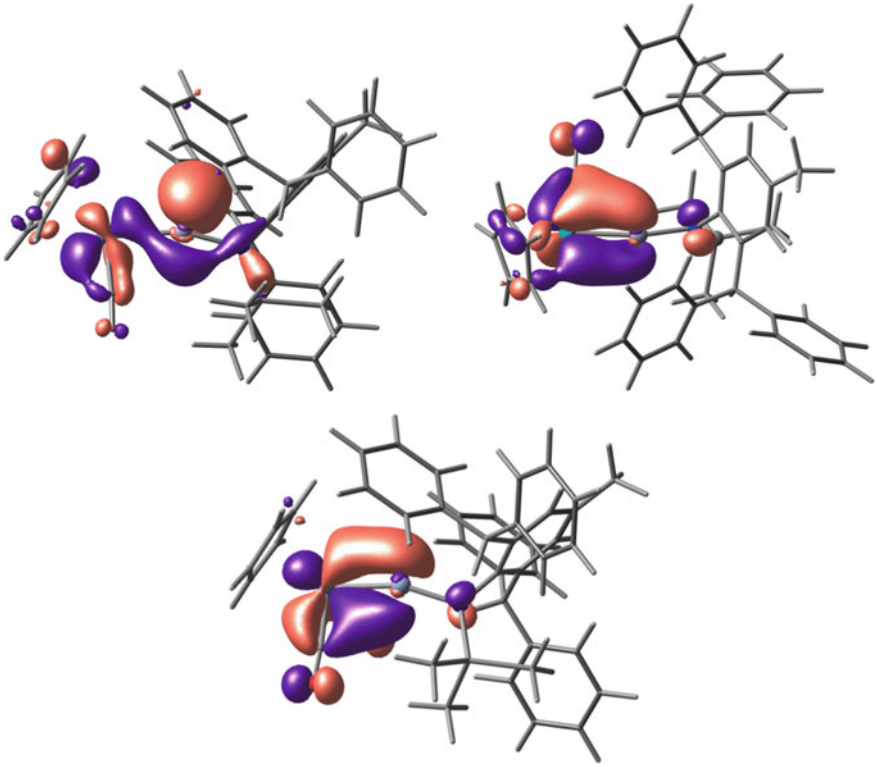

Fig. 6.5 Selected frontier orbitals calculated for **6-42**. LUMO (*top-left*), HOMO (*top-right*) and HOMO-2 (*bottom*). Iso-surface value 0.03 a.u.

and **6-42** are most likely due to large differences in electronegativities between the elements within the MoGeN fragment. This results in substantial polarization of the Mo–Ge and Ge–N bonds (calculated natural charges; Mo −1.49, Ge 1.27, N −1.43 for **6-41**; Mo −1.53, Ge 1.51, N −1.35 for **6-42**) and therefore reduces the covalent character of the Mo–Ge and Ge–N bonds, at the expense of their electrostatic component. Although the extent of this was not calculated for **6-41** or **6-42**, an energy decomposition analysis of the model complex $[Cp(CO)_2Mo{\equiv}GeMe]$ showed the covalent and electrostatic components of its Mo–Ge bond are almost equivalent [28].

In addition, quantum chemical calculations (using the same levels of theory) were also carried out on sterically reduced models of complexes **6-41** or **6-42** (viz. $[Cp(CO)_3Mo–GeN(Ph)SiMe_3]$ **6-41a** and $[Cp(CO)_2Mo{\equiv}GeN(Ph)SiMe_3]$ **6-42a**) in an attempt to determine what influence the bulky Ar* substituent has on the structure of the two isolated complexes. The geometries of **6-41a** (Mo–Ge 2.77 Å, Ge–N 1.88 Å, Mo–Ge–N 119.6°, B3LYP) optimized to be close to those in the solid state structure of **6-41**, indicating that the large steric demands of the Ar*

substituent have little effect on the overall structure of that complex. In contrast, the geometries of **6-42a** (Mo–Ge 2.31 Å, Ge–N 1.84 Å, Mo–Ge–N 170.4°, B3LYP) were optimized to have a significantly wider Mo–Ge–N angle than seen in the solid-state structure of **6-42**. This is in agreement with the proposal that the large Ar* substituent prevents the germanium centre in **6-42** from occupying a near linear geometry. Interestingly though, the calculated bond distances for **6-42** and **6-42a** are nearly identical, indicating that the significant bending of the Mo–Ge–N fragment does not greatly affect the strength of the Mo-Ge bond. This was further supported by the WBI calculations performed on **6-42a**, which calculated a WBI value of 1.60, only slightly greater than that calculated for **6-42**.

6.4 Conclusion

In summary, salt metathesis reactions between the molybdenum complex Na[CpMo$(CO)_3$] **6-04** and two bulky amido germanium chloride complexes, led to the isolation of [Cp$(CO)_3$Mo–GeN(R)Ar*] (R = Ph, **6-40**; $SiMe_3$, **6-41**), the first examples of two-coordinate molybdenum amino-germylene complexes. Compound **6-41** was found to eliminate a molecule of CO when heated to reflux in toluene, or irradiated with UV light, to give the molybdenum germylyne complex [Cp$(CO)_3$Mo≡GeN(R)Ar*] **6-42**, in essentially quantitative yields. Complex **6-42** is the first example of a transition metal amino-tetrelyne complex.

Spectroscopic and crystallographic analysis of **6-42**, including the results of various calculations, show that the complex is best viewed as having a bent Mo–Ge "triple" bond, with its Ge–N bond having little multiple bond character. Calculations on a sterically reduced model of the complex showed that the bending of the Mo–Ge–N unit was due to the large steric demands of the amino substituent.

6.5 Experimental

General methods. All manipulations were carried out using standard Schlenk and glove box techniques under an atmosphere of high purity dinitrogen. THF, hexane and toluene were distilled over molten potassium. ^{1}H NMR spectra were recorded on a Varian Inova 500 spectrometer, whereas ^{13}C and ^{29}Si were recorded on a Bruker AvanceIII 400 spectrometer and were referenced to the resonances of the solvent used. Mass spectra were obtained from the EPSRC National Mass Spectrometric Service at Swansea University. FTIR spectra were recorded using a Perkin-Elmer RX1 spectrometer as Nujol mulls between NaCl plates. Microanalyses were carried out by the Science Centre, London Metropolitan University. A reproducible microanalysis for **6-40** could not be obtained as the recrystallization of compound consistently led to contamination with small amounts of the free amine Ar*(Ph)NH. Melting points were determined in sealed glass

capillaries under dinitrogen and are uncorrected. The starting materials Na[CpMo$(CO)_3$] [34] **6-04**, [Ar*(Ph)NGeCl] [35] **2-38** and [Ar*($SiMe_3$)NGeCl] [27] **2-39** were prepared according to the literature method.

Preparation of [Cp$(CO)_3$Mo–Ge(Ph)Ar*], 6-40. To a solution of [Ar*N(Ph)GeCl] **6-38** (0.200 g, 0.321 mmol) in toluene (30 mL) was added a solution of Na[CpMo$(CO)_3$] **6-04** (0.103 g, 0.385 mmol) in THF (3 mL) at −80 °C over 5 min. The reaction produced an immediate colour change from pale yellow to orange on addition. The mixture was warmed to room temperature and stirred for a further 4 h, whereupon volatiles were removed *in vacuo*. The residue was extracted with warm hexane (100 mL), the extract filtered and volatiles removed from the filtrate *in vacuo* to give **6-40** as an orange solid (0.130 g, 48 %). N.B. X-ray quality crystals of **6-40** were obtained by crystallizing this solid from warm hexane. Mp: 164–168 °C; ^{1}H NMR (499 MHz, C_6D_6, 298 K): δ = 1.90 (s, 3H, ArCH_3), 4.52 (s, 5H, Cp*H*), 6.24 (s, 2H, Ph_2CH), 6.93–7.88 (m, 27H, Ar*H*); ^{13}C{^{1}H} NMR (126 MHz, C_6D_6) δ = 21.4 (Ar*C*H_3), 51.9 (Ph_2*C*H), 94.9 (Cp-*C*), 120.5, 123.5, 126.6, 126.8, 128.2, 128.4, 128.6, 129.2, 129.3, 130.1, 130.8, 131.4, 137.0, 143.5, 143.8, 145.3, 152.3 (Ar-*C*), 225.0 (CO, broad); IR υ/cm^{-1} (Nujol): 1972(s, CO str.), 1941(s, CO str.), 1902(s, CO str.), 1867(s, CO str.), 1860(s, CO str.), 1597(m), 1493(m), 1306(m), 1259(s), 1095(s), 1077(s), 1014(s), 868(m), 798(s), 746(m), 699 (s), 605(m), 579(m); MS/ES *m/z* (%): 833.1 (M^+, 2) 439.2 (Ar*NH_2^+, 45), 167.1 (Ph_2CH^+, 100);

Preparation of [Cp$(CO)_3$Mo–GeN($SiMe_3$)Ar*], 6-41. To a solution of [Ar*($SiMe_3$)NGeCl] **6-39** (0.200 g, 0.323 mmol) in toluene (30 mL) was added a solution of Na[CpMo$(CO)_3$] (0.104 g, 0.389 mmol) in THF (3 mL) at −80°C over 5 min. The reaction produced an immediate colour change from pale yellow to orange on addition. The mixture was warmed to room temperature and stirred for a further 4 h, whereupon volatiles were removed *in vacuo*. The residue was extracted with toluene (20 mL), and the extract filtered and concentrated to ca. 5 mL. Hexane (30 mL) was added to produce an orange precipitate of **6-41**, which was isolated by filtration (0.155 g, 58 %). N.B. X-ray quality crystals of **6-41** were obtained by recrystallizing this solid from a mixture of THF and hexane. Mp: 236–239 °C; ^{1}H NMR (499 MHz, C_6D_6, 298 K): δ = 0.79 (s, 9H, Si(CH_3)$_3$), 1.84 (s, 3H, ArCH_3), 4.69 (s, 5H, Cp*H*), 6.38 (s, 2H, Ph_2C*H*), 6.89-7.31 (m, 22H, Ar*H*); ^{13}C{^{1}H} NMR (126 MHz, C_6D_6) δ = 5.0 (Si(*C*H_3)$_3$), 21.1 (Ar*C*H_3), 52.4 (Ph_2*C*H), 96.0 (Cp-*C*), 126.7, 126.9, 128.6, 128.7, 130.3, 130.9, 131.9, 134.3, 143.5, 143.7, 144.9, 145.3 (Ar-*C*), 226.1 (CO, br.); ^{29}Si{^{1}H} NMR (80 MHz, C_6D_6) δ = 1.31 (s); IR υ/cm^{-1} (Nujol): 1966(s, CO str.), 1891(s, CO str.), 1850(s, CO str.), 1842(s, CO str.), 1830 (s, CO str.), 1598(m), 1493(m), 1250(m), 1244(m), 1194(m), 1117(m), 1108(m), 1077(m), 1031(m), 876(s), 847(s), 807(s), 750(m), 701(s), 604(m), 587(m), 555(m), 516(m), 473(m); MS/EI *m/z* (%): 801.2 (M^+–CO, 4), 745.2 (M^+ –3 CO, 7), 511.2 (Ar*N(H)$SiMe_3^+$, 100), 439.2 (Ar*NH_2^+, 33), 167.0 (Ph_2CH^+, 86); anal. calc. for $C_{44}H_{41}GeMoNO_3Si$: C 63.79 %, H 4.99 %, N 1.69 %, found: C 63.81 %, H 5.02 %, N 1.73 %.

Preparation 1 of [Cp$(CO)_2$Mo≡GeN($SiMe_3$)Ar*], 6-42. Compound **6-41** (0.200 g, 0.241 mmol) was dissolved in toluene (20 mL) and heated at reflux for

1 h. Volatiles were removed *in vacuo* to give **6-42** as an orange solid (0.189 g, 98 %). N.B. X-ray quality crystals of **6-42** were obtained from crystallizing this solid from a mixture of THF and hexane.

Preparation 2 of [Cp(CO)$_2$Mo≡GeN(SiMe$_3$)Ar*], 6-42. Compound **6-41** (0.025 g, 0.030 mmol) was dissolved in C_6D_6 and sealed in a J. Young's NMR tube. The tube was irradiated with UV light (λ = 254 nm) from a mercury vapor lamp for 20 min. A ^{1}H NMR spectrum of the resultant solution showed that it had converted to **6-42** (ca. 95 %). Mp: 230–234 °C; ^{1}H NMR (499 MHz, C_6D_6, 298 K): δ = 0.36 (s, 9H, Si(C*H*$_3$)$_3$), 1.83 (s, 3H, ArC*H*$_3$), 4.88 (s, 5H, Cp*H*), 6.30 (s, 2H, Ph$_2$C*H*), 6.90-7.19 (m, 22H, Ar*H*); ^{13}C{^{1}H} NMR (126 MHz, C_6D_6) δ = 2.8 (Si(*C*H$_3$)$_3$), 21.1 (Ar*C*H$_3$), 52.8 (Ph$_2$*C*H), 86.8 (Cp-*C*), 126.9, 127.6, 128.4, 128.8, 129.5, 130.0, 130.4, 130.6, 131.1, 135.0, 138.2, 142.1, 144.0, 144.8 (Ar-*C*), 231.3 (CO); ^{29}Si{^{1}H} NMR (80 MHz, C_6D_6) δ = 0.1 (s); IR υ/cm^{-1} (Nujol): 1926 (s, CO str.), 1853(s, CO str.), 1598(m), 1493(m), 1257(s), 1205(m), 1129(m), 1075 (m), 1030(m), 872(m), 831(m), 788(m), 761(m), 746(m), 711(m), 700(s), 604(m), 555(m), 546(m); MS/EI *m/z* (%): 801.2 (M$^+$, 45), 745.2 (M$^+$ –2 CO, 88), 511.2 (Ar*N(H)SiMe$_3^+$, 47), 439.2 (Ar*NH$_2^+$, 33), 167.0 (Ph$_2$CH$^+$, 56); anal. calc. for $C_{43}H_{41}GeMoNO_2Si$: C 64.52 %, H 5.16 %, N 1.75 %, found: C 64.41 %, H 5.20 %, N 1.79 %.

References

1. E.O. Fischer, G. Kreis, C.G. Kreiter, J. Miller, G. Huttner, H. Lorenz, Angew. Chem. **85**, 618 (1973); Angew. Chem. Int. Ed. Engl. **12**, 564 (1973)
2. See, for example: (a) H. Fischer, P. Hofmann, F.R. Kreisal, R.R. Schrock, U. Schubert, K. Weiss, *Carbyne Complexes*; VCH: New York (1988); (b) F.R. Kreisel (ed.), *Transition Metal Carbyne Complexes*; Kluwer: Dordrecht, The Netherlands (1993); (c) A. Mayer, H. Hoffmeister, Adv. Organomet. Chem. **32**, 227 (1991); d) R.R. Schrock, Chem. Rev. **102**, 145 (2002)
3. S.D. Grumbine, R.K. Chadha, T.D. Tilley, J. Am. Chem. Soc. **114**, 1518 (1992)
4. R.S. Simons, P.P. Power, J. Am. Chem. Soc. **118**, 11966 (1996)
5. L.Y. Chan, W.K. Dean, W.A.G. Graham, Inorg. Chem. **16**, 1067 (1977)
6. F. Carré, E. Colomer, R.J.P. Corriu, A. Vioux, Organometallics **15**, 741 (1984)
7. L. Pu, B. Twamley, S.T. Haubrich, M.M. Olmstead, B.V. Mork, R.S. Simons, P.P. Power, J. Am. Chem. Soc. **122**, 650 (2000)
8. L. Pauling, *The Nature of the Chemical Bond*, 3rd edn. (Cornell University Press, Ithaca, NY, 1960), p. 256
9. F.A. Cotton, G. Wilkinson, C. Murillo, M. Bochmann, *Advanced Inorganic Chemistry*, 6th edn. (Wiley, New York, 1999), p. 920
10. (a) A.C. Filippou, A.I. Philippopoulos, P. Portius, D.U. Neumann, Angew. Chem. Int. Ed. **39**, 2778 (2000); (b) A.C. Filippou, P. Portius, A.I. Philippopoulos, Organometallics **21**, 653 (2002); (c) A.C. Filippou, A.I. Philippopoulos, P. Portius, G. Schnakenburg, Organometallics **23**, 4503 (2004); (d) A.C. Filippou, G. Schnakenburg, A.I. Philippopoulos, N. Weidemann, Angew. Chem. Int. Ed. **44**, 5979 (2005); (e) A.C. Filippou, N. Weidemann, A.I. Philippopoulos, G. Schnakenburg, Angew. Chem. Int. Ed. **45**, 5987 (2006); (f) A.C. Filippou, K.W. Stumpf, O. Chernov, G. Schnakenburg, Organometallics **31**, 748 (2012); (g) H. Hashimoto, T. Fukuda, H. Tobita, M. Ray, S. Sakaki, Angew. Chem. Int. Ed. **51**, 2930

(2012); (h) A.C. Filippou, A. Barandov, G. Schnakenburg, B. Lewall, M. van Gastel, A. Marchanka, Angew. Chem. Int. Ed. **51**, 789 (2012); (i) A.C. Filippou, U. Chakraborty, G. Schnakenburg, Chem. Eur. J. **19**, 5676 (2013)
11. B.E. Eichler, A.D. Phillips, S.T. Haubrich, B.V. Mork, P.P. Power, Organometallics **21**, 5622 (2002)
12. A.C. Filippou, P. Portius, A.I. Philippopoulos, H. Rohde, Angew. Chem. Int. Ed. **42**, 445 (2003)
13. A.D. Phillips, R.J. Wright, M.M. Olmstead, P.P. Power, J. Am. Chem. Soc. **124**, 5930 (2002)
14. Selected references used in the publication for complexes with WSn single and double bonds: (a) W. Petz, Chem. Rev. **86**, 1019 (1986); (b) M.S. Holt, W.L. Wilson, J.H. Nelson, Chem. Rev. **89**, 11 (1989); (c) O. Kircher, G. Huttner, B. Schiemenz, K. Heinze, L. Zsolnai, O. Walter, A. Jakobi, A. Driess, Chem. Ber. **130**, 687 (1997); (d) T. Szymanska-Buzar, T. Glowiak, Polyhedron **17**, 3419 (1998); (e) H. Nakazawa, M. Kishishita, T. Ishiyama, T. Mizuta, K. Miyoshi, J. Organomet. Chem. **617**, 453 (2001)
15. A.C. Filippou, A.I. Philippopoulos, G. Schnakenburg, Organometallics **22**, 3339 (2003)
16. A.C. Filippou, P. Ghana, U. Chakraborty, G. Schnakenburg, J. Am. Chem. Soc. **135**, 11525 (2013)
17. A.C. Filippou, H. Rohde, H. Schnakenburg, Angew. Chem. Int. Ed. **43**, 2243 (2004)
18. L. Pu, P.P. Power, I. Boltes, R. Herbst-Irmer, Organometallics **19**, 352 (2000)
19. L. Pu, B. Twamley, P.P. Power, J. Am. Chem. Soc. **122**, 3524 (2000)
20. A.C. Filippou, N. Weidemann, G. Schnakenburg, H. Rohde, A.I. Philippopoulos, Angew. Chem. Int. Ed. **43**, 6512 (2004)
21. A.C. Filippou, N. Weidemann, G. Schnakenburg, Angew. Chem. Int. Ed. **47**, 5799 (2008)
22. B.V. Mork, T.D. Tilley, Angew. Chem. Int. Ed. **42**, 357 (2003)
23. A.C. Filippou, O. Chernov, K.W. Stumpf, G. Schnakenburg, Angew. Chem. Int. Ed. **49**, 3296 (2010)
24. (a) B.V. Mork, T. Don Tilley, A.J. Schultz, J.A. Cowan, J. Am. Chem. Soc. **126**, 10428 (2004); (b) M. Hirotsu, T. Nunokawa, K. Ueno, Organometallics **25**, 1554 (2006); (c) S.H.A. Petri, D. Eikenberg, B. Neumann, H.-G. Stammler, P. Jutzi, Organometallics **18**, 2615 (1999); (d) M. Haaf, T.A. Schmedake, R. West, Acc. Chem. Res. **33**, 704 (2000); (e) S.B. Clendenning, B. Gehrhus, P.B. Hitchcock, D.F. Moser, J.F. Nixon, R. West, J. Chem. Soc. Dalton Trans. 484 (2002)
25. A.C. Filippou, O. Chernov, G. Schnakenburg, Angew. Chem. Int. Ed. **50**, 1122 (2011)
26. A.C. Filippou, B. Baars, O. Chernov, Y.N. Lebedev, G. Schnakenburg, Angew. Chem. Int. Ed. **53**, 565 (2014)
27. J. Li, A. Stasch, C. Schenk, C. Jones, Dalton Trans. **40**, 10448 (2011)
28. K.P. Pandey, M. Lein, G. Frenking, J. Am. Chem. Soc. **125**, 1660 (2003)
29. W.-P. Leung, W.-K. Chiu, T.C.W. Mak, Organometallics **31**, 6966 (2012)
30. B. Cordero, V. Gómez, A.E. Platero-Prats, M. Revés, J. Echeverría, E. Cremades, F. Barragán, S. Alvarez, Dalton Trans. 2832 (2008)
31. See selected reviews: (a) A.J.L. Pombiero, M.F. C. Guedes da Silva, R.A. Michelin, Coord. Chem. Rev. **218**, 43 (2001); (b) R.L. Cordiner, A.F, Hill, J. Wagler, Organometallics **27**, 4532 (2008)
32. S.J. Dossett, A.F. Hill, J.C. Jeffrey, F. Marken, P. Sherwood, F.G.A. Stone, J. Chem. Soc. Dalton Trans. 2453 (1988)
33. A.C. Filippou, W. Grünleitner, E.O. Fischer, J. Organomet. Chem. **413**, 165 (1991)
34. U. Behrens, F.J. Edelmann, J. Organomet. Chem. **263**, 179 (1984)
35. J. Hicks, T.J. Hadlington, C. Schenk, J. Li, C. Jones, Organometallics **32**, 323 (2013)

Chapter 7
Appendix

7.1 General Procedures

7.1.1 X-Ray Crystallography

X-ray crystallographic measurements for all compounds reported in this thesis were made using an Oxford Gemini Ultra diffractometer, a Bruker X8 CCD diffractometer or the MX1 beamline of the Australian Synchrotron (λ = 0.7108 Å) [1]. The software package Blu-Ice [2] was used for synchrotron data acquisition, while the program XDS [3] was employed for synchrotron data reduction. All structures were solved by direct methods and refined on F^2 by full matrix least squares (SHELX97) [4] using all unique data. All non-hydrogen atoms are anisotropic with hydrogen atoms included in calculated positions (riding model), the isotropic thermal displacement and positional parameters of which were refined. Crystal data, details of data collections and refinements for all structures can be found in Tables 7.1, 7.2, 7.3, 7.4, 7.5, 7.6 and 7.7 or in their CIF files.

7.1.2 Magnetic Susceptibility Measurements

Variable-temperature solid-state magnetic susceptibility measurements for compounds [{Ar*(SiMe$_3$)NMn}$_2$] **3-15**, [Ar*(SiMe$_3$)NMnMg(^{Mes}Nacnac)] **3-16** and [CrMn{N(Si^{i}Pr$_3$)Ar†}{N(SiMe$_3$)Ar*}] **3-18** were recorded over the range 300–2 K with a Quantum Design MPMS5 SQUID magnetometer. Corrections for diamagnetism were made using Pascal's constants. All solution-state effective magnetic moment values were calculated by the Evans Method [5].

J. Hicks, *Preparation, Characterisation and Reactivity of Low Oxidation State d-Block Metal Complexes Stabilised by Extremely Bulky Amide Ligands*, Springer Theses,
DOI 10.1007/978-981-10-2905-9_7

Table 7.1 Summary of crystallographic data for compounds **2-41**–**2-47**

	2-41 $(THF)_4$	**2-42** $(toluene)_4$	**2-43** $(toluene)_4$	**2-44** $(hexane)_2$ $(THF)_2$	**2-45**	**2-46**	**2-47** $(toluene)_{1.8}$ $(hexane)_{1.2}$
Empirical formula	$C_{96}H_{120}Cl_2Cr_2N_2O_6Si_2$	$C_{130}H_{116}Cl_2Cr_2N_2Si_2$	$C_{108}H_{120}Br_2Mn_2N_2O_2Si_2$	$C_{130}H_{144}Br_2Mn_2N_2O_4Si_2$	$C_{108}H_{132}Br_2Mn_2N_2O_2Si_2$	$C_{80}H_{88}Br_2Fe_2N_2O_2Si_2$	$C_{129.8}H_{131.2}Br_2Fe_2N_2O_2Si_2$
Formula weight	1629.02	1937.33	1803.94	2124.35	1816.04	1437.22	2078.87
Crystal system	triclinic	monoclinic	triclinic	triclinic	triclinic	monoclinic	triclinic
Space group	*P*-1	*P*21/c	*P*-1	*P*-1	*P*-1	*P*21/n	*P*-1
a (Å)	11.8071(5)	15.1465(12)	11.7659(4)	14.1515(6)	11.7629(5)	16.4622(14)	14.0504(4)
b (Å)	13.1447(6)	20.9444(12)	12.7628(3)	14.3059(6)	13.3147(5)	12.6193(7)	14.5583(5)
c (Å)	15.4536(8)	17.2104(15)	17.1373(6)	14.5230(6)	15.7449(6)	18.6176(14)	15.2887(5)
α (deg.)	70.737(4)	90	106.413(3)	103.914(4)	80.282(2)	90	64.520(3)
β (deg.)	71.481(4)	111.995(10)	103.649(3)	95.548(4)	77.819(2)	114.497(10)	70.367(3)
γ (deg.)	81.584(4)	90	97.608(2)	103.950(4)	80.593(2)	90	78.910(3)
vol ($Å^3$)	2144.58(17)	5062.4(7)	2343.51(13)	2732.2(2)	2354.85(16)	3519.5(4)	2654.80(15)
Z	1	2	1	1	1	2	1
σ (calcd) ($g \cdot cm^{-3}$)	1.261	1.271	1.278	1.291	1.281	1.356	1.3
μ (mm^{-1})	0.399	0.345	1.198	1.04	1.193	1.63	1.103
F(000)	868	2040	946	1118	958	1496	1090
Reflections collected	12,924	18,451	34,600	17,958	37,572	13,984	39,120
Unique reflections	7659	9051	10,204	10,654	10,245	6877	10,417
R_{int}	0.0375	0.0613	0.0279	0.0316	0.1120	0.0617	0.0269
R1 indices [$I > 2\sigma(I)$]	0.0497	0.053	0.0299	0.0452	0.0378	0.0451	0.0318
*w*R2 indices (all data)	0.1262	0.1262	0.0766	0.128	0.0809	0.1187	0.082

Table 7.2 Summary of crystallographic data for compounds **2-48**–**2-55**

	2-48 $(toluene)_2$	**2-49** $(toluene)_{1.5}$	**2-50**	**2-51**	**2-52**	**2-53**	**2-54**	**2-55**
Empirical formula	$C_{124}H_{116}Cl_2Co_2N_2O_2Si_2$	$C_{112.5}H_{96}Cl_2Co_2N_2Si_2$	$C_{16}H_{32}Br_4Co_2O_4$	$C_{40}H_{44}BrNOSiZn$	$C_{42}H_{48}BrNOSiZn$	$C_{51}H_{42}BrNSiZn$	$C_{42}H_{48}BrNSiZn$	$C_{44}H_{52}BrNSiZn$
Formula weight	1911.13	1720.85	725.92	728.13	756.18	842.23	740.18	768.24
Crystal system	triclinic	monoclinic	triclinic	monoclinic	triclinic	triclinic	monoclinic	triclinic
Space group	*P*-1	*P*21/c	*P*-1	*C*2/c	*P*-1	*P*-1	*C*2/c	*P*-1
a (Å)	11.8902(4)	13.3383(7)	9.6952(3)	15.6064(5)	10.142(2)	10.6299(4)	45.117(9)	10.3239(5)
b (Å)	14.0389(4)	18.1137(8)	16.7946(7)	15.0567(4)	10.719(2)	10.7824(5)	11.042(2)	12.6534(6)
c (Å)	15.2789(5)	19.0342(11)	16.9815(6)	30.4145(8)	17.664(4)	19.9387(9)	35.630(7)	15.4505(8)
α (deg.)	81.973(2)	90	61.163(4)	90	95.42(3)	84.799(4)	90	82.710(3)
β (deg.)	79.402(3)	99.164(5)	84.133(3)	97.485(3)	91.34(3)	89.581(3)	123.85(3)	86.884(3)
γ (deg.)	89.569(2)	90	89.749(3)	90	92.69(3)	63.163(4)	90	72.360(2)
vol ($Å^3$)	2481.94(14)	4540.1(4)	2406.28(15)	7085.9(3)	1908.8(7)	2029.30(15)	14742(5)	1907.62(16)
Z	1	2	4	8	2	2	16	2
σ (calcd) ($g \cdot cm^{-3}$)	1.279	1.259	2.004	1.365	1.316	1.378	1.334	1.337
μ (mm^{-1})	0.467	0.502	8.038	1.887	1.753	1.656	1.813	1.754
F(000)	1006	1802	1416	3024	788	868	6176	804
Reflections collected	16,246	30,822	14,844	23,865	27,808	27,739	54,358	26,816
Unique reflections	9697	8912	8621	7732	7032	7958	13,674	7055
R_{int}	0.0297	0.0329	0.0343	0.0275	0.0821	0.0266	0.0852	0.0232
R1 indices [$I > 2\sigma(I)$]	0.0537	0.0605	0.0484	0.0347	0.0402	0.0523	0.0555	0.0362
*w*R2 indices (all data)	0.1439	0.1802	0.1069	0.0848	0.1037	0.1642	0.1481	0.1024

Table 7.3 Summary of crystallographic data for compounds **2-56**–**2-62** and **3-15**

	2-56 (cyclohexane)$_4$	(**2-57**)$_{0.7}$ (Ar*(SiPh$_3$)NH)$_{0.3}$	**2-58**	**2-59**	**2-60** (hexane)	**2-61**	**2-62**	**3-15** (toluene)$_4$
Empirical formula	$C_{100}H_{128}Cd_2I_2N_2Si_2$	$C_{51}H_{42.30}Cd_{0.70}I_{0.70}NSi$	$C_{36}H_{36}HgINSi$	$C_{38}H_{40}HgINSi$	$C_{57}H_{56}HgINSi$	$C_{42}H_{48}HgINSi$	$C_{44}H_{52}HgINSi$	$C_{100}H_{104}Mn_2N_2Si_2$
Formula weight	1892.82	864.76	838.24	866.29	1110.61	922.39	950.45	1499.91
Crystal system	triclinic	triclinic	Orthorhombic	triclinic	triclinic	triclinic	triclinic	monoclinic
Space group	*P*-1	*P*-1	*Pna*21	*P*-1	*P*-1	*P*-1	*P*-1	*P*21/c
a (Å)	10.631(2)	11.1500(6)	40.2684(12)	10.133(2)	13.403(3)	10.884(2)	10.937(2)	15.7018(6)
b (Å)	14.609(3)	11.3946(5)	17.8633(6)	15.488(3)	14.111(3)	12.792(3)	11.169(2)	10.3770(3)
c (Å)	16.783(3)	16.8845(10)	9.0713(3)	22.406(5)	14.143(3)	13.738(3)	16.882(3)	26.7505(9)
α (deg.)	71.79(3)	81.369(4)	90	81.00(3)	65.08(3)	89.16(3)	94.76(3)	90
β (deg.)	87.89(3)	71.852(5)	90	81.21(3)	85.38(3)	79.57(3)	101.54(3)	106.562(3)
γ (deg.)	71.39(3)	87.207(4)	90	86.12(3)	88.06(3)	85.73(3)	97.38(3)	90
vol (Å^3)	2340.8(8)	2015.37(18)	6525.2(4)	3428.8(12)	2418.0(8)	1875.9(7)	1991.2(7)	4177.8(2)
Z	1	2	8	4	2	2	2	2
σ (calcd) (g · cm^{-3})	1.343	1.425	1.707	1.678	1.525	1.633	1.585	1.192
μ (mm^{-1})	1.184	0.990	5.725	5.450	3.883	4.987	4.700	0.379
F(000)	972	880	3248	1688	1104	908	940	1592
Reflections collected	30,282	16,414	20,282	78,278	34,479	32,759	28,091	26,070
Unique reflections	8327	7494	8651	12745	8929	8547	7402	8203
R_{int}	0.0744	0.0360	0.0428	0.0786	0.0478	0.0805	0.0912	0.0281
R1 indices [$I > 2\sigma(I)$]	0.0508	0.0535	0.0302	0.0419	0.0494	0.0418	0.0396	0.043
wR2 indices (all data)	0.1191	0.1158	0.0579	0.0969	0.1334	0.1038	0.0918	0.1183

Table 7.4 Summary of crystallographic data for compounds **3-16**–**3-22** and **4-23**

	3-16	**3-17** (hexane)	**3-18** (hexane)$_{0.5}$	**3-19** (pentane)	**3-20** (pentane)	**3-21**	**3-22**	**4-23**
Empirical formula	$C_{67}H_{81}MgMnN_3Si$	$C_{86}H_{102}Mn_2N_2Si_2$	$C_{83}H_{95}CrMnN_2Si_2$	$C_{76}H_{101}MgMnN_3OSi$	$C_{76}H_{101}MgMnN_3O_2Si$	$C_{154}H_{202}Mg_2Mn_2N_6O_8Si_2$	$C_{74}H_{95}MgMnN_5Si$	$C_{76}H_{80}N_2Si_2Zn_2$
Formula weight	1035.69	1329.76	1283.73	1179.94	1195.94	2479.90	1161.89	1208.34
Crystal system	monoclinic	triclinic	triclinic	triclinic	triclinic	monoclinic	triclinic	mooclinic
Space group	$P2_1/n$	P-1	P-1	P-1	P-1	$P2_1/n$	P-1	$P2_1/n$
a (Å)	14.0354(10)	13.5142(7)	12.3698(4)	13.7194(5)	10.2192(4)	13.284(3)	14.7416(11)	10.627(2)
b (Å)	31.639(2)	15.1264(7)	13.9284(5)	14.4149(6)	14.5682(5)	23.108(5)	16.0335(11)	16.761(3)
c (Å)	14.0529(10)	19.1617(11)	21.8462(8)	18.7446(8)	23.4367(8)	25.148(5)	16.1827(14)	17.994(4)
α (deg.)	90	79.351(4)	75.459(2)	93.051(3)	88.295(2)	90	89.828(6)	90
β (deg.)	105.605(2)	79.778(4)	83.817(2)	91.643(2)	89.900(2)	94.31(3)	116.830(8)	90.33(3)
γ (deg.)	90	81.150(4)	70.909(2)	101.609(2)	76.256(2)	90	94.088(6)	90
vol (Å^3)	6010.3(7)	3758.7(3)	3441.6(2)	3623.1(3)	3387.7(2)	7698(3)	3402.7(5)	3205.0(11)
Z	4	2	2	2	2	2	2	2
σ (calcd) (g · cm^{-3})	1.145	1.175	1.239	1.082	1.172	1.070	1.134	1.252
μ (mm^{-1})	0.291	0.412	0.423	0.250	0.269	0.241	0.265	0.830
F(000)	2220	1420	1368	1274	1290	2668	1250	1276
Reflections collected	40,583	24,153	21,756	38,422	44,364	50,176	22,814	25,790
Unique reflections	11,145	13,843	14,108	13,439	12,546	12,504	13,248	5927
R_{int}	0.0892	0.0614	0.0388	0.0812	0.0468	0.0747	0.0552	0.0585
R1 indices [$I > 2\sigma(I)$]	0.0616	0.0623	0.0529	0.0964	0.0485	0.0866	0.0622	0.0387
wR2 indices (all data)	0.1727	0.1518	0.1208	0.2913	0.1187	0.2710	0.1695	0.1042

Table 7.5 Summary of crystallographic data for compounds **4-24–4-30**

	4-24	**4-25**	**4-26a**	**4-26b**	**4-27**	**4-28** (pentane)	**4-29** (pentane)	**4-30** (pentane)
Empirical formula	$C_{76}H_{80}Cd_2N_2Si_2$	$C_{76}H_{80}Hg_2N_2Si_2$	$C_{67}H_{81}MgN_3SiZn$	$C_{65}H_{77}MgN_3SiZn$	$C_{84}H_{96}Hg_2N_2Si_2$	$C_{89}H_{108}N_2Si_2Zn_2$	$C_{89}H_{108}N_2Si_2Zn_3$	$C_{89}H_{108}CdN_2Si_2Zn_2$
Formula weight	1302.40	1478.78	1046.12	1018.07	1590.99	1392.69	1458.06	1505.09
Crystal system	Monoclinic	Monoclinic	Monoclinic	Monoclinic	triclinic	monoclinic	triclinic	triclinic
Space group	$P2_1/n$	$P2_1/n$	$P2_1/n$	$P2_1/n$	P-1	$P2_1/c$	P-1	P-1
a (Å)	10.630(2)	10.660(2)	13.855(3)	13.5124(5)	11.608(2)	17.670(4)	10.704(2)	10.709(2)
b (A)	16.806(3)	16.853(3)	31.731(7)	31.1931(12)	13.169(3)	13.486(3)	12.459(3)	12.471(3)
c (Å)	18.319(4)	18.287(4)	14.032(3)	14.3764(5)	13.350(3)	32.343(7)	16.608(3)	16.643(3)
α (deg.)	90	90	90	90	76.49(3)	90	74.86(3)	75.46(3)
β (deg.)	90.31(3)	90.45(3)	105.771(7)	109.160(2)	72.56(3)	90.75(3)	86.03(3)	86.42(3)
γ (deg.)	90	90	90	90	65.09(3)	90	80.70(3)	81.74(3)
vol ($Å^3$)	3272.6(11)	3285.2(11)	5937(2)	5723.9(4)	1752.1(6)	7707(3)	2109.0(7)	2128.4(7)
Z	2	2	4	4	1	4	1	1
σ (calcd) ($g \cdot cm^{-3}$)	1.322	1.495	1.170	1.181	1.508	1.200	1.148	1.174
μ (mm^{-1})	0.730	4.748	0.468	0.502	4.457	0.699	0.917	0.876
F(000)	1348	1476	2240	2176	802	2976	774	792
Reflections collected	49,507	24,335	35,602	60,067	26,423	56,606	30,023	31,538
Unique reflections	6674	6063	11,030	10,547	6469	14,309	7744	7812
R_{int}	0.0788	0.0553	0.0803	0.0448	0.0454	0.1014	0.0812	0.0363
R1 indices [$I > 2\sigma(I)$]	0.0329	0.0301	0.0577	0.0458	0.0270	0.0956	0.1118	0.0603
wR2 indices (all data)	0.0837	0.0781	0.1623	0.1186	0.0699	0.2849	0.3529	0.1753

Table 7.6 Summary of crystallographic data for compounds **4-31–4-32**, **5-43–5-45** and **6-40–6-41**

	4-31 (pentane)	**4-32**	**4-43** $(benzene)_{2.5}$	**5-44** $(fluorobenzene)_{1.75}$	**5-45a** $(diethyl\ ether)_{0.75}$	**5-45b** (pentane)	**6-40**	**6-41**
Empirical formula	$C_{89}H_{108}HgN_2Si_2Zn_2$	$C_{48}H_{64}BrN_3SiZn_2$	$C_{72}H_{63}CoNSi$	$C_{112.5}H_{92.75}Co_2F_{1.75}N_2Si_2$	$C_{65}H_{69.5}CoN_3O_{0.75}Si$	$C_{67}H_{74}CoN_3Si$	$C_{47}H_{37}GeMoNO_3$	$C_{44}H_{41}GeMoNO_3Si$
Formula weight	1593.28	921.76	1029.25	1679.93	991.76	1008.31	832.31	828.4
Crystal system	triclinic	triclinic	monoclinic	triclinic	triclinic	monoclinic	triclinic	triclinic
Space group	*P*-1	*P*-1	$P2_1/n$	*P*-1	*P*-1	$P2_1/c$	*P*-1	*P*-1
a (Å)	10.709(2)	10.8421(8)	13.9259(9)	14.930(3)	12.495(3)	22.050(4)	9.6979(6)	10.5025(3)
b (Å)	12.471(3)	14.6580(12)	18.1348(11)	17.230(3)	19.107(4)	10.082(2)	14.1058(9)	11.1486(3)
c (Å)	16.643(3)	16.0589(14)	23.0194(13)	18.810(4)	24.377(5)	25.070(5)	14.7614(10)	17.1700(4)
α (deg.)	75.46(3)	68.562(8)	90	104.15(3)	105.22(3)	90	97.177(4)	97.282(2)
β (deg.)	86.42(3)	86.097(6)	106.420(6)	96.94(3)	89.89(3)	96.23(3)	94.713(4)	98.670(2)
γ (deg.)	81.74(3)	71.518(7)	90	100.74(3)	104.40(3)	90	107.018(3)	103.088(2)
vol ($Å^3$)	2128.4(7)	2249.7(3)	5576.3(6)	4539.0(16)	5426.8(19)	5540.3(19)	1900.7(2)	1908.59(9)
Z	1	2	4	2	4	4	2	2
σ (calcd) ($g \cdot cm^{-3}$)	1.243	1.361	1.226	1.229	1.214	1.209	1.454	1.441
μ (mm^{-1})	2.428	2.016	0.374	0.446	0.383	0.375	1.164	1.188
F(000)	824	964	2172	1759	2110	2152	848	848
Reflections collected	32,314	17,691	21,335	65,267	77,655	42,378	8925	27,485
Unique reflections	7881	8364	10,314	16,803	20,142	10,783	8688	7476
R_{int}	0.1211	0.0510	0.0406	0.0754	0.0942	0.0551	0.0516	0.0285
R1 indices $[I > 2\sigma(I)]$	0.0851	0.0446	0.0474	0.0627	0.0583	0.0718	0.041	0.0267
*w*R2 indices (all data)	0.2435	0.0956	0.1205	0.1858	0.1553	0.2058	0.0969	0.0657

Table 7.7 Summary of crystallographic data for compounds **6-42** and **7-01–7-03**

	6-42	**7-01**	**7-02**	**7-03** $(toluene)_{1.5}$
Empirical formula	$C_{43}H_{41}GeMoNO_2Si$	$C_{88}H_{104}Mn_2N_2OSi_2$	$C_{78}H_{84}GeN_2Si_2Zn$	$C_{94.5}H_{114}CoN_7Si$
Formula weight	800.39	1371.79	1243.61	1434.95
Crystal system	triclinic	triclinic	monoclinic	triclinic
Space group	*P*-1	*P*-1	$P2_1/c$	*P*-1
a (Å)	10.4466(4)	11.8629(5)	15.100(3)	10.501(2)
b (Å)	10.7223(3)	12.6271(6)	19.540(4)	18.201(4)
c (Å)	18.7882(6)	13.6370(7)	23.140(5)	21.760(4)
α (deg.)	92.295(3)	88.3340(3)	90	96.68(3)
β (deg.)	103.169(3)	87.055(3)	106.57(3)	99.75(3)
γ (deg.)	111.411(3)	67.856(3)	90	93.70(3)
vol ($Å^3$)	1890.03(11)	1889.47(15)	6544(2)	4055.9(14)
Z	2	1	4	2
σ (calcd) ($g \cdot cm^{-3}$)	1.406	1.206	1.262	1.175
μ (mm^{-1})	1.195	0.413	0.908	0.277
F(000)	820	732	2624	1542
Reflections collected	27,586	13,351	97,539	54,486
Unique reflections	7418	6763	12,163	14,896
R_{int}	0.0369	0.0445	0.1519	0.535
R1 indices $[I > 2\sigma(I)]$	0.0387	0.0499	0.0462	0.0639
*w*R2 indices (all data)	0.1053	0.1096	0.1114	0.1708

7.1.3 EPR Spectroscopy Studies

The EPR spectroscopy studies in Chap. 3 were obtained in collaboration with Prof. Damien Murphy, Cardiff University, Cardiff, UK. Continuous Wave (CW) EPR spectra were measured at X- and Q-band frequencies. The spectra were recorded as frozen solutions (in dried solvents) at 10 K. All manipulations were done in a glovebox, including transferring the solutions to the EPR tubes. The X-/Q-band CW measurements were performed on a Bruker ESP300E series spectrometer using a standard Bruker ER4102ST X-band cavity or using a Bruker ER5106 QT-E Q-band resonator incorporating an Oxford Helium cryostat. The EPR simulations were performed using the Easyspin toolbox [6].

7.1.4 Computational Studies

All theoretical calculations in Chap. 3 were obtained in collaboration with Prof. L. Gagliardi, University of Minnesota, Minneapolis, USA. The bimetallic

complexes [{Ar*($SiMe_3$)NMn}$_2$] **3-15**, [CrMn{N(Si^iPr_3)$Ar^\dagger$}{N($SiMe_3$)Ar*}] **3-18**, in addition to the sterically reduced model complex [Ar*($SiMe_3$)NMnMg (^{Mes}Nacnac)] **3-16^{Me}** were studied using density functional theory (DFT) and the complete active space self-consistent field (CASSCF) method [7], followed by a multi-configurational second-order perturbation theory (CASPT2) method [8]. Previous studies on similar systems have demonstrated that this approach is successful in predicting accurate results for ground and electronically excited states of bimetallic systems [9].

All theoretical calculations in Chap. 4 were obtained in collaboration with Prof. Laurent Maron, Laboratoire de Physique et Chimie des Nano-objets, Toulouse, France. The bi- and trimetallic complexes [{$Ar^\dagger$($SiMe_3$)NM}$_2$] (M=Zn **4-23**, Cd **4-24**, Hg **4-25**), [Ar*(Si^iPr_3)NZnMg(^{Mes}Nacnac)] **4-26b** and [{Ar*(Si^iPr_3)NZn}$_2$Zn] **4-29** were studied using B3LYP and B3PW91 levels of theory.

All theoretical calculations in Chap. 6 were obtained in collaboration with Dr. Christian Schenk, Universität Heidelberg, Heidelberg, Germany. The bimetallic complexes [Cp(CO)$_3$Mo–GeN($SiMe_3$)Ar*] **6-41** and [Cp(CO)$_2$Mo≡GeN($SiMe_3$)Ar*] **6-42** were studied using quantum chemical calculations (B3LYP/6-311G(d)/LANL2DZ and BP86/6-311G(d)/LANL2DZ).

7.2 Miscellaneous Data

See Figs. 7.1, 7.2 and 7.3.

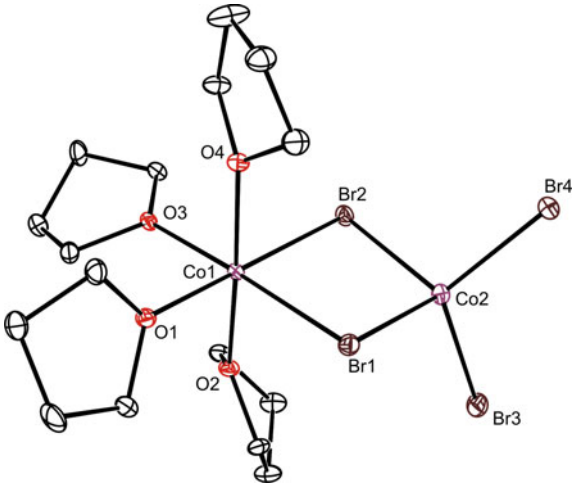

Fig. 7.1 Thermal ellipsoid plot (25 % probability surface) of the molecular structure of [(THF)$_4$Co(μ-Br)$_2$CoBr$_2$] **2-50**. Hydrogen atoms have been omitted for clarity. Selected bond lengths (Å): Co(1)-Br(1) 2.6444(12), Co(1)-Br(2) 2.5783(12), Co(2)-Br(1) 2.4411(13), Co(2)-Br(2) 2.4582(13), Co(2)-Br(3) 2.3761(13), Co(2)-Br(4) 2.3816(13), Co(1)-O(1) 2.085(5), Co(1)-O(2) 2.116(5), Co(1)-O(3) 2.114(5), Co(1)-O(4) 2.117(5)

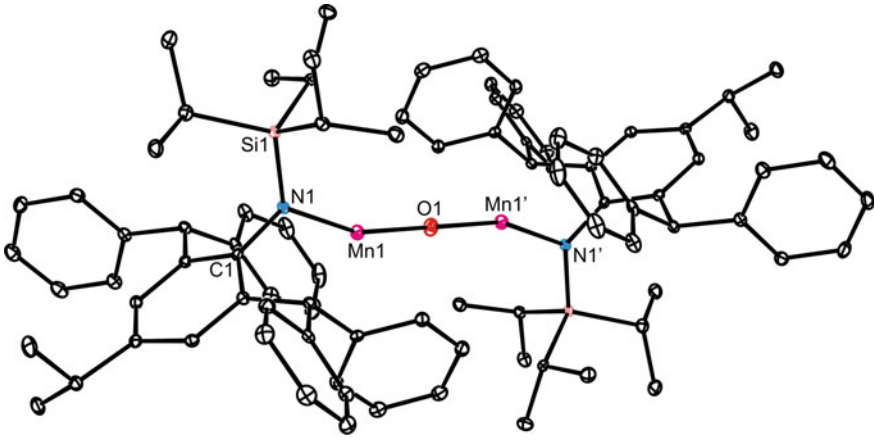

Fig. 7.2 Thermal ellipsoid plot (25 % probability surface) of the molecular structure of [{Ar†(Si^{i}Pr$_3$)NMn}$_2$(μ-O)] **7-01**. Hydrogen atoms have been omitted for clarity. Selected bond lengths (Å) and angles (°): Mn(1)-O(1) 1.8109(3), N(1)-Mn(1) 1.9890(15), N(1)-Mn(1)-O(1) 160.46(4), Mn(1)-O(1)-Mn(1′) 180.000(2)

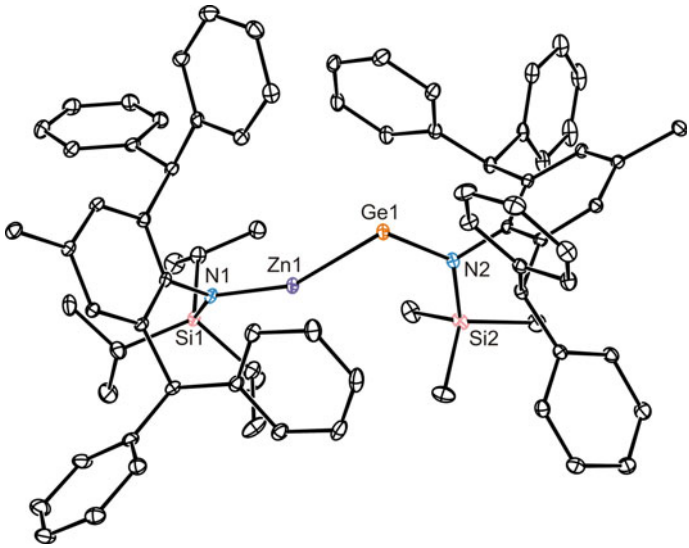

Fig. 7.3 Thermal ellipsoid plot (25 % probability surface) of the molecular structure of [Ar*(Si^{i}Pr$_3$)NZnZnN(SiMe$_3$)Ar*] **7-02**. Hydrogen atoms have been omitted for clarity. Selected bond lengths (Å) and angles (°): Zn(1)-Ge(1) 2.4947(9), N(1)-Zn(1) 1.902(2), Ge(1)-N(2) 1.859(2), N(1)-Zn(1)-Ge(1) 156.23(7), Zn(1)-Ge(1)-N(2) 110.62(7)

7.3 Summary of Crystallographic Data

See Figs. 7.4, 7.5 and 7.6.

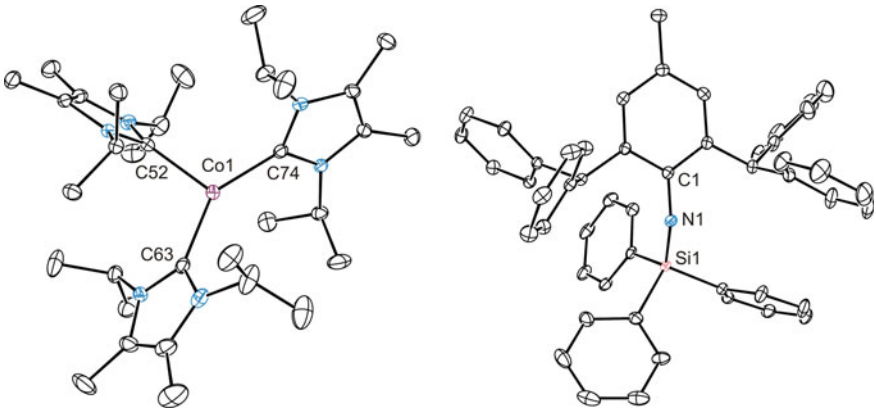

Fig. 7.4 Thermal ellipsoid plots (25 % probability surface) of the cation (*left*) and the anion (*right*) of $[Co(IPriMe)_3]^+[Ar^*NSiPh_3]^-$ **7-03**. Hydrogen atoms have been omitted for clarity. Selected bond lengths (Å) and angles (°): Co(1)-C(52) 1.973(3), Co(1)-C(63) 1.996(3), Co(1)-C(74) 1.991(3), N(1)-C(1) 1.354(3) N(1)-Si(1) 1.634(2), C(52)-Co(1)-C(63) 111.37(11), C(63)-Co(1)-C(74) 104.73(11), C(74)-Co(1)-C(52) 143.63(11), C(1)-N(1)-Si(1) 144.45(18)

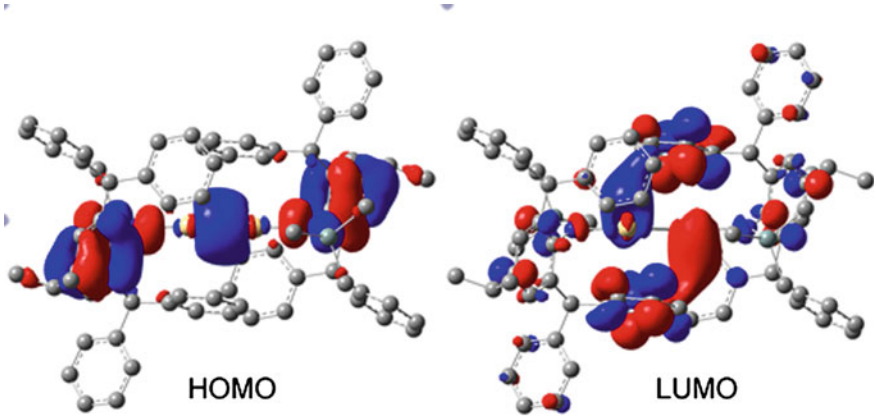

Fig. 7.5 Selected calculated frontier orbitals for $[\{Ar^{\dagger}(SiMe_3)NCd\}_2]$ **4-24**. HOMO (*left*) and LUMO (*right*)

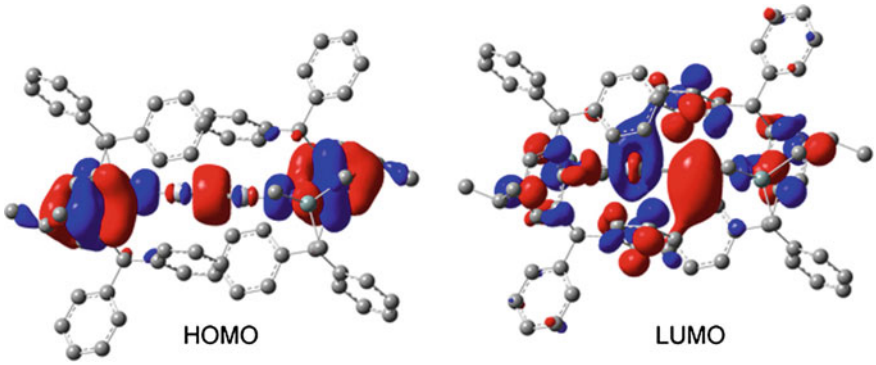

Fig. 7.6 Selected calculated frontier orbitals for [{Ar†(SiMe$_3$)NHg}$_2$] **4-25**. HOMO (*left*) and LUMO (*right*)

References

1. N.P. Cowieson, D. Aragao, M. Clift, D.J. Ericsson, C. Gee, S.J. Harrop, N. Mudie, S. Panjikar, J.R. Price, A. Riboldi-Tunnicliffe, R. Williamson, T. Caradoc-Davies, J. Synchrotron Radiat **22**, 187 (2015)
2. T.M. McPhillips, S.E. McPhillips, H.-J. Chiu, A.E. Cohen, A.M. Deacon, P.J. Ellis, E. Garman, A. Gonzalez, N.K. Sauter, R.P. Phizackerley, S.M. Soltis, P. Kuhn, J. Synchrotron Radiat **9**, 401 (2002)
3. W. Kabsch, J. Appl. Crystallogr. **26**, 795 (1993)
4. G. M. Sheldrick, *SHELX-97*, University of Göttingen (1997)
5. (a) D. F. Evans, J. Chem. Soc., **2003** (1959); (b) E. M. Schbert, J. Chem. Educ., **69**, 62 (1992)
6. S. Stoll, A. Schweiger, J. Magn. Reson. **178**, 42 (2006)
7. B.O. Roos, P.R. Taylor, P.E.M. Siegbahn, Chem. Phys. **48**, 157 (1980)
8. K. Anderson, P.-Å. Malmqvist, B.O. Roos, J. Chem. Phys. **96**, 1218 (1992)
9. A few selected examples include: (a) B. N. Briggs, D. R. McMillin, T. K. Todorova, L. Gagliardi, F. Poineau, K. R. Czerwinski, A. P. Sattelberger, Dalton Trans. **39**, 11322 (2010); (b) F. Poineau, L. Gagliardi, P. M. Forster, A. P. Sattelberger, K. R. Czerwinski, Dalton Trans., **5954** (2009); (c) F. Ferrante, L. Gagliardi, B. E. Bursten, A. P. Sattelberger, Inorg. Chem., **44**, 8476 (2005); (d) L. Gagliardi, B. O. Roos, Inorg. Chem., **42**, 1599 (2003); (e) F. Poineau, P. M. Forster, T. K. Todorova, L. Gagliardi, A. P. Sattelberger, K. R. Czerwinski, Inorg. Chem., **49**, 6646 (2010); (f) C. M. Zall, D. Zherebetskyy, A. L. Dzubak, E. Bill, L. Gagliardi, C. C. Lu, Inorg. Chem, **51**, 728 (2012); (g) L. Fohlmeister, S. Liu, C. Schulten, B. Moubaraki, A. Stasch, J. D. Cashion, K. S. Murray, L. Gagliardi, C. Jones, Angew. Chem., Int. Ed., **51**, 8294 (2012)